RESPONSE OF HIGH STRENGTH CONCRETE COLUMNS UNDER FIRE-INDUCED BIAXIAL BENDING

By

Nikhil Raut

A DISSERTATION

Submitted to
Michigan State University
in partial fulfillment of the requirements
for the degree of

DOCTOR OF PHILOSOPHY

Civil Engineering

2011

ABSTRACT

MODELING THE FIRE RESPONSE OF HIGH STRENGTH CONCRETE COLUMNS UNDER BIAXIAL BENDING

BY

Nikhil Raut

Reinforced concrete (RC) columns, under fire conditions, can experience biaxial bending which can arise due to eccentricity in loading, uneven spalling, or significant thermal gradients generated through 1-, 2-, or 3-sides of fire exposure. High strength concrete (HSC) columns are especially prone to such biaxial bending due to fire induced spalling. However, there is limited data and understanding in the literature on the effect of fire-induced biaxial bending on the response of RC columns under realistic loading and fire conditions. To overcome some of these knowledge gaps, a comprehensive study was undertaken to develop an understanding on the fire performance of RC columns under biaxial bending.

A numerical model, in the form of a computer program, is developed for tracing the fire response of RC column. The model, based on macroscopic finite element approach, utilizes time dependent moment-curvature (M-κ) relationships for establishing the response of RC columns under fire conditions. The model accounts for fire-induced spalling, biaxial bending, various strain components, and high temperature material properties. Fire-induced biaxial bending is incorporated in the analysis through M-κ curves generated along both axes of bending while spalling is accounted through hydro-thermal analysis.

For validating the numerical model, fire resistance tests were carried out on six RC columns under realistic loading, and fire scenarios. The columns comprised of one NSC, three HSC and two HSC columns with polypropylene fiber, and were tested under a standard and two design

fires. Results from the tests show that HSC columns exhibit lower fire resistance due to occurrence of spalling and faster degradation of strength. But these HSC columns can survive burnout conditions (no failure) under typical design fire scenarios encountered in buildings. Also, the addition of polypropylene fibers mitigates spalling and thus significantly enhances fire resistance of HSC columns. Data from these fire tests, as well as that reported in literature, was utilized to validate the above numerical model by comparing concrete and rebar temperatures, extent of spalling, axial and lateral deformations, and failure times.

The validated model was applied to carry out parametric studies to quantify the effect of various factors on the fire response of RC columns. Data from parametric studies show that the significant factors that influence fire resistance of RC columns are fire scenario, concrete strength (permeability), biaxial bending arising from 1-, 2-, or 3-face exposure, load eccentricity, or uneven spalling, load ratio, and slenderness ratio.

Results from the parametric studies are utilized to develop a rational design approach for evaluating fire resistance of RC columns. The proposed approach comprises of evaluating fire resistance under standard fire conditions and then establishing equivalency between standard and design fire scenarios. The fire resistance under standard fire is evaluated through an equation that accounts for critical factors, such as fire scenario, spalling, load ratio, load eccentricity (uniaxial and biaxial), different face exposure (1-, 2-, 3-, or 4-side), concrete strength, and slenderness ratio. Then, an equivalency between standard and design fire scenarios is established based on the area under the fire curve concept, where in the survivability of column under design fire evaluated. The validity of the proposed approach is established by comparing resulting fire resistance predictions with those obtained from detailed finite element analysis and fire tests.

ACKNOWLEDGMENT

I would like to express my gratitude to my advisor, Prof. Venkatesh Kodur for his continued support and guidance during the course of my studies. I would also like to thank Prof. Ronald Harichandran, Prof. Parviz Soroushian and Prof. K.N. Subramanian for joining my Ph.D. committee, and for their valuable advice throughout my education at MSU.

This research was primarily supported by the National Science Foundation CMMI program (Grant number CMS 0601178) and Portland Cement Association, and I would like to thank them for their resources.

I would like to thank the lab manager, Mr. Siavosh Ravanbakhsh for his support and help during the experimental program in this research. And, I would like to extend my thanks to Laura Taylor, Mary Mroz, and Margaret Conner for all the help they provided.

I would like to thank Aqeel Ahmad, Megan Vivian, Nickolas Hatinger, Rustin Fike Raut, Purushutham Pakala, Wasim Khaliq, Mahmud Dwaikat, Monther Dwaikat, Monther Dwaikat, Baolin Yu, Esam Aziz, Nnaemeka Ezekwmba, Nishan Harichandran, Nikhil Chaudhary and Dr. X.Y. Mao for their support, particularly in the experimental part of this study.

Additionally, I would like to thank all the faculty members and students at the Civil and Environmental Engineering department at Michigan State University for their help and support during my Ph.D. study.

TABLE OF CONTENTS

List of Tables ix

List of Figures xi

Chapter 1 1
1 Introduction 1
1.1 General 1
1.2 Concrete under Fire 2
1.3 Behavior of RC Columns under Fire Conditions 3
1.4 Research Objectives 8
1.5 Scope 9

Chapter 2 15
2 State-of-the-Art Review 15
2.1 General 15
2.2 Experimental Studies 16
2.3 Numerical Studies 22
2.4 Codes of Practice 26
2.5 Factors Influencing Fire Performance of RC Columns 28
2.5.1 Concrete Strength 29
2.5.2 Concrete Moisture Content 29
2.5.3 Concrete Density 29
2.5.4 Fire Intensity 30
2.5.5 Column Dimensions 30
2.5.6 Lateral Reinforcement 30
2.5.7 Fiber Reinforcement 31
2.5.8 Load Intensity and Type 31
2.5.9 Type of Aggregate 32
2.6 Material Properties at Elevated Temperatures 32
2.6.1 General 32
2.6.2 Concrete Properties 34
2.6.3 Reinforcing Steel Properties 45
2.7 Knowledge Gaps 48

Chapter 3 76
3 Experimental Study 76
3.1 General 76
3.2 Experimental Details 77
3.2.1 Test Specimens 77
3.2.2 Instrumentation 79
3.2.3 Test Apparatus 79
3.2.4 Test Conditions and Procedure 80
3.2.5 During and Post-Test Observations 82
3.3 Results 82

3.3.1 Thermal Response 83
3.3.2 Spalling Pattern 84
3.3.3 Structural Response 85
3.3.4 Fire Resistance 89
3.4 Summary 90

Chapter 4 107
4 Numerical Model 107
4.1 General 108
4.2 Selection of Modeling Technique 108
4.3 Finite Element Model 109
4.3.1 General Approach 110
4.3.2 Fire Temperatures 111
4.3.3 Hydro-Thermal Analysis and Spalling Prediction 112
4.3.4 Strength Analysis 134
4.4 Computer Implementation 146
4.4.1 Column Idealization 146
4.4.2 Time Domain 149
4.4.3 Fire Scenario 150
4.4.4 Exposure Condition 150
4.4.5 Structural Parameters 151
4.4.6 Material Properties 151
4.4.7 Failure Criteria 152
4.4.8 Output Results 152
4.5 Summary 153

Chapter 5 172
5 Validation Studies 172
5.1 General 173
5.2 Validation of Numerical Model 173
5.2.1 Column Discretization and Material Models 174
5.2.2 Columns Tested in Literature 175
5.2.3 Columns Tested at MSU 180
5.3 Summary 185

Chapter 6 201
6 Parametric Studies 201
6.1 General 202
6.2 Factors Influencing Fire Resistance 202
6.3 Numerical Studies 203
6.3.1 Column Characteristics 204
6.3.2 Analysis Details 204
6.4 Results of Parametric Studies 205
6.4.1 Effect of Fire Exposure Conditions 205
6.4.2 Effect of Load Eccentricity 207
6.4.3 Effect of Column Size 209

6.4.4 Effect of Fire Severity 210
6.4.5 Effect of Load Level 211
6.4.6 Effect of Concrete Strength (Permeability) 212
6.5 Summary 213

Chapter 7 228
7 Design Guidelines 228
7.1 General 228
7.2 Critical Factors Influencing Fire Resistance 228
7.2.1 Effect of Load Ratio 229
7.2.2 Effect of Slenderness Ratio 230
7.2.3 Effect of Cover Thickness 231
7.2.4 Effect of Reinforcement Ratio 231
7.2.5 Effect of Aggregate Type 232
7.2.6 Effect of Load Eccentricity 232
7.2.7 Effect of Number of Sides of Fire Exposure 233
7.2.8 Effect of Concrete Strength 234
7.2.9 Summary 235
7.3 Methodology for Evaluating Fire Resistance 235
7.4 Fire Resistance Equation for Standard Fire Conditions 236
7.4.1 General 236
7.4.2 Accounting for Different Face Exposures 237
7.4.3 Accounting for Concrete Strength (Permeability) 238
7.4.4 Accounting for Eccentric Loading 238
7.4.5 Proposed Fire Resistance Equation 238
7.5 Fire Resistance under Design Fire Exposure 241
7.6 Validation of Proposed Approach 243
7.6.1 RC Columns Exposed to Standard Fire Scenario 243
7.6.2 RC Columns Exposed to Design Fire Scenarios 245
7.6.3 Comparison with Codes and Standards 246
7.7 Design Applicability 247
7.7.1 General 247
7.7.2 Design Example 248
7.7.3 Limitations 249
7.8 Summary 249

Chapter 8 270
8 Conclusions and Recommendations 270
8.1 General 270
8.2 Key Findings 271
8.3 Recommendations for Future Research 273
8.4 Research Impact 275

Appendix A 278
High Temperature Material Relationships 278

Appendix B 291
Calculation Load Carrying Capacity of the Testes Columns 291

Appendix C 297
Worked Example using Proposed Simplified Approach 297

References 303

LIST OF TABLES

Table 2.1 Experimental studies on fire resistance of reinforced concrete columns..... 51

Table 2.2 Analytical studies on fire resistance of reinforced concrete columns. 60

Table 2.3 Provisions in building standards of various countries 66

Table 2.4 Prediction of fire resistance values for column III 14 [Lie and Woolerton, 1988] using different codes..... 68

Table 3.1 Concrete mix proportions for fabricating different RC columns..... 92

Table 3.2 Summary of test parameters and results for fire resistance tests 93

Table 3.3 Compartment and Material Characteristics assumed for Developing Design Fire Scenarios 93

Table 5.1– Properties and results for RC columns used in the validation study 186

Table 5.2 Summary of test parameters and comparison with fire resistance tests at MSU..... 187

Table 5.3 Summary of spalling predictions and measurements 188

Table 6.1 Properties and results for RC columns used in the numerical study 215

Table 7.1(a). Fire resistance of RC columns with concentric loads obtained in standard fire tests 251

Table 7.1(b). Fire resistance of RC columns with eccentric load as obtained in standard fire tests 252

Table 7.2 (a). Fire resistance data of rectangular RC columns used for validating proposed equation..... 254

Table 7.2 (b). Fire resistance data of circular RC columns used for validating proposed equation 256

Table 7.3: Fire resistance equivalency as predicted by macroscopic finite element model (MFEM) (Chapter 4) and the proposed approach..... 257

Table 7.4. Fire resistance comparison from proposed equation with code provisions..... 258

Table A.1 – Constitutive Relationships for High Temperature Properties of Concrete 278

Table A.2. Values for the Main Parameters of the Stress-strain Relationships of NSC and HSC at Elevated Temperatures (Eurocode 2)..... 286

Table A.3 – Constitutive Relationships for High Temperature Properties of Reinforcing Steel 287

Table A.4. Values for the Main Parameters of the Stress-strain Relationships of Reinforcing Steel at Elevated Temperatures (Eurocode 2)..... 290

Table B.1 –Parameters Assumed for 8 X 8 inch Columns 291

Table B.2 – Summary Table 291

Table C.1. Prediction of fire resistance values for column III 14 using different codes. 301

LIST OF FIGURES

Fig. 1.1: Relative performance of NSC and HSC under fire conditions (For interpretation of the references to color in this and all other figures, the reader is referred to the electronic version of this dissertation.) 11

Fig. 1.2: Variation of axial deformation with fire exposure time for an RC column 12

Fig. 1.2 Contd: Variation of axial deformation with fire exposure time for an RC column..... 13

Fig. 1.3: Factors influencing behavior of RC column under fire..... 14

Fig. 2.1 Heating rates used for fire tests on RC columns [Ali et al., 2001]..... 69

Fig. 2.2 - Typical layout of ties used in RC columns [Kodur, 2003]..... 69

Fig. 2.3 Comparison of fire resistance predictions from simplified equation and test data [Franssen and Dotreppe, 2003]. 70

Fig. 2.4 - Variations of measured and predicted of thermal conductivity for NSC as a function of temperature 70

Fig. 2.5 - Variations of measured and predicted of thermal capacity for NSC as a function of temperature 71

Fig. 2.6 - Variation of compressive strength as a function of temperature for NSC 71

Fig. 2.7 - Variation of compressive strength as a function of temperature for HSC 72

Fig. 2.8 - Variation of residual compressive strength as a function of temperature [Kumar 2003] 72

Fig. 2.9 - Variations of measured and predicted of thermal expansion for concrete as a function of temperature 73

Fig. 2.10 – Illustration of occurrence of spalling..... 73

Fig. 2.11 – Illustration of thermal dilation mechanism for fire induced spalling 74

Fig. 2.12 – Variations of measured and predicted ultimate and yield strength of reinforcing steel as a function of temperature..... 74

Fig. 2.13 – Measured residual yield strength of reinforcing steel [Neves et al. 1996] 75

Fig. 2.14 – Variation of thermal strain of reinforcing steel as a function of temperature [ASCE Manual 1992] 75

Fig. 3.1 – Layout of Steel Reinforcement before Concrete Placement 94

Fig. 3.2 – View of RC columns after Fabrication..... 94

Fig. 3.3. Column dimensions and locations of thermocouple and strain gauges..... 95

Fig. 3.4 – View of a Thermocouple and a Strain Gage attachment to Columns 96

Fig. 3.5. Structural Fire Test Furnace at MSU's Civil and infrastructure laboratory..... 97

Fig. 3.6. Time temperature curves for fire scenarios used in the fire tests 98

Fig. 3.7. Measured rebar and concrete temperatures for RC columns..... 99

Fig. 3.8. Fire induced spalling in RC columns under respective fire exposure 102

Fig. 3.9. Measured axial deformations as a function of time for the tested RC columns..... 103

Fig. 3.10. Measured axial strains as a function of time for the tested RC columns..... 103

Fig. 4.1 - Layout of a Typical RC Column and its Idealization for Analysis..... 155

Fig. 4.2 (a) - Flowchart showing the steps associated with the analysis of an RC column exposed to fire..... 156

Fig. 4.2 (b) - Flowchart showing the steps associated with the stiffness analysis subroutine.... 158

Fig. 4.3 - Cross-section of an RC column and its Discretization for Fire Resistance Analysis . 160

Fig. 4.4 - Illustration of Spalling Prediction in a Concrete Segment..... 161

Fig. 4.5 - Variation of Strain, Stress and Internal Forces in a Typical RC Column Cross-section Exposed to Fire 162

Fig. 4.6 - Illustration of Curvature Controlled Iterative Procedure used for Structural Analysis163

Fig. 4.7– Independent deformation of a column segment 164

Fig. 4.8–Elevation and cross-section of the RC column used for discretization effect case study 164

Fig. 4.9– Effect of mesh size on fire-induced spalling and thermal response predictions 165

Fig. 4.11–Effect of time step on fire response prediction in RC columns..... 167

Fig. 4.12– Different fire scenarios incorporated in the model..... 168

Fig. 4.13– Typical response parameters generated in the fire resistance analysis..... 169

Fig. 5.1. Cross-sectional dimensions and comparison of predicted and measured temperatures and deformations for concentrically loaded NSC column I3..... 189

Fig. 5.2. Cross-sectional dimensions and comparison of predicted and measured temperatures and deformations for concentrically loaded HSC column HSC2-1..... 190

Fig. 5.3. Cross-sectional dimensions and comparison of predicted and measured temperatures and deformations for eccentrically loaded NSC column III3. 192

Fig. 5.4. Cross-sectional dimensions and comparison of predicted and measured temperatures and deformations for eccentrically loaded HSC column HSC2-9. 193

Fig. 5.5. Cross-sectional dimensions and comparison of predicted and measured temperatures and deformations for concentrically loaded circular NSC column III11..... 195

Fig. 5.6. Cross-sectional dimensions and comparison of predicted and measured temperatures and deformations for concentrically loaded circular NSC column III12..... 196

Fig. 5.7. Cross-sectional dimensions and comparison of predicted and measured temperatures, deformations and spalled area for concentrically loaded RC columns tested at MSU. 198

Fig. 6.1. Details of column analyzed in numerical studies. 218

Fig. 6.2. Various Fire Scenarios used in the Analysis. 219

Fig. 6.3. Thermal gradients after 45 minutes in RC columns CE0, CE1, CE3 and CE4..... 219

Fig. 6.4. Axial deformation of RC columns (CE0, CE1, CE3, & CE4) exposed to different face exposure 220

Fig. 6.5. Lateral deformation of RC columns (CE0, CE1, CE3, & CE4) exposed to different face exposure 220

Fig. 6.6. Axial deformation of RC columns (CE0, CE5, CE6, CE54 & CE58) under different eccentric loadings..... 221

Fig. 6.7. Lateral deformation of RC columns (CE0, CE5, CE6, CE54 & CE58) under different eccentric loadings..... 221

Fig. 6.8. Axial deformation of RC columns (CE0, CE8, and CE16) under different sizes 222

Fig. 6.9. Lateral deformation of RC columns (CE0, CE8, and CE16) under different sizes..... 222

Fig. 6.10. Axial deformation of RC columns (CE3, CE11, and CE19) under different sizes 223

Fig. 6.11. Lateral deformation of RC columns (CE3, CE11, and CE19) under different sizes.. 223

Fig. 6.12. Axial deformation of RC columns (CE58, CE60, CE61, CE63, and CE63) under different fire scenarios 224

Fig. 6.13. Lateral deformation of RC columns (CE58, CE60, CE61, CE63, and CE63) under different fire scenarios 224

Fig. 6.14. Axial deformation of RC columns (CE58, CE64, CE65, CE66, and CE67) under different load levels..... 225

Fig. 6.15. Lateral deformation of RC columns (CE58, CE64, CE65, CE66, and CE67) under different load levels..... 225

Fig. 6.16. Spalled area after 30 minutes for columns CE24 and CE39 226

Fig. 6.17. Progression of spalling with time for columns CE24 and CE39..... 226

Fig. 6.18. Axial deformation of RC columns (CE0, CE24, and CE39) under different concrete types. 227

Fig. 6.19. Lateral deformation of RC columns (CE0, CE24, and CE39) under different concrete types. 227

Fig. 7.1- Fire resistance as a function of load-ratio for RC columns..... 259

Fig. 7.2- Fire resistance as a function of slenderness-ratio for RC columns 259

Fig. 7.3- Fire resistance as a function of cover thickness for RC columns..... 260

Fig. 7.4- Fire resistance as a function of percentage of steel for RC columns 260

Fig. 7.5- Fire resistance as a function of load eccentricity for RC columns..... 261

Fig. 7.6- Variation of fire resistance with eccentricity along Y axis for different eccentricities along X axis 261

Fig. 7.7- Variation of fire resistance with eccentricity and exposure condition..... 262

Fig. 7.8- Variation of fire resistance with permeability under 4-side exposure for different column sizes conditions..... 262

Fig. 7.9- Variation of fire resistance with permeability under 3-side exposure for different column sizes conditions..... 263

Fig. 7.10- Variation of fire resistance with permeability under 2-adjacent side exposure for different column sizes conditions 263

Fig. 7.11- Variation of fire resistance with permeability under 2-opposite side exposure for different column sizes conditions 264

Fig. 7.12- Variation of fire resistance with permeability under 1-side exposure for different column sizes conditions 264

Fig. 7.13- Variation of equivalent eccentricity for different exposure conditions..... 265

Fig. 7.14- Calculation of time equivalency between design fire and standard fire 265

Fig. 7.15- Comparison of predicted and measured fire resistance for NSC columns with concentric load under standard fire..... 266

Fig. 7.16- Comparison of predicted and measured fire resistance for NSC columns with eccentric load under standard fire 266

Fig. 7.17- Comparison of predicted fire resistance form the proposed equation with the predicted fire resistance from numerical model 267

Fig. 7.18- Comparison of predicted fire resistance from the proposed equation with actual fire resistance values (tests) and values from model for circular columns..... 267

Fig. 7.19- Comparison of fire resistance predicted from the proposed equation with ACI provisions..... 268

Fig. 7.20- Comparison of fire resistance predicted from the proposed equation with Eurocode equation..... 268

Fig. 7.21- Comparison of fire resistance predicted from the proposed equation with Australian code provisions 269

Fig. B.1. P-M Diagram for NSC column..... 292

Fig. B.2. Load Carrying Capacity of NSC column..... 293

Fig. B.3. P-M Diagram for HSC column..... 295

Fig. B.4. Load carrying capacity of HSC Column..... 296

Fig. C.1- Elevation and cross-sectional details of Columns III14 [Lie and Woolerton, 1988] .. 297

CHAPTER 1

1 INTRODUCTION

1.1 General

Concrete is widely used as a primary structural material in building construction where fire resistance is one of the key considerations in design. Generally, concrete structural members exhibit good performance under fire situations. Over the last three decades, there have been significant research and development activity in improving the properties of concrete. This has led to new types of concrete which are often referred to as high strength concrete (HSC), fiber reinforced concrete (FRC), high performance concrete (HPC) and ultra HPC. The construction industry has shown significant interest in the use of these new concrete types. This is due to the improvements in structural performance, such as high strength and durability, that it can provide compared to the traditional normal-strength concrete (NSC). High strength concrete is quite often used in columns of high rise building since the higher compressive strength can be utilized effectively.

Results from a number of studies have shown that there are well-defined differences between the properties of HSC and NSC at high temperatures. Also, concern has developed regarding the occurrence of explosive spalling when HSC is subjected to rapid heating, as in the case of a fire. Such spalling, which was observed in several experimental studies [Phan, et al. 2001; Kodur and McGrath 2003; Sullivan 2004], has detrimental effect on the fire resistance of concrete members. Hence, provision of appropriate fire safety measures for columns is one of the major safety requirements in building design since when other measures for containing the fire fail, structural integrity is the last line of defense.

The fire safety of a structural member is measured in terms of fire resistance. Fire resistance is the duration during which a structural member exhibits adequate resistance with respect to structural integrity, stability and temperature transmission under fire conditions. Fire resistance rating requirements are specified in building codes and these provisions are based on standard fire tests carried out on a limited number of specimens. In these provisions fire resistance requirements are expressed based on factors such as member dimensions and concrete cover to reinforcement and do not account for critical factors that are specific to new concrete types such as HSC, HPC, and to specific cases of columns exposed to either 1-, 2-, 3-sides exposed. These specifications are based on fire resistance tests and the test specimens in most of these studies were limited in size due to the size limitations of the testing furnace. Thus they did not represent the realistic fire scenarios and actual loading and restraint conditions the column may be subjected to as discussed in the further sections. Furthermore, the fire resistance tests are very costly, involve special experimental setup and are unrepresentative of the actual conditions the structure might be subjected to in the occurrence of a fire. Thus there are a number of drawbacks in the current approach of evaluating fire resistance.

1.2 Concrete under Fire

Concrete generally provides the best fire resistance of any building material. This excellent fire resistance is due to concrete's constituent materials (i.e. cement and aggregates) which, when chemically combined, form a material that is essentially inert and has low thermal conductivity, high heat capacity, and slower strength degradation. It is this slow rate of heat transfer and strength loss that enables concrete to act as an effective fire shield not only between adjacent spaces but also to protect itself from fire damage.

Concrete, similar to other materials, loses its strength and stiffness properties when exposed to fire. The variation in strength and stiffness is dependent on the type of concrete (see Figure 1.1 (a)). Figure 1.1 (a) shows the reduction in compressive strength with temperature for the commonly used building materials. It can be seen that though concrete loses its strength much slower as compared to other building materials, the rate of loss of strength in HSC is steeper than that of NSC.

In addition to degradation in strength and stiffness, fire induced spalling, is more predominant in HSC members under severe fire conditions and was observed in several experimental studies [Diederichs, et al. 1988; Castillo and Durrani 1990; Hertz 1991; Hammer 1995; Phan 1996; Phan, et al. 2000; Kodur and McGrath 2003; Sullivan 2004]. The break-up of chunks of concrete, from the surface of concrete member during exposure to fire, is termed as fire induced spalling and primarily results from the build-up of pore pressure within the concrete [Diederichs, et al. 1995; Kodur 2000; Kodur and Phan 2007]. The extremely high water vapor pressure, generated during exposure to fire, cannot escape due to the high density (and low permeability) of HSC. When effective pore pressure exceeds the tensile strength of concrete, chunks of concrete fall off from the structural member. This process of spalling can be explosive and depends on fire and concrete characteristics [Anderberg and Thelandersson 1976; Harmathy 1993]. In addition, HSC is normally subjected to higher stress levels than NSC which may create conditions which are conducive to fire induced spalling. Figure 1.1 (b) shows the comparison of spalling resulting in fire exposed HSC column as compared to that of NSC column.

1.3 Behavior of RC Columns under Fire Conditions

Generally building codes require columns in high rise buildings to have a fire resistance rating of 1-4 hours based on the use and occupancy of the building. Columns made of NSC can provide

the required fire resistance without any external fire proofing. However numerous experiments have shown that the fire resistance of HSC columns is lower than that of NSC columns. Through these experiments, effect of various parameters such as cross sectional size, cover thickness, reinforcement ratio, aggregate type, load, and load eccentricity on fire resistance was investigated. Data from reported fire tests can be used to illustrate the typical behavior of NSC and HSC column under fire. Figure 1.2(a) shows the elevation and cross-section of typical columns tested in the laboratory [Lie and Woolerton 1988, Kodur et al. 2003]. Figure 1.2(b) shows the variation of axial deformation of these columns with fire exposure time.

Figure 1.2(b) shows that both the columns expand in the initial stages of fire exposure mainly due to the thermal expansion occurring in both concrete and steel. When the steel reinforcement starts to lose its strength, because of increasing temperatures, both columns start to contract. Since the reinforcing steel is in the outer core of the section, the temperature rises much faster in steel than the inner core of concrete. When the steel yields, the concrete carries a progressively increasing portion of the load. The strength of the concrete also decreases with time due to deteriorating properties of concrete, and ultimately, when the column can no longer support the load, failure of the column occurs. The large deformations prior to failure, results from high mechanical strains (due to significant loss of strength and stiffness of the column) and also due to significant levels of high temperature creep. The time to reach the failure point is defined as the fire resistance of the column.

However, the expansion in HSC column is much smaller due to the loss of cross-section due to spalling which induced additional axial deformation in the column. Further the loss of strength is faster in concrete leading to higher axial deformations and lesser fire resistance.

The behavior of a RC column illustrated above is under standard fire, axial load and absence of end restraints and thus represents idealistic behavior. But under realistic situations, columns are integrated members of the structural system and thus have other significant parameters influence its behavior under fire. The RC column is subject to fire induced restraint forces due to the adjoining members. The column may undergo bending (uni-axial or bi-axial) due to eccentric loading and uneven exposure to fire. Also columns (especially those made of HSC) may experience spalling and may be subjected to fire scenario different from a standard fire based on the fuel and ventilation available in the building.

To illustrate the occurrence and effect of these parameters in a RC column, a structural frame, shown in Figure 1.3(a), is exposed to fire. In current fire design practice, this type of structure is modeled as either simply supported or a fixed column (Figure 1.3(b)). However, due to the restraint offered by the adjacent members, the columns are likely to behave as a restrained member (Fig. 1.3(c)). When the column expands under increasing temperatures, the adjacent members impose both axial and rotational restraints (K_a and K_r) on the column that prevents it from free expansion. This generates axial force (P) and bending moment (M_r). Further, the fire induced axial force (P) causes additional bending moment on the column due to P-δ effect. The increase in the bending moment (M) produces additional deflections and hence further deterioration in the response of the RC column.

Columns usually are subjected to bending under ambient conditions due to the eccentricity of the load that comes from forces transferred from adjoining members (or beams). But in case of fire, the columns may also undergo bending due to the development of thermal gradients or due to occurrence of non-uniform spalling. In a structural frame under fire, perimeter columns act as beam-columns and hence they also need to be designed for bending. Perimeter columns are

found on the perimeter of a building or adjacent to an opening (e.g., shaft) in the floor system. A column is often treated as a two-dimensional planar structure and therefore designed to resist bending moments acting in the plane of the frame. While this idealization is true for peripheral columns, in an actual building framework columns are frequently subjected to bending moments acting in two perpendicular directions in addition to an axial compression (biaxial bending). The obvious example is a corner column in a space frame of a building. Also in case of fire, a column may be exposed to fire on 1-side, 2-sides, 3-sides or all four sides. This causes the development of thermal gradients which can result in uniaxial (1-side or 3- sided) or biaxial (2 adjacent sides) bending of the column. The additional moments on the column reduce the load carrying capacity of the column and also cause addition deformations thus reducing its fire resistance.

Figure 1.3(d-h) shows the development of thermal gradient in the center column, peripheral column and corner column respectively under fire. It can be seen that the occurrence of uniaxial bending (peripheral column) and biaxial bending (corner column) can be common in buildings. The presence of uniaxial bending induces an eccentricity in an originally axially applied load due to the shift in neutral axis due to the degradation of concrete and reinforcing steel strength and stiffness. Thus the column is subjected to an additional moment along with the applied load and thus affecting the fire resistance of the column. In the case of a corner column (biaxial bending), the neutral axis shifts and also rotates thus inducing eccentricity along both the axes. This causes the column to experience additional moments along both the axes (two directions). The fire-induced load eccentricity in both the cases also increases the lateral and axial deformations due to the P-δ effect. Also spalling can occur in the columns, especially those made of HSC. Spalling depends on a number of factors such as thermal gradient, porosity distribution, moisture distribution and strength of concrete. Depending on all the above factors the columns may

undergo non uniform spalling thus causing the applied load to act eccentrically. For example if the initial loading on the column is concentric (at the centre of gravity in figure 1.3 (i)) and a small chunk of concrete spalls, as shown in the figure, then the neutral axis of the column shifts and thus causes the column to bend biaxially. The current provisions in codes and standards are based on standard tests with all four sides exposed to fire and hence cannot be applied to one, two or three side exposure.

When exposed to fire, thermal gradients develop in the concrete cross section as illustrated above. As the temperatures increase the moisture in concrete transforms to vapor and thus creates pore pressure. When this pressure exceeds the tensile strength of concrete chunks of concrete peel off referred to as spalling. This is explained in Figure 1.3(i). Spalling leads to loss of cross-section and thus there is lesser mass of concrete to absorb the heat and thus there is faster rise in temperature in the cross section leading to rapid loss of strength and stiffness. Also the loss of cross section leads to loss of stiffness and thus it leads to lower fire resistance. Few recent studies have shown that the incorporation of fibers (polypropylene or steel) help in improving the fire resistance of RC columns by mitigating spalling and enhancing tensile strength. However, there are no numerical models that account for fire induced spalling in fire resistance calculations.

Further, the type of fire scenario has a significant influence on the development of restraint forces in RC columns. Much of the current knowledge is based on fire resistance tests on RC columns where the exposure is typically assumed to be that of a standard fire. However, in buildings the fire exposure is likely to be different and dependent on fuel load and ventilation characteristics in the fire compartment [Buchanan 2002]. Figure 1.3(j), illustrates the difference between standard fire and realistic (design) fire scenarios. The main difference between the two

is that in standard fire exposure the temperature of the fire is assumed to increase without any decaying (cooling). However, fires in buildings die down and the compartment enters a cooling phase as a result of exhaustion of fuel and/or ventilation (oxygen). This decay phase results in cooling of concrete and reinforcing steel and thus helps regain some of the lost strength and stiffness. This aspect of cooling phase has significant influence on the fire response of RC columns [Buchanan, 2002; Dwaikat. 2009]. Thus it can be seen that factors such as end restraint, uniaxial/biaxial bending and spalling are important factors which affect the fire resistance of RC columns significantly and thus need to be incorporated in fire resistance predictions. The current models do not fully account for these factors. Thus there is a need to develop a numerical model which can incorporate these factors and thus provide an accurate estimate of fire resistance.

1.4 Research Objectives

From the above discussion, it is clear that there is lack of knowledge on the fire response of RC columns under realistic fire, biaxial bending effects, 1-, 2-, 3- side of fire exposure and new concrete types. To address this knowledge gap the following research objectives were set-out as a part of this dissertation:

- Conduct a detailed state-of-the-art review on the fire response of RC columns. The comprehensive review will cover experimental and numerical studies, provisions in codes and standards, and high temperature material properties.
- Undertake fire resistance experiments on RC columns, with and without fibers, under standard and design fire scenarios to evaluate the behavior under different parameters.
- Develop a comprehensive macroscopic finite element based model for predicting the response of RC columns under realistic fire, loading and failure conditions. Such model should account for nonlinear high temperature material properties, various strain

components, fire induced restraint effects, fire-induced spalling in concrete and uniaxial/biaxial bending of columns.

- Validate the above developed computer program using data from fire resistance tests on NSC and HSC columns.
- Carry out parametric studies to quantify the influence of various factors, specially those arising from biaxial bending effects, on the fire resistance of RC columns.
- Develop a simplified expression, using data from fire tests and parametric studies, for evaluating the fire resistance of RC columns.

1.5 Scope

The research, undertaken to address the above objectives, is presented in seven Chapters. Chapter 1 provides a general background to the fire response of RC columns and presents the objectives of this study. Chapter 2 summarizes a state-of-the-art review on the behavior of RC columns exposed to fire. The review includes summary of experimental and analytical studies, as well as the fire design provisions for RC columns in current codes of practice. Also, a review of the high temperature material properties and associated constitutive relationships of concrete and reinforcing steel is reviewed in Chapter 2.

Chapter 3 deals with fire resistance experiments on six RC columns under realistic fire, and loading scenarios. Results from the fire tests are used to discuss the response of RC columns under these realistic conditions. Chapter 4 presents details of macroscopic finite element based numerical modeling of the fire response of RC column. The validation of the finite element model (thermal and structural) is presented in Chapter 5, where predictions from the model are compared with available test data from literature, and also with results from the fire tests reported in Chapter 3.

Chapter 6 presents results from parametric studies on the effect of significant parameters on fire resistance of RC columns. A detailed discussion on the trends along with the definitions and ranges of parameters governing the fire resistance of RC columns is described in Chapter 6. In Chapter 7, statistical analysis is presented and a simplified expression and guidelines for predicting the fire resistance of RC columns are developed. Results from the parametric studies are applied to verify the proposed approach for evaluating the fire resistance of RC columns under different realistic conditions. Finally, Chapter 8 summarizes the main findings arising from the current study and lays out recommendations for further research.

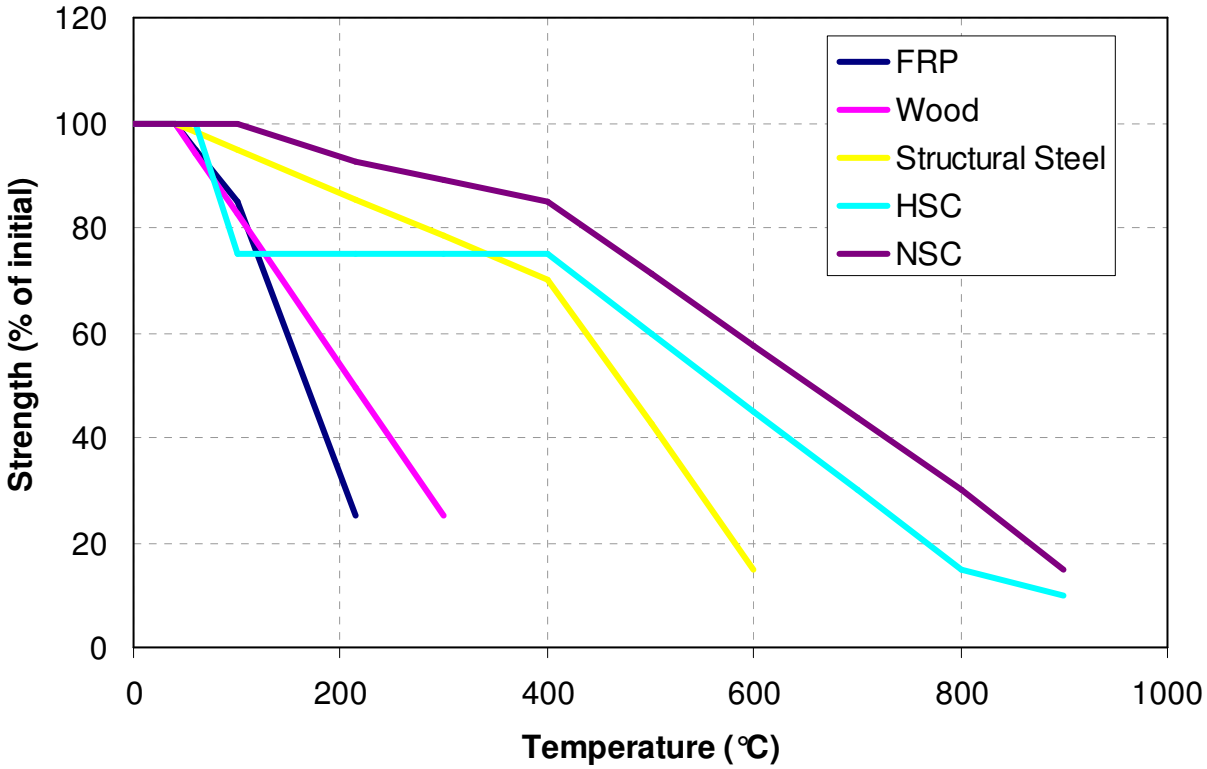

(a) Compressive strength of concrete

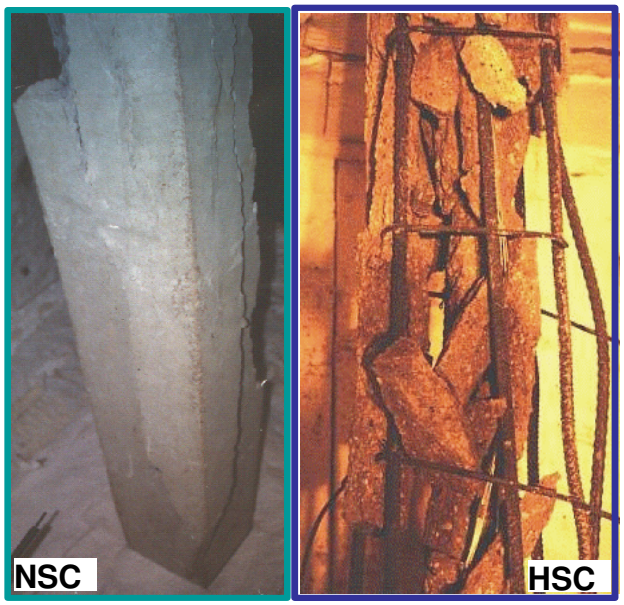

(b) Spalling of columns

Fig. 1.1: Relative performance of NSC and HSC under fire conditions (For interpretation of the references to color in this and all other figures, the reader is referred to the electronic version of this dissertation.)

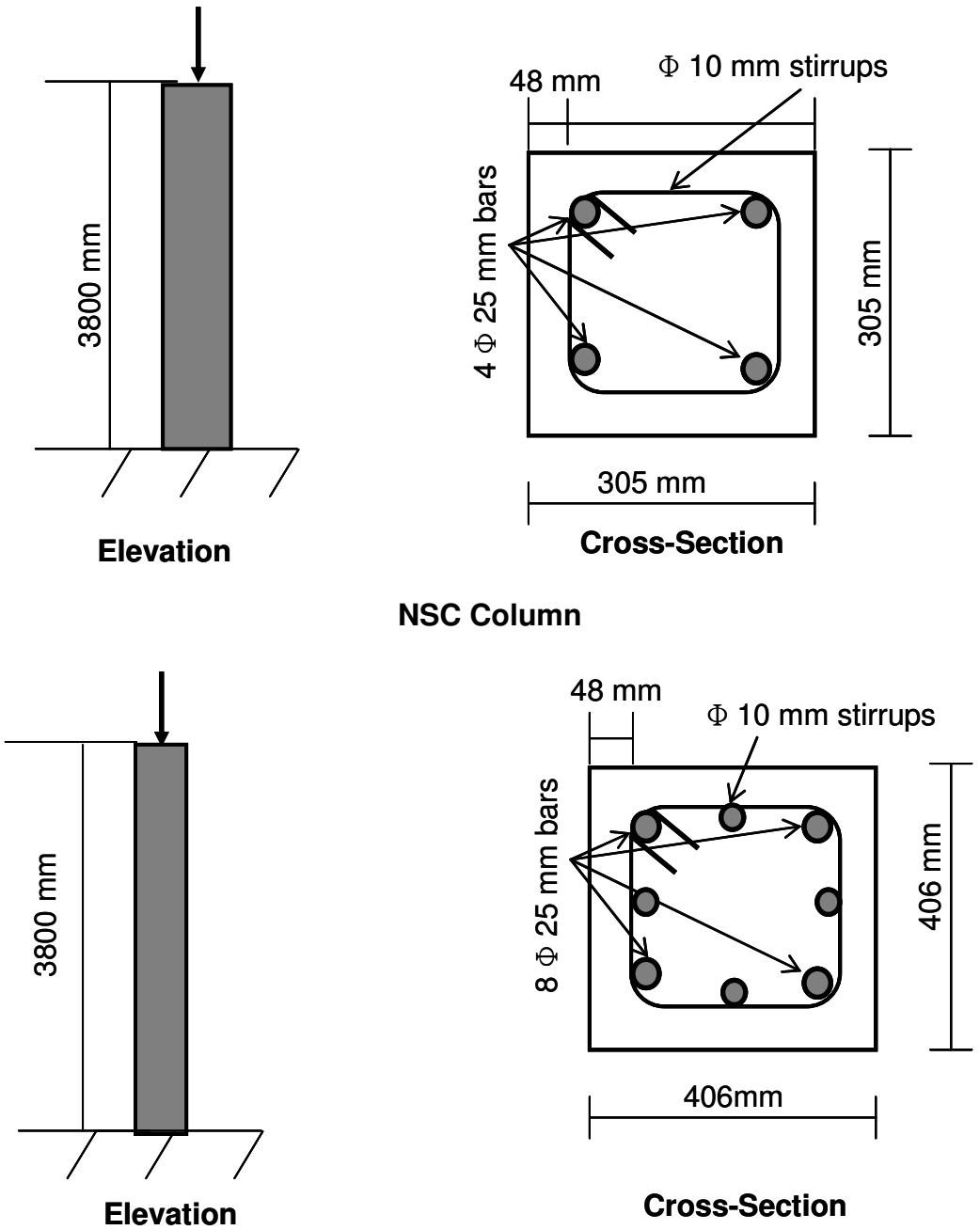

(a) Column layout

Fig. 1.2: Variation of axial deformation with fire exposure time for an RC column

Fig. 1.2 Contd: Variation of axial deformation with fire exposure time for an RC column

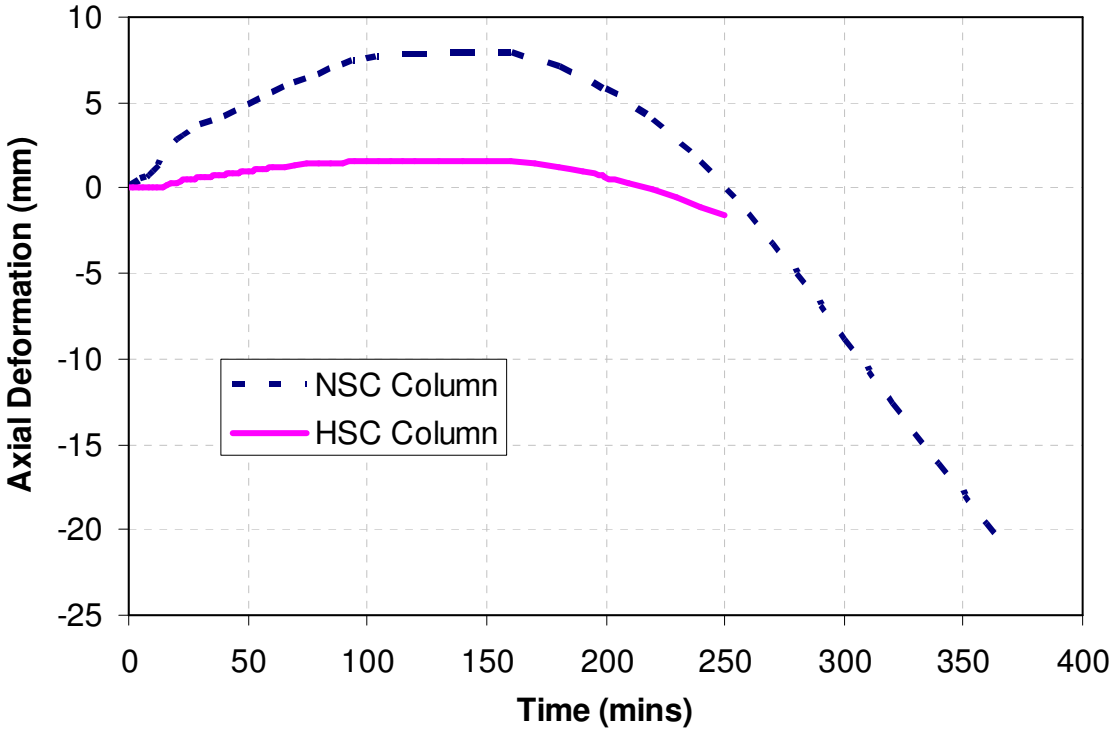

(b) Axial deformation

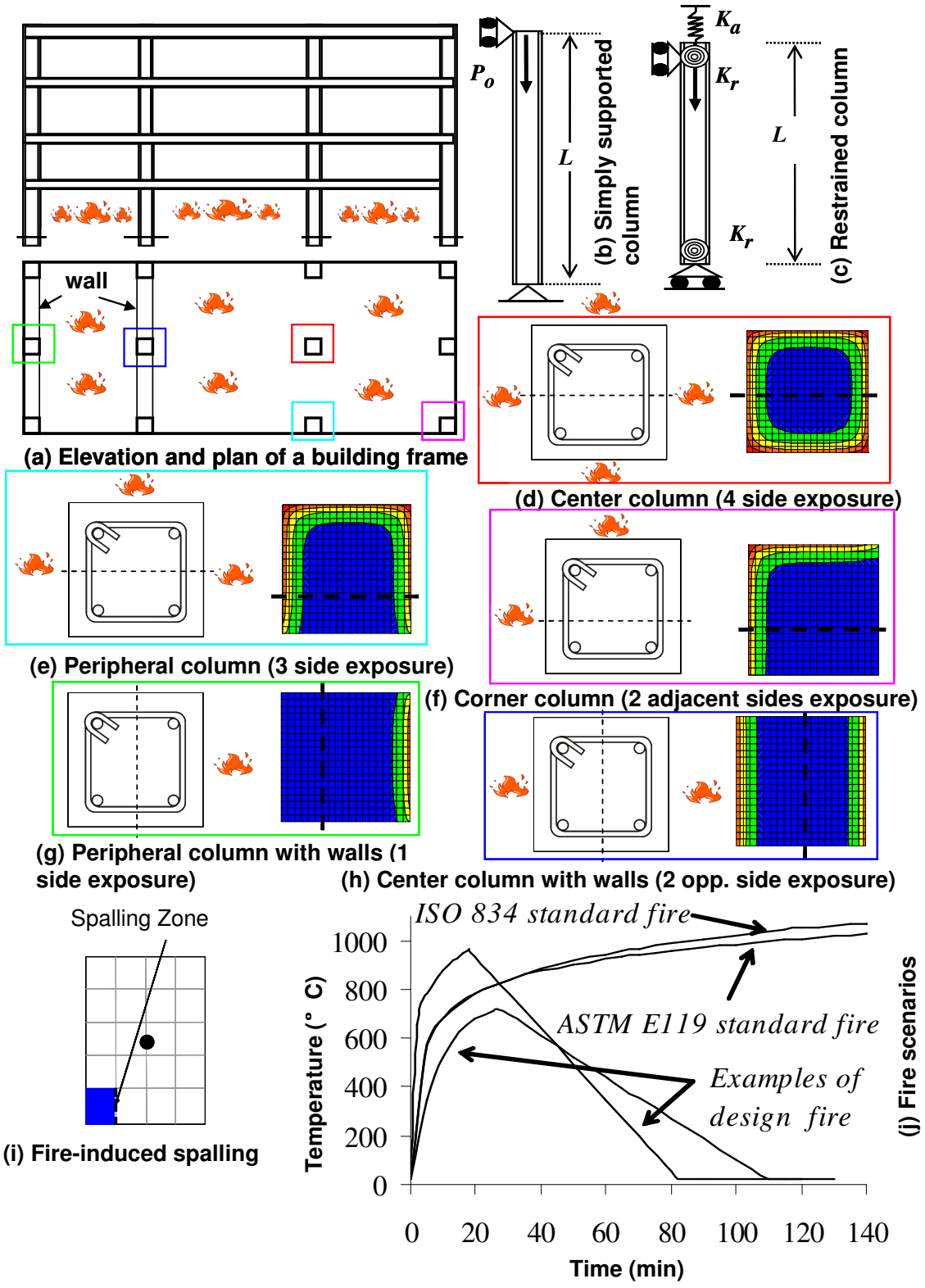

Fig. 1.3: Factors influencing behavior of RC column under fire

CHAPTER 2

2 STATE-OF-THE-ART REVIEW

This chapter is mainly based on the following journal paper:

- Kodur, V. and Raut, N. (2007), "Fire Resistance of Reinforced Concrete Columns – State-of-the-Art and Research Needs", ACI SP-255-5 CD-ROM: Designing Concrete Structures for Fire Safety, American Concrete Institute, pp. 97-124.

2.1 General

Fire resistance of RC columns is influenced by a number of factors including fires scenario, exposure conditions, load level, restraint, and concrete strength. However many of these factors are not taken into consideration in fire design of RC columns. The current code provisions for evaluating fire resistance of concrete columns is based on a prescriptive methodology and assumes the column to have failed when steel rebar reaches a critical temperature. These provisions are derived based on the standard fire tests carried out on RC columns. Since 1970's, there have been numerous studies, both experimental and analytical, to develop an understanding on the behavior of RC columns under fire conditions. Most of these studies focused on the behavior of columns under standard fire scenario without any consideration to structural interaction (such as column-beam interaction), biaxial bending, and realistic fire scenarios. Also due to dearth of data on high temperature thermal and mechanical properties for newer types of concrete no consideration is given to variation of high temperature properties in fire resistance evaluation. This section provides a state-of-the-art review on experimental and analytical studies

related to fire performance of RC columns. Also, a review of fire resistance provisions in various codes and standards is provided.

2.2 Experimental Studies

The common approach for evaluating fire resistance of RC columns is through fire tests under standard fire conditions. A number of test programs were undertaken in the last three decades to study the fire performance of RC columns. The main objectives of most of the fire resistance experiments included:

- Observing and monitoring the column behavior under a standard fire exposure,
- Generating fire resistance ratings for RC columns, of specific size and load intensity,
- Generating data over a range of variables for verification of computer models, and
- Investigating the conditions under which spalling might occur in HSC columns.

A summary of notable fire resistance tests is presented in Table 2.1. For each of the study, the objectives, the test parameters, the test methods/features and major conclusions have been summarized in the table. In addition, the strengths and drawbacks, if any, in each of the study are also presented. Additional details, including significant findings in these studies are discussed below.

Lie and Woolerton [1988] tested 41 RC columns under standard fire conditions to study the effect of various parameters like shape of cross section, cover thickness, reinforcement, aggregate type, load, and load eccentricity on the fire resistance of RC columns. The tested columns were full-size columns and were loaded. The study concluded that carbonaceous aggregate increased the fire resistance of RC columns. Also, columns with heavy reinforcement were observed to provide higher fire resistance and the end conditions affected the slenderness ratio of the column, which in turn decreased the fire resistance with increasing slenderness ratio.

Aldea et al. [1997) conducted six fire tests on NSC and HSC short columns to quantify the parameters influencing fire induced spalling. The NSC columns had a concrete strength in the range of 20 MPa to 50 MPa, while the HSC had a compressive strength of 90 MPa. The parameters considered were reinforcement, number and diameter of steel bars, and concrete strength. The study observed that HSC columns showed early spalling at the corners while no spalling took place in NSC columns. The authors concluded that the material characteristics have higher influence on failure modes under fire conditions than the structural detailing. But again the study was limited to standard fire exposure under concentric loading.

Ali et al. [2001] carried out fire tests on six sets (three columns per set) of short RC columns. Two different fire scenarios were studied (see Figure 2.1) but the variation was limited to the heating rates of the fire and thus decay phase (cooling of fire) was not considered. During the fire tests, the degree of spalling was monitored. The authors concluded that increasing the load level decreased failure time and failure temperatures in both heating cases. Increasing the loading level did not increase the probability of spalling both under high and low heating regimes, but low heating rates minimized the risk of explosive spalling. Also, explosive spalling occurred when a column was expanding (initial stages of fire exposure) and no spalling took place when the column was contracting.

Franssen and Dotreppe [2003] performed tests on four circular RC columns to examine the effect of circular shape on the fire behavior of concrete columns. The main conclusions, derived based on the test observations and analyses of the test data, were that circular shape did not prevent the occurrence of spalling, the diameter of the longitudinal reinforcement had no significant influence on surface spalling, and increase in load level lead to a significant decrease in fire resistance.

Kodur [2003] carried out comprehensive experimental study on large number of full-scale RC columns and RC wall segments (blocks) aimed at developing fire resistance design guidelines for HSC columns. The test variables included column dimensions, concrete strength (34 MPa – 110 MPa), aggregate type in the concrete, tie configuration, addition of fiber reinforcement, type of fiber, load intensity and eccentricity of loading. Based on these detailed fire experiments, Kodur quantified the influence of major factors on fire resistance and developed the following guidelines (some of which have been incorporated in ACI 216.1 [2007] for enhancing the fire performance of HSC columns.

- Concrete strength: Strengths higher than 70 MPa are more susceptible to spalling and may result in lower fire resistance.
- Concrete moisture content: HSC columns are prone to higher spalling as HSC maintains higher relative humidity (moisture content) due to its lower permeability compared to NSC columns.
- Concrete density: The extent of spalling is much greater in HSC columns when the lightweight aggregate is used.
- Fire intensity: The spalling of HSC is much more severe in fires characterized by fast heating rates or high fire intensities.
- Specimen dimensions: The risk of explosive thermal spalling increases with the specimen cross sectional dimensions. The recommended minimum dimensions for a particular fire rating are provided in ACI 216.1.
- Lateral reinforcement: Higher fire resistance in the HSC columns can be achieved by providing an improved tie configuration (provision of bent ties at 135° back into the core

of the column and increased lateral reinforcement) and with a closer tie spacing (at 0.75 times that required for the NSC columns). Typical tie layouts are illustrated in Figure 2.1.

- Fiber reinforcement: The addition of polypropylene fibers (about 0.1-0.15% by volume) minimizes spalling in the HSC members under fire conditions. Addition of steel fibers (1.75% by weight) enhances tensile strength and reduces spalling.
- Load intensity and type: Higher load intensity leads to lower fire resistance. Further, the extent of spalling is higher if the load is of an eccentric (or bending) type since this will induce additional tensile stresses caused by the bending of the column.
- Type of aggregate: Of the two commonly used aggregates, carbonate aggregate (predominantly limestone) provides higher fire resistance and better spalling resistance than the siliceous aggregate (predominantly quartz) due to enhanced heat capacity of carbonate aggregates that occur in 600-800°C range as a result of an endothermic reaction.
- Sufficient concrete cover thickness to reinforcement as specified in design standards, based on structural (corrosion) considerations, should be provided in order to enhance fire resistance.

In another major study, Kodur et al. [2003] carried out fire experiments on five sets (each set comprised of 3 columns) of RC columns to evaluate the effect of strength and fiber reinforcement on the fire resistance of HSC columns. The variables considered in these tests included concrete strength (NSC and HSC), aggregate type (siliceous and carbonate aggregate), and fiber reinforcement (steel and polypropylene fibers). The results show that, for similar aggregate type and other characteristics, the fire resistance of an NSC column is higher than that of an HSC column. From this study, the authors concluded that the addition of steel and

polypropylene fibers in HSC can improve the ductility of HSC columns and thus fire resistance. Also, the addition of polypropylene fibers in HSC batch mix reduces spalling and enhances fire resistance.

Kodur and McGrath [2003] conducted fire resistance tests on six square RC columns to study the factors influencing the thermal and structural behavior of HSC columns under standard fire conditions. In the column with high relative humidity, some spalling was observed at 10 to 20 minutes into the fire resistance test. From this study, it was concluded that HSC columns have lower fire resistance than NSC columns. The fire resistance of HSC columns increases with decreasing load, and carbonate aggregate concrete columns provides about 10% higher fire resistance than column made with siliceous aggregate concrete.

Ali et al. [2004] investigated the effect of structural parameters on the fire performance of NSC and HSC columns by testing 99 short RC columns under fire. Four loading levels, three levels of axial restraint (where restraint degree is defined as the ratio of applied axial stiffness to the column axial stiffness), and two heating rates (high and low) were considered in the study. These tests showed that loading levels up to 60% of the design strength have no significant effect on concrete spalling both under high and low heating regimes. It was also noted that low heating rates reduced the risk of explosive spalling for HSC columns. Moreover, the authors observed that explosive spalling could directly contribute to premature column failure (buckling) as major parts of the column section can be lost due to spalling. In the study, fifty-four columns were tested under three degrees of axial restraint (α_L) of 0, 0.1 and 0.2. The study showed that the "generation factor" of the restraint forces (generation factor = generated forces/column's strength) decreases if the axial loading levels are increased. It was seen that despite HSC columns showing the same susceptibility to spalling under zero restraint as for NSC, they

suffered less spalling when they are under axial restraint. The study revealed that higher tensile strength in HSC balances or overcomes the low permeability effect to some extent. Therefore, NSC could show more susceptibility for spalling due its low tensile strength (which is approximately half the tensile strength of HSC). This observation is in contradiction to many other studies in the literature which reported that HSC is more susceptive to explosive spalling. Also, the tests confirmed that addition of polypropylene fibers was very effective in reducing explosive spalling. The average degree of spalling (defined as the ratio of mass of concrete lost due to spalling to the original mass of the column) for the six tested HSC columns with polypropylene fibers was less than 1% compared with 22% for HSC columns without polypropylene fibers.

Benmarce and Guenfoud [2005] studied the fire behavior of HSC columns by conducting fire tests on twelve HSC columns. The parameters studies were load ratio, restraint ratio (the ratio of the stiffness of the column to the restraint stiffness provided by the structure) and heating rate. From these fire tests, it was concluded that fire resistance of HSC columns reduced with the increase in load ratio. The large load ratios reduced the steel and concrete temperatures at which the failure occurred in the columns. The drop in failure temperatures was as anticipated, since less restraint force was required for the failure load to be reached. Imposing a restraint against axial expansion (of column), leads to lesser forces generated in the column. Also, the increase in the applied load requires less additional force to produce structural failure. The axial deformation that occurs during fire exposure is independent of the rate of heating and is influenced by load levels in the column. The failure time of columns under low heating rate is almost twice the failure time of columns under high heating rate, for the same degree of restraint and load ratio.

The above review illustrates that there have been a number of experimental studies on the behavior of RC columns under fire. These studies have investigated the effect of various parameters, such as column size, type of concrete, load intensity, tie configuration, presence of fibers, strength of concrete etc., on the fire response of RC columns and generated valuable data for validation of computer models. However, most of the tests were carried out on small specimens (columns) due to the limitation of test equipment. Also, most of the tests were carried out under standard fire scenarios and all sides exposed. Thus there is limited information on the behavior of RC columns under realistic fire, loading and restraint conditions. Behavior of columns exposed to biaxial bending arising from different faces (1-, 2-, 3-) of exposure, uneven spalling, and bi-eccentric loading was not studied. Also spalling was qualitatively monitored during the test and thus not much data is available on the amount of spalling which is crucial for validation of spalling and fire resistance models.

2.3 Numerical Studies

A review of literature indicates that a fair number of analytical studies have been conducted on the fire behavior of RC columns. The main objective in many of these studies was to trace the response of columns under fire conditions and to demonstrate the inherent fire resistance of RC columns. Most of the studies concentrated on developing numerical models, which were generally based on finite element or finite difference methods. In majority of these studies, the focus was mainly on NSC columns. In cases where HSC was considered, spalling was not fully incorporated in the analysis. A summary of various analytical studies dealing with the structural response of concrete columns exposed to fire is outlined in Table 2.2.

Lie and Celikkol [1991] developed a mathematical model for calculating the fire resistance of circular RC columns. Finite difference method was used for calculating the column temperatures

and a sectional analysis was applied to derive the strength of the columns at incremental time steps. The model was validated by comparing predictions with data from 40 full-scale fire tests conducted by NRC and PCA [Lie and Woolerton 1988]. The temperatures predicted by the model were in good agreement with those measured in the tests. Lie and Irwin [1993] developed another model for predicting the fire resistance of rectangular RC columns. This model was developed on the same lines as the one discussed above for circular columns. In this study, the column was also assumed to be exposed to fire on all four sides and the fire temperature was assumed to follow that of standard fire described in ASTM E119 [2007] or CAN/ULC-S101 [2004].

The above two studies formed the basis for further development of numerical models. But these models were limited to sectional analysis. The models assumed a representative section (usually at mid-height of the column) and predicted the behavior of the entire column based on this representative section. Thus the applicability of these models could be limited to prediction of behavior of columns with regular support conditions or without any axial or rotational restraint. Also the rectangular columns were exposed to fire on all four sides. Thus biaxial bending was not incorporated in the model. Also fire-induced spalling was ignored.

Franssen and Dotreppe [2003] utilized data from their fire tests, as well as that in the literature, to develop simplified calculation methods. The first of the two methods developed is an empirical equation, which expresses the fire resistance of RC columns as a function of influencing parameters. This method has been incorporated into Eurocode EC2-1-2 [2004] and yields conservative predictions. The second model developed by the authors is more elaborate and is classified as a simplified calculation method in Eurocode (level II according to EC2-1-2). This method has been validated against data from four circular columns tested by authors. In this

model, the ultimate load capacity of the heated RC column is expressed as a fraction of the plastic crushing load of the section. This formulation gives safe, though rather conservative, fire resistance values for design purposes. Again these methods are applicable for standard fire exposure only as they were derived based on standard fire tests and do not account for fire-induced biaxial bending. Figure X.4 shows a graphic presentation of the comparison of fire resistance obtained with this method and experimental results.

Kodur et al. [2004] developed a numerical model for tracing the fire behavior of HSC columns under standard fire exposure. The approach used (for heat transfer and structural analysis) is similar to the one used in Lie and Celikkol [1991] for normal strength concrete (NSC) columns. However, the model has been extended to include high temperature properties of HSC and also a simplified spalling sub-model. Thus the model is capable of accounting for high temperature properties, aggregate type, spalling, fibers and moisture content.

The study completed by Tan and Yao [2003, 2004] used a theoretical formulation for deriving the fire resistance of RC columns. The study was initially performed for rectangular RC columns subject to fire on all four sides and was then extended to columns subject to heating on 1-, 2- and 3- faces. The effect of elevated temperature on material deterioration with regard to strength and stability of the columns were quantified. Both uniaxial and biaxial bending of columns was considered. The computer program, SAFIR [Franssen, Kodur et al. 2004], was used to analyze and simulate the deformation response of RC columns. The approach comprised of determining the respective strength and modulus of elasticity reduction factors in concrete and steel at elevated temperature on the basis of numerical simulations using SAFIR. Then balanced failure point of the column section was calculated so as to determine whether the eccentricity of the

applied load is small or large. Finally the failure load was determined by a trial and error process. This method can be regarded as an extension of the existing ACI method for ultimate strength predictions of RC columns at ambient temperature. This method also includes a parameter (suggested in literature) in order to account for spalling. Though this method provides a model for different fire exposures, it is derived based on standard fire exposure only. Also it predicts load carrying capacity of the column but does not provide detailed response parameters of the columns such as axial deformation and temperature gradients as a function of fire exposure time.

Bratina et al. [2005] developed a numerical model for tracing the behavior of RC columns in fire. The study describes a two-step finite element formulation for the thermo-mechanical non-linear analysis of the behavior of the RC columns in fire and compares these predictions with the results from the Eurocode 2 [2004]. In the mechanical analysis, new "strain-based 2D geometrically exact" and "materially non-linear beam finite elements" were used to model the column. These special elements satisfy the equilibrium and compatibility conditions of axial forces and bending moments at the integration points.

The above review illustrates that there have been a fair number of analytical studies on the fire behavior of RC columns. While factors such as load, concrete strength, sectional dimensions and rebar configurations were addressed, other factors such as spalling, fire scenarios have not been fully included in the models. Further these analysis methods do not include the effect of spalling or use a very simplistic (crude) model for the same [Tan and Yao 2003; Kodur, Wang et al. 2004; Tan and Yao 2004]. Also, the methods are mainly based on sectional analysis and neglect the behavior of the column as a whole and thus did not incorporate fire-induced bending (uniaxial and biaxial). In addition the models were validated for standard fire scenarios only and have not been validated for design fire situations.

2.4 Codes of Practice

In most countries, the specifications for fire resistant design are included in building codes and national standards and these provisions are prescriptive in nature. In the prescriptive approach, the codes and standards provide tabulated values of fire resistance which are based on standard fire tests. These tabulated fire resistance values are mostly dependent on concrete cover thickness and minimum dimensions. The highlights of the provisions in various codes and standards are provided in Table 2.3.

In the USA, concrete structures are to be designed in accordance with the American Concrete Institute (ACI-318) [2008] standard. While ACI 318 does not contain any fire provisions, it refers to ACI 216.1 [2007] standard which gives prescriptive based specifications for fire design of concrete and masonry structures. ACI 216.1 standard specifies concrete cover thickness and minimum sectional dimensions required for achieving a required fire resistance rating in RC columns. These provisions are given for both siliceous and carbonate aggregate concrete types. Different values have been specified based on the number of sides of the column that are exposed to ASTM E119 standard fire. The specification for the ties and their spacing is provided in order to maintain integrity in fire situation. The recent edition of ACI 216.1 standard contains some additional provisions for achieving fire resistance ratings in HSC structural columns. In addition to minimum sectional dimensions and concrete cover thickness requirements, it also proposes the use of 135° bent ties [Kodur 2003] for achieving required fire ratings.

Eurocode 2, Part 1–2 [2004] gives a choice of simplified, tabular (tables) or advanced methods for determining fire resistance of RC columns. Tables, which are based on prescriptive approach, provide the fastest and most direct method for determining the minimum dimensions and cover thickness in RC columns. The tabular method gives a minimum concrete cover, based on

nominal axis distance, which is the distance from the center of the main reinforcing bar to the surface of the member.

The simplified equation may give more economical fire resistant designs, especially for small columns and/or high fire resistance periods. The simplified equation adopted in Eurocode is based on the equation developed by Franssen and Dotreppe [2003] details of which is presented in the previous section.

There are two simplified methods given in Eurocode 2 Part 1–2. Method A and method B are both equally applicable; although Method A, which is slightly simple, has smaller limits on load eccentricity than Method B. For columns supporting the uppermost storey, the eccentricity often exceeds the limits for both methods, A and B, and requires the column to be treated as a beam. In addition to satisfying the rules for cover thickness (or normal axis distance), the code specifies a minimum percentage of steel and spacing requirements for achieving required fire resistance.

Australian Code AS 3600 [2001] has two different clauses for calculating the fire resistance of columns. The first clause is for columns with all faces exposed to fire and the second clause is for columns partially exposed to fire. The code provides an equation to calculate the fire resistance of RC columns based on steel ratio, compressive strength of concrete, dimensions of column, axial load on the column and the effective length.

A closer examination of fire resistance specifications in different codes of practice reveals significant variation in fire resistance provisions. To illustrate this wide variation, the provisions from three codes of practice were applied to compute fire resistance of a typical RC column. The column selected for analysis (column III 14) is the one tested by Lie and Woolerton [1988] under ASTM E119 (similar to ISO 834) fire exposure (see Table 2.4). The measured fire resistance in the test for the RC column was 183 minutes. Using the ACI 216.1 provisions, the fire resistance

(rating) of the column was computed to be 180 minutes. It can be said that ACI provisions are very close to the observed fire resistance in tests. But it needs to be noted that the fire resistance (rating) provisions specified in ACI 216.1 are based on the concrete cover thickness to the rebar (and minimum cross sectional dimensions) and would still provide the same fire resistance for a similar RC column under different load level, slenderness of the column, percentage of steel etc. The empirical equation in Eurocode predicts the fire resistance to be 161 minutes, while the Australian code provisions (simplified equation) give a prediction of 234 minutes. Thus it can be seen that there is a wide variation in the fire resistance predictions based on the provisions in current codes and standards.

Until recently, for fire resistance evaluation of RC columns has been based on the prescriptive approach specified in building codes, with little or no opportunity for designers to apply a rational engineering approach. Recently some countries have moved towards performance-based design in the form of rational fire engineering approaches involving thermal and structural analysis for fire design. Such an approach, based on rational engineering principles, leads to alternate and cost-effective fire designs. Also with the increasing use of newer materials, like HSC, which are more prone to phenomenon like spalling, the existing fire resistance provisions may not be fully applicable. The development of numerical models can facilitate performance based design solutions without the necessity for carrying out fire resistance tests. One of the major obstacles for undertaking performance based fire design is the unavailability of validated numerical models and calculation methods for fire resistance assessment.

2.5 Factors Influencing Fire Performance of RC Columns

A review of results from the experimental and analytical studies reveal that RC columns made of NSC exhibit good fire performance. Also, a review of previous studies indicate that fire behavior

of HSC columns, and fire-induced spalling in particular, is complex phenomenon and is affected by a number of factors. Based on the analysis of model predictions, test data, and the visual observations reported in previous studies, some of the factors that influence the fire performance of the RC columns are briefly discussed here.

2.5.1 Concrete Strength

The results from the review of fire resistance tests show that high fire resistance (three hours or more) can be obtained for RC columns, made of NSC, even under full service loads. However, a comparison of the fire resistance of the HSC columns with that of the NSC columns indicates that the HSC columns have the lower fire resistance of the two [Kodur, et al. 2003; Kodur and McGrath 2003]. Concrete compressive strengths higher than 70 MPa are more susceptible to spalling and may result in lower fire resistance.

2.5.2 Concrete Moisture Content

The moisture content in concrete, expressed in terms of relative humidity (RH), influences the extent of spalling in RC columns with higher RH levels leading to higher spalling [Ali, et al. 2004]. Fire-resistance tests on full-scale HSC columns have shown that significant spalling occurs when the RH is higher than 80%, due to the built-up or pore pressure. This has further negative effect on HSC columns since the time required to attain acceptable RH level longer for HSC columns as compared to NSC columns.

2.5.3 Concrete Density

The effect of concrete density was studied through fire tests on the normal and lightweight columns and blocks [Kodur 1999]. The extent of spalling was much greater when the lightweight aggregate was used. This could be partly attributed to higher free moisture present in the

lightweight aggregate, which creates higher vapor pressure under severe fire exposures, which in turn lead to fire-induced spalling of concrete.

2.5.4 Fire Intensity

Fire intensity affects the spalling and thus fire resistance of RC columns. As spalling is not a major phenomenon in NSC columns, heating rate has minimal effect on fire performance of NSC columns. The spalling of HSC is much more severe in fires characterized by fast heating rates or high fire intensities, typical of hydrocarbon fires [Danielsen 1997; Bilodeau, et al. 1998]. This can be attributed to the faster rise in temperatures in concrete leading to higher pore pressure development and to a higher thermal gradient across the concrete cross-section. Thus, higher heating rates or higher fire intensities significantly reduce fire resistance of RC columns.

2.5.5 Column Dimensions

Generally, the fire resistance of RC columns increases with column size. However, the risk of explosive thermal spalling increases with the size of HSC columns [Kodur and Phan 2007]. This is due to the fact that the specimen size is directly related to the heat and moisture transport through the structure, as well as the capacity of larger structures to store more energy. When spalling mitigation measures are incorporated, the risk of explosive spalling decreases and the fire resistance increases with the size of the members. As spalling is not a major phenomenon in NSC columns, fire resistance increases with the size of NSC column.

2.5.6 Lateral Reinforcement

Results from fire resistance studies clearly show that the layout (configuration) of ties and confinement of columns have an influence on the fire performance of RC columns. Higher fire resistance in RC columns can be achieved by providing an improved tie configuration (provision

of bent ties at 135^{o} back into the core of the column) and with a closer tie spacing (at 0.75 times that required for the NSC columns). The extent of spalling in columns, with bent tie configuration, is relatively less compared to that in columns without bent tie configuration. The columns containing only 90^{o} bent ties typically lose a significant portion of the columns section upon failure. The columns with 135^{o} bent ties exhibit the classic pyramid compression failure section with the failed section being confined locally within one or two tie spacing. Thus, the tie configuration has significant influence in the fire resistance of HSC columns [Kodur 2003; ACI-216.1 2007].

2.5.7 Fiber Reinforcement

The addition of fibers into concrete mix has an influence on fire induced spalling and fire resistance of RC columns. Results from experimental studies show that the addition of polypropylene fibers (about 0.1-0.15% by volume) to concrete mix minimizes spalling in the HSC columns under fire conditions and thus enhances its fire resistance. The polypropylene fibers melt at 160 to 170°C (320 to 340°F) and increase concrete permeability which helps to alleviate the pore pressure in the concrete [Bilodeau et al. 1998; Kodur 2000; Hertz 2003]. Thus the HSC column does not decrease in cross-section due to spalling and can sustain the load longer. The addition of steel fibers (about 1.75% by weight) enhances the tensile strength of concrete and thus reduces spalling [Kodur 1999; Kodur, et al. 2003], which in turn increases the fire resistance time of the column.

2.5.8 Load Intensity and Type

The type of load and its intensity have a significant influence on spalling and the resulting fire resistance. Higher load intensity leads to lower fire resistance [Kodur and McGrath 2003; Ali, et

al. 2004; Kodur and McGrath 2006]. The effect is more pronounced in HSC columns since the loss of strength with rise in temperature is greater for HSC than for NSC. A loaded HSC structural column is susceptible to higher spalling than an unloaded column. This occurs because a loaded structural member is subjected to stresses due to load in addition to the pore pressure generated by steam. Further, the extent of spalling is higher if the load is of an eccentric (or bending) type since this induces additional tensile stresses.

2.5.9 Type of Aggregate

Of the two commonly used aggregates, the carbonate aggregate (predominantly limestone) provides higher fire resistance and better spalling resistance in concrete than does the siliceous aggregate (predominantly quartz). In general, the fire resistance of the RC columns made with carbonate aggregate concrete is about 10% higher than the RC columns made with siliceous aggregate concrete [Kodur 2000; Kodur, et al. 2003]. This trend is applicable for both NSC and HSC columns.

2.6 Material Properties at Elevated Temperatures

2.6.1 General

Properties of constituent materials, namely concrete and reinforcing steel, influence the fire response of RC columns. These properties include: (a) thermal (b) mechanical (c) deformation and (d) material specific properties such as spalling in concrete. The thermal properties determine the extent of heat transfer to the column, whereas the mechanical properties determine the extent of strength loss and stiffness deterioration in the column. The deformation properties (in conjunction with the mechanical properties) determine the deformations and strains in the column. In addition, fire induced spalling can play a significant role on the performance of RC

members fabricated with new types of concrete. All these material properties vary as a function of temperature and depend on the composition and characteristics of concrete as well as those of reinforcing steel [Kodur, et al. 2008; Dwaikat 2009].

Thermal properties such as thermal conductivity and specific heat of concrete and reinforcing steel influence the temperature rise and distribution in an RC column. The mechanical properties that determine the fire performance of RC members are strength, modulus of elasticity of the constituent materials. The deformation properties that influence the development of strain and deformation are thermal expansion, creep of concrete and steel, and transient strain of concrete. Creep, often referred to as creep strain, is defined as the time-dependent plastic deformation of the material. At normal stresses and ambient temperatures, the deformation due to creep may not be significant, especially under service load levels. At higher stress levels and extreme temperatures, however, the rate of deformation caused by creep can be substantial. The main factors that influence high temperature creep are temperature, stress level, and their duration.

In addition to thermal, mechanical, and deformation properties, fire induced spalling in concrete influences the fire performance of an RC column. For predicting such spalling, additional properties such as porosity and permeability of concrete are required.

All of the above material properties vary as a function of temperature and have to be properly accounted for in tracing the fire response of RC members. Further, the variation of many of the properties at high-temperatures is quite sensitive to small changes in concrete ingredients and environmental conditions (humidity and temperature rise). As an illustration, the thermal properties are significantly influenced by the type of aggregate and composition of the concrete mix [Flynn 1999]. This section provides a review on high temperature properties of concrete and reinforcing steel.

2.6.2 Concrete Properties

2.6.2.1 Thermal Properties

As per Dwaikat [2009] the thermal properties that influence on the thermal response of concrete structures are thermal conductivity, specific heat (or heat capacity), and mass loss. There have been limited test programs for characterizing high temperature thermal properties of concrete [Lie and Kodur 1995; Lie and Kodur 1996; Saad, et al. 1996; Van-Geem, et al. 1996; Van-Geem, et al. 1997; Shin, et al. 2002; Kodur and Sultan 2003]. Based on the test data, empirical formulae for thermal properties of different types of concrete have been developed [Lie 1992; Lie and Kodur 1996; Kodur and Sultan 2003; EC2-1-2 2004].

Figure 2.2 illustrates the variation in thermal conductivity of NSC plotted as a function of temperature, while Figure 2.3 shows heat capacity of NSC. The test data is compiled from different studies [Harmathy 1970; Harada, et al. 1972; Harmathy and Allen 1973; Lie and Kodur 1995; Lie and Kodur 1996; Shin, et al. 2002; Kodur and Sultan 2003]. The large variation in this data can be attributed to the differences in test methods, conditions, procedures and measurement techniques. It can be seen from Figure 2.3 that the aggregate type has significant influence on thermal capacity of concrete. The high heat capacity for carbonate aggregate concrete in temperature range 600 -800˚C is due to the endothermic reaction, which results from the decomposition of dolomite and absorbs a significant amount of energy. This high heat capacity in carbonate aggregate concrete helps in minimizing spalling and enhancing fire resistance.

Very few studies were carried out to characterize other high-temperature thermal properties of concrete, such as density changes and porosity structure. These tests usually came along with elemental tests, and were not characterized for performance-based design (due to the fact that

test conditions, heating rates and other parameters were not well reported for these tests). Therefore, such properties were not addressed properly in the literature.

Test data generated in previous studies have been used to develop constitutive models, such as those specified in the ASCE manual [Lie 1992] and Eurocode 2 [2004], for the temperature dependent thermal properties of concrete. Thermal conductivity and heat capacity from the available constitutive models in Eurocode 2 [2004] and ASCE manual of practice [Lie 1992] are also plotted in the Figures 2.2 and 2.3. The high-temperature constitutive models for thermal properties of concrete are presented in Table A.1 in the Appendix. These properties are generally expressed as a function of temperature in the Eurocode, and as a function of aggregate type and temperature in ASCE manual. While the ASCE constitutive model accounts for significant changes in heat capacity that occurs in carbonate aggregate concrete in the temperature range of 600-800˚C, Eurocode constitutive model ignores this effect and has the same heat capacity models for both siliceous and carbonate aggregate concrete. The ASCE constitutive model is valid for NSC only, whereas the Eurocode constitutive model is valid for both NSC and HSC. Based on experimental studies, Kodur et al. [Kodur, Wang et al. 2004] extended the ASCE constitutive model, applicable for NSC, to HSC (see Table A.1 in Appendix A).

2.6.2.2 Mechanical Properties

2.6.2.2.1 Mechanical Properties in Heating Phase

Dwaikat [2009] stated that generally the mechanical property tests were carried out in two ways, namely; high temperature tests and residual tests. In high temperature tests, the concrete specimen is heated up to achieve a certain temperature and its response is measured at that temperature [Castillo and Durrani 1990; Furumura, et al. 1995; Lie and Kodur 1995; Khoury 1996; Lie and Kodur 1996; Chan, et al. 1999; Lawson, et al. 2000; Balendran, et al. 2003; Wang,

et al. 2003; Cheng, et al. 2005; Khoury 2006; Khoury 2006; Khoury 2006]. In the residual tests, the response is measured after exposure to elevated temperatures [Felicetti, et al. 1996; Li, et al. 2004; Fu, et al. 2005; Savva, et al. 2005; Chang, et al. 2006; Lau and Anson 2006; Nassif 2006; Xiao, et al. 2006]. In such residual tests, the specimens are subjected to various temperature increments and after attaining a specific target temperature in concrete, the specimen was cooled to room temperature and then loaded to failure to measure its mechanical response. There is a good amount of high-temperature test data on the strength properties of both NSC and HSC with different types of aggregates.

Figures 2.4 and 2.5 show variation of concrete compressive strength with temperature for NSC and HSC, respectively. Figure 2.4 shows large, but uniform variation, of the compiled test data for NSC throughout the temperature range as seen in the shaded area. However, Figure 2.5 shows a larger variation in the compressive strength with temperature for HSC in the range 200˚C to 500˚C, and less variation above 500˚C. This is mainly because fewer test data points were reported for temperatures higher than 500˚C either due to occurrence of spalling or due to limitations in test apparatus. However, wider variation is observed for NSC in this temperature range (above 500 °C) when compared to HSC as can be seen from Figures 2.4 and 2.5. This is mainly because of the higher number of data points reported for NSC in the literature and also due to lower tendency of NSC to spalling under fire. It can be seen that the variations in the mechanical properties of concrete at high-temperatures are quite high. These variations from different tests can further be attributed to using different heating and loading rates, specimen curing, condition at testing (moisture content and age of specimen), and the use of different quantities of admixtures in concrete.

Among the factors that directly affect the high-temperature mechanical property test results are the initial curing, moisture content at the time of testing and the addition of admixtures and silica fume to the concrete mix [Dwaikat 2009]. These factors were not addressed in the literature, and there is no test data that shows the influence of these factors on the high-temperature mechanical properties of concrete.

Another main reason for the significant variation in the high-temperature properties of concrete is the use of different testing conditions (such as heating rate and strain rate) and test procedures (hot strength test and residual strength test) due to lack of standardized test methods for carrying out property tests. Further, much of the data reported in literature does not provide full details on the type of aggregate, moisture content, heating or loading rates under which the tests were conducted. Therefore, the constitutive models developed from such test data may not be fully reliable.

Based on the data from mechanical property tests, researchers have proposed different constitutive models for high temperature mechanical properties of concrete. The most widely used constitutive models present in the Eurocode 2 [2004] (see Table A.2 in Appendix A), ASCE manual of practice [Lie 1992] and Kodur et al. [Kodur, et al. 2004] are reproduced in Table A.1 in the Appendix A. The ASCE model is valid for NSC, Eurocode model is valid for both NSC and HSC, and Kodur et al. model is valid for HSC. These relations give the rate of degradation of concrete as a function of temperature only, and without any consideration to variations in other significant parameters such as rate of loading, heating, material composition. Figures 2.4 and 2.5 show variation of concrete strength with temperature for NSC and HSC respectively according to the models in Eurocode 2, ASCE 1992 and Kodur et al.and from test data reported in literature.

It can be seen from Figure 2.4 and 2.5 that there is a large variation in the reported test data and also from the different models present in ASCE, Eurocode and Kodur et al. For example, the reduction in NSC compressive strength with temperature based on ASCE model seems to be closer to the upper bound of the reported experimental data. However, the Eurocode 2 curve for the strength reduction of NSC is closer to the lower bound of the reported test results.

Phan and Carino [2003] reviewed the current high-temperature constitutive models for the compressive strength of HSC and proposed a lower bound model for the compressive strength of HSC (shown in Figure 2.5). However, even this model is not conservative throughout the temperature range of 100-500˚C as can be seen from Figure 2.5. Overall, the model proposed in Eurocode 2 for Class 3 of HSC gives conservative values for concrete compressive strength reduction with temperature.

The above review clearly illustrates the large variation in the available test data and constitutive relationships in codes and standards for high-temperature strength properties. Consequently, fire resistance calculations using these constitutive models produce diverse fire resistance predictions. However, Kodur et al. [2008] showed that using the ASCE model (which is most commonly used for fire resistance evaluation in North America) produces better fire resistance predictions for NSC columns when compared to the Eurocode model.

2.6.2.2.2 Mechanical Properties in Cooling Phase

Upon cooling (in the decay phase of the fire scenario), concrete continue to lose its strength and stiffness. This can be mainly attributed to the hydration of some of the dehydrated cement components upon cooling. The products of such hydration are of larger volumes than those of the original components and this leads to further cracking in the concrete. Thus, the residual strength of concrete is generally less than the strength of heated concrete (provided both are heated to the

same temperature). The residual strength of concrete is important in evaluating the response of RC members exposed to design (or real) fire scenarios where a cooling phase always exists. The literature review shows that there is a large variation in the residual strength of concrete as shown in Figure 2.6. This large variation can be attributed to using different heating (or cooling) rate or loading rate, specimen and test conditions, and the use of admixtures. Codes and standards, such as Eurocode 2 and ASCE manual, do not specify relationships for the residual strength of concrete after fire exposure. Thus, the best fit of the reported test data, which is generally used for evaluating the residual strength of concrete, is plotted in Figure 2.6 [Kumar 2004].

2.6.2.3 Deformation Properties

Deformation properties are highly dependent on the chemical composition, the type of aggregate and the chemical and physical reactions that may occur in the concrete during heating [Schneider 1988]. Deformation properties include thermal expansion, creep strain and transient strain [Dwaikat 2009].

2.6.2.3.1 Thermal Expansion

The coefficient of thermal expansion represents the change in length of a material due to temperature changes. The coefficient of thermal expansion, which is defined as the change in a unit length of a material due to a unit (degree) increase in temperature, is important as a measure of the expansion of the member and thermal stresses resulting from temperature changes [Kodur, Dwaikat et al. 2008].

Date from the literature indicates that there is large variation in the measured thermal expansion of concrete as shown in Figures 2.7. This can be attributed to the fact that the coefficient of

thermal expansion of concrete is affected by the aggregate type and its composition, moisture content and many other factors. The thermal expansion of siliceous aggregate concrete is greater than that for carbonate aggregate concrete. At high temperatures (600°C to 800°C) most concretes no longer exhibit any expansion and in some cases contract as shown in Figure 2.7.

2.6.2.3.2 Creep and Transient Strain

Creep is defined as the time-dependent plastic strain under constant stress and temperature. Creep strains generally occur due to the movement of moisture in concrete [Mindess et al., 2003] and thus are largely influenced by concrete temperature. At room temperature, the movement of moisture in concrete is limited; therefore, creep deformations occur at very slow pace. However, at elevated temperatures, significant moisture movement occurs in concrete resulting in larger creep strains. Because creep affects strains, deflections, and stress redistribution, it plays an important role on the fire response of structural members. Since high temperature causes degradation of the concrete properties, creep properties will be also be affected.

A review of the literature shows that high temperature creep of concrete is a complex phenomenon that depends on many factors including temperature, loading, and mix proportions. The review indicates that creep generally increases with temperature. It also shows that low-modulus aggregate exhibit increased creep deformations. Creep rates were found to be significantly higher at elevated temperatures than under ambient conditions. In addition, it was found that creep increases with increasing load level or at high stress level.

Transient strain occurs during the first time heating of concrete under load, but not on subsequent heating [Khoury et al. 1985]. Transient strain is essentially due to the thermally induced incompatibilities between the aggregate and the cement paste [Purkiss 2007]. During heating of concrete, there are complex changes in the moisture content and chemical composition of the

cement paste, and also there is a mismatch in thermal expansion between the cement paste and the aggregate. Such mismatch in thermal expansion leads to the development of internal stresses and micro-cracking in the concrete constituents (aggregate and cement paste) and results in transient strain in concrete [Schneider 1988].

A review of literature shows that there is very limited information on creep and transient strain of concrete at elevated temperature [Kodur, et al. 2008]. However, based on the limited available data in literature, Anderberg and Thelandersson [1976] developed constitutive models for creep and transient strain in concrete at elevated temperatures [Harmathy 1993]. According to Anderberg and Thelandersson, the creep strain and transient strain of concrete at elevated temperatures are given by the following two equations, respectively:

$$\varepsilon_{cr} = \beta_1 \frac{\sigma}{f_{c,T}} \sqrt{t}\ e^{d(T-293)} \qquad [2.1]$$

$$\varepsilon_{tr} = k_2 \frac{\sigma}{f_{c,20}} \varepsilon_{th} \qquad [2.2]$$

where: ε_{cr} = creep strain, ε_{tr} = transient strain, $\beta_1 = 6.28\times10^{-6}$ $s^{-0.5}$, $d = 2.658\times10^{-3}$ K^{-1}, T = concrete temperature (°K) at time t (s), $f_{c,T}$ = concrete strength at temperature T, and σ = stress in the concrete at the current temperature, k_2 = a constant ranges between 1.8 and 2.35, ε_{th} = thermal strain, and $f_{c,20}$ = concrete strength at room temperature.

2.6.2.4 Fire Induced Spalling

2.6.2.4.1 General

Fire induced spalling in concrete members can broadly be classified into three stages, namely; early spalling, intermediate spalling, and late spalling [Dwaikat and Kodur, 2009; Dwaikat,

2009]. In typical RC members (beams and columns), early spalling can start immediately after fire exposure (5 to 10 minutes) and can continue up to 30 to 45 minutes. This type of spalling is generally of explosive nature and often results due to the development of high thermal gradients within the parts (surface close to fire exposure) of concrete members. Early spalling results in the break-up of large chunks of concrete and thus may have detrimental effect on the fire resistance of RC members, particularly when spalling reduces the concrete cover thickness to the main reinforcement.

Intermediate spalling occurs mid-way into fire exposure (about 30 to 45 minutes) and results in the form of surface scaling (breaking off small pieces of concrete) and this can continue through final stages of fire exposure. Such type of spalling has less effect on the fire resistance of RC members since it generally results in break-up of thin layers of concrete. Late spalling occurs just prior to failure of structural members and primarily results from significant loss of strength and stiffness of structural member due to prolonged fire exposure. This late spalling has minor influence on the overall fire response of RC members. Such type of spalling occurs even in room temperature conditions prior to failure of concrete members.

Spalling generally results in reduced cross-sections and rapid loss in load carrying capacity, thereby lowering the fire resistance of a concrete member. A review of literature indicates that the main factors influencing fire induced spalling in concrete are moisture content, concrete permeability, concrete strength, fire scenario (rate of heating) and stress levels [Phan 1996, Phan, et al. 2000, Kodur and Phan 2007]. Compared to NSC, HSC has a higher susceptibility to fie induced spalling. This is probably because the low permeability and the high density of HSC prevent water vapor from escaping at elevated temperatures and lead to high pore pressure which

produces spalling. In addition, HSC is normally subjected to higher stress levels than NSC which might enhance the conditions for the occurrence of fire induced spalling in the case of HSC.

2.6.2.4.2 Causes of Spalling

Dwaikat [2009] stated that the review of literature presented a conflicting picture on the occurrence of spalling in RC members and also on the exact mechanism for spalling. While some researchers, based on fire test data, reported explosive spalling in concrete members, a number of other studies reported little or no significant spalling. One possible explanation for this confusing trend of observations is the large number of factors that influence the spalling and the inter-dependency of some of these factors. However, most researchers agree that major causes for spalling in concrete are due to low permeability of concrete and also due to moisture migration at elevated temperatures.

There are two broad theories on which the spalling phenomenon can be explained [Kodur 2000]:

- **Pressure build-up:** Spalling is believed to be caused by the build-up of pore pressure during heating. HSC is believed to be more susceptible to this pressure build-up than NSC because of its low permeability. The extremely high water vapour pressure, generated during exposure to fire, cannot escape due to the high density (and low permeability) of HSC. When the effective pore pressure (porosity times pore pressure) exceeds the tensile strength of concrete, chunks of concrete fall off from the structural member as shown in Figure 2.8. This falling off can often be explosive depending on the fire and concrete characteristics [Harmathy 1993 and Anderberg 1997].
- **Restrained thermal dilatation:** This hypothesis considers that spalling results from restrained thermal dilatation close to the heated surface, which leads to the development of compressive stresses parallel to the heated surface as shown in Figure 2.9. These

compressive stresses are released by brittle fractures of concrete (spalling). The pore pressure can play a significant role in the onset of instability in the form of explosive thermal spalling [Bazant 1997].

2.6.2.4.3 Factor Affecting Spalling

From the previous experimental studies it is clear that spalling of concrete is a very complex phenomenon that depends on a number of factors [Kodur and Phan, 2007];

- Concrete strength: HSC is more susceptible to spalling than NSC.
- Concrete moisture content: moisture content increases the potential for spalling in concrete.
- Concrete density: the extent of spalling is much greater when the lightweight aggregate is used.
- Heating rate: higher heating rate increases the fire induced spalling in concrete.
- Specimen dimensions: the risk of explosive thermal spalling increases with the specimen size.
- Tie configuration and spacing: spalling in HSC columns can be minimized by providing an improved tie configuration (provision of bent ties at 135° back into the core of the column and increased lateral reinforcement) and with a closer tie spacing (at 0.75 times that required for the NSC columns).
- Fiber reinforcement: addition of polypropylene or steel fibers reduces fire induced spalling in HSC members.
- Type of aggregate: carbonate aggregate concrete is less prone to spalling than siliceous aggregate concrete.

2.6.2.4.4 Codes and Standards

A review of the literature indicates that there is very limited guideline in current codes and standards to predict fire induced spalling in concrete. The specifications in Eurocode 2 state that spalling is unlikely to occur when the moisture content in concrete is lower than 3% without any due considerations to concrete permeability and the tensile strength of concrete. ACI 216.1 standard [2007] does not have any specifications for predicting spalling in concrete. However, this standard provides some guidelines for mitigating spalling through the addition of polypropylene fibers to concrete mix. It should be noted that the guidelines on fire induced spalling in current codes are mainly derived from fire tests on small specimens and they do not account for moisture migration and pore pressure build up (which is thought to be the main cause of spalling). The lack of calculation methodologies for predicting spalling is one of the main reasons for slow progress in developing effective spalling mitigation measure in concrete structures.

2.6.3 Reinforcing Steel Properties

High temperature properties of reinforcing steel (thermal properties, mechanical properties, deformation properties and specific properties such as bond strength) that influence the fire response of concrete structures has been reviewed by Kodur et al. [2008].

2.6.3.1 Thermal Properties

The thermal properties of reinforcing steel depend on the type and temperature of steel. These properties include thermal conductivity and thermal capacity. The thermal conductivity of reinforcing steel is high in comparison to concrete and thus heat is distributed through steel rebars quite rapidly. In addition, steel reinforcement is embedded in concrete and is of very small

area as compared to concrete. For these reasons, in fire resistance calculations steel reinforcement is generally assumed to be a perfect conductor, which implies that temperature is uniform within the steel area, and thus do not separately account for steel reinforcement in thermal analysis. As temperature rises, the thermal properties of steel become more dependent on temperature and are influenced less by steel composition [Williams 2004]. However, it has been shown that reinforcing steel has small influence on the temperature distribution within the RC cross-section [Lie and Irwin 1993]. Thus, thermal properties of reinforcing steel are not very important for predicting the temperature distribution in RC members.

2.6.3.2 Mechanical Properties

Mechanical properties of reinforcing steel include yield strength, ultimate strength and modulus of elasticity. These properties are generally represented by the stress-strain-temperature relationships of steel and decrease with temperature. The literature review shows that there is a variation in the yield and ultimate strength of steel as shown in Figure 2.10 [Harmathy 1993]. Some of this variation is due to the differences in steel composition and the lack of definition for the yield strength of steel [Buchanan 2002]. The variation of yield and ultimate strength of reinforcing steel as a function of temperature, specified in the ASCE Manual [1992] are also shown in Figure 2.10. It can be seen that the ASCE model follows the lower bound yield strength of steel. However, for ultimate strength, the ASCE model is overly conservative for temperatures below 500°C and unconservative for temperatures above 700°C.

A review of literature indicates that reinforcing steel recovers nearly all of its original yield strength upon cooling as long as heating temperatures do not exceed 500°C [Neves et al. 1996]. However, for steel heated to temperatures above 500°C the residual strength start to degrease gradually as shown in Figure 2.11. The behavior of reinforcing steel in the cooling phase is

crucial for modeling the response of RC structural members exposed to real (design) fire scenarios. The high-temperature constitutive models for mechanical properties of reinforcing steel are presented in Table A.3 in Appendix A.

2.6.3.3 Deformation Properties

Deformation properties of reinforcing steel include thermal strain and creep strain. The thermal strain of reinforcing steel at elevated temperatures is directly related to the temperature rise and generally increases with temperature. The variation for the thermal strain as a function of temperature as per the ASCE Manual [1992] is shown in Figure 2.12.

Creep strain is the gradual increase in strain with time under a constant stress. Creep strain occurs due to the movement of dislocations in the slip plane (in the microstructure of steel). Normally, steel (metal) composition contains variety of defects, for example solute atoms, that act as obstacles to dislocation movement. At room temperature, the amount and distribution of these defects remain almost uniform and thus creep strains occur at very slow time pace. However, at high temperatures, vacancies in the crystal structure can diffuse to the locations of a dislocation and cause the dislocations to move faster to an adjacent slip plane; therefore allowing for further deformation to occur. Thus, creep strain becomes significant at elevated temperatures, particularly above 450°C, and should be included in modeling the fire response of RC members. A review of literature indicated that there is very little information on high temperature creep strain of reinforcing steel. The available creep models, such as the one proposed by Harmathy [1967], are based on Dorn's theory which relates the creep strain to the temperature, stress, and time. More information on Harmathy's creep model is provided in Chapter 4. The high-temperature constitutive models for deformation properties of reinforcing steel are presented in Table A.3 in the Appendix.

2.6.3.4 Other Properties

Other properties of reinforcing steel that may influence the fire response of concrete structures include bond between concrete and reinforcing steel, which arises primarily from friction and adhesion between concrete and steel were also studied by Kodur et al. [2008] and Dwaikat [2009]. Generally, bond strength is a function of (1) mix proportions of concrete (cement type, admixtures, water-cement ratio), (2) mechanical properties of the steel (size and spacing of the ribs if any), and (3) rebar position within the concrete member (under tension or compression). Permissible bond stresses are generally specified as percentages of concrete's compressive strength [Naus 2006].

The bond between concrete and steel at room temperature has been considerably studied. However, there are very limited studies on the effect of elevated-temperature exposure on the bond properties between steel and concrete. The most notable study is that reported by Harmathy [1993] and showed that in the case of deformed bars, the bond strength degrades at elevated temperatures in a trend similar to that of the compressive strength of concrete. Thus, the reduction in the bond strength is similar to the reduction in concrete compressive strength at elevated temperature for deformed bars (which are the most widely used steel bars in concrete structures). Thus, bond failure is not likely to occur in RC columns at elevated temperatures due to the fact that the degradation in the strength of reinforcing steel is faster than the degradation in the bond strength (which is similar to that in concrete compressive strength).

2.7 Knowledge Gaps

From the above state-of-the-art review, it can be seen that most of the efforts thus far have been directed towards understanding the behavior of RC columns under standard fire. In order to predict resistive fire performance of NSC columns, and also to extend it to HSC columns, more

detailed analysis is required for including phenomenon such as biaxial bending, 1-, 2-, 3-side fire exposure, spalling, creep and other features including realistic fire, and different strains (mechanical, thermal, transient and creep). Thus the future work in this area should be focused on developing detailed analytical models which should be capable of accounting for all these factors. The availability of such models will facilitate performance-based approach to fire safety design, which often leads to cost-effective and innovative fire safety solutions. Following are some of the tasks needed to close the current knowledge gaps on fire performance of RC columns:

1. Sophisticated analytical models, based on whole member behavior as opposed to sectional analysis, are to be developed for the analysis of RC columns. Such models should account for fire induced spalling, biaxial bending (due to bi-eccentric loading, uneven spalling, or different face exposure), nonlinear high temperature properties, restraint conditions and various failure criteria.
2. Reliable test data needs to be generated for validating the developed model under different fire scenarios (e.g. design fire scenarios) and loading conditions. This requires detailed experimental studies with sophisticated test data including (strains) and observations made on spalling progression as a function of fire exposure time.
3. Using the validated models, parametric studies have to be carried out to quantify the influence of various parameters on the fire performance of RC columns.
4. Based on the experimental studies and parametric studies, design guidelines have to be developed in order to improve fire performance of RC columns. Also, simple equations (calculation methods) have to be developed to evaluate the fire resistance of RC columns. Such design guidelines should include spalling mitigation techniques for HSC columns.

5. A framework for performance-based design of RC structures is to be developed. Such a framework should lay out specifics on design fire scenarios, material properties at different temperatures, loading configurations and failure criterion (including spalling predictions) for various design scenarios. The availability of validated numerical models, together with design guidelines and a framework for performance-based design will facilitate a rational approach to fire safety design of RC columns.

Table 2.1 Experimental studies on fire resistance of reinforced concrete columns

Study/Investigation	Study Objectives / Detail	Features and Methodology	Observations / Conclusions	Strengths/Draw backs
Lie and Woolerton [1988]	The study presents the results of the extensive tests carried on 41 RC (NSC) columns. Objectives: • To generate experimental data on fire resistance of RC columns. • To develop general methods for the calculation of the fire resistance of concrete columns and walls for a wide range of applications. The effect of size and shape of cross section, cover thickness, reinforcement, aggregate type, load, load eccentricity, axial restraint and fire exposure intensity on fire resistance was investigated.	• All columns were 3810 mm long. Square cross sections of side 203 mm, 305 mm and 406 mm, rectangular cross sections of 305 x 457 mm and 203 x 915 mm and circular cross section of 355 mm diameter were used in the study. • One column had 48 mm cover while the remaining columns had a cover of 38 mm. • Three types of aggregates were used: siliceous sand, carbonate sand and lightweight expandable shale. • All loads were applied at least 40 mins before the test in four or more stages. • Most columns were subjected to standard ASTM-E119 temperature-time curve. Two columns were first exposed to two hours of standard fire and then cooled and loaded to failure. One column was exposed to high intensity fire.	• Data and observations made during the test were used for quantifying the effect of :- type of aggregate, concrete strength, end restraint and end conditions, heavy reinforcement, size and amount of reinforcement, cross section shape, fire scenario, eccentric loading, sections with brackets and load intensity • Carbonaceous aggregate increased the fire resistance of RC columns. • HSC columns (Concrete with compressive strength more than 50 MPa were considered as HSC) provided more fire resistance that NSC as spalling did not occur. • Columns with heavy reinforcement provided higher fire resistance. • The end conditions affected the slenderness ratio and affected the fire resistance accordingly.	• This extensive experimental study provides valuable test data for understandin g the fire response of RC column and to validate numerical models. • Detailed observations made during tests and have been appropriately categorized. • Focused mostly on standard fire exposure and NSC columns.

Table 2.1 Contd. Experimental studies on fire resistance of reinforced concrete columns

Aldea et al. [1997]	Objectives: • To quantify some of the parameters influencing fire induced spalling in NSC and HSC columns. • To examine the influence of the diameter of the rebars on spalling of concrete.	• Six columns were tested and the parameters considered were reinforcement (by number and diameter of steel bars) and concrete type. • Columns were made of three different types. NSC and HSC with two different rebar configurations. • The columns were simply supported and a force that equals to 50% of the column design strength was applied. • ISO 834 standard fire exposure was used.	• HSC columns showed early spalling at the corners. Premature heating of the steel rebars in the reduced section, resulted in buckling of the steel rebars just before failure by crushing of concrete core. Consequently a considerable reduction in fire resistance was noticed. • Spalling of NSC columns under fire was not noticed. • Tests showed that the material behavior has more significant influence on failure than the structural behavior.	• This study presents a good comparison between NSC and HSC columns as relates to spalling. • Many important parameters were not considered in the study. • Effect of cross section on the spalling phenomena is not addressed.
Ali et al. [2001]	Presents an experimental program on the behavior of HSC columns under fire. The research includes testing reinforced HSC columns subjected to various loading levels and heating rates.	• 18 columns were tested under four loading levels and two heating rates. • All the columns were tested at about 100 days. The columns were simply supported at both ends and were tested under three loading levels: 0.2, 0.4 and 0.6 of the design strength as per BS 8110. Each column was tested under two heating regimes	• Of the 18 columns, 17 suffered various types of spalling which was classified as “explosive”. • Despite the good agreement in the measured parameters an obvious deviation in the values of spalling degrees can be noticed between the three tested specimens for each case. Increasing the load level decreased failure time and failure temperatures in both heating cases.	• Despite the conclusion that increasing loading level does not increase the risk of spalling, the limited experiments indicate an increase in the degree of spalling at loading level of 0.4 for low heating rate. Therefore such a general conclusion cannot be adopted until further tests are carried out for both

Table 2.1 Contd. Experimental studies on fire resistance of reinforced concrete columns

	Objective: To determine the effect of loading and heating rates on fire induced explosive spalling of HSC columns in fire	(BS 476 and low heating rate). • Concrete of strength (28 days) 90 to 110 N/mm^2 were used. • Spalling was classified as minor, major and severe.	• In all the tests, explosive spalling happened in the first 45 min of the heating. Minor spalling always took place first, followed by major and severe spalling. Explosive spalling did not occur in later stages of fire exposure. • Explosive spalling always occur when the column is expanding. No spalling took place in the columns in contraction phase. • Increasing the loading level did not increase the probability of spalling both under high and low heating regimes. • Low heating rates minimized the risk of explosive spalling. Columns tested under high heating rate showed less fire resistance.	• heating regimes, perhaps for loading levels of 0.3 and 0.5. • The study includes a good amount of parameters and thus provides a good understanding on the phenomenon of fire induced spalling in RC columns. • Further studies are needed to quantify the influence of various parameters on spalling. Column size are scaled-ones (length and cross section) and hence had to extrapolate test results.
Franssen, and Dotreppe [2003].	To study the influence of the circular shape on the behavior of columns under fire condition, the authors present the experimental research on circular RC columns.	Test Features: • Four columns of circular cross section were tested. • Two different percentages of longitudinal reinforcement and siliceous aggregates were used in the specimens.	The following observations were made during the test: • Sloughing off of concrete was seen in many places in all columns. • In the columns with lesser longitudinal steel there was significant increase in the damage after sloughing.	• The effects of parameters such as type of aggregate, addition of fibers, strength of concrete were not studied. • Data from tests was used in developing simplified calculation methods.

Table 2.1 Contd. Experimental studies on fire resistance of reinforced concrete columns

	Objectives: • To investigate if the circular sections are less prone to spalling, due to the fact that there is no corner in a circular section, and that spalling in the rectangular sections is usually first observed at corners. • To evaluate the feasibility of using calculation methods, that have been developed for rectangular sections, for circular section RC columns.	• The columns were simply supported at the ends giving a slenderness ratio of 28. • The temperature in the furnace varied according to ISO 834 fire curve. • The data led to the development of a simple method for calculating the fire resistance of RC columns.	• Large longitudinal cracks were observed. Conclusions: • The circular shape of the column does not prevent spalling. • No explosive spalling occurred in HSC (60 MPa) columns.	
Kodur [2003]	Objectives: • To compare the fire performance of HSC column with that of NSC columns. • Discuss the various factors influencing the structural behavior of HSC columns under fire conditions.	• Columns were subjected to ASTM E119 standard fire. The parameters studied in tests: • Concrete strength was varied from 34 MPa (typical for NSC) to 110 MPa (typical for HSC). • Type of aggregate in concrete. • Tie configuration.	• The cross sectional temperatures in HSC columns are generally lower than NSC columns. • Large cracks occurred in HSC columns after 3 hours. • The axial deformation in HSC columns is much lower than NSC columns. • Spalling occurred in HSC columns in the later stags of fire. Main conclusions/findings from the study:	• Data from the tests provides an understanding into the behavior of RC columns under fire. • The test data helped in developing design guidelines to improve the fire performance of HSC columns. • All tests focused on standard fire exposure. • Size of the columns were limited by the test equipment.

Table 2.1 Contd. Experimental studies on fire resistance of reinforced concrete columns

		• Addition of fiber reinforcement. • Type of fiber. • Load intensity. • Eccentricity of load.	• Concrete strength: Strengths higher than 70 MPa are more susceptible to spalling and may result in lower fire resistance. • Concrete moisture content: Higher spalling occurs in HSC as the time required to attain acceptable relative humidity level is more. • Other factors influencing fire resistance and spalling are: - concrete density - fire intensity - specimen dimensions - lateral reinforcement - fiber reinforcement - load intensity and type • - type of aggregate	
Kodur et al. [2003]	The study presents the results from fire resistance experiments carried out on five sets of RC columns. The variables considered in the study include concrete strength, aggregate type and fiber reinforcement. Objectives: • To compare the fire resistance performance of	• Five sets of columns (3 per set) were studied. • Four sets of columns were made of HSC (set 2 through 5) while the first set was made of NSC. • Steel and polypropylene fiber reinforcements were added to sets 4 and 5.	• There are slight differences in the temperature propagation between NSC and HSC columns. The temperature propagation for various types of HSC columns was found to be very similar. • The temperatures in the NSC column are generally lower than the corresponding temperatures in the HSC column throughout the fire exposure due to the variation in thermal properties of the two concretes and to the higher compactness resulting in a lower porosity. • In the case of HSC columns, the deformation-time response is significantly lower than that of NSC	• The study considered a number of factors affecting fire resistance and compares the changes in behavior due to these factors. • The tests provide a good understanding of the behavior of concrete columns under elevated temperatures. • The effect of change in cross section,

Table 2.1 Contd. Experimental studies on fire resistance of reinforced concrete columns

	• HSC columns with that of fiber reinforced HSC columns. • To discuss the factors that influence thermal and structural behavior of HSC concrete columns under fire conditions. To obtain test data for the development of computer programs that can model the behavior of HSC columns under fire conditions.	• All sets were made with siliceous aggregate, except set 3, which was made with carbonaceous aggregate. • The end conditions were fixed-fixed for all tests. • The columns were tested under concentric loads. • The tests were performed under ASTM E119 standard fire exposure.	columns in the expansion zone. • While there was no spalling in the NSC columns, significant spalling at the corners was observed before failure occurred in the HSC columns. • Columns with carbonate aggregate were less prone to spalling as compared to the one with siliceous aggregate. • The fire resistance of HSC columns was lower than that of NSC columns. It improved with the addition of fibers. Conclusions: • The presence of carbonate aggregate in HSC increases fire resistance. • The addition of steel and polypropylene fibers in HSC can improve the ductility of HSC columns and increase their fire endurance. • The presence of polypropylene fibers in HSC columns can reduce spalling and enhance their fire resistance.	eccentricity and cover thickness is not considered in the study. • The fire exposure is limited to standard fire exposure.
Kodur and McGrath [2003]	Objective: Generate data on the fire resistance of HSC columns, and identify the factors (such as tie configuration) that influence the behavior of HSC columns.	• Six columns of 3810 mm length were studied. • The cross section size and the aggregate type was varied. • Columns were tested under concentric load	• All six columns failed in compression mode and there was noticeable spalling at the end of the test. • The cracks in the columns progressed with time, at the corners of the cross-section, and led to spalling of chunks of concrete. While minute hairline cracks could be noticed in corners at about 20 to 30 minutes, the widening of these cracks occurred after about 60 minutes.	• The study covers major parameters affecting fire endurance of HSC columns exposed to standard fire. • The detailed data and test observations generated shall help in developing models

Table 2.1 Contd. Experimental studies on fire resistance of reinforced concrete columns

		varying from 54% to 123% of full service load determined according to the CSA Standard CSA-A23.3. • The end conditions were fixed • ASTM E119 fire scenario was used in fire tests. • Ties were bent at 90° in 3 columns and at 135° in the remaining.	• In most columns the rebars yielded before failure occurred. Ties bent to 135^{o} did not open-up, while the ones bent at 90° opened up. • Generally, there was no significant spalling in the first few minutes. In the column with high relative humidity, some spalling was observed about 10–20 minutes into the fire endurance test. In columns where there were wider cracks, significant spalling at the corners was observed as the test progressed. Further, prior to the failure of the column, significant spalling was noticed in all columns. Conclusions: • HSC columns have lower fire endurance than NSC • Ties bent at 135^{o} improve fire endurance as compared to ties bent at 90^{o}. • The fire endurance of a column increases with decreasing load. • The fire endurance of column made with carbonate aggregate concrete is about 10% higher than those with siliceous aggregate concrete.	for evaluating fire resistance. • The effect of end restraints and eccentricity of load were not studied which might have considerable effect on fire resistance. • The sizes of the column were limited by test equipment. • Only standard fire scenarios were used in the test.
Ali et al. [2004]	• This study investigated the effect of degree of restraint, loading level and heating rates on the performance of RC	• 99 NSC and HSC columns were tested. • High and low heating rates were used. • High (106 MPa) and normal (43 MPa) strength	• Of the 30 columns tested under different loads and heating intensities, 22 columns suffered various types of explosive spalling. • In all tests, explosive spalling happened in the first 45 mins of the heating where minor spallings took place. This was followed by major and severe spallings. • Tests also showed that loading levels up to 60% of the design strength have no significant effect on the probability of concrete spalling both under high and low heating regimes.	• The study considers major factors affecting fire resistance and compares the changes in behavior. • The tests provide a good

Table 2.1 Contd. Experimental studies on fire resistance of reinforced concrete columns

	columns subjected to fire, with a special attention directed towards explosive spalling. Objectives: • To investigate the effect of structural parameters on the performance of NSC and HSC columns under fire. To study the feasibility of using polypropylene fibers to prevent explosive spalling.	concrete were considered. • The failure criterion adopted in the tests was that a failure occurs when the column displacement (in contracting phase) passed the zero datum line (displacement before heating). The parametric study investigated the effect of degree of restraint, loading level and heating rates on the performance of RC columns subjected to fire. • Four loading levels were involved. • Three vales for the degree of restraint were involved, = applied axial stiffness/column axial stiffness.	• Low heating rates minimized the risk of explosive spalling. • Restraint forces decrease if the loading levels are increased. It also showed that increasing the degree of restraint increased the restraint forces generated in the columns.	understanding of the behavior of RC columns under fire exposure. • The effect of changing cross section, eccentricity and concrete cover thickness is not considered in the study.
Benmarce and Geunfoud [2004]	Objectives: to investigate the influence of: 1. boundary conditions. 2. different load ratios on HSC columns under fire. 3. restraint force.	• Twelve HSC columns subjected to three different load ratios, (20, 40 and 60% of design load from BS8110), at two restraining ratios, (0.1 and 0.2) and two heating rates, (high BS476 and at a lower rate were tested. • Each column was reinforced with four 12 mm dia. steel bars • To provide the variable stiffness that was required for the test specimens, a number of rubber springs with different stiffness	• Minor spalling was observed in fire tests. • Failure due to excessive axial deflection was noticed on most specimens. • The restraint system generally produced the desired effect of a linear increase of force with axial deformation, which translated to a linear increase of force with temperature. • Increasing the load	• The study provides a good understanding on the behavior of RC columns subjected to fire. • Very detailed observations are made during the test on the effect of load ratio and restraint ratio.

Table 2.1 Contd. Experimental studies on fire resistance of reinforced concrete columns

		were introduced into the restraint system.	ratio from 0.2 to 0.6 reduced the axial expansion values to almost one third. • The rate of heating has an inverse effect on failure time. • Imposing a restraint against axial expansion, leads to less forces generated in the column. • The maximum value of axial deformation is independent of the rate of heating and it is dependent on the load that has been applied.	• Effect of parameters such as aggregate type, addition of fibers and eccentricity were not considered in the study.

Table 2.2 Analytical studies on fire resistance of reinforced concrete columns.

Study	Objective / Study Details	Analysis/Model Features	Observations / Conclusions	Strengths/Drawbacks
Lie and Celikkol [1991]	Develop a mathematical model for predicting the fire resistance of circular RC columns.	Analysis Technique: • Finite Difference Method Features: • Standard fire given by ASTM E119 CAN4 - S101. Validation against: • Full scale fire resistance tests on RC columns tested by NRC and PCA.	• Fire resistance predictions can be done with an accuracy adequate for practical purposes. • The temperature predicted was very similar but varied slightly towards the center due to not accounting for moisture migration.	• The model can also be used to calculate fire resistance of RC columns with different concrete types if relevant material properties are known • Only standard fire scenarios were used in the model. • Applicable for circular cross-sections only.
Lie and Irwin [1993].	Develop a mathematical model for predicting the fire resistance of rectangular RC columns.	Analysis Technique: • Finite Difference Method (FDM) Features: • Standard fire given by ASTM E119 or CAN4 - S101. Validation against: • Full scale fire resistance tests on RC columns tested by NRC and PCA.	• Predictions of fire resistance can be done with accuracy adequate for practical purposes. • The temperature predicted was very similar but varied slightly towards the center due to migration of moisture. • Performance of rectangular RC columns under fire was found to be better than square RC columns of same c/s area.	• The model can also be used to calculate fire resistance of RC columns with different types of concrete if relevant material properties are known • Only standard fire scenarios were used in the model. • Applicable for rectangular or square cross sections only.
Franssen, and Dotreppe [2003].	To develop two simplified methods for calculation of fire resistance of RC columns.	• Method 1: This is a simple empirical equation which expresses fire resistance as an exponential function of five different variables,	The first simplified approach is easier to use and quick but gives very conservative results. • The second more elaborate method takes into account	• A simple model for spalling is used in the proposed method which is incapable of considering explosive spalling phenomena. • The proposed methods are fast,

Table 2.2 Contd. Analytical studies on fire resistance of reinforced concrete columns.

		such as axis distance, the buckling length and section dimension to list a few. Method 2: This method is a more elaborate and can be considered as a simplified calculation method. The ultimate load capacity is expressed as a fraction of the plastic crushing load of the section. Validation against: Four columns of circular cross section of diameter 300 mm and a length of 2100 mm were tested.	spalling, but the results were too conservative leading to the following considerations: • Despite the circular shape of the columns, surface spalling was observed in the four tests thus stating the need to account for it. A new calibration for the circular geometry was needed and accordingly made.	conservative and a good substitute for generating rough estimate of fire resistance. • Applicable for NSC columns only.
Kodur [2003]	To develop fire resistance design guidelines for HSC columns.	Features: • Columns of square cross section 305 mm x 305 mm and 3810 mm long were studied. • ASTM E119 fire exposure. The parameters studied: • Concrete strength from 34 MPa (typical for NSC) to 110 MPa (typical for HSC). • Type of aggregate in concrete. • Tie configuration. • Addition of fiber reinforcement. • Type of fiber. • Load intensity. • Eccentricity of load.	• Concrete Strength: Strengths higher than 70 MPa are more susceptible to spalling and may result in lower fire resistance. • Concrete moisture content: Higher spalling occurs in HSC as the time required to attain acceptable relative humidity level is more. • Other factors influencing fire resistance and spalling are: concrete density, fire intensity, specimen dimensions, lateral reinforcement, fiber reinforcement, load intensity, and type of aggregate	• Simple guidelines are proposed to improve the fire performance of HSC columns. • However the guidelines are broad in nature and does not quantify the extent of the influence of specific parameters.

Table 2.2 Contd. Analytical studies on fire resistance of reinforced concrete columns.

Kodur et al. [2004].	To develop a numerical model for tracing the behavior of HSC columns exposed to fire. Columns studied: • Non slender square columns.	Analysis Technique: • Finite difference method (FDM) Features: • Standard fire given by ASTM E119 or CAN/ULC S101. • Variation of temperature across each member is possible in the program. • Accounts for spalling. Validation against: • Full scale fire resistance tests on 15 RC columns with varied parameters like aggregate type, fibers added in concrete and moisture content.	• The predicted fire resistances were within 10% of the measured value for plain HSC and within 20% for fiber reinforced HSC column. • Due to ties bent at 135o, most of the spalling occurred outside the reinforcing core • The model can also be used for the calculation of fire resistance of columns made with other concrete if relevant material properties are used.	• More accurate model for spalling needs to be used for better prediction of fire resistance. • The model is validated only for standard fire scenarios.
Tan and Yao [2003]	To develop simplified method to predict the fire resistance of RC columns subjected to four-face heating. Numerical simulations: • Large number of RC columns with different slenderness ratios, load levels,	Analysis Technique: • Extension of ACI method at room temperature. Features: • SAFIR computer program was used for numerical simulations. • Material properties of concrete at elevated temperature were taken as given by Dotreppe et al. (1997). ISO 834 fire scenario was considered. • Both uniaxial and biaxial bending of columns were considered. • Only rectangular sections were considered. • Columns were assumed to be heated on all four sides.	• The study shows good agreement with the test results. • Gives a simplified approach for determining the fire resistance. • The results using this approach are consistent and conservative. • The method assumes slenderness ratio less than or equal to 100 and load eccentricity less than or equal to half of longer cross sectional dimension.	• Uniaxial and biaxial bending of columns considered. • Gives a simplified approach for determining the fire resistance. • The limitation is that different fire scenarios cannot be

Table 2.2 Contd. Analytical studies on fire resistance of reinforced concrete columns.

	eccentricities, cross-section areas and concrete covers were analyzed using SAFIR and compared with the results from the simplified model.			used for calculations. • Changes in behavior of concrete due to use of HSC, aggregate type, fibers added in concrete cannot be incorporated. • Spalling is neglected. • The method is applicable only to columns heated on all four sides.
Tan and Yao [2004]	To predict the fire resistance of RC columns subjected to 1-, 2- and 3-face heating. This study builds on the model "four-face heating" developed by the authors. Numerical Simulations: • Sixty four RC column tests from three laboratories were collected from literature and were analyzed using computer program SAFIR.	Analysis Technique: • Extension to ACI method at room temperature Features: • SAFIR computer program was used for numerical simulations. • Material properties of concrete at elevated temperature were taken as given by Dotreppe et al. (1997) and ISO 834 fire scenario was considered. • Both uniaxial and biaxial bending of columns were considered. • Assumed that there are no convective heat losses between fire and the heated surface. • Only rectangular sections were considered.	• The study shows fair agreement with the results from SAFIR and tends to be conservative as the model includes the effect of spalling. • Gives a simplified approach for determining the fire resistance.	• The advantages and limitations are the same as the model for four face heating presented above. • This model can be used for 1, 2, 3, or 4 sides of columns exposed to fire.

Table 2.2 Contd. Analytical studies on fire resistance of reinforced concrete columns.

Bratina et al. [2005]	To develop a two-step finite element formulation for the thermo-mechanical non-linear analysis of the behavior of RC columns in fire. The authors compare the results from the model with the results from the Eurocode.	Features: • The temperature in the steel bar is assumed as being that of concrete at its location. • The moisture transport, its evaporation and condensation in concrete is ignored, although the effect of moisture distribution histories may be significant, particularly for a higher initial moisture content. Thus the flame emissivity of fire, which has more significant effect than the moisture, can safely be ignored. • The formulation is based on the modified Hu–Washizu functional of the kinematically exact planar beam theory of Reissner (1972). The only unknown functions in the functional (the extensional strain, 'e', and the pseudo-curvature, 'j') are approximated by the Lagrangian interpolation scheme. The remaining unknown functions, i.e. displacements, the rotation and the internal forces and moments, appear in the functional only through their boundary values.	• The comparison of predictions from the model with test data shows a good agreement in the fire resistance values. • The agreement in the variation of the axial displacement with time was only qualitative. • The comparison of predictions showed that Eurocode gives a less conservative value of fire resistance.	• The behavior of HSC is not incorporated. • Spalling is ignored.

Table 2.2 Contd. Analytical studies on fire resistance of reinforced concrete columns.

Kodur [2005]	To develop resistance design guidelines for HSC columns.The various factors that influence the structural behavior of HSC columns under fire conditions were discussed. Design guidelines were presented for mitigating spalling and enhancing fire endurance of HSC columns.	• Data from fire experiments is used to quantify the influencing factors on spalling and fire resistance of HSC columns. The test columns were 3810 mm in length and of a cross section of 305x305 mm. The test variables included column dimensions, concrete strength, type of aggregate, tie configuration, addition of fiber reinforcement, type of fiber, load intensity and eccentricity of loading. Data from both NSC and HSC columns were considered in the analysis. The fire exposure was that of ASTM E119 standard temperature–time curve. • The behavior of HSC under fire is studied and summarized. • The factors governing fire performance are also discussed in detail.	Guidelines for fire resistant design of HSC columns on the following factors are provided: • Size of the member. • Tie configuration. • Addition of polypropylene fibers. • Addition of steel fibers. • Effect of aggregate type. • Cover thickness.	• The paper gives a good idea on the effect of fire and the characteristics of the phenomena. • It states the factors which influence fire performance and provides a good explanation for their effect. • The paper does not talk about how to use the design guidelines for achieving optimum fire performance. i.e. it does not quantify the extent of influence of various factors on spalling in fire resistance.

Table 2.3 Provisions in building standards of various countries

Standard	Provisions	Strengths/Drawbacks
ACI 216, USA	• The concrete cover provisions for a required fire resistance rating have been given. • The provisions are divided in two categories based on concrete strength ($f_c' < 12$ ksi and $f_c' > 12$ ksi). • For columns having design compressive strength of 12 ksi (83 MPa) or less the least dimension of RC columns of different types of concrete are specified in a table based on the aggregate type and the resistance time required. • Two different tables have been given for four side exposure and the other for 2 parallel side exposure. • The values given on two parallel side exposure can be used for three and four sides provided that one set of the two parallel sides of the column is at least 36 in. (915 mm) long. • The least dimension for RC columns of compressive strength on greater than 12 ksi (83 MPa) for a rating of 1-4 hours is given as 24 in. (600 mm). • Specifications on the ties have been given in order to ensure required fire performance.	• The provisions are prescriptive in nature. • The fire resistance is based on the concrete cover thickness, aggregate type and the dimension of the column and thus ignores other important factors affecting the fire resistance.
National Building code, Canada	• Simple empirical formulas are provided to compute the minimum column dimensions based on the required fire resistance rating in hours. • Similarly the minimum cover thickness required for given fire resistance rating is also provided. • Additional provisions for the provision of plaster are also provided.	• The provisions are prescriptive in nature. • The fire resistance is only based on concrete cover thickness, aggregate type and the dimension of the column and ignores a number of other factors influencing fire resistance.

Table 2.3 Contd. Provisions in building standards of various countries

Eurococde 2, Europe	• Part 1–2: Structural fire design, gives a choice of tables, simplified or advanced methods for determining fire resistance of columns • The tables (based on standard fire tests) give the minimum dimensions and the cover required for attaining the desired fire resistance. • Two methods have been given for determining the fire resistance. One being more detailed and the other simpler. • Specifications for the minimum percentage of steel and its spacing have also been provided.	• The "advanced method" provisions are of more detailed nature and can be used in performance-based design. • The advanced method suggested for calculating the fire design account for the majority of the factors influencing fire resistance.
AS 3600, Australia	• Two different clauses for calculating the fire resistance of columns are specified: for four (all) face exposure and the other for all faces exposed but satisfying some special conditions. • An equation to calculate the fire resistance of columns based on various parameters is given.	• The equation accounts for many of the influencing parameters. • Spalling is not considered. • Aggregate types are not considered in the equation.

Table 2.4 Prediction of fire resistance values for column III 14 [Lie and Woolerton, 1988] using different codes

Fire Resistance (min)	Measured (test)	ACI	Eurocode	Australian Code
Column III14	183	180	161	234

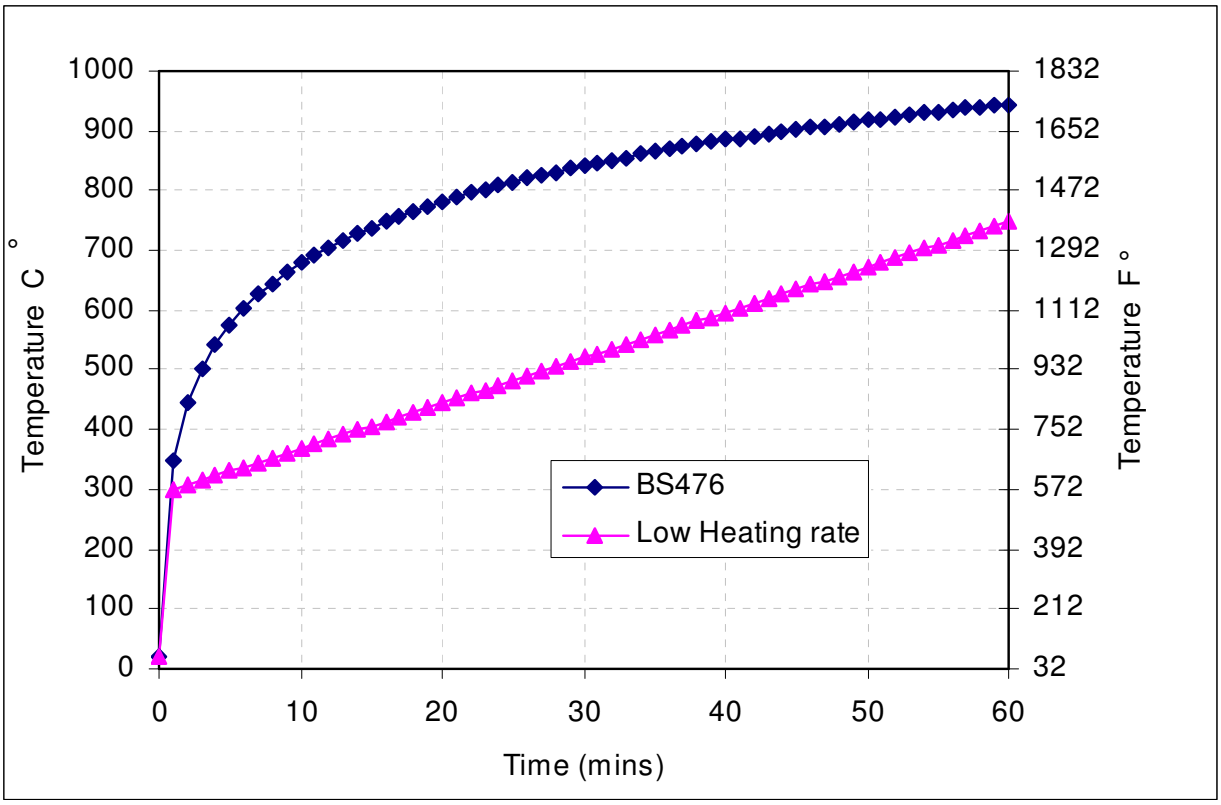

Fig. 2.1 Heating rates used for fire tests on RC columns [Ali et al., 2001].

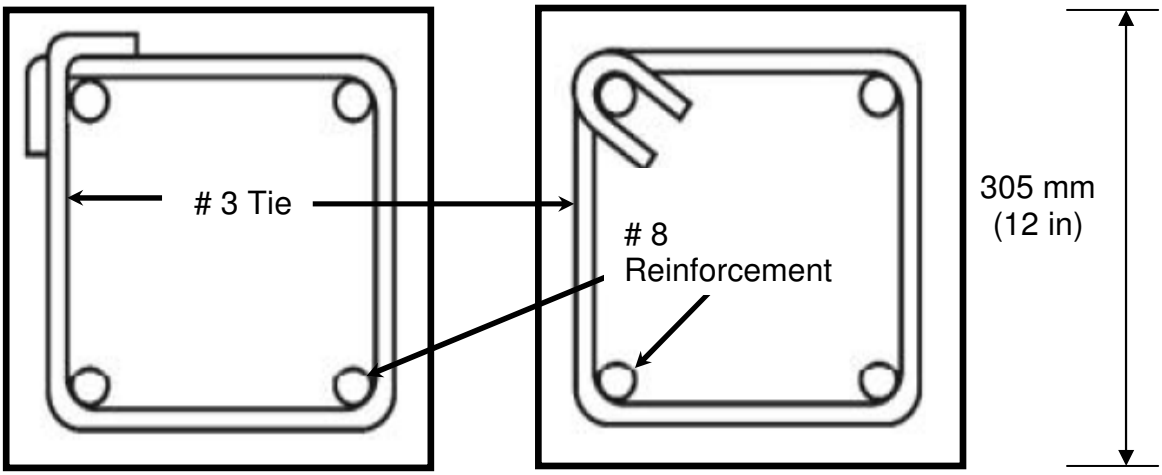

(a) Ties bent at 90° (b) Ties bent at 135°

Fig. 2.2 - Typical layout of ties used in RC columns [Kodur, 2003].

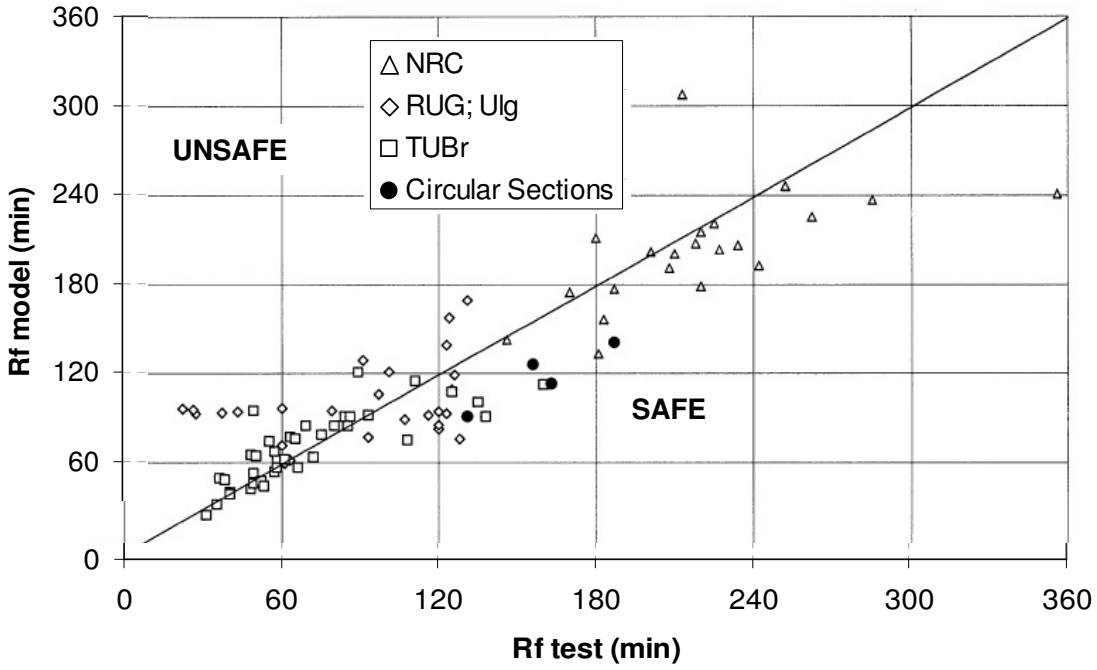

Fig. 2.3 Comparison of fire resistance predictions from simplified equation and test data [Franssen and Dotreppe, 2003].

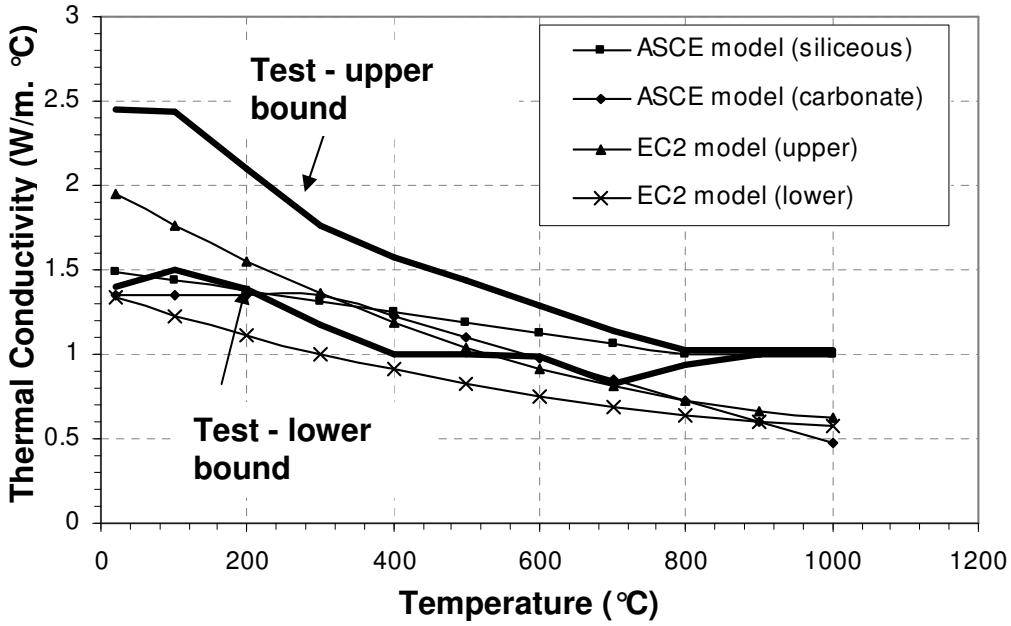

Fig. 2.4 - Variations of measured and predicted of thermal conductivity for NSC as a function of temperature

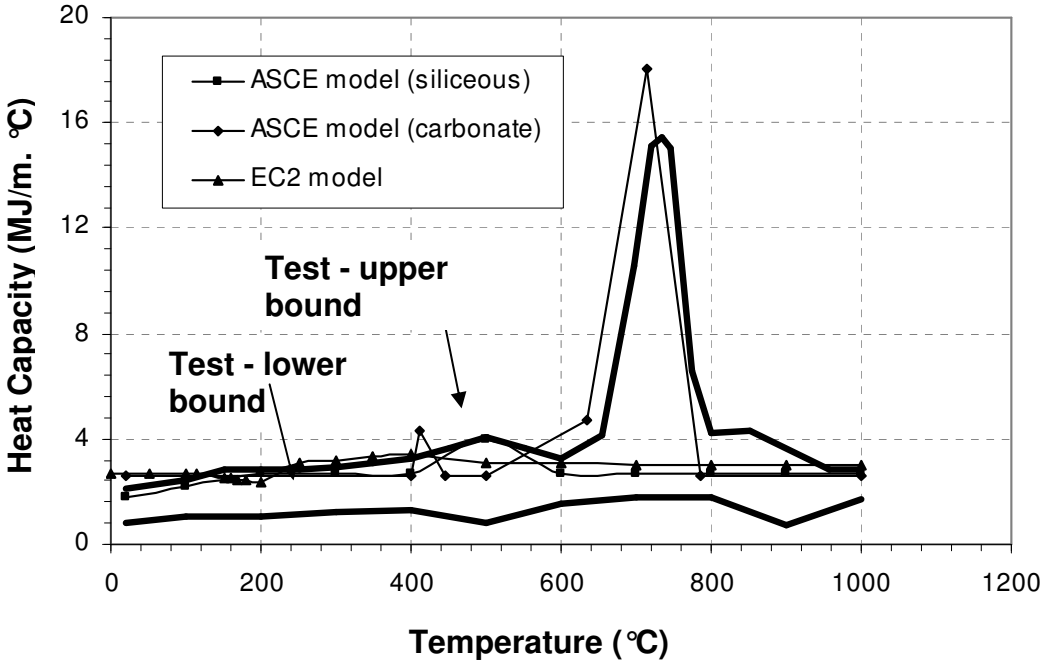

Fig. 2.5 - Variations of measured and predicted of thermal capacity for NSC as a function of temperature

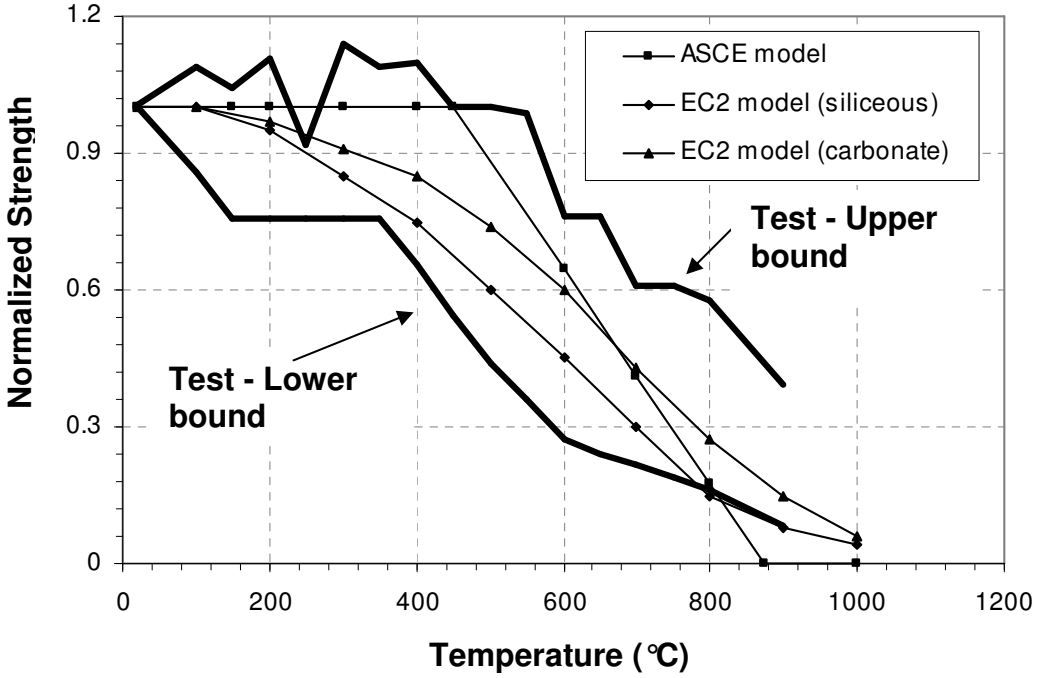

Fig. 2.6 - Variation of compressive strength as a function of temperature for NSC

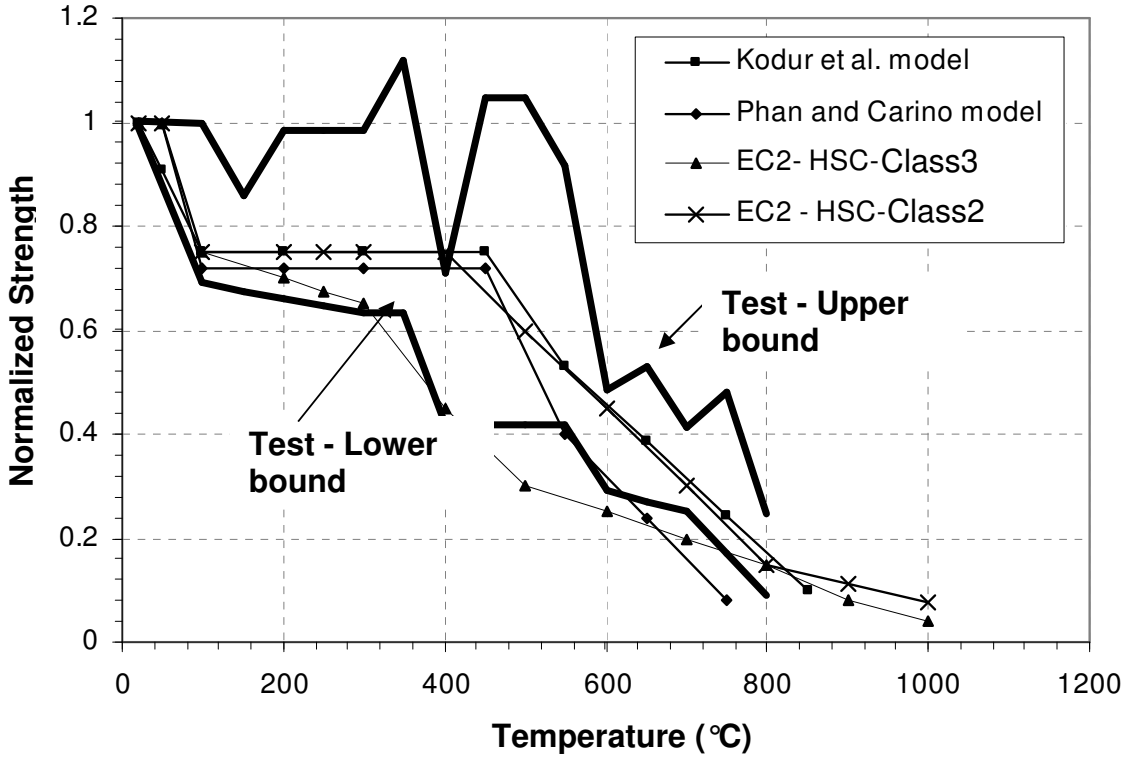

Fig. 2.7 - Variation of compressive strength as a function of temperature for HSC

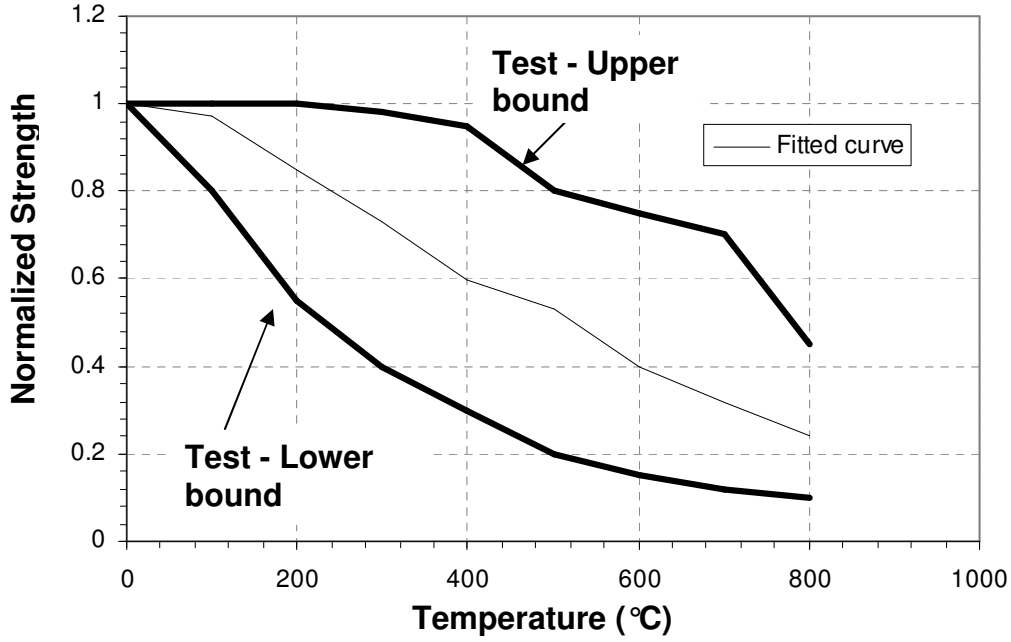

Fig. 2.8 - Variation of residual compressive strength as a function of temperature [Kumar 2003]

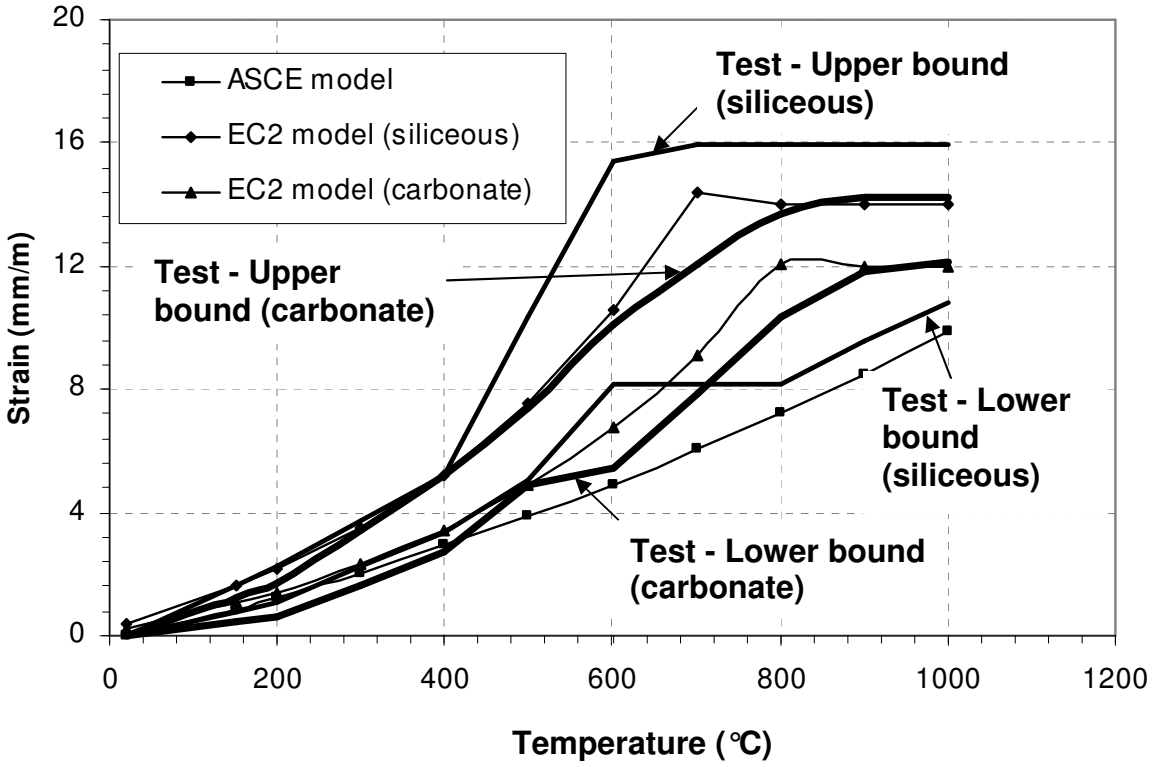

Fig. 2.9 - Variations of measured and predicted of thermal expansion for concrete as a function of temperature

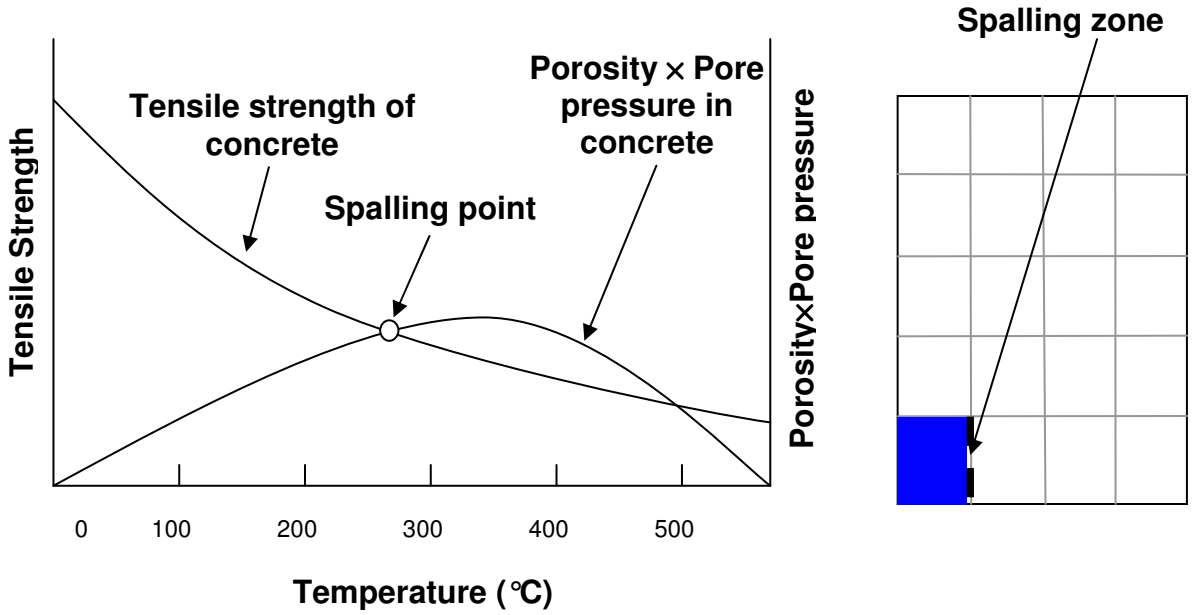

Fig. 2.10 – Illustration of occurrence of spalling

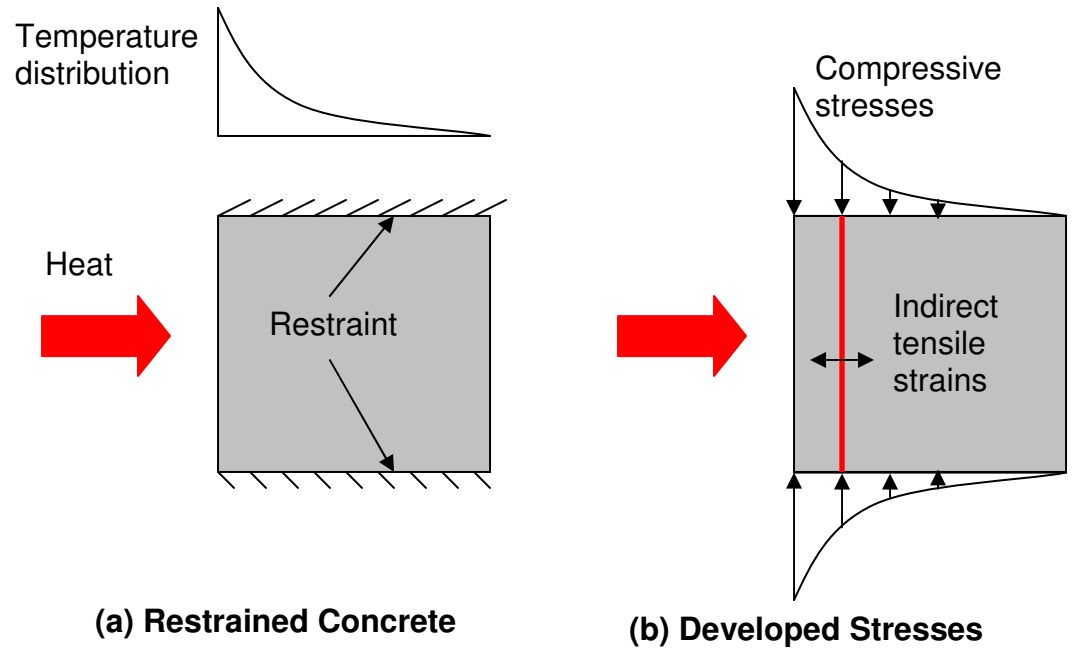

Fig. 2.11 – Illustration of thermal dilation mechanism for fire induced spalling

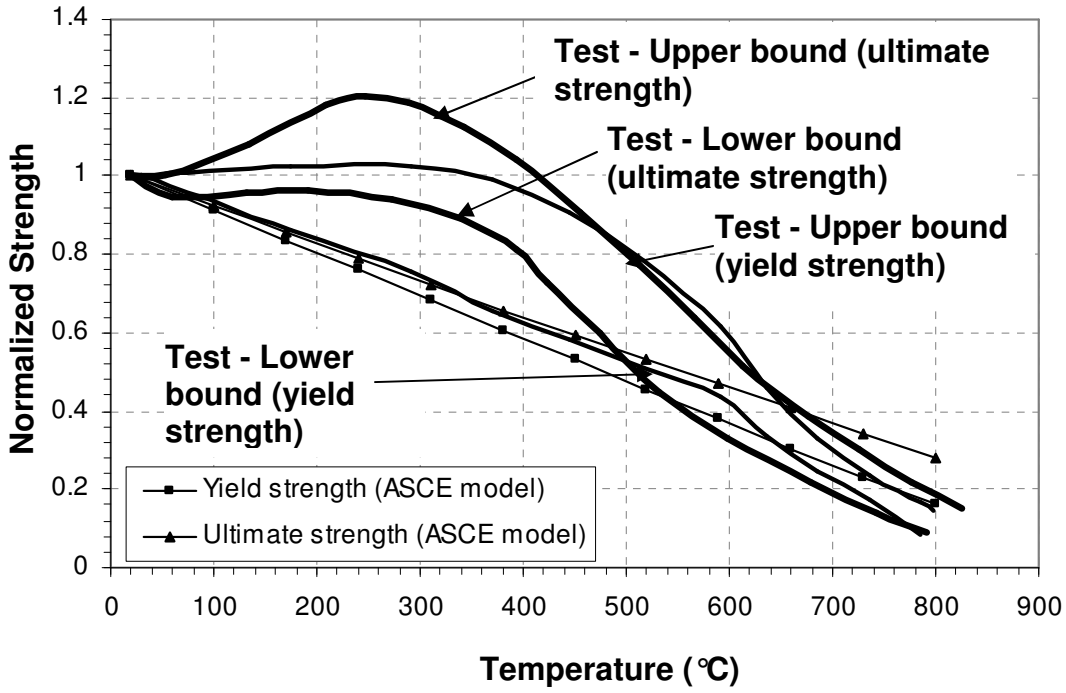

Fig. 2.12 – Variations of measured and predicted ultimate and yield strength of reinforcing steel as a function of temperature

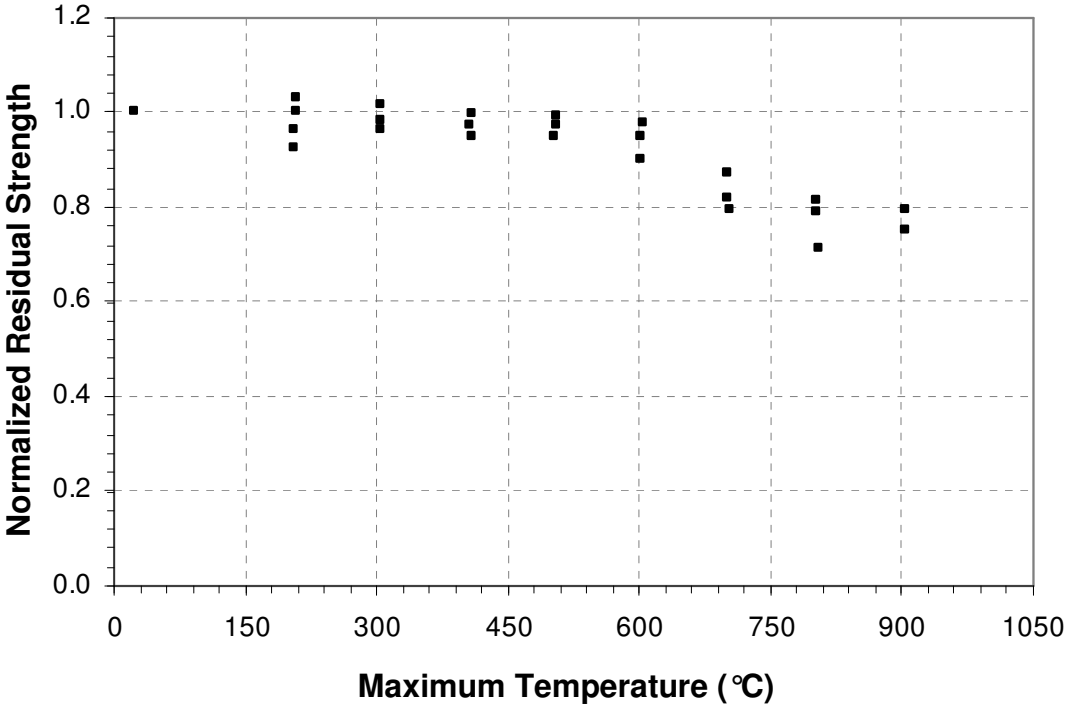

Fig. 2.13 – Measured residual yield strength of reinforcing steel [Neves et al. 1996]

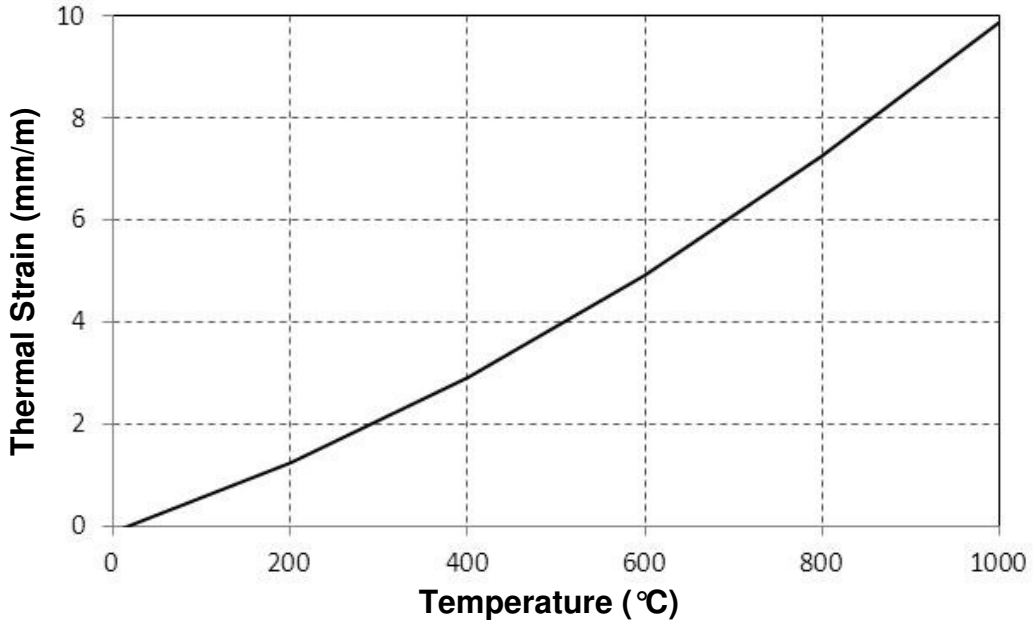

Fig. 2.14 – Variation of thermal strain of reinforcing steel as a function of temperature [ASCE Manual 1992]

CHAPTER 3

3 EXPERIMENTAL STUDY

This chapter is mainly based on the following journal papers:

- Raut N. and Kodur V., (2011) "Response of High Strength Concrete Columns under Design Fire Exposure", In Press, ASCE – Journal of Structural Engineering.
- Kodur, V.R, Raut N., (2009) "Enhancing the Fire Performance of HSC Columns through Polypropylene Fibers", Proceedings of NSF Engineering Research and Innovation Conference, Honolulu, Hawaii.

3.1 General

The state-of-the-art review indicated that numerous fire tests have been conducted on RC columns. However, most of these experiments were carried out under standard fire conditions without any consideration for critical factors such as realistic fire exposure, load level, and presence of polypropylene fibers, which influence the fire resistance of RC columns. Also spalling was qualitatively monitored during these tests and thus not much data is available on the amount of spalling which is crucial for validation of spalling sub-models. To overcome these limitations discussed, an experimental study was undertaken to develop a better understanding on the behavior of NSC and HSC columns under realistic fire, and loading scenarios. This chapter presents results of fire resistance experiments that were carried out on six RC columns under realistic conditions. These tests were aimed at investigating the effect of load level, concrete strength, fire scenario and addition of polypropylene fibers on the response of RC columns. The tests were designed to collect large amount of data including cross-sectional

temperatures, axial deformations, spalling progression, and failure time and modes, for validation of finite element model presented in Chapter 4. Full details of the fire experiments, including specimens' instrumentation, fire tests procedure and measured parameters are presented in this chapter.

3.2 Experimental Details

The experimental program consisted of conducting fire resistance tests on six reinforced concrete columns (1 normal strength concrete (NSC), 3 high strength concrete (HSC), and 2 high strength concrete with polypropylene fibers (HSCP)) designated NSC1, HSC1, HSC2, HSC3, HSCP1 and HSCP2 based on the type of concrete. Following are the details of the experimental program.

3.2.1 Test Specimens

The steel of main reinforcing bars and stirrups had specified yield strengths of 420 MPa. Based on the tensile strength tests the yield strength, ultimate strength, and ultimate strain of steel rebars were found to be about 450 MPa, 705 MPa and 0.17, respectively. In each beam, the bars were tied with the stirrups to form a steel cage as shown in Figure 3.1. Then, each steel cage is placed horizontally in wooden formwork which was properly designed and fabricated to have the same internal dimensions as those of the tested beams. To achieve good quality control, concrete mix was ordered from a local concrete plant.

Three batches of concrete were used for fabricating columns. Column NSC1 was fabricated from NSC mix (Batch 1), while columns HSC1 through HSC3 were fabricated from HSC mix (Batch 2). For columns HSCP1 and HSCP2 the batch mix consisted of HSC with polypropylene (HSCP) fibers (Batch 3). All batches of concrete were made with general purpose, Type I Portland cement and carbonate aggregate. The mix proportions, per cubic meter of concrete are presented

in Table 3.1. The average compressive cylinder strength of concrete measured at 28 days and on the day of the testing is provided in Table 3.2. Three cylinders from each batch were tested to evaluate compressive strength at 7, 28 and 90 days respectively.

All columns were cast horizontally and the HSC and HSCP columns were moist cured in the forms for 7 days, whereas the NSC columns were sealed in the forms for 7 days (see Figure 3.2). Then all the specimens were lifted from the forms and stored in air maintained at about 25°C and 40% relative humidity. The moisture condition (relative humidity) was measured at a depth of 100 mm of the column using a relative humidity probe on the day of the test (about 8 months after fabrication of these columns). The relative humidity of HSC and HSCP columns is higher than that of NSC columns as can be seen from the tabulated values in Table 3.2. This can be attributed to the fact that the depth of 100 mm, where the relative humidity was measured, is at the center of the column (most humid location) and the low permeability of HSC and HSCP columns, due to higher compactness of these mixes, leads to lesser evaporation of moisture. Since the permeability of these concretes is lower than NSC, the rate of loss of water present in the columns is slower and thus the relative humidity is high.

All columns were 3350 mm long and were of square cross section of 203×203 mm. All columns had 4 ϕ20 mm bars as longitudinal reinforcement and had ϕ10 mm stirrups, with a spacing of 200 mm, over the length of the column as transverse reinforcement. The ties were anchored in the core to a length of 3 inches (as per ACI 318, 2008 provisions) (see Appendix B). Steel plates 400×400×25 mm were attached to the top and the bottom of the column in order to fix the column in position and for load transfer from the actuator. The plates were bolted using four steel angles of 100×100×12mm per end of the column. The bottom end of the column was bolted to a steel plate fixed to the floor and thus the bottom end can be assumed to be fully restrained

against rotation for numerical analysis. The top end, as it is bolted to the actuator which rests on a structural frame, does not provide full rotational fixity and has a rotational stiffness of 250KN.m/μrad. Figure 3.3 shows the elevation and cross-sectional details of the columns, while Table 3.2 gives additional details of column specifics.

3.2.2 Instrumentation

The instrumentation in the columns included thermocouples, strain gauges and displacement transducers. Type-K Chromel-alumel thermocouples, 0.91 mm thick, were installed at the mid-height cross section in each column for measuring concrete and rebar temperatures. Each of the columns was instrumented with 7 thermocouples. Also strain gauges (both high temperature and normal temperature types) were mounted on the rebars at mid-height of columns. The location and numbering of thermocouples and strain gauges in the cross-section are shown in Figure 3.3. Figure 3.4 shows thermocouples and strain gauge after being installed in position within the reinforcement cage. The axial deformation of each column was measured at the top of the column using displacement transducers (LVDTs).

3.2.3 Test Apparatus

The fire resistance tests on RC columns were carried out using structural fire testing furnace recently commissioned at Michigan State University. The test furnace has been specially designed to produce conditions, such as temperature, loads and heat transfer, to which a structural member might be exposed during a fire. The furnace, shown in Figure 3.5(a), has the capacity to supply both heat and applied loads that are present in a typical building exposed to fire.

The furnace consists of a steel framework supported by four steel columns, with a fire chamber that is 2.44 m wide, 3.05 m long, and 1.68 m high. The maximum heat power the furnace can produce is 2.5 MW. Six natural gas burners located within the furnace provide thermal energy, while six type-K Chromel-alumel thermocouples as per ASTM E119 [2008], distributed throughout the test chamber, monitor the furnace temperature during a fire test. During the fire test, these furnace temperatures are used to manually adjust fuel supply, and maintain a temperature course consistent with the pre-determined standard or realistic fire scenario. In this way, the furnace temperature can be maintained along a desired curve. Two small view ports on either side of the furnace wall are provided for visual monitoring of the fire-exposed specimens during a test. The furnace accommodates two columns at a time and different load levels can be applied on each column.

3.2.4 Test Conditions and Procedure

The fire resistance tests were carried out by placing two RC columns in the furnace and exposing them to a desired fire exposure. The columns were of 3.35 m high, with the middle 1.7 m of the column height exposed to fire as seen in Figure 3.5(b).

To investigate the effect of fire scenario on column response, the RC columns were tested under three fire scenarios. Columns NSC1 and HSC1 were tested under ASTM E119 standard fire exposure [ASTM 2008], while the remaining four columns were tested under two design fire exposures. These design fires represent parametric fires in Eurocode 1 [1994] wherein resulting fire consists of a growth phase and decay phase. Both phases of the fire are influenced by the compartment characteristics including fuel load (amount of combustible materials), ventilation openings, and wall lining materials [Feasey and Buchanan, 2002].

The short fire (SF) selected for fire test on columns HSC2 and HSC3 corresponds to Eurocode 1 parametric fire for a room with dimensions of 6 m × 4 m × 3 m having a fuel load of 250MJ/m^2 and a ventilation factor of 0.04. Similarly, the long fire (LF) selected for columns HSCP1 and HSCP2 corresponds to a Eurocode 1 parametric fire for the same size room but with a fuel load of 600MJ/m^2. Further in the long fire it is assumed that the ventilation factor increases to 0.2 after attaining peak temperature due to breakage of windows (glass). The values of fuel load and opening dimensions are given in Table 3.3.

The time temperature curve for the three fire scenarios (ASTM E119 standard fire, SF, LF) is shown in Figure 3.6. It can be seen that design fires SF and LF follow similar temperature profile as that of ASTM E119 in the growth phase of the fire, but have a well-defined decay (cooling) phase, obtained by controlling the temperatures in the furnace (by blowing air through the furnace) to decay at a predetermined rate of cooling, as encountered in real fires in buildings.

All columns were slender columns as per ACI 318 [2008] and were tested under a concentric axial load with fixed supports. The columns were tested under concentric axial loads. Since special care was taken to align the center of the loading actuator and the top steel plate the eccentricities are within ± 5mm. The type of fire exposure and the load ratio for the various columns are tabulated in Table 3.2. The load ratio is the ratio of the applied (test) load to the column capacity computed according to ACI 318 [2008].

The load was applied approximately 30 minutes before the start of the fire test and was maintained until a condition was reached at which no further increase of the axial deformation of the column could be measured. During the test, the column was exposed to heat controlled in such a way that the average temperature in the furnace followed, as closely as possible, the targeted fire scenario (measured in terms of time temperature curve of ASTM E119 standard fire,

SF, or LF). The load was maintained constant throughout the fire test duration. The columns were considered to have failed when the hydraulic jack could no longer maintain the load.

3.2.5 During and Post-Test Observations

During the test, the columns were exposed to heat controlled in such a way that the average temperature in the furnace followed, as closely as possible, the targeted time-temperature curve (ASTM E119 standard fire, SF, or LF). The load was controlled such that it was maintained constant throughout the test. The test data including furnace temperatures, specimen temperatures, strains, axial deformations, and loading were recorded every 5 seconds through the data acquisition system. Observations were made every 5 minutes through the view ports in the furnace to record any major changes in the specimens such as fire induced spalling or visible cracks. The columns were considered to have failed and the tests were terminated when the hydraulic jack could no longer maintain the load.

After the fire tests, post-fire inspection was carried out to record any fire induced spalling, and concrete cracking in the tested columns. In addition, the columns were stored to conduct volumetric measurements to quantify the volumes of spalled concrete from each column during the fire tests. The exposed length of each column was divided into a number of segments and the volume of each segment is computed by taking measurements with respect to a reference axes system. The total volume of a damaged column was then computed as the sum of the volumes of all the segments, and used to compute the spalled volume of concrete in that column.

3.3 Results

The comparative performance of NSC, HSC, HSCP columns under different conditions is evaluated by studying the thermal response, structural response, spalling progression, as well as fire resistance, and is presented in the following sections.

3.3.1 Thermal Response

The thermal response of all six columns is presented in Figure 3.7 by plotting rebar and concrete temperatures at various thermocouple locations. The locations of the thermocouples are as shown in Figure 3.3 (section BB). Columns NSC1 and HSC1 were exposed to ASTM E119 standard fire (without a decay phase) but the remaining four columns were exposed to design fires with a well-defined decay phase as shown in Figures 3.6. In all six columns the rebar and concrete temperatures plateau at about 100°C and this can be mainly attributed to the utilization of heat energy (from fire) for the evaporation of water in concrete. After the plateau, the temperatures in rebar and concrete increase with fire exposure time. It can be seen that the measured temperature at mid-depth of concrete is lower than that at the rebars and this is due to the lower thermal conductivity and higher thermal capacity of concrete which slows down heat penetration to the inner layers of concrete.

Since the initial portion of the design fires (prior to the decay phase) followed the time temperature curve as per ASTM E119 standard fire, all three columns had same fire exposure up to 90 minutes and cross-section temperatures can be compared directly. It can be seen from Figure 3.7 that the measured temperatures in rebars and concrete (at 100 mm concrete depth) in the NSC column (NSC1) are lower than the corresponding temperatures in the HSC columns (HSC1, HSC2, and HSC3) throughout the fire exposure. This variation in temperature profiles can be partly attributed to slight differences in thermal properties of the two concretes resulting from higher compactness (lower porosity) of HSC and also due to the occurrence of spalling in the HSC columns. The higher thermal conductivity of HSC resulting from lower porosity slightly increases the rebar and concrete temperatures in the HSC column. Also, in the case of HSC

columns there was some surface spalling and this loss of concrete led to faster rise in temperatures.

The rebar and the cross section temperatures in column HSCP1 and HSCP2 are similar to that of column NSC1. This is on expected lines since polypropylene fibers in these two columns helped to mitigate spalling by alleviating pore pressure. The polypropylene fibers melt at around 160°C [Khalifa et al. 2001] and thus columns are likely to have similar permeability as that of column NSC1. Polypropylene fibers mitigate spalling by alleviating pore pressure through: (a) working as reservoirs (air bubbles or micro cracks) or (b) as continuous channels for moisture migration (pressure induced tangential space or through space vacated by vaporization of pp fibers) [Khoury, 2009]. This theory of pressure release through melting of pp fibers is widely accepted to be the mechanism for spalling mitigation.

3.3.2 Spalling Pattern

The extent of spalling during the fire tests was monitored by making observations through the window ports of the furnace and through post-test observations of columns. Based on test results the extent of spalling in the six tested columns was classified as minor, moderate, and severe and is given in Table 3.2. Spalling is said to be 'minor' when only small chunks of concrete peels-off of the surface (from outer layers) of the RC column. Spalling is said to be 'moderate' when the extent of spalling does not reach the steel reinforcement, while it is said to be 'severe' when spalling results in reinforcement (longitudinal and transverse) being exposed to fire.

Minor spalling, in the form of surface scaling, occurred in column NSC1. However, severe spalling occurred in columns HSC1, HSC2 and HSC3. This can be attributed to the higher compactness and lower permeability of high strength concrete which facilitates the pore pressure build-up within the cross section and when this pressure exceeds the tensile strength of concrete,

chunks of concrete fall-off from the surface. In case of HSC columns when the concrete temperatures reach about 250-300°C the fire induced pore pressure exceeds the reduced tensile strength of concrete and at this stage chunks of concrete fall off from the surface of the column. There was no spalling in columns HSCP1 and HSCP2, and this is because polypropylene fibers melt at relatively low temperatures (around 160°-170°C) and this melting increases the permeability of the concrete. This creates 'channels' for the generated steam pressure (within the concrete) to escape, thus preventing the small 'explosions' (spalling).

Figure 3.8 shows pictures of all six columns after fire resistance test. It can be seen that significant spalling occurred in the HSC column as compared to the NSC column. This can be attributed to the low permeability of HSC which significantly increases the fire induced spalling as discussed above. The presence of fibers helped to mitigate spalling in columns HSCP1 and HSCP2.

3.3.3 Structural Response

3.3.3.1 Axial Deformations

The measured axial deformations for the six tested columns are shown in Figure 3.9 as a function of fire exposure time. All columns expanded in early stages of fire exposure which is mainly due to the thermal expansion of both concrete and steel. With increased fire exposure time, the columns contract as a result of loss of strength in steel reinforcement due to increasing cross-sectional temperatures and also due to load redistribution to concrete from reinforcement. Since the reinforcement (longitudinal) is in the outer core of the section, the temperature rises much faster in steel than the inner core of concrete. When the steel (reinforcement) yields, concrete carries a progressively increasing portion of the load. The strength of the concrete also decreases

with time due to deteriorating properties of concrete, and ultimately, when the column can no longer support the load, failure of column occurs.

Previous fire resistance tests have indicated that the large deformation prior to failure results from high mechanical strains (due to significant loss of strength and stiffness of the column) and also from significant levels of high temperature creep [SFPE, 2008]. The high temperature creep is one of the main reasons for the significant increase in the deformations in columns HSC1 and HSC3 towards later stages of fire exposure. These columns experienced very high temperatures (in concrete and steel) prior to failure resulting in high stress ratio (where stress ratio is the ratio of the existing stress on the column to the strength of the column at a particular fire exposure time) which produces high creep deformations. However, due to the presence of a cooling phase, columns HSC2 and HSCP1 did not attain such high temperatures and thus significant creep deformation might not have occurred in these columns. Though column HSCP2 was subjected to a fire scenario with a cooling phase, it experienced higher deformations as compared to HSCP1 due to the higher stress ratios, caused by the higher load, and thus higher creep deformations.

The effect of concrete strength on the fire response of RC columns can be illustrated by comparing the axial deformation vs. time curves of columns NSC1 and HSC1 (subjected to ASTM E119 fire). It is seen that column HSC1 exhibits lesser expansion than column NSC1. This can be attributed to the higher rebar temperature in column HSC1 and also due to the faster degradation of strength and stiffness of HSC at elevated temperatures. Also, column HSC1 experienced severe spalling resulting in the loss of concrete cross-section thus reducing its load carrying capacity. This in turn leads to contraction or buckling (global) of column. The higher axial deformation in HSC1 led to early failure of the column resulting in lower fire resistance.

The effect of fire scenario on the structural response can be gauged by comparing the axial deformation trends of the columns HSC1 and HSC2 exposed to ASTM E119 standard fire and design fire (SF) respectively. Both columns show an expansion phase followed by a contraction phase. However column HSC1, which has a very short expansion phase, contracts at a faster rate and fails in a brittle manner at about 61 minutes. This behavior is mainly due to significant spalling that occurred in early stages of fire exposure. The loss of concrete resulted in higher temperatures which in turn led to higher fire induced creep deformations.

Columns HSC2 which was exposed to design fire with a cooling phase shows slower rate of axial deformations. Ideally column HSC1 and HSC2 should have demonstrated similar behavior up to 75 minutes of fire exposure as both columns were subjected to similar temperature profiles. However the post fire test observations show that column HSC1 suffered high amount of spalling from 1 face making the spalling pattern non uniform and thus causing additional bending moments in the column. This also led to quick rise in rebar temperatures in the highly spalled area leading to faster degradation of strength. This non uniform spalling can be attributed to the spatial variation in the permeability in concrete cross-section as discussed by Dwaikat [2009]. Since the spalling in column HSC2 (as observed from post fire test observations) was more uniform the temperature profile was symmetric and thus did not cause early buckling of the column. This helped column HSC2 to survive the heating phase. Following the growth phase of fire, it could withstand the applied load due to recovery in the strength and stiffness as the temperatures in the column cooled down.

Column HSC3, with higher applied load, failed even though the column was subjected to a fire scenario with a cooling phase. This is because this column failed before the rebar temperature

moved toward the cooling phase and thus no strength recovery was possible in this column. This can mainly be attributed to the higher load level on this column.

The effect of polypropylene fibers on the fire response of HSC columns can be seen by comparing the axial deformations of columns HSC1 and HSCP1. As discussed before HSC1 experienced moderate to severe spalling and thus had lesser expansion and higher axial deformations in the later stages of fire exposure. HSCP1 as stated earlier did not suffer any spalling due to the melting of polypropylene fibers and thus it behaved similar to NSC1. The mitigation of spalling helped this column to retain cross sectional area which in turn helped the column to sustain the applied load for a longer time.

The effect of load on the structural response of HSC columns can be gauged by comparing the axial deformations in columns HSC2 (40% load ratio) and HSC3 (60% load ratio) exposed to short design fire (SF). HSC3 experienced higher deformations mainly due to higher mechanical and creep strains occurring from increased load ratio.

3.3.3.2 Strain in Steel Rebars

The strains in the longitudinal reinforcement of the columns were monitored during the test using high temperature and normal temperature strain gages as shown in Figure 3.3 (section A-A). The measured strain in the longitudinal reinforcement of the central section in the six tested columns is plotted as a function of time in Figure 3.10.

It can be seen from Figure 3.10 that the strain data from NSC column, NSC1, seems to be record nonsensical measurements. This can be attributed to the cracking of concrete near the strain gauge, or de-bonding of the strain gauge from the reinforcing steel due to the increase in rebar temperature during exposure to fire. However, the strain gauges could collect sensible data for HSC columns HSC1, HSC2 and HSC3, the data could be collected only for up to 10 minutes of

fire exposure. One reason for this could be that the strain gauges were damaged due to the occurrence of spalling and/or due to being exposed to fire directly. The lack of spalling in HSC columns with polypropylene (HSCP1 and HSCP2) seemed to ascertain the continual operation of the strain gauges in these columns. The data recorded for the columns HSCP1 and HSCP2 correlated quite well with the axial deformations measure by the LVDT's. Thus it can be concluded that formation of cracks (and mainly spalling) damage the strain gauges easily and also possibly subject them to direct heat.

It should be noted that high temperature strain gages are generally unreliable due to the many complex physical and chemical processes that occur at elevated temperatures [Dwaikat, 2009]. The problem associated with the reliability of high temperature strain gages was also encountered by other researchers [Dwaikat 2009, Williams 2004, Bisby 2003]. Some previous researcher attributed the problem in strain gages to the electrical interference from the operation of the high voltage ignition and the control systems [Williams 2004]. One other reason for this problem could be that the strain gages were designed for low heating rate compared to the high rate of heating encountered (about 10℃ per minute for rebars) in fire exposure. Due to the lack of consistency, the strain gage data can not be confidently used to infer any strain trends in the tested RC columns.

3.3.4 Fire Resistance

A comparison of fire resistance of the six columns is given in Table 3.2. The time to reach failure is defined as the fire resistance and failure is said to occur when the strength of the column decreases to a level at which the column can not sustain the applied load. Only four of the six tested columns failed. Two of the columns which failed were exposed to ASTM E119 standard fire while the remaining two columns were exposed to design fire, but were subjected to higher

loads. Columns HSC2 and HSCP1 did not attain failure and survived burnout conditions. These failure patterns can be attributed to variation in test conditions (fire) and column characteristics (loading and concrete strength).

The fire resistance of columns HSC1 (61 minutes) was found to be lower than that of column NSC1 (183 minutes). This can be mainly attributed to the faster degradation of strength properties and the occurrence of moderate to severe spalling in HSC as discussed earlier. Due to the presence of polypropylene fibers, column HSCP1 did not experience any spalling and survived the burn-out conditions. This shows that the addition of polypropylene fibers can help mitigate spalling and thus achieve the desired fire resistance for HSC columns. Columns HSC3 and HSCP2 were both subjected to a higher load ratio (60%) as compared to columns HSC2 and HSCP1 respectively, which were subjected to a load ratio of 40%. Thus they attained failure and could not survive the burn-out condition. Column HSC3 due to spalling failed in 75 minutes, but column HSCP2 due to the presence of polypropylene fibers mitigated fire induced spalling and enhanced the failure time to 221 minutes.

3.4 Summary

Fire tests were conducted to study the behavior of axially loaded RC columns under different loading, concrete type, fire scenarios and presence of polypropylene fibers. Based on the fire tests undertaken, the following observations can be drawn on the behavior of slender HSC columns under design (non-standard) fire scenarios:

- The strength of concrete, and associated decrease in permeability, has significant influence on the fire resistance of RC columns. The fire resistance of HSC columns can decrease by as much as 65% of the fire resistance of NSC columns under some scenarios.

- The addition of about 0.1-0.2% (by weight) polypropylene fibers mitigates fire induced spalling in HSC columns and thus helps to achieve higher fire resistance. The fire resistance of HSC columns nearly tripled with the addition of polypropylene fibers to concrete mix.
- The type of fire exposure has significant influence on the fire resistance of RC columns and both NSC and HSC columns can survive burn out conditions under most realistic fire scenarios. The conventional method of evaluating fire resistance, based on "standard" fire exposure, is conservative under design fire scenarios.
- Concrete permeability and load level have significant influence on spalling and fire resistance of HSC columns. HSC, due to low permeability, is more prone to spalling (around 40% in 33 minutes) than NSC (no spalling). The extent of spalling can be severe in the case of HSC columns with low permeability and under higher load levels.

Table 3.1 Concrete mix proportions for fabricating different RC columns

	Batch 1	Batch 2	Batch 3
Columns fabricated	NSC1	HSC1, HSC2, HSC3	HSCP1, HSCP2
Concrete type	NSC	HSC	HSCP
Cement (kg/m^3)	390	513	513
Coarse aggregate (kg/m^3)	1037	1078	1078
Fine aggregate (kg/m^3)	830	684	684
Water (kg/m^3)	156	130	130
Water reducing agent (kg/m^3)	2	15	15
Silica fume (kg/m^3)	0	43	43
Polypropylene fibers (% by volume)	0	0	2
Water Binder Ratio	0.4	0.23	0.23
Concrete Strength 28 Day (MPa)	39 ± 0.6	91 ± 0.3	85 ± 0.5
Concrete Strength 90 Day (MPa)	48 ± 0.4	105 ± 0.3	90 ± 0.3
Slump (mm)	100	100	90
Density (Kg/m^3)	2429	2490	2464

Table 3.2 Summary of test parameters and results for fire resistance tests

Column designation	Test #	Fire exposure	Concrete type	Concrete Strength (MPa)		Test day Concrete Strength (MPa)	Load		Relative Humidity (%)	Fire resistance (minutes)	Extent of spalling	
				28 day	Test day		kN	%		Measured	% vol	Qualitative
NSC1	I	ASTM E119	NSC	39	51	51	280	40	81.5	183	15	Minor
HSC1	I	ASTM E119	HSC	91	106	106	500	40	81.1	61	40	Medium - Severe
HSC2	II	SF	HSC	91	107	107	500	40	87.5	NF	43	Severe
HSC3	II	SF	HSC	91	107	107	760	60	86.6	75	40	Severe
HSCP1	III	LF	HSCP	85	93	93	500	40	91.8	NF	0	Nil
HSCP2	III	LF	HSCP	85	93	93	760	60	92.5	221	0	Nil

NF - No Failure

Table 3.3 Compartment and Material Characteristics assumed for Developing Design Fire Scenarios

Design Fire	Lining material	Thermal capacity of lining material ($W.s^{0.5}/m^2.K$)	Opening dimension (m)	Fire load (MJ/m^2 floor area)
SF	Concrete	1900	2.25 x 1.5	250
LF	Concrete	1900	2.25 x 1.5	600

Fig. 3.1 – Layout of Steel Reinforcement before Concrete Placement

Fig. 3.2 – View of RC columns after Fabrication

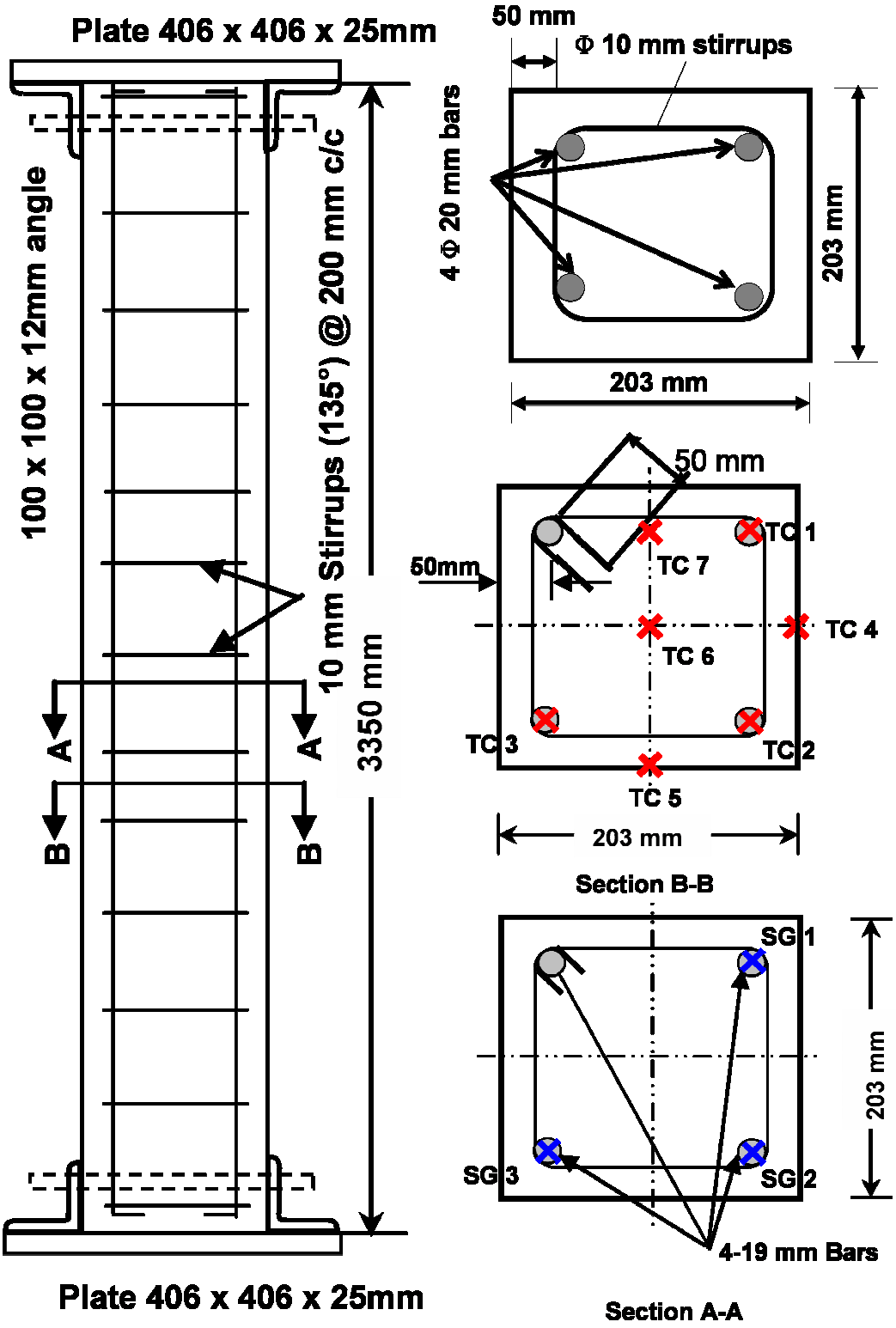

Fig. 3.3. Column dimensions and locations of thermocouple and strain gauges

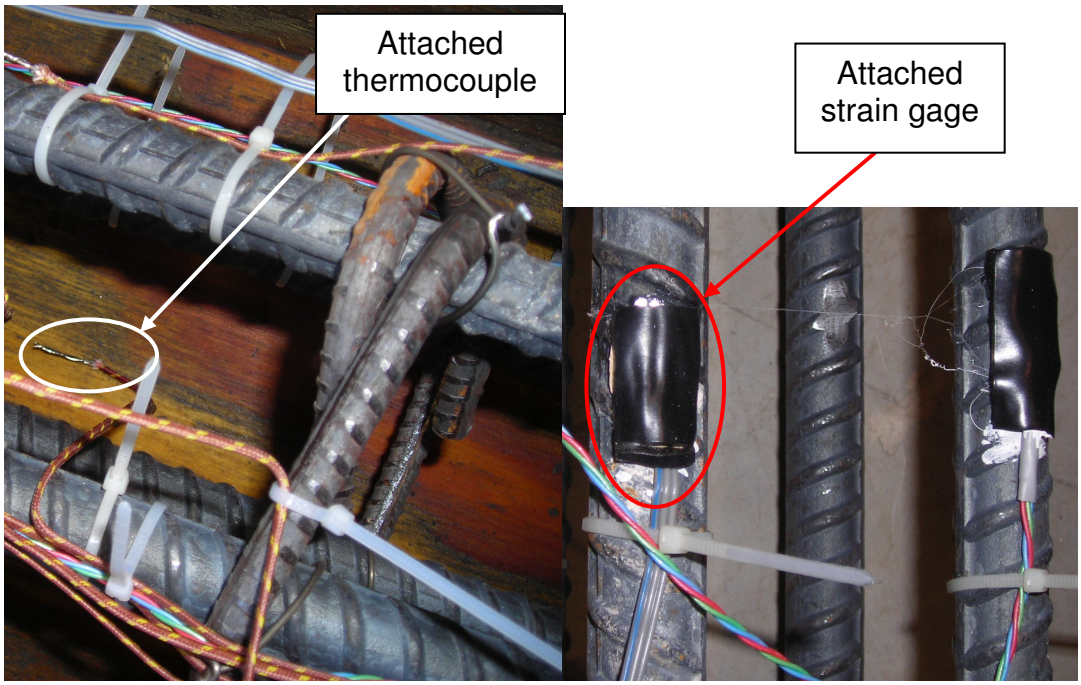

Fig. 3.4 – View of a Thermocouple and a Strain Gage attachment to Columns

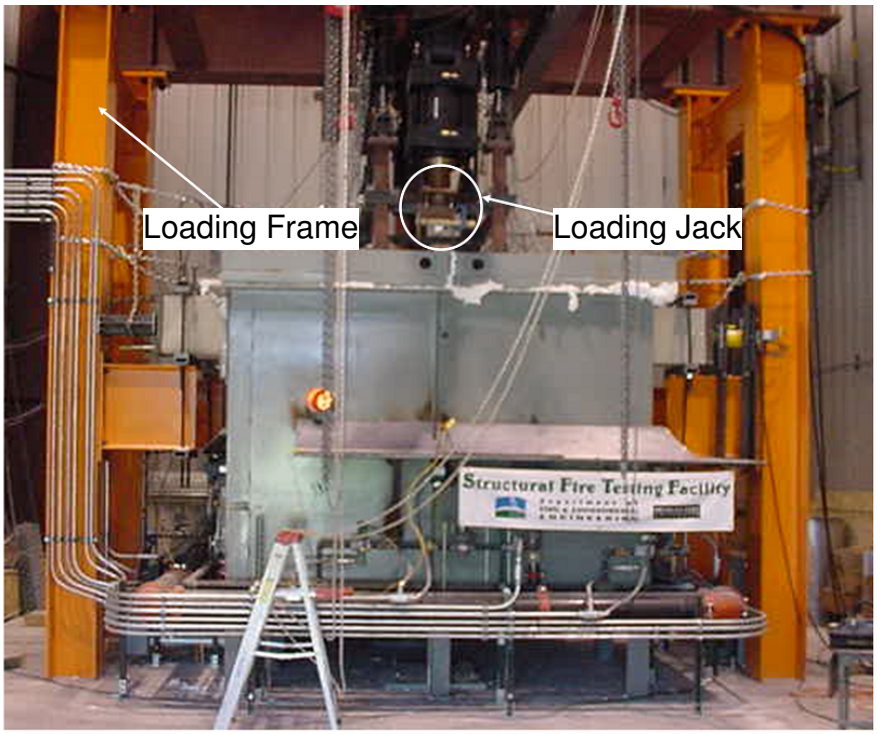

(a) Furnace and loading frame

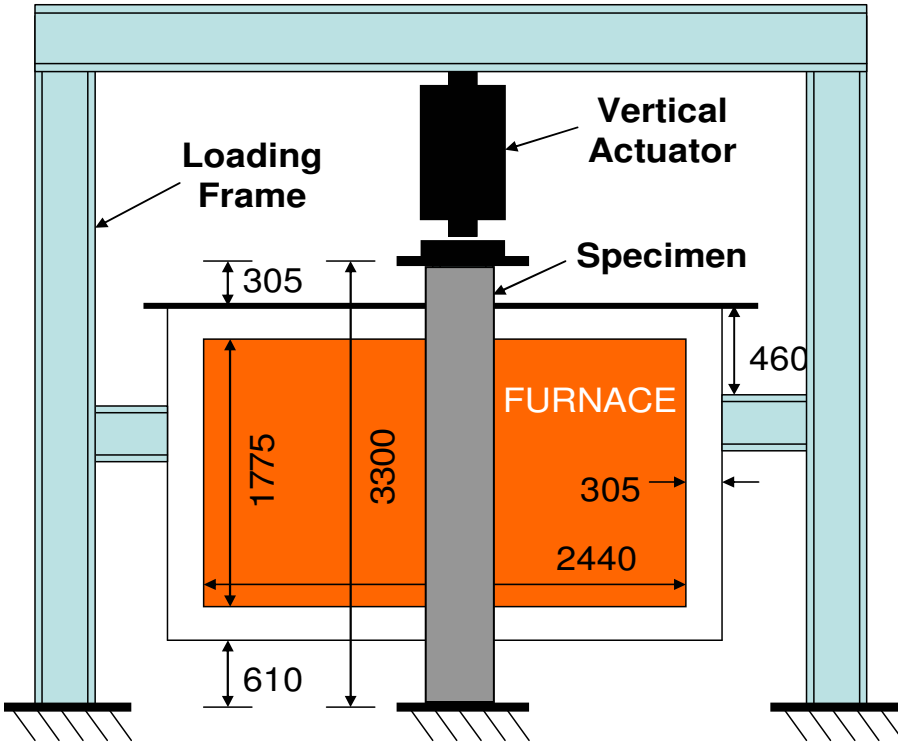

(b) Schematic for furnace front view

Fig. 3.5. Structural Fire Test Furnace at MSU's Civil and infrastructure laboratory

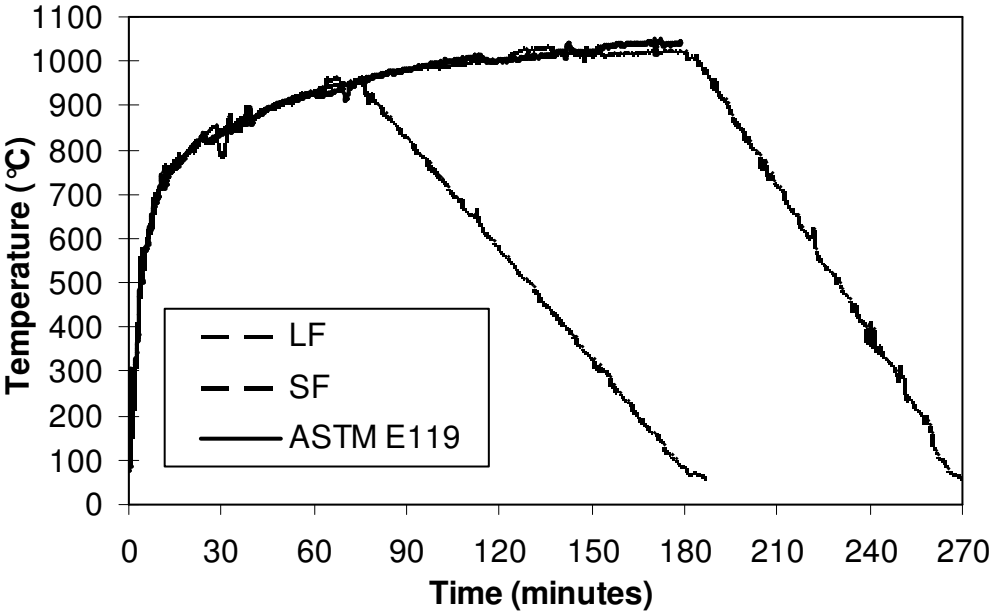

Fig. 3.6. Time temperature curves for fire scenarios used in the fire tests

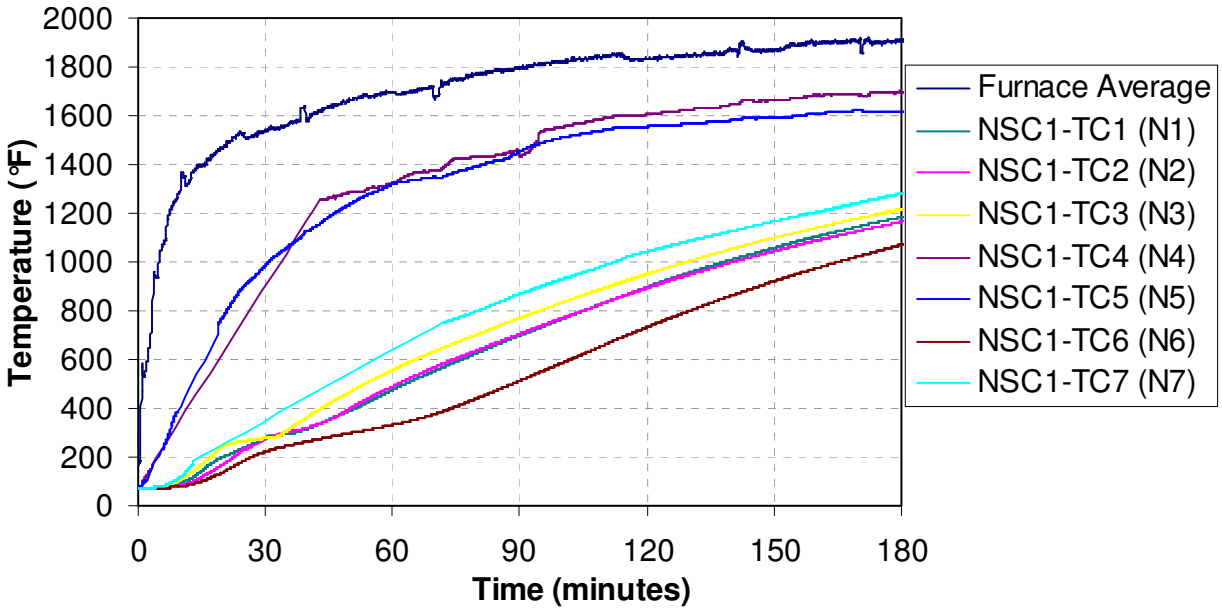

(a) NSC1

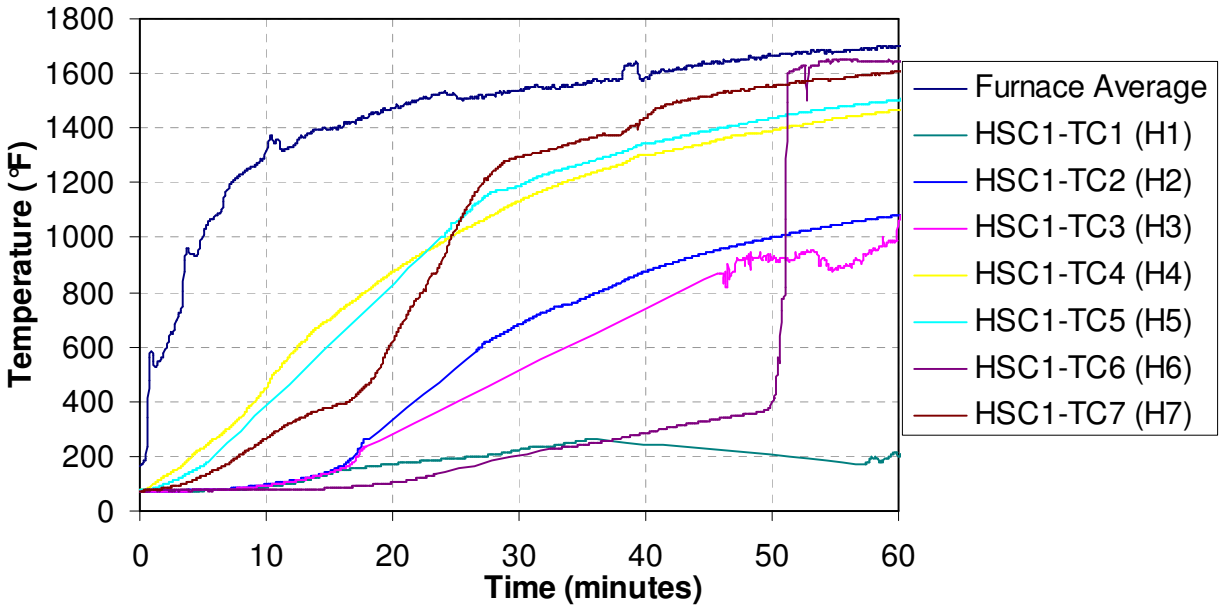

(b) HSC1

Fig. 3.7. Measured rebar and concrete temperatures for RC columns

Fig. 3.7. Contd. Measured rebar and concrete temperatures for RC columns

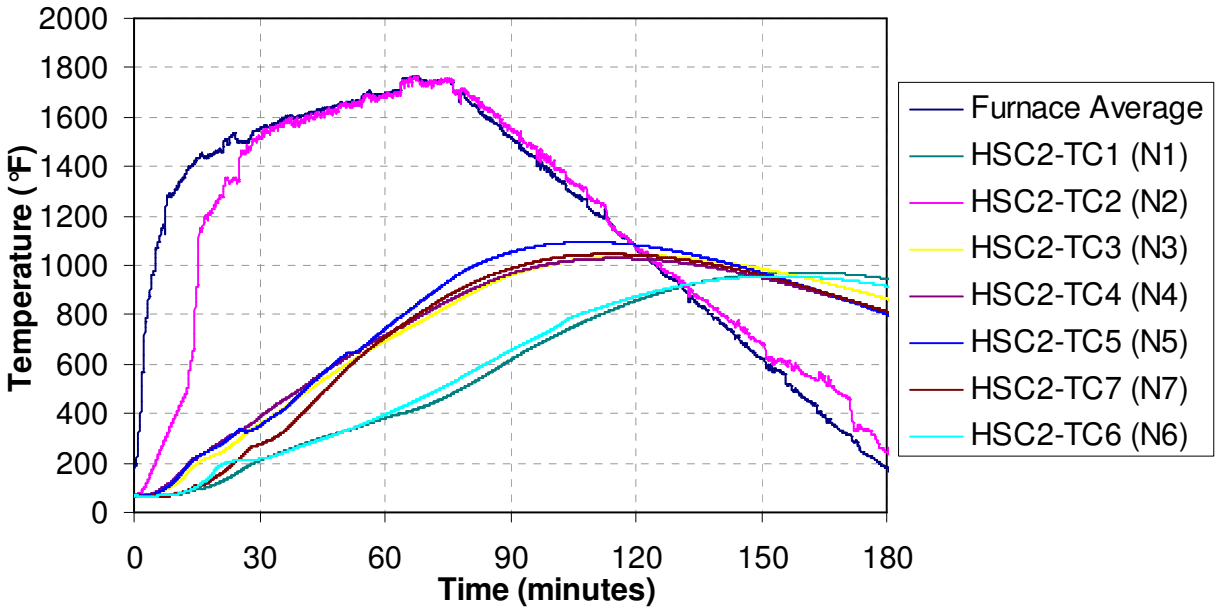

(c) HSC2

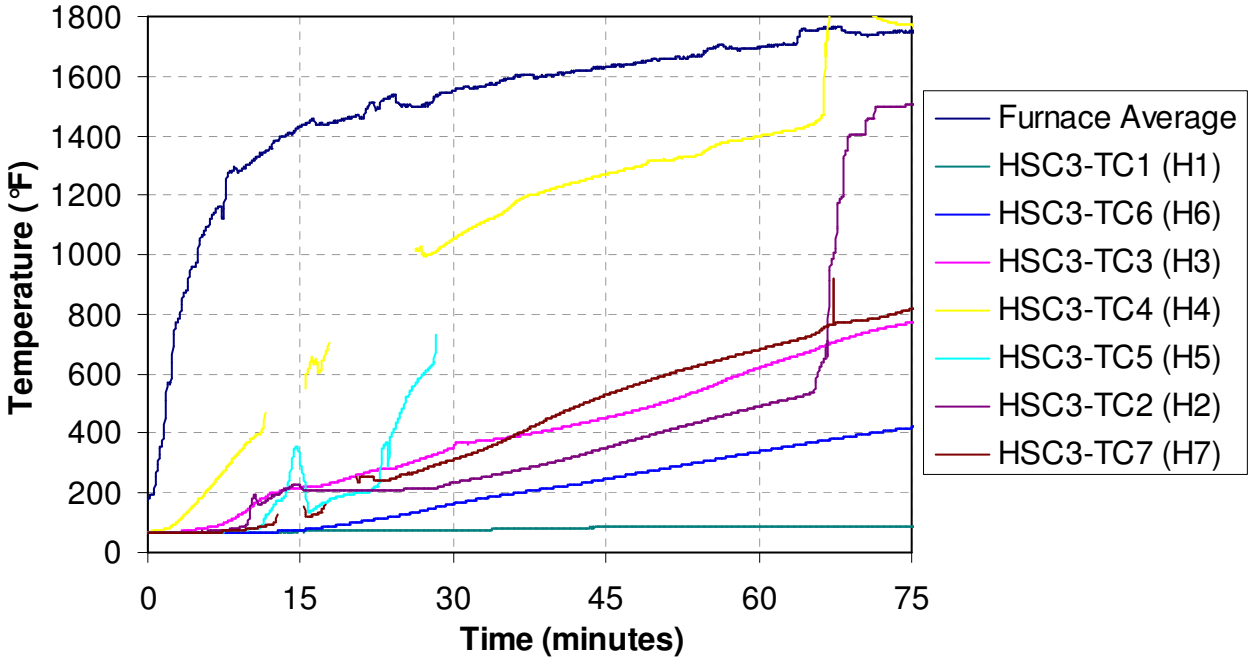

(d) HSC3

(e)

Fig. 3.7. Contd. Measured rebar and concrete temperatures for RC columns

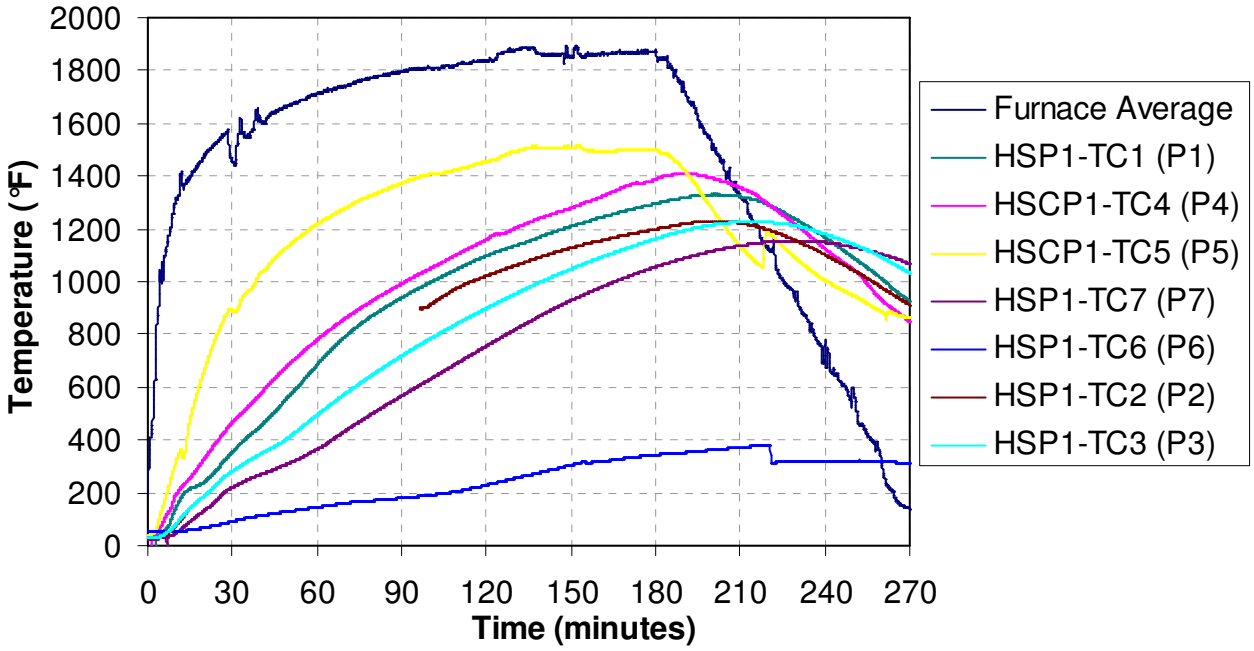

(f) HSCP1

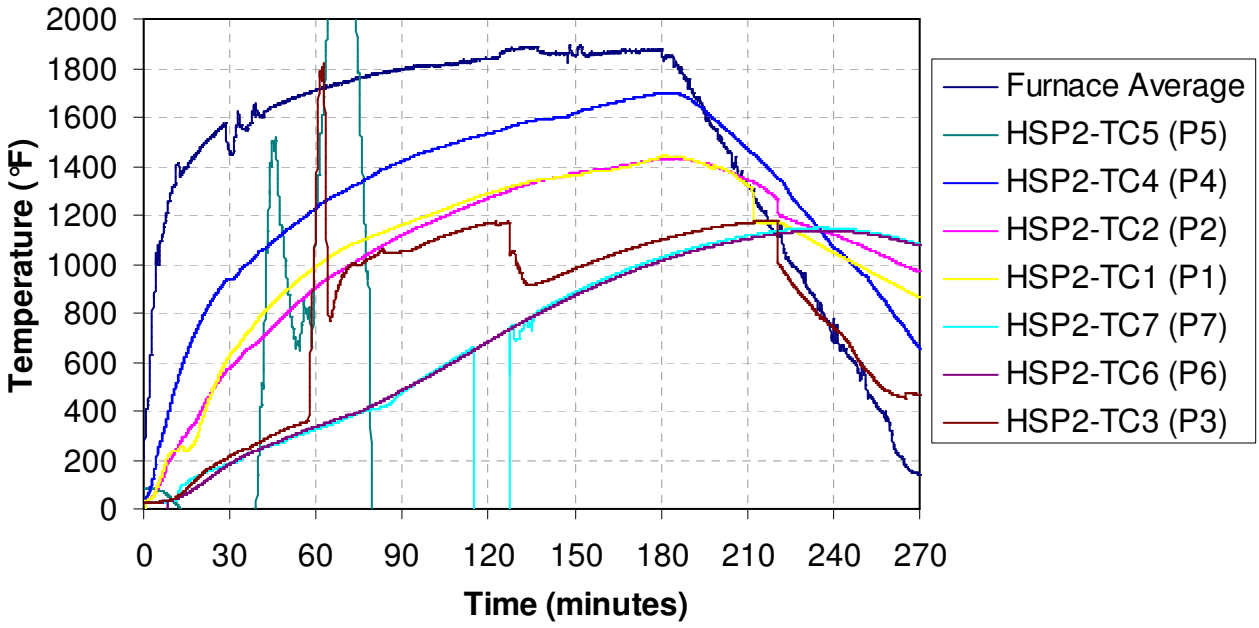

(f) HSCP2

(a) NSC1

(b) HSC1

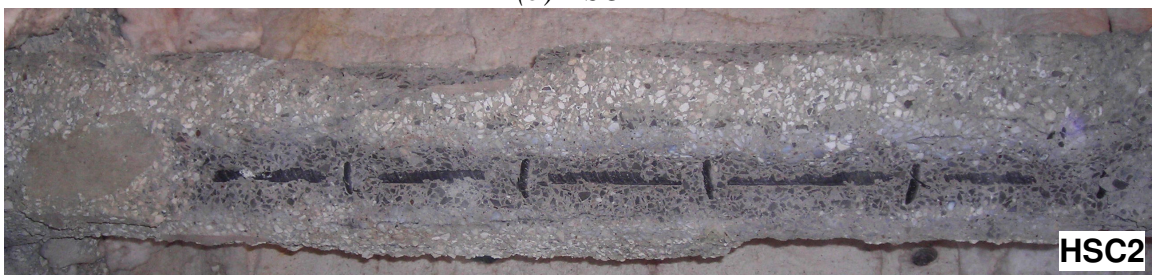

(c) HSC2

(d) HSC3

(e) HSCP1

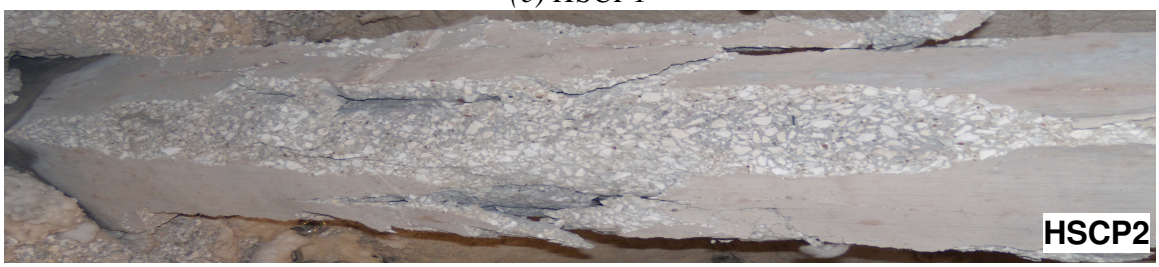

(f) HSCP2

Fig. 3.8. Fire induced spalling in RC columns under respective fire exposure

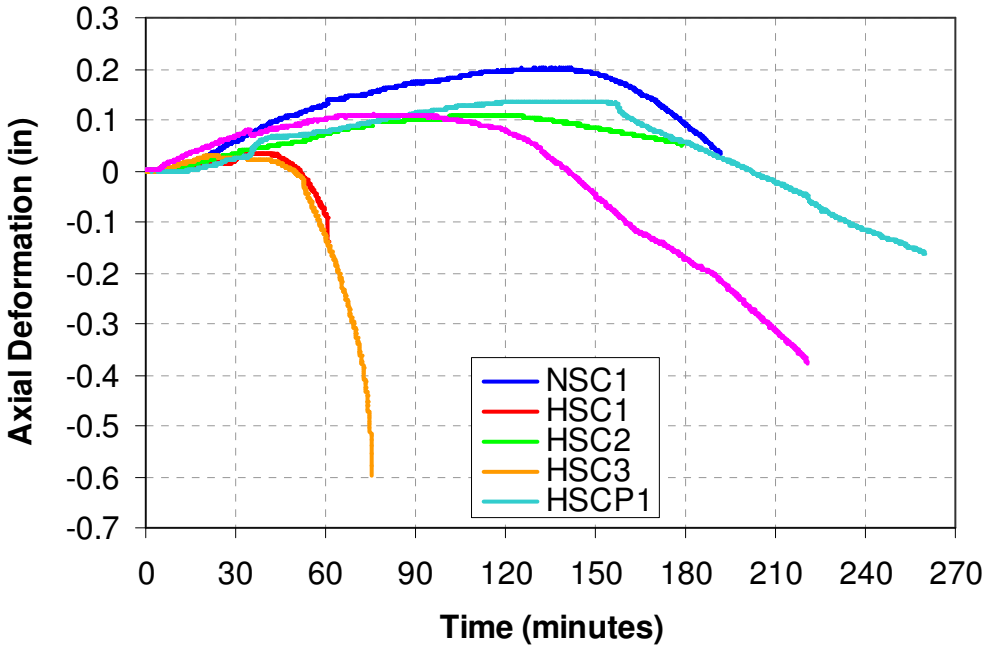

Fig. 3.9. Measured axial deformations as a function of time for the tested RC columns

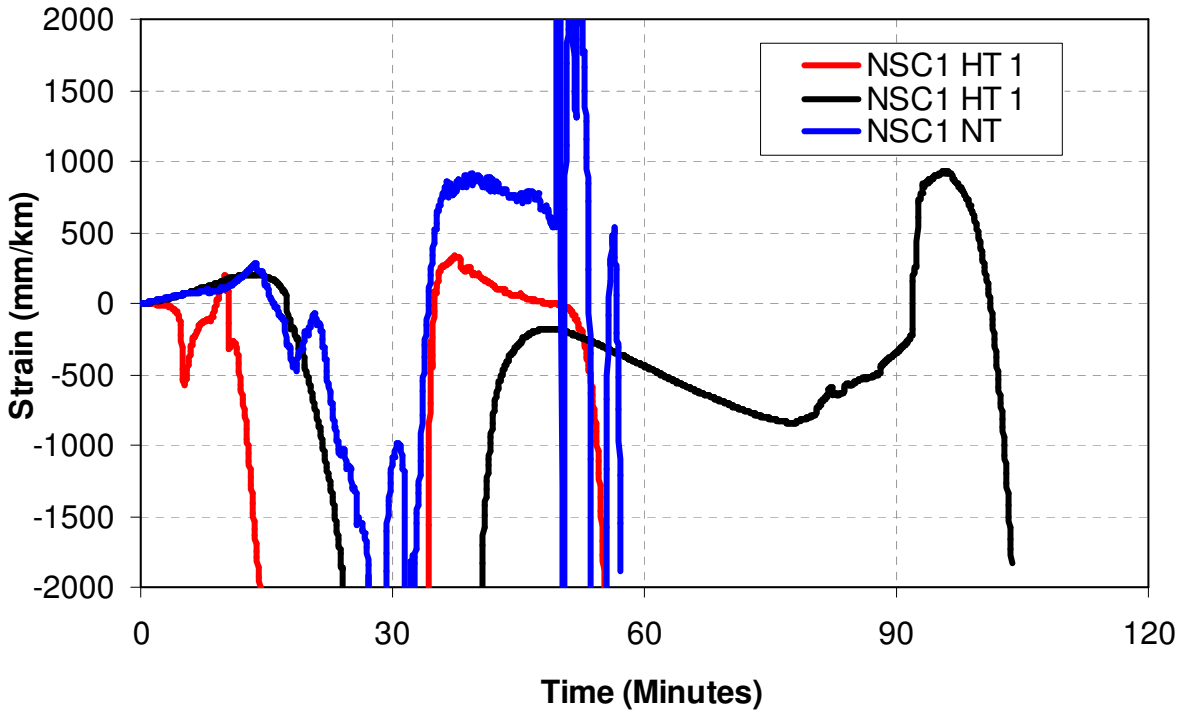

(a) NSC1

Fig. 3.10. Measured axial strains as a function of time for the tested RC columns

Fig. 3.10. Contd. Measured axial strains as a function of time for the tested RC columns

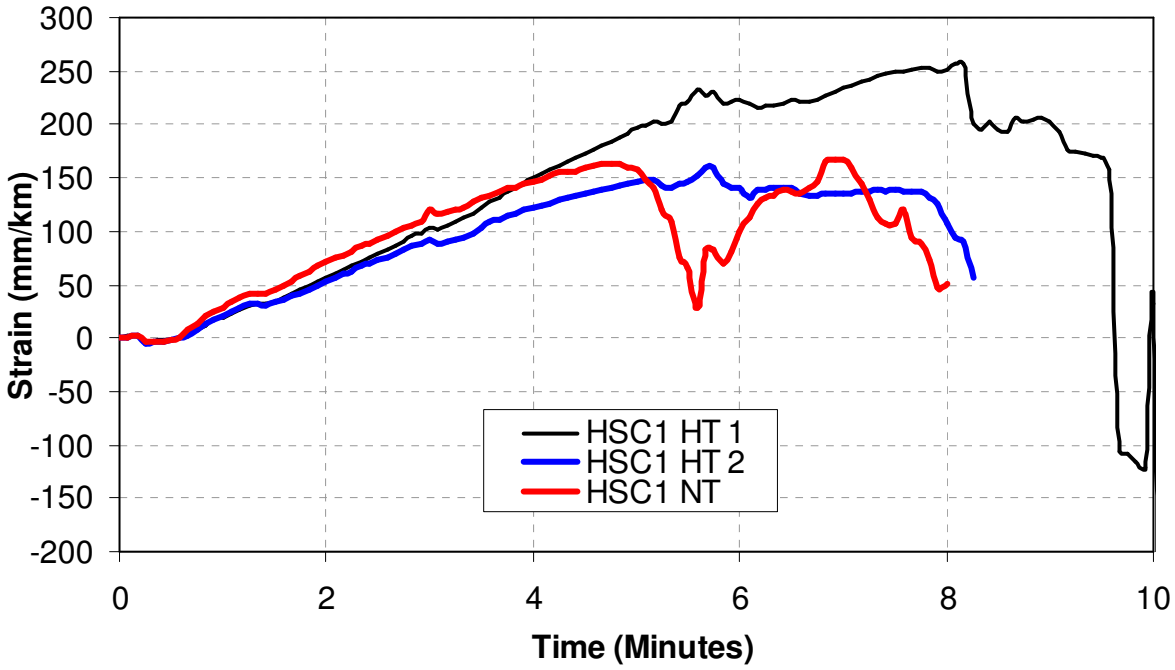

(b) HSC1

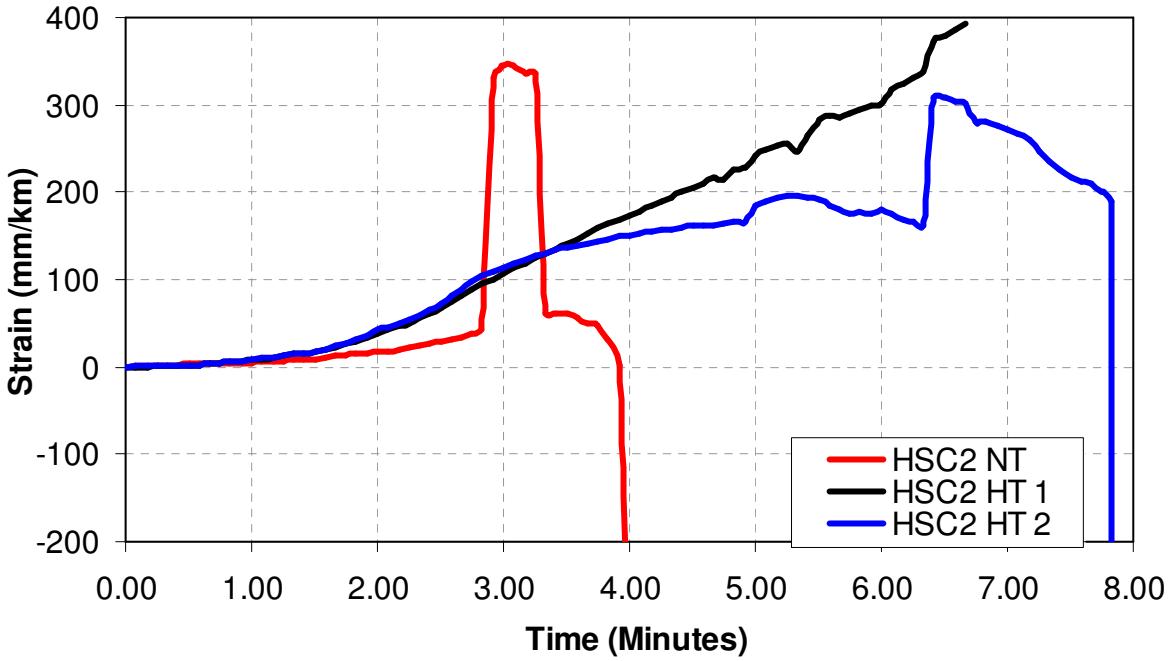

(b) HSC2

Fig. 3.10. Contd. Measured axial strains as a function of time for the tested RC columns

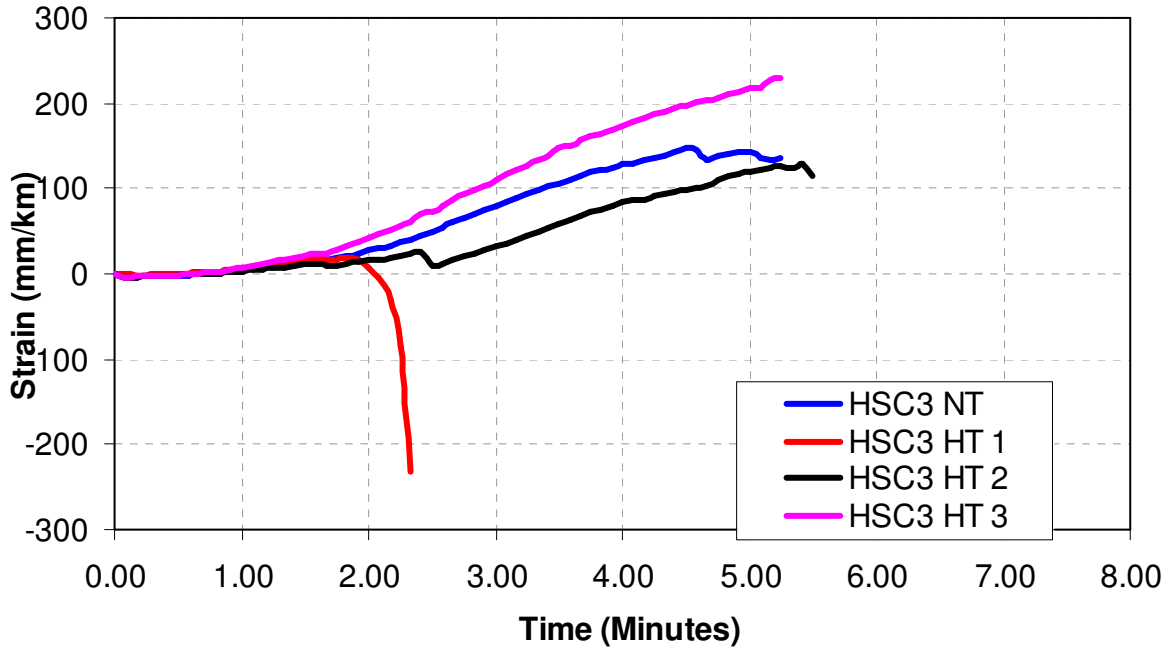

(d) HSC3

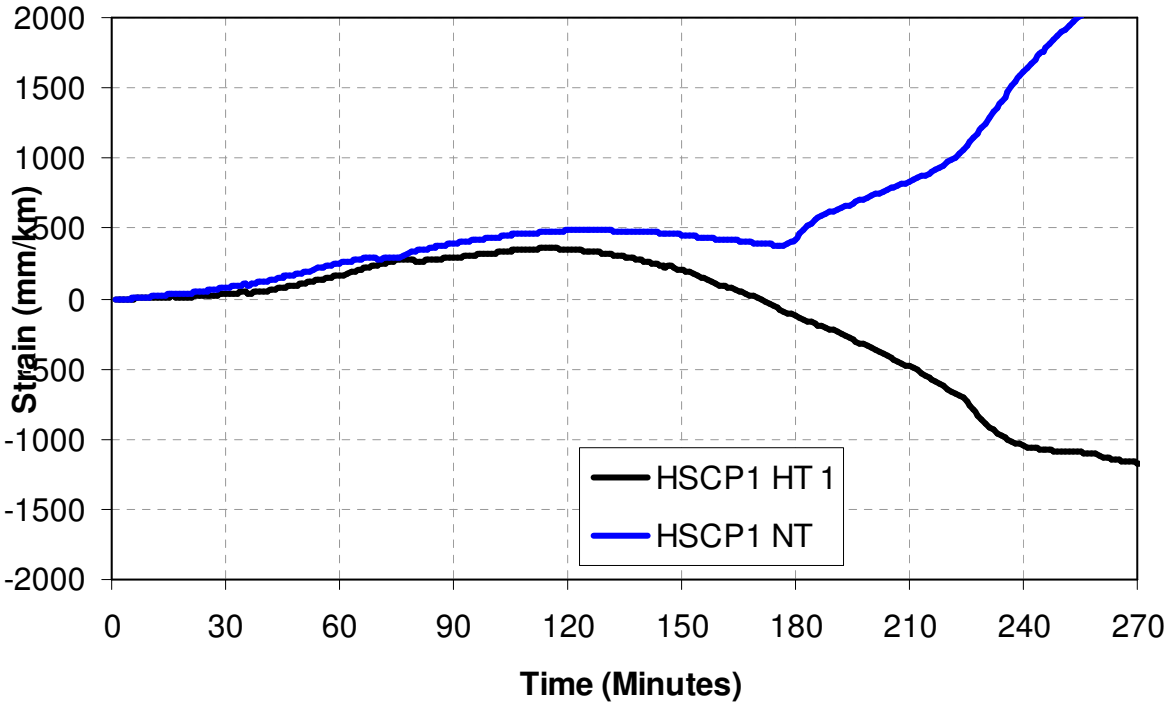

(g) HSCP1

Fig. 3.10. Contd. Measured axial strains as a function of time for the tested RC columns

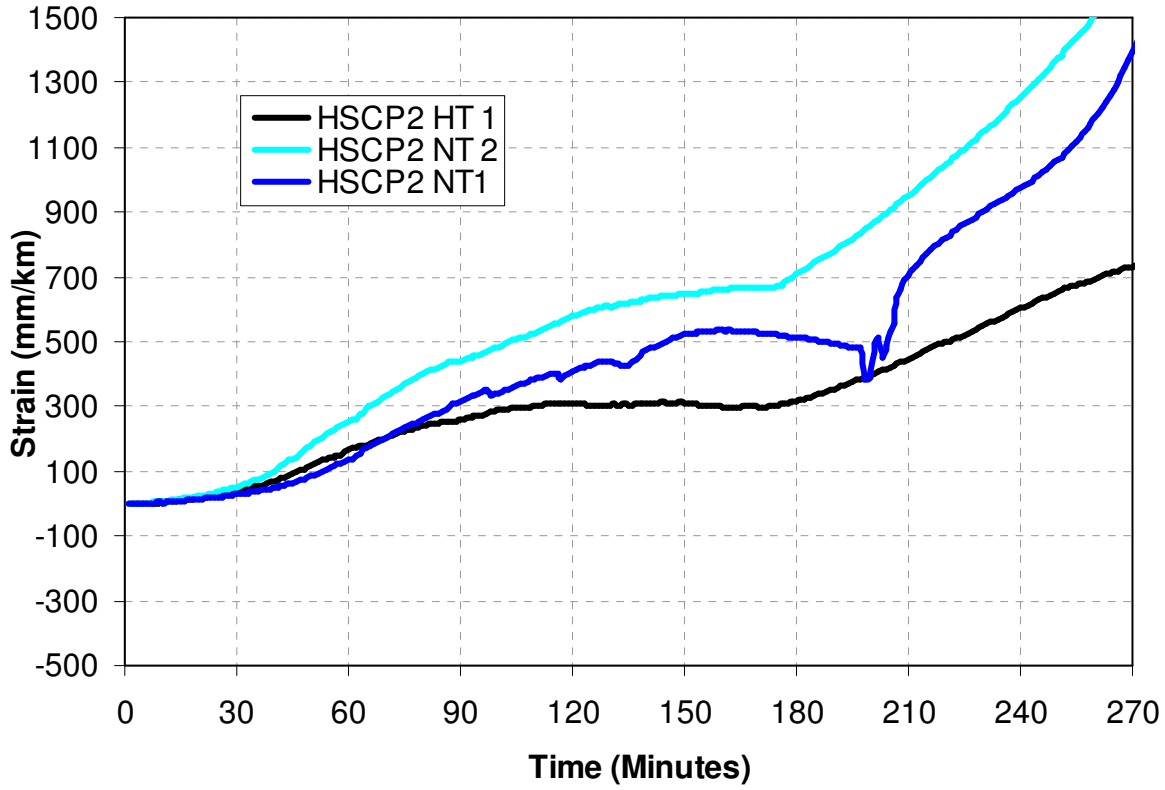

(f) HSCP2

CHAPTER 4

4 NUMERICAL MODEL

This chapter is mainly based on the following journal papers:

- Kodur, V., Dwaikat M. and Raut N., (2007) "Macroscopic Finite Element Models for Tracing the Response of Concrete Structures Under Fire Conditions", Proceedings: Fire Design of Concrete Structures from Materials Modeling to Structural Performance, FIB Workshop, University of Coimbra, Portugal, pp 327-341.
- Kodur V., Dwaikat M. and Raut N., (2009) "Macroscopic FE Models for Tracing the Fire Response of Reinforced Concrete Members", Engineering Structures Journal, V. 31 No. 10, pp. 2368-2379.
- Raut N. and Kodur V., (2009) "Behavior of High Strength Concrete Columns under Design Fire Scenarios", Proceedings: ASCE Structures Congress, Austin, TX.
- Raut N., Kodur V., and Szoke S (2010) "A Macroscopic Finite Element Computer Model for Tracing Fire Response of Reinforced Concrete Columns", Proceedings: ACI Spring Convention, Chicago, IL.
- Raut N. and Kodur V., (2010) "Modeling the Fire Response of Reinforced Concrete Columns under Biaxial Bending", 6th International Conference on Structures in Fire, East Lansing, USA.
- Raut N. and Kodur V., (2010) "Modeling the Fire Response of Reinforced Concrete Columns Under Biaxial Bending", Accepted, ACI Structural Journal.
- Raut N. and Kodur V., (2010) "Behavior of Circular Reinforced Concrete Columns Under Fire Conditions", Communicated, Journal of Structural Fire Engineering.

- Raut N. and Kodur V., (2010) "Computer Model for Predicting the Fire Response of Reinforced Concrete Columns ", Accepted, ACI Special Publication.

4.1 General

Undertaking fire tests is quite expensive, complex, and time consuming. An alternative is to use numerical models to investigate the influence of critical parameters on the fire response of RC columns. As discussed in Chapter 2, there have been a fair number of analytical studies on the fire behavior of RC columns. These analysis methods do not include the effect of spalling or use a very simplistic model for the same. Also, these methods are mainly based on sectional analysis and neglect the behavior of the column as a whole and thus did not incorporate buckling (uniaxial and biaxial). Thus, sophisticated analytical models, based on global approach (consideration of whole member as opposed to sectional analysis), are to be developed for the analysis of RC columns. Such models should account for fire induced spalling, buckling, nonlinear high temperature properties, restraint conditions and various failure criteria. For this purpose, a numerical model was developed using FORTRAN95. The fire response is evaluated through two stages of analysis, namely, thermal and structural analysis. In this chapter, the development of finite element model for thermal and structural analyses is presented.

4.2 Selection of Modeling Technique

The behavior of RC columns under fire can be simulated through the use of advanced numerical models. Such models are generally based on microscopic or macroscopic finite element formulations. In the case of microscopic finite element based models (eg. ANSYS, ABAQUS and SAFIR), a structural member is generally discretized into a three dimensional mesh, and

coupled (or uncoupled) thermal and structural analyses are carried out to trace the fire behavior. However, such an analysis is complex, requires significant effort and the results are often difficult to interpret. Although, such models are capable of accounting for high temperature material properties and different strain components, and can generate detailed output parameters, most of the commercial finite element programs are not capable of modeling fire induced spalling of concrete. Also, some of the sophistication and complexity used in three dimensional modeling is of limited use since high temperature constitutive relationships for concrete in more than one dimension are not available.

An alternative to complex microscopic finite element methods is the use of macroscopic finite element approach for tracing the fire behavior of RC columns. In the macroscopic finite element method, a sectional analysis is carried out at a number of cross-sections along the length of the column and moment-curvature (M-κ) relationships are generated for these sections as a function of time. These sectional M-κ relations are then utilized to predict the overall fire response of the RC column. Various strain components, high temperature constitutive relationships, fire induced spalling, and restraint effects can be accounted for in such models. In this way, the necessity of three dimensional material properties is avoided and the results obtained from the model are easier to interpret and use. However, such macroscopic finite element models are not currently available for modeling the fire response of RC columns and thus a macroscopic finite element based model was developed as a part of this study to trace the response of RC columns exposed to fire.

4.3 Finite Element Model

4.3.1 General Approach

The numerical model, proposed here, uses moment curvature (M-κ) relationships to trace the response of an RC column in the entire range of loading up to collapse under fire. A RC column is divided into a number of segments along its length (as shown in Figure 4.1) and the mid-section of the segment is assumed to represent the behavior of the whole segment. The fire resistance analysis is carried out by incrementing time in steps. At each time interval, the analysis is performed through three main steps, namely:

- Establishing fire temperature due to fire exposure,
- Carrying out coupled hydro-thermal analysis in each segment to predict cross-sectional temperature and fire-induced spalling, and
- Performing strength and deformation analysis through three sub-steps, namely:
  - Calculating fire induced axial restraint force in the RC column,
  - Generating sectional M-κ relationships (utilizing the axial restraint force computed above) for each column segment, and
  - Performing structural analysis of the overall column to compute deflections and internal forces.

The first step in the analysis is to establish the fire temperature using standard or design fire scenarios. Following this, a hydro-thermal analysis is performed to evaluate cross-sectional temperatures and fire-induced spalling (if any) in each segment of the column. Then the axial restraint force is computed based on the axial deformation of the column. Once the axial restraint force in the column is computed, the next step is the generation of M-κ relationships for each segment of the column [Campbell and Kodur 1990]. In the current model, such M-κ relationships are established as a function of time for various segments and they are in turn used to trace the

response of the column under fire conditions. Material nonlinearity and fire induced restraint effects are implicitly accounted for in the moment curvature generation. Using the M-κ relationships, the load (axial load and moment) the column can carry at a particular time step is evaluated. Also, the axial and lateral deformations at that time step are calculated through a stiffness approach by evaluating average stiffness of the column. The average stiffness of the column is computed using segmental stiffness, which is estimated by means of known M-κ relationships. A flowchart showing the numerical procedure for fire resistance calculations is given in Figure 4.2.

The model generates various critical output parameters, such as temperatures, stresses, strains, axial restraint force, axial deformation, lateral deformation, and axial load and moment capacities at various fire exposure times. The temperatures and strength capacities for each segment are used to evaluate failure of the column at each time step. Details of the analysis procedure are presented in the following sections.

4.3.2 Fire Temperatures

The temperatures due to fire are calculated by assuming that sides of the column (1-, 2-, 3- or 4) are exposed to a fire, whose temperature follows that of the standard fire exposure such as ASTM E119 [2008] or any other design fire scenario [SFPE 2004, Eurocode 1 2002]. The time-temperature relationship for the ASTM E119 standard fire can be approximated by the following equation:

$$T_f = T_0 + 750\left(1 - exp\left(-3.79553\sqrt{t_h}\right)\right) + 170.41\sqrt{t_h} \qquad [4.1]$$

where: t_h = time (hours), T_0 = initial temperature (°C), and T_f = fire temperature (°C).

For design fires, the time-temperature relationship specified in Eurocode 1 [2002] for typical fuel load and ventilation factor are built into the model. Also, to simulate hydrocarbon fire scenarios, the time-temperature relationship specified in ASTM E1529 [1993] is incorporated into the model.

4.3.3 Hydro-Thermal Analysis and Spalling Prediction

The hydro-thermal analysis is performed to compute the temperature and pore pressure distributions within the column cross-section. At each time step, hydro-thermal analysis is carried out in two steps, namely; thermal analysis and pore pressure calculations. RC columns are constructed predominantly in two shapes, rectangular (or square) and circular. Circular RC columns, though less common as compared to rectangular (or square) ones, still find applications in built environment (such as parking structures) due to several advantages they possess. Hence the model developed incorporates for both rectangular and circular cross-sections. Since the circular RC columns are mostly exposed to fire throughout its circumference, axisymmetry can be used to calculate the cross-sectional temperature and to predict spalling. Hence the thermal analysis and pore pressure calculations have been presented separately for rectangular and circular cross-sections in the following sub-sections.

4.3.3.1 Columns with Rectangular Cross-section

4.3.3.1.1 Thermal Analysis

The temperatures within the cross-section of each segment are computed using the finite element approach. The fire temperature established in Section 4.3.2 forms the input into thermal analysis. The cross-sectional area of each segment is subdivided into a number of elements and temperature rise in a column segment is derived by establishing a heat balance for each element.

The temperature is assumed to be uniform along the length of the segment and thus the calculations are performed for a unit length of each segment. Steel reinforcement is not specifically considered in the thermal analysis because it does not significantly influence the temperature distribution in the column cross-section [Lie and Irwin 1993].

Based on the conservation of energy, the following equation can be obtained for one dimensional heat transfer problems:

$$\rho c \frac{dT}{dt} = -\frac{dq}{dx} + Q \qquad [4.2]$$

Applying Fourier's law, which relates the heat flux to the temperature gradients as $q = -k\frac{dT}{dx}$, Eq. [4.2] can be written as

$$\rho c \frac{dT}{dt} = \frac{d\left(k\frac{dT}{dx}\right)}{dx} + Q \qquad [4.3]$$

Thus, the governing heat transfer equation within a rectangular column cross-section, which represents a two dimensional problem, can be written as:

$$\rho c \frac{dT}{dt} = \nabla k \nabla T + Q \qquad [4.4]$$

where: k = thermal conductivity, ρc = heat capacity, T = temperature, t = time, Q = heat source, and q = heat flux.

At the fire-column interface, the mechanism for heat transfer is through radiation and convection. The heat flux on the boundary due to convection and radiation can be given by the following two equations which relates the heat flux due to convection and radiation to the temperature of fire (or ambient temperature for faces not exposed to fire):

$$q_{rad} = h_{rad}\left(T - T_E\right) \qquad [4.5]$$

$$q_{con} = h_{con}\left(T - T_E\right) \quad [4.6]$$

where:

q_{rad} and q_{con} = radiative and convective heat fluxes,

h_{rad} and h_{con} = radiative and convective heat transfer coefficient,

$h_{rad} = 4\sigma\varepsilon\left(T^2 + T_E^2\right)\left(T + T_E\right)$,

T_E = temperature of the environment surrounding the boundary,

σ = Stevan-Boltzman constant = 5.67×10^{-8} (W/m^2.°K^4), and

ε = emissivity.

Hence, the total heat flux on the olumn boundaries (q_b) can be given by the following equation:

$$q_b = \left(h_{con} + h_{rad}\right)\left(T - T_E\right) \quad [4.7]$$

Using Fourier's Law, the governing heat transfer equation on the boundary of the column can be written as:

$$k\left(\frac{\partial T}{\partial y}n_y + \frac{\partial T}{\partial z}n_z\right) = -h\left(T - T_f\right) \quad [4.8]$$

where:

n_y and n_z = components of the vector normal to the boundary in the plane of the cross-section, and

$h = h_{con} + h_{rad}$.

Since the column may be exposed to fire from 1-, 2-, 3-, or 4- sides, two types of boundary equations are to be considered for thermal analysis, namely:

- Fire exposed boundaries where the heat flux is governed by the following equation:

$$k\left(\frac{\partial T}{\partial y}n_y + \frac{\partial T}{\partial z}n_z\right) = -h_f\left(T - T_f\right) \quad [4.9]$$

- Unexposed boundary where the heat flux equation is given by:

$$k\left(\frac{\partial T}{\partial y}n_y + \frac{\partial T}{\partial z}n_z\right) = -h_c\left(T - T_0\right) \quad [4.10]$$

where:

h_f and h_c = heat transfer coefficient of the fire side and the cold side, respectively, and

T_f and T_0 = fire and cold side temperature, respectively.

4.3.3.1.2 Pore Pressure Calculations

To evaluate fire induced spalling, pore pressure calculations are carried out for each segment at each time step as proposed by Dwaikat and Kodur [2009] and Dwaikat [2009].

Assumptions

The following assumptions are made in the development of spalling sub-model:

- Concrete is a continuum medium. This assumption is based on the fact that the heterogeneity scale (length over which the medium changes from one phase to another) of concrete is much smaller than the length over which a change can be observed in the temperature, moisture content, and pressure.
- Water vapor is an ideal gas, which is valid for most engineering applications [Harmathy 1969, 1971 and Huang 1979].

- Mobility of liquid water is ignored. This assumption is valid because Darcy's coefficient (permeability) for liquid water in concrete is much smaller than that for water vapor [Harmathy 1969 and Sahota 1979].
- The effect of air is ignored in the analysis. This assumption is considered to be valid because the mass of air in concrete is much smaller than the mass of water.
- The solid skeleton (concrete structure) is assumed to be undeformable. This is because the mechanical and thermal deformation of the solid phase is small when compared to the volume changes due to other processes such as evaporation.
- Water is incompressible liquid. This assumption is valid because the volumetric deformation of liquid water due to pressure is much smaller than the volumetric changes due to other processes such as evaporation.
- The applied loading on the RC column has no influence on the hydro-thermal analysis. The applied loading generally causes damage in concrete which increases the concrete permeability. Thus, by ignoring such effect, conservative spalling predictions can be obtained.
- The effect of latent heat and heat of dehydration is not accounted for in the analysis. Accounting for latent heat and heat of dehydration will slightly reduce the predicted temperatures. Thus, latent heat and heat of dehydration can be conservatively ignored in the analysis.

Governing Equations

The governing equations for the calculation of vapor pressure in concrete are derived using four main principles; namely:

- Conservation of mass for liquid water,

- Ideal gas law,
- Total volume of all different components in a unit volume of concrete equals unity, and
- Conservation of mass for water vapor.

- The basic equations that govern the conservation of mass for liquid water is given by:

$$E = m_{LW0} - m_L + m_D \qquad [4.11]$$

Differentiating with respect to time, Eq. [4.11] can be written as:

$$\frac{dE}{dt} = -\frac{dm_L}{dt} + \frac{dm_D}{dt} \qquad [4.12]$$

Using the chain rule to elaborate $\frac{dm_L}{dt}$, Eq. [4.12] can be written as:

$$\frac{dE}{dt} = -\frac{dm_L}{dP_V}\frac{dP_V}{dt} - \frac{dm_L}{dT}\frac{dT}{dt} + \frac{dm_D}{dT}\frac{dT}{dt} \qquad [4.13]$$

where: E = mass of evaporated water, m_{LW0} = mass of liquid water at $t = 0$, (initial mass of liquid water), m_L = mass of liquid water at any time, t, m_D = mass of liquid water formed due to dehydration, T = temperature, P_V = vapor pressure, and t = time.

- The ideal gas law is used to relate the pressure, the volume, the mass, and the temperature for water vapor as follows:

$$P_V V_V = n_V RT \qquad [4.14]$$

$$n_V = \frac{m_V}{M} \qquad [4.15]$$

Hence, $P_V = \frac{R}{M}\frac{m_V T}{V_V}$ [4.16]

$$\frac{dP_V}{dt} = \frac{R}{M}\left(\frac{TV_V\,\frac{dm_V}{dt} + m_V V_V\,\frac{dT}{dt} - m_V T\,\frac{dV_V}{dt}}{V_V^2}\right) \quad [4.17]$$

Rearranging Eq. [4.17]:

$$\frac{dm_V}{dt} = \frac{V_V M}{RT}\frac{dP_V}{dt} - \frac{m_V}{T}\frac{dT}{dt} + \frac{m_V}{V_V}\frac{dV_V}{dt} \quad [4.18]$$

where: m_V = mass of water vapor, R = gas constant, n_V = number of moles of water vapor, M = molar mass of water, V_V = volume fraction of water vapor, and T = temperature (°K).

- For a unit volume of concrete, the sum of the volume fractions of all phases equals unity, which leads to:

$$V_V + V_L + (V_{S0} - V_D) = 1 \quad [4.19]$$

Eq. [4.19] can be rearranged as:

$$V_V = 1 - V_L - (V_{S0} - V_D) \quad [4.20]$$

Using the volume-mass-density relationship, Eq. [4.20] can be written as:

$$V_V = 1 - \frac{m_L}{\rho_L} - \left(V_{S0} - \frac{m_D}{\rho_L}\right) \quad [4.21]$$

Differentiating both sides of Eq. [4.21] with respect to time, Eq. [4.21] transforms to:

$$\frac{dV_V}{dt} = \frac{1}{\rho_L}\left(\frac{dm_D}{dt} - \frac{dm_L}{dt}\right) - \frac{1}{\rho_L^2}\frac{d\rho_L}{dT}\frac{dT}{dt}(m_D - m_L) \quad [4.22]$$

Substituting Eq. [4.12] in Eq. [4.22] results in:

$$\frac{dV_V}{dt} = \frac{1}{\rho_L}\frac{dE}{dt} - \frac{1}{\rho_L^2}\frac{d\rho_L}{dT}\frac{dT}{dt}(m_D - m_L) \quad [4.23]$$

By substituting Eq. [4.23] in Eq. [4.18], Eq. [4.24] can be obtained.

$$\frac{dm_V}{dt} = \frac{V_V M}{RT}\frac{dP_V}{dt} - \frac{m_V}{T}\frac{dT}{dt} + \frac{m_V}{V_V \rho_L}\left(\frac{dE}{dt} - \frac{1}{\rho_L}\frac{d\rho_L}{dT}\frac{dT}{dt}(m_D - m_L)\right) \qquad [4.24]$$

where: V_L = volume fraction of liquid water, V_{S0} = initial volume fraction of solid, V_D = volume fraction of dehydrated liquid water, and ρ_L = density of liquid water.

- Based on the conservation of mass of water vapor, the following equation can be obtained for one dimensional problems:

$$\frac{dm_V}{dt} = -\frac{dJ}{dx} + \frac{dE}{dt} \qquad [4.25]$$

Using Darcy's Law, which relates the mass flux to the pressure gradients as $J = -\lambda\frac{dP_V}{dx}$, Eq. [4.25] can be written as:

$$\frac{dm_V}{dt} = \frac{d\left(\lambda\frac{dP_V}{dx}\right)}{dx} + \frac{dE}{dt} \qquad [4.26]$$

Darcy's coefficient, λ, can be written as:

$$\lambda = m_V \frac{k_T}{\mu_V} \qquad [4.27]$$

Substituting for λ, Eq. [4.26] can be written as:

$$\frac{dm_V}{dt} = \frac{d\left(\left(m_V \frac{k_T}{\mu_V}\right)\frac{dP_V}{dx}\right)}{dx} + \frac{dE}{dt} \qquad [4.28]$$

For two dimensional problems, Eq. [4.28] can be written as:

$$\frac{dm_V}{dt} = \nabla\left(m_V \frac{k_T}{\mu_V}\right)\nabla P_V + \frac{dE}{dt} \qquad [4.29]$$

By substituting Eq. [4.24] in Eq. [4.29]:

$$\frac{V_V M}{RT}\frac{dP_V}{dt} - \frac{m_V}{T}\frac{dT}{dt} + \frac{m_V}{V_V \rho_L}\left(\frac{dE}{dt} - \frac{1}{\rho_L}\frac{d\rho_L}{dT}\frac{dT}{dt}(m_D - m_L)\right) = \nabla\left(m_V \frac{k_T}{\mu_V}\right)\nabla P_v + \frac{dE}{dt} \quad [4.30]$$

Hence, the governing differential equation for pore pressure is given by:

$$\frac{V_V M}{RT}\frac{dP_V}{dt} = \nabla\left(m_V \frac{k_T}{\mu_V}\right)\nabla P_V + \left(1 - \frac{m_V}{V_V \rho_L}\right)\frac{dE}{dt} + \frac{m_V}{T}\frac{dT}{dt} + \frac{m_V}{V_V \rho_L^2}\frac{d\rho_L}{dT}\frac{dT}{dt}(m_D - m_L) \quad [4.31]$$

Substituting $\frac{dE}{dt}$ from Eq. [4.13] in Eq. [4.31]:

$$\frac{V_V M}{RT}\frac{dP_V}{dt} = \nabla\left(m_V \frac{k_T}{\mu_V}\right)\nabla P_V + \left(1 - \frac{m_V}{V_V \rho_L}\right)\left(-\frac{dm_L}{dP_V}\frac{dP_V}{dt} - \frac{dm_L}{dT}\frac{dT}{dt} + \frac{dm_D}{dT}\frac{dT}{dt}\right) + \frac{m_V}{T}\frac{dT}{dt} + \frac{m_V}{V_V \rho_L^2}\frac{d\rho_L}{dT}\frac{dT}{dt}(m_D - m_L) \quad [4.32]$$

which can be rearranged as:

$$\left[\left(1 - \frac{m_V}{V_V \rho_L}\right)\frac{dm_L}{dP_V} + \frac{V_V M}{RT}\right]\frac{dP_V}{dt} = \nabla\left(m_V \frac{k_T}{\mu_V}\right)\nabla P_V + \left[\left(1 - \frac{m_V}{V_V \rho_L}\right)\left(-\frac{dm_L}{dT} + \frac{dm_D}{dT}\right) + \frac{m_V}{T} + \frac{m_V}{V_V \rho_L^2}\frac{d\rho_L}{dT}(m_D - m_L)\right]\frac{dT}{dt} \quad [4.33]$$

where: J = mass flux of water vapor, λ = Darcy's coefficient of permeability, k_T = intrinsic permeability of concrete at temperature, T, and μ_V = dynamic viscosity of water vapor.

Equation [4.33] can be simplified by introducing three parameters, A, B, and C as follows:

$$A\frac{dP_V}{dt} = \nabla B \nabla P_V + C \quad [4.34]$$

where:

$$A = \left[\left(1 - \frac{m_V}{V_V \rho_L} \right) \frac{dm_L}{dP_V} + \frac{V_V M}{RT} \right]$$

$$B = m_V \frac{k_T}{\mu_V}$$

$$C = \left[\left(1 - \frac{m_V}{V_V \rho_L} \right) \left(- \frac{dm_L}{dT} + \frac{dm_D}{dT} \right) + \frac{m_V}{T} + \frac{m_V}{V_V \rho_L^2} \frac{d\rho_L}{dT} \left(m_D - m_L \right) \right] \frac{dT}{dt}$$

Initial and Boundary Conditions

The initial and boundary conditions for pore pressure calculations are assumed as follows:

- Initial pore pressure (P_{V0}) can be computed as:

  $$P_{V0} = RH \cdot P_{S0} \qquad [4.35]$$

  where: RH = initial relative humidity in the concrete, and P_{S0} = initial saturation pressure which can be computed based on the initial temperature of concrete.

- On the boundaries (surface) of the column the water vapor is assumed to be transferred through diffusion. Thus, the governing mass transfer equation of water vapor at the column boundaries can be written as:

  $$\lambda \left(\frac{\partial P_V}{\partial y} n_y + \frac{\partial P_V}{\partial z} n_z \right) = -D_0 \left(\rho_V - \rho_{V\infty} \right) \qquad [4.36]$$

  where: D_0 = diffusion coefficient of water vapor at the boundaries of the column, ρ_V = density of water vapor in the concrete boundaries, and $\rho_{V\infty}$ = density of water vapor in the surrounding environment. By assuming $\rho_{V\infty}$ to be constant during fire exposure (due

to the lack of information on the changes that take place in the surrounding environment of the column), Eq. [4.36] can be written as:

$$\lambda\left(\frac{\partial P_V}{\partial y}n_y+\frac{\partial P_V}{\partial z}n_z\right)=-\frac{D_0 M}{RT}\left(P_V-\frac{RT\rho_{V\infty}}{M}\right) \qquad [4.37]$$

where: T = temperature (°K).

4.3.3.2 Columns with Circular Cross-section

4.3.3.2.1 Thermal Analysis

As mentioned earlier, since circular columns are assumed to be exposed to fire throughout the circumference, the thermo-mechanical analysis can be reduced to one dimension using axisymmetry. Thus the governing equation for transient heat conduction (Eq. [4.3]) can be written as:

$$\rho c\frac{dT}{dt}=\frac{d\left(k\frac{dT}{dr}\right)}{dr}+Q \qquad [4.38]$$

where: k = thermal conductivity, ρc = heat capacity, T = temperature, t = time, and Q = heat source, r = the radial distance from the surface of the column.

Since the column is exposed to fire throughout the circumference, only one type of boundary condition (fire exposed boundary) is to be considered for thermal analysis, where the heat flux is governed by:

$$k\frac{\partial T}{\partial r}=-h_f\left(T-T_f\right) \qquad [4.39]$$

where: h_f = heat transfer coefficient of the fire side, T_f = fire side temperature And T = the temperature in that particular location of the column.

4.3.3.2.2 Pore Pressure Calculations

Similar to thermal analysis, the conservation of mass of water vapor Equation (Eq.[4.28]) is expressed in radial coordinates as:

$$\frac{dm_V}{dt} = \frac{d\left(\left(m_V \frac{k_T}{\mu_V}\right)\frac{dP_V}{dr}\right)}{dr} + \frac{dE}{dt} \qquad [4.40]$$

where: r = the radial distance from the surface of the column.

By substituting Eq. [4.24], Eq. [4.40] can be written as:

$$\frac{V_V M}{RT}\frac{dP_V}{dt} - \frac{m_V}{T}\frac{dT}{dt} + \frac{m_V}{V_V \rho_L}\left(\frac{dE}{dt} - \frac{1}{\rho_L}\frac{d\rho_L}{dT}\frac{dT}{dt}\left(m_D - m_L\right)\right) = \frac{d\left(\left(m_V \frac{k_T}{\mu_V}\right)\frac{dP_V}{dr}\right)}{dr} + \frac{dE}{dt} \qquad [4.41]$$

Hence, the governing differential equation for pore pressure in RC columns with circular cross-section is given by:

$$\frac{V_V M}{RT}\frac{dP_V}{dt} = \frac{d\left(\left(m_V \frac{k_T}{\mu_V}\right)\frac{dP_V}{dr}\right)}{dr} + \left(1 - \frac{m_V}{V_V \rho_L}\right)\frac{dE}{dt} + \frac{m_V}{T}\frac{dT}{dt} + \frac{m_V}{V_V \rho_L^2}\frac{d\rho_L}{dT}\frac{dT}{dt}\left(m_D - m_L\right) \qquad [4.42]$$

Using Eq. [4.13], Eq. [4.42] can be written as:

$$\frac{V_V M}{RT}\frac{dP_V}{dt} = \frac{d\left(\left(m_V \frac{k_T}{\mu_V}\right)\frac{dP_V}{dr}\right)}{dr} + \left(1 - \frac{m_V}{V_V \rho_L}\right)\left(-\frac{dm_L}{dP_V}\frac{dP_V}{dt} - \frac{dm_L}{dT}\frac{dT}{dt} + \frac{dm_D}{dT}\frac{dT}{dt}\right) + \frac{m_V}{T}\frac{dT}{dt} + \frac{m_V}{V_V \rho_L^2}\frac{d\rho_L}{dT}\frac{dT}{dt}\left(m_D - m_L\right) \qquad [4.43]$$

which can be rearranged as:

$$\left[\left(1-\frac{m_V}{V_V\rho_L}\right)\frac{dm_L}{dP_V}+\frac{V_V M}{RT}\right]\frac{dP_V}{dt}=\frac{d\left(\left(m_V\frac{k_T}{\mu_V}\right)\frac{dP_V}{dr}\right)}{dr}$$
$$+\left[\left(1-\frac{m_V}{V_V\rho_L}\right)\left(-\frac{dm_L}{dT}+\frac{dm_D}{dT}\right)+\frac{m_V}{T}+\frac{m_V}{V_V\rho_L^2}\frac{d\rho_L}{dT}(m_D-m_L)\right]\frac{dT}{dt} \quad [4.44]$$

where: J = mass flux of water vapor, λ = Darcy's coefficient of permeability, k_T = intrinsic permeability of concrete at temperature, T, and μ_V = dynamic viscosity of water vapor.

Similar to Equation [4.33], Equation [4.44] can be simplified by introducing three parameters, A, B, and C as follows:

$$A\frac{dP_V}{dt}=\frac{d\left(B\frac{dP_V}{dr}\right)}{dr}+C \quad [4.45]$$

where: A, B, and C are same as defined in Equation [4.34].

Equation [4.36] is modified to radial coordinates and the initial and boundary condition is written as:

$$\lambda\left(\frac{dP_V}{dr}\right)=-\frac{D_0 M}{RT}\left(P_V-\frac{RT\rho_{V\infty}}{M}\right) \quad [4.46]$$

where: D_0 = diffusion coefficient of water vapor at the boundaries of the column, ρ_V = density of water vapor in the concrete boundaries, and $\rho_{V\infty}$ = density of water vapor in the surrounding environment. T = temperature (°K).

4.3.3.3 Finite Element Solution

4.3.3.3.1 Rectangular Columns

Galerkin finite element formulation is applied to solve the heat transfer equation Eq. [4.4] and the differential equation for pore pressure development Eq. [4.34]. Both equations can be written in the following form:

$$A_1 \frac{du}{dt} = \nabla B_1 \nabla u + C_1 \qquad [4.47]$$

The governing equation at the column boundaries for both heat and mass transfer can be written as:

$$A_{11}\left(\frac{\partial u}{\partial y} n_y + \frac{\partial u}{\partial z} n_z\right) = -B_{11}\left(u - C_{11}\right) \qquad [4.48]$$

The cross-section of an RC column is divided into elements as shown in Figure 4.3. According to the finite element formulation, the material property matrices and the equivalent nodal heat or mass flux (stiffness matrix K_e, mass matrix M_e, and nodal heat or mass flux F_e) are generated for each element. These matrices are given by the following equations [William 1990]:

$$K_e = \int_A \left[B_1 \frac{\partial N}{\partial x} \frac{\partial N^T}{\partial x} + B_1 \frac{\partial N}{\partial y} \frac{\partial N^T}{\partial y} \right] dA + \int_\Gamma N B_{11} N^T ds \qquad [4.49]$$

$$M_e = \int_A A_1 N N^T dA \qquad [4.50]$$

$$F_e = \int_A N C_1 dA + \int_\Gamma N B_{11} C_{11} ds \qquad [4.51]$$

where: N = vector of the shape functions, A_1, B_1, C_1, A_{11}, B_{11} and C_{11} = parameters computed by comparing equations [4.4], [4.9], [4.10], [4.34] and [4.37] with equations [4.47] and [4.48] for heat and mass transfer, Γ = boundary of the column, and s = distance along the boundary Γ.

4.3.3.3.2 Circular Columns

For one dimensional analysis Eq. [4.38] and Eq. [4.45] can be written in the following form:

$$A_2 \frac{dP_V}{dt} = \frac{d\left(B_2 \frac{dP_V}{dr} \right)}{dr} + C_2 \qquad [4.52]$$

The governing equation at the column boundaries for both heat and mass transfer can be written as:

$$A_{22}\left(\frac{du}{dr} \right) = -B_{22}\left(u - C_{22} \right) \qquad [4.53]$$

Similar to rectangular columns, stiffness matrix K_e, mass matrix M_e, and nodal heat or mass flux F_e are generated for each element. These matrices are given by:

$$K_e = \int_r \left[B_2 \frac{dN}{dr} \frac{dN^T}{dr} \right] dr + NB_{22}N^T \qquad [4.54]$$

$$M_e = \int_r A_2 NN^T dr \qquad [4.55]$$

$$F_e = \int_r NC_2 dr + NB_{22}C_{22} \qquad [4.56]$$

where: N = vector of the shape functions, A_2, B_2, C_2, A_{22}, B_{22} and C_{22} = parameters computed by comparing Eqs. [4.38], [4.39], [4.45], and [4.46] with Eqs. [4.52] and [4.53] for heat and mass transfer Γ.

Solution of the Differential Equation

Once the element matrices are computed, they are assembled into a system of differential equations which can be written as:

$$M\dot{u} + Ku = F(t) \qquad [4.57]$$

where: K = global stiffness matrix, M = global mass matrix, F = equivalent nodal heat flux, and $\dot{u}$ = the derivative of u with respect to time.

A finite difference procedure (θ algorithm) in the time domain is used to solve Eq. [4.57] [William 1990]. The algorithm assumes:

$$u_{n+1} = u_n + h\left(\theta \dot{u}_{n+1} + (1-\theta)\dot{u}_n\right) \qquad [4.58]$$

Multiplying both sides of Eq. [4.58] by M and using Eq. [4.57] at the beginning and the end of the time interval (t_n, t_{n+1}), the following equation can be obtained:

$$(M + h\theta K)u_{n+1} = (M - h(1-\theta)K)u_n + h(\theta F_{n+1} + (1-\theta)F_n) \qquad [4.59]$$

where: h = time step, u_n and u_{n+1} = values of u at the beginning and the end of time step, respectively, F_n and F_{n+1} = equivalent nodal heat flux at the beginning and the end of time step, and θ = a constant between 0 and 1.

For unconditional stability of numerical calculations, θ has to be greater than or equal to 0.5 [William 1990]. By knowing the values of u at ambient conditions, Eq. [4.59] can be applied to obtain the time history for temperature or pressure at the following time step, and this can be repeated for subsequent time steps. In each time step, an iterative process is required to solve Eq. [4.59] due to the nonlinearity of both material properties and boundary conditions.

4.3.3.4 Spalling Predictions

Once the pore pressure in various concrete elements is calculated, a simplified approach is applied to determine spalling. The computed effective pore pressure (pore pressure multiplied by the porosity of concrete) is compared against the temperature dependent tensile strength of concrete as shown in Figure 4.4. When the effective pore pressure exceeds the temperature

dependent tensile strength at that time step, spalling is assumed to occur in that concrete element; i.e.:

$$nP_V > f_{tT} \quad [4.60]$$

where:

n = porosity of concrete = $V_V + V_L$, and

f_{tT} = tensile strength of concrete for temperature, T.

Once spalling occurs, that concrete element is assumed to be lost and the reduced concrete section and new boundary surface is considered in the subsequent hydro-thermal and strength analyses. In this way, the coupling between spalling and hydro-thermal analysis will be accounted for in the model.

4.3.3.5 Constitutive Relationships

4.3.3.5.1 Isotherms

Isotherms are used to predict the mass of liquid water inside concrete as a function of pore pressure and temperature. The isotherms, used in the analysis, are assumed to follow the semi empirical isotherms developed by Bazant and Thonguthai [1978] and presented by Dwaikat and Kodur [2009]. The main assumption in Bazanat's isotherms is that water in concrete is capillary water (adsorbed water is ignored). This assumption may not be applicable for HSC at room temperature where adsorbed water is a large portion of water in concrete. However, Bazant showed that the adsorbed water significantly decreases at elevated temperatures and thus capillary water becomes the dominant state of water in HSC. According to Bazant's isotherms, the mass of liquid water can be given as:

$$m_L = \begin{Bmatrix} \rho_C \left(\dfrac{m_0}{\rho_C} \dfrac{P_V}{P_S} \right)^{1/m(T)} & , \dfrac{P_V}{P_S} \le 0.96 \\ m_{0.96} + \left(\dfrac{P_V}{P_S} - 0.96 \right) \dfrac{m_{1.04} - m_{0.96}}{0.08} & , 0.96 < \dfrac{P_V}{P_S} < 1.04 \\ m_{L0} \left[1 + 0.12 \left(\dfrac{P_V}{P_S} - 1.04 \right) \right] & , \dfrac{P_V}{P_S} \ge 1.04 \end{Bmatrix} \quad [4.61]$$

The case of relative humidity (P_V/P_S) exceeding 100% represents the case of condensation of water vapor. According to Bazant's isotherms, the mass of liquid water (m_L) exceeds the saturation mass of liquid water (m_{L0}) at room temperature when the relative humidity exceeds 100%. This can be attributed to the condensation of water vapor transferred to the high pressure region. The increase in pressure is associated with an increase in concrete porosity due to elastic deformation and cracking. This provides more space for the increase in the mass of liquid water at room temperature.

Thus, the derivatives of m_L with respect to pore pressure and temperature (which are essential to compute A and C in Eq. [4.34]) are:

$$\frac{dm_L}{dP_V} = \begin{Bmatrix} \dfrac{m_0}{m(T) P_S} \left(\dfrac{m_0}{\rho_C} \dfrac{P_V}{P_S} \right)^{1/m(T)-1} & , \dfrac{P_V}{P_S} \le 0.96 \\ \dfrac{m_{1.04} - m_{0.96}}{0.08} & , 0.96 < \dfrac{P_V}{P_S} < 1.04 \\ 0.12 \dfrac{m_{L0}}{P_S} & , \dfrac{P_V}{P_S} \ge 1.04 \end{Bmatrix} \quad [4.62]$$

$$\frac{dm_L}{dT} = \begin{cases} -m_L\left[\dfrac{\dfrac{dm(T)}{dT}}{m(T)^2} ln\left(\dfrac{m_0 P_V}{\rho_C P_S}\right) + \dfrac{\dfrac{dP_S}{dT}}{m(T)P_S}\right] & ,\dfrac{P_V}{P_S} \le 0.96 \\ \dfrac{dm_{0.96}}{dT} - \dfrac{P_V}{P_S^2}\dfrac{\dfrac{dP_S}{dT}}{}\left(\dfrac{m_{1.04} - m_{0.96}}{0.08}\right) + X & ,0.96 < \dfrac{P_V}{P_S} < 1.04 \\ \dfrac{dm_{L0}}{dT}\left[1 + 0.12\left(\dfrac{P_V}{P_S} - 1.04\right)\right] - 0.12\dfrac{m_{L0} P_V \dfrac{dP_S}{dT}}{P_S^2} & ,\dfrac{P_V}{P_S} \ge 1.04 \end{cases} \qquad [4.63]$$

where:

ρ_C = mass of cement per unit volume of concrete,

m_0 = mass of water for saturation at 25 °C per unit volume of concrete,

m_{L0} = mass of water for saturation at any temperature per unit volume of concrete,

P_S = saturation pressure,

$$m(T) = 1.04 - \frac{(T+10)^2}{22.3(25+10)^2 + (T+10)^2},$$

$$m_{0.96} = \rho_C\left(0.96\frac{m_0}{\rho_C}\right)^{1/m(T)},$$

$$m_{1.04} = m_{L0} = \rho_L(1 - V_{S0}) + m_D,$$

$$\frac{dm(T)}{dT} = -\frac{2(T+10)\left(22.3(T0+10)^2 + (T+10)^2\right) - 2(T+10)^3}{\left(22.3(T0+10)^2 + (T+10)^2\right)^2},$$

$$\frac{dm_{0.96}}{dT} = -m_{0.96} \frac{ln\left(0.96 \frac{m_0}{\rho_{cem}}\right) \frac{dm(T)}{dT}}{(m(T))^2},$$

$$\frac{dm_{1.04}}{dT} = \frac{dm_{L0}}{dT} = (1 - V_{S0}) \frac{d\rho_L}{dT} + \frac{dm_D}{dT},$$

$$X = \left(\frac{P_V}{P_S} - 0.96\right) \frac{\frac{dm_{1.04}}{dT} - \frac{dm_{0.96}}{dT}}{0.08}, \text{ and}$$

T = temperature (°C).

4.3.3.5.2 Permeability Model

Permeability of concrete varies significantly with temperature and pore pressure. However, even to date, such variation is not well understood. Thus, in the spalling sub-model, the variation of permeability as a function of pore pressure and temperature is assumed to follow the relationship developed by Gawin et al. [1999] based on the experimental results conducted by Schneider and Herbst [1989]. Accordingly, the intrinsic permeability of concrete at any temperature is give as:

$$k = k_0 10^{C_T (T - T_0)} \left(\frac{P_V}{P_0}\right)^{0.368} \quad [4.64]$$

k_T = intrinsic permeability of concrete at temperature T (°C), k_0 = initial intrinsic permeability of concrete at room temperature, P_0 = 101,325 Pa, P_V = pore pressure (Pa), T_0 = initial temperature (°C), and C_T = factor to account for the increase in concrete permeability at elevated temperatures.

Mechanical and thermo-chemical damage increases the permeability of concrete which leads to the development of lower pore pressure and in turn less spalling. Thus, the effect of mechanical and thermo-chemical damage on permeability of concrete is conservatively ignored.

Gawin et al. [1999] suggested a value of 0.005 for C_T. However, this value of C_T seems to overestimate the increase in permeability of concrete at elevated temperatures (especially for concrete with high initial permeability) when compared with test results reported by Kanema et al. [2007] and Dwaikat [2009]. The higher the permeability at elevated temperatures, the lower the (developed) vapor pressure and this will reduce the fire induced spalling in concrete. A review of the literature indicates that there is lack of test data on the variation of permeability as a function of temperature. Thus, the factor C_T in Eq. [4.64] is conservatively assumed to be 0.0025, which is lower than all the values obtained from test results.

4.3.3.5.3 Dehydration

Two types of water; namely, evaporable and nonevaporable water, are present in cement paste. Evaporable water is lost when cement paste is oven-dried at 110 °C, while nonevaporable water is lost when oven-dried cement paste is heated to temperature of about 800 °C in a process called dehydration. Dehydration of cement paste is a complex phenomenon that depends on many factors including temperature and chemical composition of the cement paste itself. Even to date, such phenomenon is not completely understood. The amount of nonevaporable water, which is chemically bound with cement, increases with the degree of hydration of the concrete mix. Thus, for spalling predictions, it will be conservative to assume that the concrete is fully hydrated. In the spalling model, dehydration of cement paste is considered based on the simplified approach

suggested by Bazant and Kaplan [1996]. In this approach (where concrete is assumed to be fully hydrated at room temperature) the mass of dehydrated water, m_D, can be given as:

$$m_D = \begin{cases} 0 & T \le 100\,°C \\ 0.04\rho_C \dfrac{T-100}{100} & 100°C < T \le 700°C \\ 0.24\rho_C & T > 700°C \end{cases} \qquad [4.65]$$

4.3.3.5.4 Tensile Strength of Concrete

Tensile strength of concrete, at elevated temperatures, is assumed to vary as per Eurocode 2 [2004] provisions but with some modifications to minimize the convergence problems when the tensile strength becomes zero at relatively low temperature (600 °C). In such conditions, the model might predict spalling to occur at very low values of pore pressure, which is unrealistic as observed in fire tests [Dwaikat, 2009]. Thus, variation of tensile strength of concrete with temperature is assumed to follow the following expression:

$$f_{tT} = \begin{cases} f_t & T \le 100\,°C \\ f_t \dfrac{600-T}{500} & 100°C < T \le 550°C \\ f_t \dfrac{1200-T}{6500} & 550°C < T \le 1200°C \\ 0 & T > 1200°C \end{cases} \qquad [4.66]$$

where:

f_{tT} = tensile strength of concrete at temperature T (°C), and f_t = tensile strength of concrete at room temperature.

It should be noted that the modifications to Eurocode equation for the temperature dependent tensile strength is to avoid numerical instability and it has very small effect on the accuracy of

the spalling predictions. This is because, according to Eq. [4.66], more than 90% of the room temperature tensile strength will be lost for concrete heated to above 600°C.

4.3.3.6 Limitations

The spalling sub-model presented here is capable of predicting early and intermediate stages of spalling. "Late" stage spalling which occurs just prior to failure is not considered in the analysis since it primarily results from significant loss of strength and stiffness. However, such type of spalling, due to the fact that it occurs just prior failure, does not significantly influence the overall fire resistance of RC columns.

4.3.4 Strength Analysis

The strength analysis procedure is similar for RC columns with both rectangular and circular cross-section. This is because in the structural analysis, the column is represented as a 1-dimensional frame element and the cross-section effect is incorporated through the generated M-κ relationships as explained later.

4.3.4.1 General Analysis Procedure

The third step in the numerical model is the strength analysis at the mid-section of each segment. The cross-sectional temperature distribution generated from hydro-thermal analysis is used as input to the strength analysis. For the strength analysis, the following assumptions are made:

- Plane sections before bending remain plane after bending.
- There is no bond-slip between steel reinforcement and concrete.
- Concrete of strength higher than 70 MPa is considered to be HSC.

At each time step, the strength analysis is performed in three sub-steps; namely, estimating the axial force in each segment of the restrained column, generating the M-κ relationship for each

segment, and carrying out nonlinear stiffness analysis to trace the response of the column under fire conditions. The axial force, due to fire induced restraint, is computed based on the axial deformation of the column. This axial force is assumed to be zero at the first time step (room temperature). For the subsequent time steps, the axial deformation from the preceding time step is utilized to compute the axial force. The use of the curvatures from the preceding time step does not have a significant influence on the restraint force provided the time increments are small.

The M-κ relationships, at various time steps, are generated using the calculated axial restraint force and the constitutive relationships for concrete and reinforcement. The interaction between axial force and bending moment capacity (and stiffness of the column) is automatically accounted for in the generated M-κ relationships. In the nonlinear stiffness analysis, the deformation of the column at each time step can be calculated through a stiffness approach which utilizes generated M-κ relationships to compute the stiffness for each column segment.

Various strain components including mechanical strain, thermal strain, and creep strain for both concrete and reinforcing steel, and transient strain for concrete are accounted for in the model. The creep and transient strains, which are often not accounted for in fire resistance calculations, might play a significant role on the fire response of RC columns particularly, deflections. Spalling of concrete is incorporated into fire resistance calculations through the pore pressure predictions as discussed above.

The strength calculations are carried out using the same rectangular network described above and shown in Figure 4.3(b). The temperatures, deformations and stresses in each element are represented by those at the center of the element. The temperature at the center of the concrete element is obtained by averaging the temperatures of the nodes of that element in the network.

The same procedure is used for steel reinforcement, with the values of stress, strain components, and temperature of each bar are represented by those at the center of the bar. The temperature at the centre of a steel bar is approximated by the temperature at the location of the center of the bar cross-section (in concrete).

The total strain in a concrete element, at any fire exposure time, is taken as the sum of the thermal expansion, the mechanical strain, the creep strain, and the transient strain:

$$\varepsilon_t = \varepsilon_{th} + \varepsilon_{me} + \varepsilon_{cr} + \varepsilon_{tr} \qquad [4.67]$$

where: ε_t = total strain, ε_{th} = thermal strain, ε_{me} = mechanical strain, ε_{cr} = creep strain, and ε_{tr} = transient strain.

Thermal strain is directly dependent on the temperature in the element and can be obtained by knowing the temperature and thermal expansion of the concrete. Creep strain is assumed to be function of time, temperature, and stress level, and is computed based on Harmathy's [1993] approach using the following expression:

$$\varepsilon_{cr} = \beta_1 \frac{\sigma}{f_{c,T}} \sqrt{t}\ e^{d(T-293)} \qquad [4.68]$$

where: $\beta_1 = 6.28\times10^{-6}$ s$^{-0.5}$, $d = 2.658\times10^{-3}$ K^{-1}, T = concrete temperature (°K) at time t (s), $f_{c,T}$ = concrete strength at temperature T, and σ = stress in the concrete at the current temperature.

The transient strain, which is specific for concrete under fire conditions, is computed based on the relationship proposed by Anderberg and Thelandersson [1976]. The transient strain is related to thermal strain as follows:

$$\Delta\varepsilon_{tr} = k_2 \frac{\sigma}{f_{c,20}} \Delta\varepsilon_{th} \qquad [4.69]$$

where: k_2 = a constant ranges between 1.8 and 2.35 (a value of 2 will be used in the analysis), $\Delta\varepsilon_{th}$ = change in thermal strain, $\Delta\varepsilon_{tr}$ = change in transient strain, and $f_{c,20}$ = concrete strength at room temperature.

For steel reinforcement, the total strain, at any fire exposure time, is calculated as the sum of three components, as given by the following equation:

$$\varepsilon_{ts} = \varepsilon_{ths} + \varepsilon_{mes} + \varepsilon_{crs} \qquad [4.70]$$

where: ε_{ts}, ε_{ths}, ε_{mes} and ε_{crs} are total strain, thermal strain, mechanical strain, and creep strain in the steel reinforcement, respectively.

Similar to concrete, thermal strain in steel can be directly calculated from the knowledge of rebar temperature and the thermal expansion coefficient of the reinforcing steel. Creep strain is computed based on Dorn's theory and the model proposed by Harmathy [1967] with some modifications made to account for different values of yield strength of steel. According to Harmathy's model, creep strain in steel is given by the following expression:

$$\varepsilon_{crs} = \left(3Z\varepsilon_{t0}^2\right)^{1/3}\theta^{1/3} + Z\theta \qquad [4.71]$$

where:

$$Z = \begin{Bmatrix} 6.755\times10^{19}\left(\dfrac{\sigma}{f_y}\right)^{4.7} & \dfrac{\sigma}{f_y} \le \dfrac{5}{12} \\ 1.23\times10^{16}\left(e^{10.8\left(\sigma/f_y\right)}\right) & \dfrac{\sigma}{f_y} > \dfrac{5}{12} \end{Bmatrix},$$

$\theta = \int e^{-\Delta H/RT} dt$, $\frac{\Delta H}{R} =$ 38900°K, t = time (hours), $\varepsilon_{t0} = 0.016\left(\frac{\sigma}{f_y}\right)^{1.75}$, σ = stress in steel, and f_y = yield strength of steel.

Figure 4.5 shows the distributions of total strain, stress, and internal forces for the column cross-section at any fire exposure time. The total strain in any element (concrete or rebar) can be related to the curvature of the column by the following expression:

$$\varepsilon_t = \varepsilon_0 + \kappa y \qquad [4.72]$$

where: ε_0 = total strain at the geometrical centroid of the column cross-section, κ = curvature, and y = the distance from the geometrical centroid of the column cross-section.

In the model, Eq. [4.67] to Eq. [4.72] can be used to carry out strain computation of a segment at any given fire exposure time. At any time step, and for an assumed value of ε_0 and κ, the total strain in each element (concrete or rebar) can be determined using Eq. [4.72]. Then the thermal, transient (for concrete only), and creep strains in the concrete and rebars are evaluated using known temperatures and corresponding equations derived above. Using the knowledge of total, thermal, transient, and creep strains, the mechanical strain in concrete or steel element can be evaluated by rearranging Eqs. [4.67] and [4.70]:

$$\varepsilon_{me} = \varepsilon_t - \varepsilon_{th} - \varepsilon_{cr} - \varepsilon_{tr} \qquad \text{for concrete} \qquad [4.73]$$

$$\varepsilon_{mes} = \varepsilon_{ts} - \varepsilon_{ths} - \varepsilon_{crs} \qquad \text{for steel} \qquad [4.74]$$

Then for the estimated mechanical strain, the stress in the element can be established using the stress strain relationships for steel and concrete.

4.3.4.2 Calculation of Fire Induced Axial Force

RC columns can develop significant restraint forces under fire exposure. The degree of restraint is dependent on the support conditions and will determine the behavior and fire resistance of an RC column. Generally, the axial restraint force in an RC column is compressive during the expansion phase of the column and tensile when the column starts contracting. Thus the axial restraint force is computed as:

$$P_r = k_r \Delta \qquad [4.75]$$

where: P_r = axial restraint force, k_r = axial restraint stiffness provided by adjoined beams supported by the column, Δ = axial deformation of the column.

4.3.4.3 Generation of M-κ Relationships

The M-κ generation, at elevated temperatures, is carried out using the same rectangular and circular networks described above and shown in Figure 4.3. Once the axial restraint force in the column is computed, the M-κ relationships are generated through an approach analogous to the method used for the analysis of prestressed concrete beams. In this approach, M-κ relationships are established by iterating the central total strain (ε_0) and the curvature (κ).

At the beginning of the analysis, values for curvature and central total strain (in concrete) are assumed. Then, the total strain in each of the rebars and concrete elements is computed from the assumed strain and curvature. The stresses in the rebars and the concrete elements are determined using the constitutive laws of the materials. The temperature of a rebar is assumed to be equal to the temperature at the location of the center of the rebar. Once the stresses are known, the forces are computed in the concrete and the rebars. The curvature is then iterated until equilibrium of forces is satisfied (internal force equal to the fire induced axial restraint force).

Once the equilibrium is satisfied, the moment and the corresponding curvature are calculated. Thus, the values of moment and curvature are stored to represent a point on the M-κ curve.

The value of the central total strain is incremented to generate subsequent points on the moment curvature curve. This procedure is repeated for each time step of fire exposure. The generated M-κ curves are used for tracing the behavior of the column through nonlinear structural analysis. The generation of M-κ relationships is an important part of the numerical model since these relationships form the basis for the fire resistance analysis of the column. In the case of rectangular columns there is a possibility of biaxial bending due to eccentricity of load, 1-, 2-, 3-, sided exposure and uneven fire-induced spalling as explained in Chapter 1. Hence to account for this the moment curvature relationships are generated along both the axes. This is not necessary for circular columns since the temperature profile and spalling are always axisymmetric. The eccentricity of the load may lead to uniaxial bending only since during analysis the bending axis can be chosen to pass through the point of application of the load.

4.3.4.4 Column (Member) Analysis

The M-κ relationships and the axial restrained force generated for various segments are used to trace the response of the whole column exposed to fire. At each time step the deformations in the column are evaluated through a stiffness approach. The secant stiffness for each segment is determined from the M-κ relationships, based on the moment level reached in that particular segment.

Each node in the idealized column is assumed to have five degrees of freedom (namely; two rotations and three displacements) in the case of rectangular columns and three degrees of freedom (namely; rotation and two displacements) in the case of circular columns. The deformation of the column is computed using an iterative procedure described by Campbell and

Kodur [1990]. Accordingly, the first step in the analysis is to conduct a linear analysis using the initial rigidity of the column (EI_0) to determine the moment distribution along the span of the column. The segment having the maximum bending moment is selected to be the critical segment.

The second step is to increment the curvature in the critical segment and the curvature and moment distributions along the span of the column (in each segment) are computed for each increment of the curvature. An iterative procedure is employed to obtain the solution at each increment of curvature such that equilibrium, compatibility, and convergence conditions are satisfied.

The iterative procedure used for the column analysis is illustrated in Figure 4.6. For each increment, a target curvature is selected for the critical segment. The analysis is carried out using secant stiffness of the column computed from the generated moment curvature relationships. The column is analyzed under a unit load and the bending moment and the curvature in each segment are computed. The curvature in each segment is multiplied by a scaling factor that is computed through dividing the target curvature in the critical element by the computed curvature in the same element. The new secant rigidity for the next iteration can be computed from the generated M-κ relationship. The iterative procedure continues until convergence is achieved where the rigidity in each segment is approximately maintained within a certain tolerance.

In the iterative procedure described above, the stiffness matrix and the loading vector are computed for each longitudinal segment. Then these matrices are assembled in the form of nonlinear global stiffness equation, which can be written as:

$$K_g \, \delta = P_f + P_s \qquad [4.76]$$

where: K_g = global stiffness matrix, δ = nodal displacements, P_f = equivalent nodal load vector due to applied loading, and P_s = equivalent nodal load vector due to P-δ effect.

The effect of the second order moments, developed due to the axial restraint force, is calculated using the following equation:

$$P_s = -K_{geo}\delta \qquad [4.77]$$

where: K_{geo} = geometric stiffness matrix, δ = nodal displacements, and P_s = equivalent nodal load vector due to *P*-δ effect.

The second order moments are then added to the external loads in the stiffness analysis as given by equation [4.76]

Thus, for any given time step, the temperatures (in concrete and steel), moment capacity and curvatures, as well as deformations in the column are known for a given fire exposure. These output parameters are used to evaluate the failure of the column at local (in each segment) and global (whole column) levels using two sets of failure criteria which include strength and thermal limit states. The analysis is continued until strength failure of the column is reached. The two sets of failure criterion used to define failure of an RC column are:

1) When the temperature in steel rebars (tension reinforcement) exceeds the critical temperature which is 593 °C for reinforcing steel.
2) When the column is unable to resist the specified applied service load.

4.3.4.5 Column Analysis

4.3.4.5.1 Rectangular Columns

The global stiffness matrix (K_g), in equation [4.76], needs to be defined. The solution to a biaxially loaded column (representing the case of a beam-column) requires due consideration of geometry, boundary conditions and thermal gradients. The instability of the member arising from the magnification of the primary moments by the axial load acting on the laterally deflecting beam-column must also be considered. To account for biaxial bending arising from uneven spalling or loading or 1-, 2-, 3-sides fire exposure, a 3-D frame element as shown in Figure 4.7 is used. The five different degrees of freedom to be considered in a beam-column segment at each node are shown in Figure 4.7. The segmental stiffness matrix *[k(10×10)]* is computed considering axial and bending deformations separately. The sectional properties are assumed to be constant within the segment at a given time step. Thus elastic analysis can be performed. The segmental matrix is derived by solving separately the axial and flexural components, using the force-displacement relations. The flexural components in Y and Z directions and the three force components in X, Y, Z directions are given by:

$$P = -EAu_x'\,;\; m_y = -EI_y u_z''\,;\; m_z = -EI_z u_y'' \qquad [4.78]$$

where: P = axial force acting on the column; m_y and m_z = moment about the Y and Z axis; EA = axial rigidity of the segment; EI_y and EI_z = flexural rigidity of the segment about Y and Z axis.

The final stiffness matrix for each segment can be written as

$$\left[k(10\times 10)\right] = \begin{bmatrix} k_{AA}(5\times 5) & k_{AB}(5\times 5) \\ k_{BA}(5\times 5) & k_{BB}(5\times 5) \end{bmatrix} \qquad [4.79]$$

In Eq. (4.79) the stiffness matrices K_{AA}, K_{BB} and K_{AB} are expressed as:

$$[k_{AA}]=\begin{bmatrix} \frac{EI_y k_y^3 S_y}{2-2C_y-k_y LS_n} & 0 & 0 & 0 & \frac{EI_y k_y^2(1-C_y)}{2-2C_y-k_y LS_n} \\ 0 & \frac{EI_z k_z^3 S_z}{2-2C_z-k_z LS_z} & 0 & -\frac{EI_z k_z^2(1-C_z)}{2-2C_z-k_z LS_z} & 0 \\ 0 & 0 & \frac{EA}{L} & 0 & 0 \\ 0 & -\frac{EI_z k_z^2(1-C_z)}{2-2C_z-k_z LS_z} & 0 & \frac{EI_z k_z(S_z-k_z LC_z)}{2-2C_z-k_z LS_z} & 0 \\ \frac{EI_y k_y^2(1-C_y)}{2-2C_y-k_y LS_n} & 0 & 0 & 0 & \frac{EI_y k_y(S_y-k_y LC_y)}{2-2C_y-k_y LS_y} \end{bmatrix}$$

[4.80]

$$[k_{BB}]=\begin{bmatrix} \frac{EI_y k_y^3 S_y}{2-2C_y-k_y LS_n} & 0 & 0 & 0 & \frac{EI_y k_y^2(1-C_y)}{2-2C_y-k_y LS_n} \\ 0 & \frac{EI_z k_z^3 S_z}{2-2C_z-k_z LS_z} & 0 & -\frac{EI_z k_z^2(1-C_z)}{2-2C_z-k_z LS_z} & 0 \\ 0 & 0 & \frac{EA}{L} & 0 & 0 \\ 0 & -\frac{EI_z k_z^2(1-C_z)}{2-2C_z-k_z LS_z} & 0 & \frac{EI_z k_z(S_z-k_z LC_z)}{2-2C_z-k_z LS_z} & 0 \\ \frac{EI_y k_y^2(1-C_y)}{2-2C_y-k_y LS_n} & 0 & 0 & 0 & \frac{EI_y k_y(S_y-k_y LC_y)}{2-2C_y-k_y LS_y} \end{bmatrix}$$

[4.81]

$$[k_{BA}]=\begin{bmatrix} -\frac{EI_y k_y^3 S_y}{2-2C_y-k_y LS_n} & 0 & 0 & 0 & -\frac{EI_y k_y^2(1-C_y)}{2-2C_y-k_y LS_n} \\ 0 & -\frac{EI_z k_z^3 S_z}{2-2C_z-k_z LS_z} & 0 & \frac{EI_z k_z^2(1-C_z)}{2-2C_z-k_z LS_z} & 0 \\ 0 & 0 & -\frac{EA}{L} & 0 & 0 \\ 0 & \frac{EI_z k_z^2(1-C_z)}{2-2C_z-k_z LS_z} & 0 & \frac{EI_z k_z(S_z-k_z LC_z)}{2-2C_z-k_z LS_z} & 0 \\ -\frac{EI_y k_y^2(1-C_y)}{2-2C_y-k_y LS_n} & 0 & 0 & 0 & \frac{EI_y k_y(S_y-k_y LC_y)}{2-2C_y-k_y LS_y} \end{bmatrix}$$

[4.82]

where: $$C_y = \cos k_y L; S_y = \sin k_y L; C_z = \cos k_z L; S_z = \sin k_z L;$$

$$k_y = \sqrt{\frac{P}{EI_y}}; k_z = \sqrt{\frac{P}{EI_z}}$$

Using the time dependant M-κ relationships developed above the flexural rigidity (EI) of each segment along both the axes can be computed. The global stiffness matrix is generated by assembling the stiffness matrices for each segment and the strength analysis is carried out.

4.3.4.5.2 Circular Columns

As discussed before, circular columns can be subject to uniaxial bending only. Thus in the case of circular columns a 2-D frame element (see Figure 4.7(b)) is utilized. This member has three degrees of freedom per node thus making the global stiffness matrix (K_g) of the order 6×6. The above Equation [4.79] can be reduced as:

$$[k(6\times 6)] = \begin{bmatrix} k_{AA}(3\times 3) & k_{AB}(3\times 3) \\ k_{BA}(3\times 3) & k_{BB}(3\times 3) \end{bmatrix} \quad [4.83]$$

In Eq. (5) the stiffness matrices K_{AA}, K_{BB} and K_{AB} are expressed as:

$$[k_{AA}] = \begin{bmatrix} \frac{EI_y k_y^3 S_y}{2-2C_y-k_y LS_n} & 0 & \frac{EI_y k_y^2 (1-C_y)}{2-2C_y-k_y LS_n} \\ 0 & \frac{EA}{L} & 0 \\ \frac{EI_y k_y^2 (1-C_y)}{2-2C_y-k_y LS_n} & 0 & \frac{EI_y k_y (S_y-k_y LC_y)}{2-2C_y-k_y LS_y} \end{bmatrix} \quad [4.84]$$

$$[k_{BB}]=\begin{bmatrix} \dfrac{EI_y k_y^3 S_y}{2-2C_y-k_y LS_n} & 0 & \dfrac{EI_y k_y^2(1-C_y)}{2-2C_y-k_y LS_n} \\ 0 & \dfrac{EA}{L} & 0 \\ \dfrac{EI_y k_y^2(1-C_y)}{2-2C_y-k_y LS_n} & 0 & \dfrac{EI_y k_y(S_y-k_y LC_y)}{2-2C_y-k_y LS_y} \end{bmatrix} \quad [4.85]$$

$$[k_{BA}]=[k_{AB}]=\begin{bmatrix} -\dfrac{EI_y k_y^3 S_y}{2-2C_y-k_y LS_n} & 0 & -\dfrac{EI_y k_y^2(1-C_y)}{2-2C_y-k_y LS_n} \\ 0 & -\dfrac{EA}{L} & 0 \\ -\dfrac{EI_y k_y^2(1-C_y)}{2-2C_y-k_y LS_n} & 0 & \dfrac{EI_y k_y(S_y-k_y LC_y)}{2-2C_y-k_y LS_y} \end{bmatrix} \quad [4.86]$$

where: $C_y = \cos k_y L; S_y = \sin k_y L; C_z = \cos k_z L; S_z = \sin k_z L;$

$$k_y = \sqrt{\frac{P}{EI_y}}; k_z = \sqrt{\frac{P}{EI_z}}$$

4.4 Computer Implementation

The numerical procedure described above requires a large amount of computations since an iterative approach has to be used. Therefore, to facilitate the above set of calculations, the numerical procedure was incorporated into a computer program, written in FORTRAN. Figure 4.2 shows flowcharts of the numerical procedure associated with the computer program. Details regarding input parameters such as idealization, material properties, fire scenarios, structural parameters and output results are presented below.

4.4.1 Column Idealization

The RC column is idealized to be a set of longitudinal frame elements (segments). For hydro-thermal and mechanical analysis of RC columns, the cross-section of each segment is idealized

as a mesh of elements as shown in Figure 4.3. The number of longitudinal segments and the number of elements and the grid size in each direction are to be specified in the input file. The program allows for non-uniform grid size in the cross-sectional mesh.

In finite element analysis discritization parameters such as segment length, and mesh (element) size can significantly influence model predictions. Thus, for accurate and realistic predictions the appropriate discritization parameters need to be used as input parameters. To develop optimum discritization parameters numerical studies were carried out by varying these parameters over a range and quantifying their effect on fire resistance predictions.

4.4.1.1 Effect of Mesh Size

To study the effect of mesh size on fire resistance predictions, a mesh-sensitivity study was undertaken. Details of the RC column used for the analysis is shown in Figure 4.8. The column is divided into 40 segments of equal length. The column was subjected to ASTM E119 standard fire and was axially loaded to 50% of its room temperature capacity. The results which included both spalling predictions and rebar temperatures are shown in Figure 4.9.

Since the mesh size influences cross-sectional temperatures and spalling predictions (which in turn affect fire resistance) these are plotted as a function of time. Figure 4.9 (a) shows the progression of spalling for various element sizes. It can be seen that there are sudden jumps in spalling predictions when the mesh is coarse. This smoothens out with decrease in element size (finer mesh). The predictions from a 10 mm (0.4 in) element mesh and a 1 mm (0.04 in) element mesh are identical. There is a slight difference in predictions from the 25 mm (1 in) mesh that of 10 mm (0.4 in) mesh. The 10 mm (0.4 in) mesh predicts spalling to start earlier than that in the case of 25 mm (1 in) mesh. This is because of elimination of elements once the pore pressure exceeds the tensile strength of concrete at the interface of the element. In the case 25 mm (1 in)

mesh longer time is required for the pore pressure to rise so that spalling can occur compared to a 10 mm (0.4 in) mesh wherein the lesser time is required and thus the element spalls off indicating earlier onset of spalling.

Figure 4.9 (b) shows the rebar temperature as a function of fire exposure time for different mesh sizes. Again the rise in temperature with a coarser mesh is more sudden due to the loss of an element (resulting from spalling) thus making the inner element (and eventually the rebar) exposed to higher temperatures. But it can be seen that the temperatures with mesh size of 25 mm (1 in) or smaller are similar and thus it can be said that an element size of 25 (1 in) mm or smaller can provide accurate temperatures. Therefore a 25 mm (1 in) mesh size is recommended for fire resistance analysis using this model.

4.4.1.2 Effect of Segment Length

The effect of segment length on fire resistance predictions is investigated by varying the length of segments in fire resistance analysis. As discussed in the numerical model section, the program utilizes moment curvature relationships for tracing the fire response of RC columns. Therefore the curvature variation along the length of the column depends on the length of the segments. Theoretically the higher the number of segments (smaller the segment length), more accurate is the predicted stiffness of the column. To arrive at an optimum length of segments a parametric study was carried out by varying the number of segments along the column length. The number of segments rather than segment length was chosen since the variation of curvature along the column length can be better represented with larger number of segments.

Same column as studied in the mesh sensitivity study was selected for this analysis. An elemental mesh size of 25 mm (1 in) was used in the analysis. The number of segments of the column was varied from 5, 10, 20, 40, and 100 segments. Figure 4.10 shows the axial

deformations predicted for the column using various numbers of segments (divisions). It can be seen that all columns behave the same during the expansion phase. This is because the axial deformation in this phase solely depends on the thermal expansion of the column. Since the temperature rise resulting from thermal analyses for these columns were identical, the expansion is also the same. When the column starts losing its stiffness and starts contracting, then the curvature of the column plays an important role in determining its stiffness. For lesser segments the column is inherently stiffer and thus the axial deformations are smaller. This in turn lead to smaller lateral deflection and thus small moments acting on the column due to reduced P-δ effects. Thus with the use of lesser segments the column is predicted to have a higher fire resistance and this is not realistic. It can be seen that at least 40 segments are required to achieve reasonable accurate predictions. For undertaking fire resistance analysis using the model, discretizing the column with 40 segments gives reliable predictions.

4.4.2 Time Domain

The complete time domain (time to failure of a column under fire conditions) in divided into smaller time steps for the analysis and fire resistance analysis is carried out by incrementing time step. Separate time steps can be input for the hydro-thermal analysis and the structural analysis. The program computes and iterates until convergence is attained at each time step. Then the result from that time step is used as for the subsequent time step. Also, as mentioned below the high temperature material properties are also highly nonlinear and temperature dependent. Thus the problem is highly nonlinear and sensitive to the time steps used.

Similar to the mesh size and number of segments, the time increment selected for fire resistance analysis can influence on the model predictions. Hence the same column studied above was analyzed with an element size of 25 mm (1 in) and 40 segments along the length with different

time increments. Figure 4.11 (a) shows the rebar temperature predictions from thermal analysis corresponding to time steps of 0.5, 1, 5 and 10 minutes. It can be seen that smaller time increments of 1 minute is required for accurate predictions from the model. This is also due to the fact that the spalling sub-model is also sensitive to the time increments and thermal properties of concrete are highly nonlinear.

Figure 4.11 (b) shows the predicted axial deformations for the same columns for time steps of 0.5, 1, 5 and 10 minutes. The results from thermal analysis with 1 minute time step were used as input for these structural analyses. From the figure it can be seen that the model gives reasonable predictions with a maximum time step of 5 minutes. The higher time step in structural analysis, as compare to that of thermal analysis, is because the structural analysis is not as sensitive to the time step as long as accurate predictions are available from the thermal analysis.

4.4.3 Fire Scenario

Time temperature curves corresponding to standard fire scenarios; namely, ASTM E119 standard fire, hydrocarbon standard fire, external standard fire, as well as two design fire scenarios (shown in Figure 4.12) are built into the program. The user has the option of selecting any of the five fire exposures by specifying in the input file. Alternatively the user can define any other time temperature relationship in the input file.

4.4.4 Exposure Condition

As discussed earlier the column can be exposed to fire on different sides (1-, 2-, 3-, or all 4) and this information needs to be provided in the model. The appropriate boundary conditions for the thermal analysis are then automatically considered in the program.

4.4.5 Structural Parameters

The basic input for the program consists of structural parameters which are critical for realistic predictions. These are:

4.4.5.1 Support Conditions and End Restraint

The end conditions for the column need to be specified as input parameters. Also, the values of axial and rotational end restraint, if any, are to be provided (as spring stiffnesses) and the numerical model can account the restraint force developed in the column.

4.4.5.2 Load and Load Eccentricity

The load level and any eccentricity of the loading needs to be specified. A minimum eccentricity is assumed in the model if the load is concentric. This is necessary in order to account for imperfections and initiate the non-linear analysis.

4.4.6 Material Properties

4.4.6.1 Concrete

The user can specify any of the material models in the input file. Three sets of high temperature concrete properties (both thermal and mechanical) as specified in Eurocode 2 [2004], ASCE Manual [1992], and Kodur et al. [2004] (see Appendix A) are built into the program. Both siliceous aggregate concrete and carbonate aggregate concrete properties are built into the program. In addition, the program allows for general material properties read from other input files where the material properties should be given in a tabular format as a function of temperature. In the input file the user has to specify 28-day compressive strength of concrete,

initial moisture content, initial concrete permeability, tensile strength of concrete, concrete model (Eurocode, ASCE, or Kodur), and the type of aggregate in the concrete.

4.4.6.2 Steel Reinforcement

The mechanical properties of reinforcing steel (stress-strain-temperature relationships) that are given in ASCE Manual [1992] and the Eurocode 2 [2004] (see Appendix A) are built into the program. In addition, the program allows for general stress strain relationships as a function of temperature which should be tabulated in another input file. When the ASCE or Eurocode model is selected, the user has to specify the yield strength of steel in the input file and the program automatically uses the built in stress-strain relationships.

4.4.7 Failure Criteria

As mentioned in section 4.3.1 the results generated in the program are utilized to evaluate failure of the column. Different failure criteria, such as (a) limiting rebar temperature, or (b) Strength limit state, are built into the program and the failure (and thus fire resistance) can be computed based on the choice of the user.

4.4.8 Output Results

The output from the program includes the results from the hydro-thermal and structural analyses. At each incremental time step results such as cross-sectional temperature profile and rebar temperature, spalled area of concrete, axial and lateral deformations, axial strains, and fire resistance are computed. Figure 4.13 shows typical results obtained from analysis of an RC column, similar to the one shown in Fig 1.2 using the program. Figure 4.13 (a) shows typical temperature gradient across the column cross-section after 60 minutes of ASTM E119 standard

fire exposure. Figure 4.13 (b) shows typical rebar temperature for the column as a function of fire exposure time.

Figure 4.13 (c) shows typical spalled area for the column exposed to ASTM E119 fire for 30 minutes while Figure 4.13 (d) shows the axial deformation as a function of time as predicted by the numerical model. Similarly the lateral deformations of the column can also be obtained as illustrated in Fig 4.13 (e).

The model accounts for different strains (thermal, mechanical, creep and transient for concrete and thermal, mechanical and creep for steel). These strains at a particular location are computed at every time step and can be computed and can indicate the contribution of each strain at a particular instant in a fire scenario. Thus, it can be seen that the computer model generates a lot of useful data which can be used for undertaking rational design approach for fire resistant design.

4.5 Summary

This chapter presents a numerical model, in the form of a computer program, for tracing the response of RC column exposed to fire. The three stages associated with the fire resistance analysis, namely; fire growth, thermal, and structural analysis, are explained. Equations governing the hydro-thermal and mechanical analyses for fire exposed RC columns are derived. The proposed model accounts for high temperature material properties, various fire scenarios, fire induced axial restraint effects, geometrical nonlinearity, and various strain components. In the nonlinear structural analysis, the model uses a curvature controlled iterative procedure in which the softening of the column is accounted for. Also, a sub-model, which involves pore pressure calculations, is incorporated into the numerical model to account for fire induced spalling. The model can account for biaxial bending of column due to eccentricity of load,

different exposure conditions and uneven spalling. The proposed model is applicable for both circular and rectangular (or square) RC columns. The validity of the proposed computer model in tracing fire response of RC columns will be established in the following chapter.

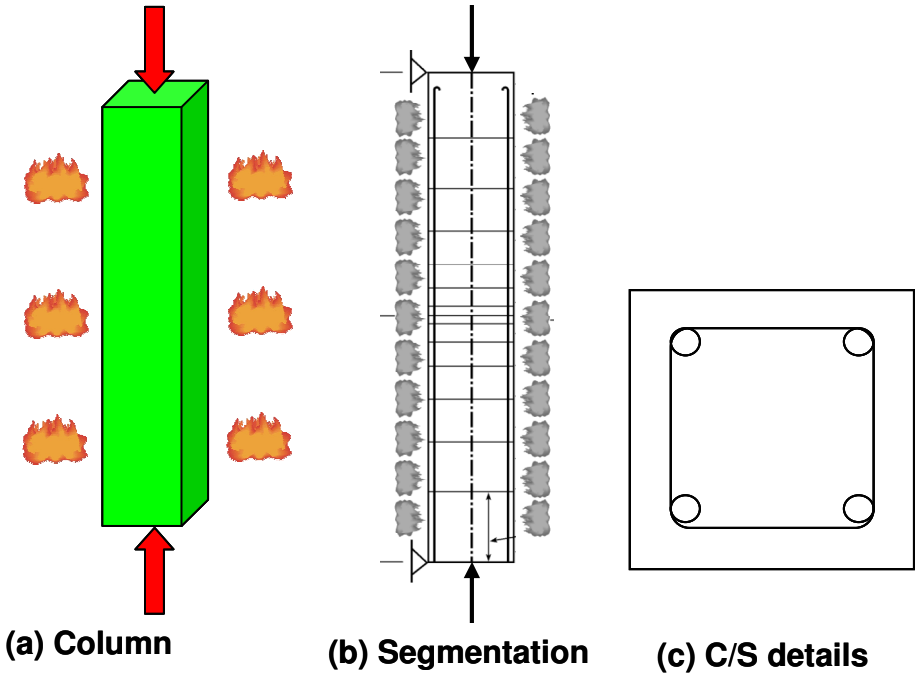

Fig. 4.1 - Layout of a Typical RC Column and its Idealization for Analysis

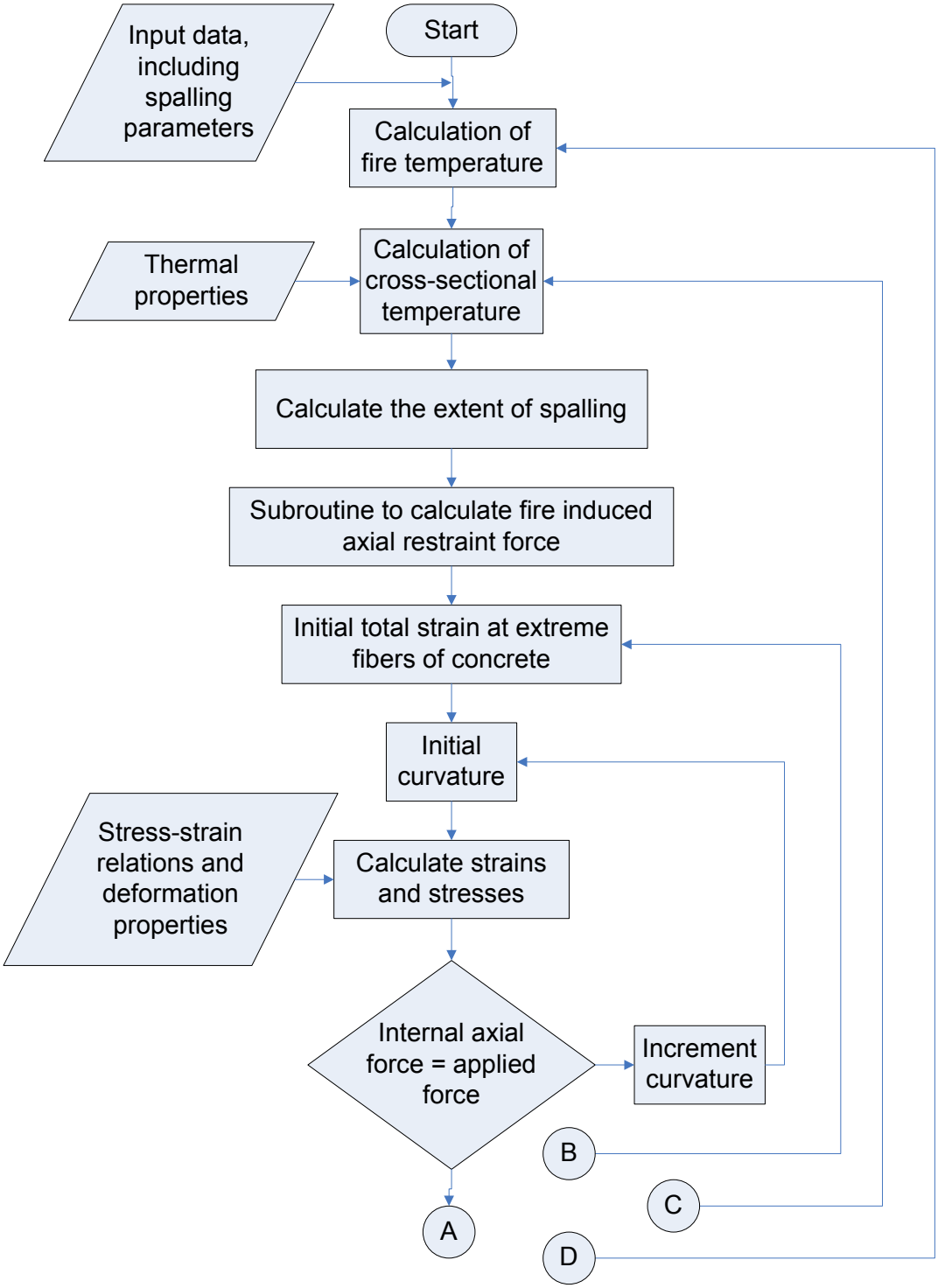

Fig. 4.2 (a) - Flowchart showing the steps associated with the analysis of an RC column exposed to fire

Fig. 4.2 (a) – (Contd.) Flowchart showing the steps associated with the analysis of an RC column exposed to fire

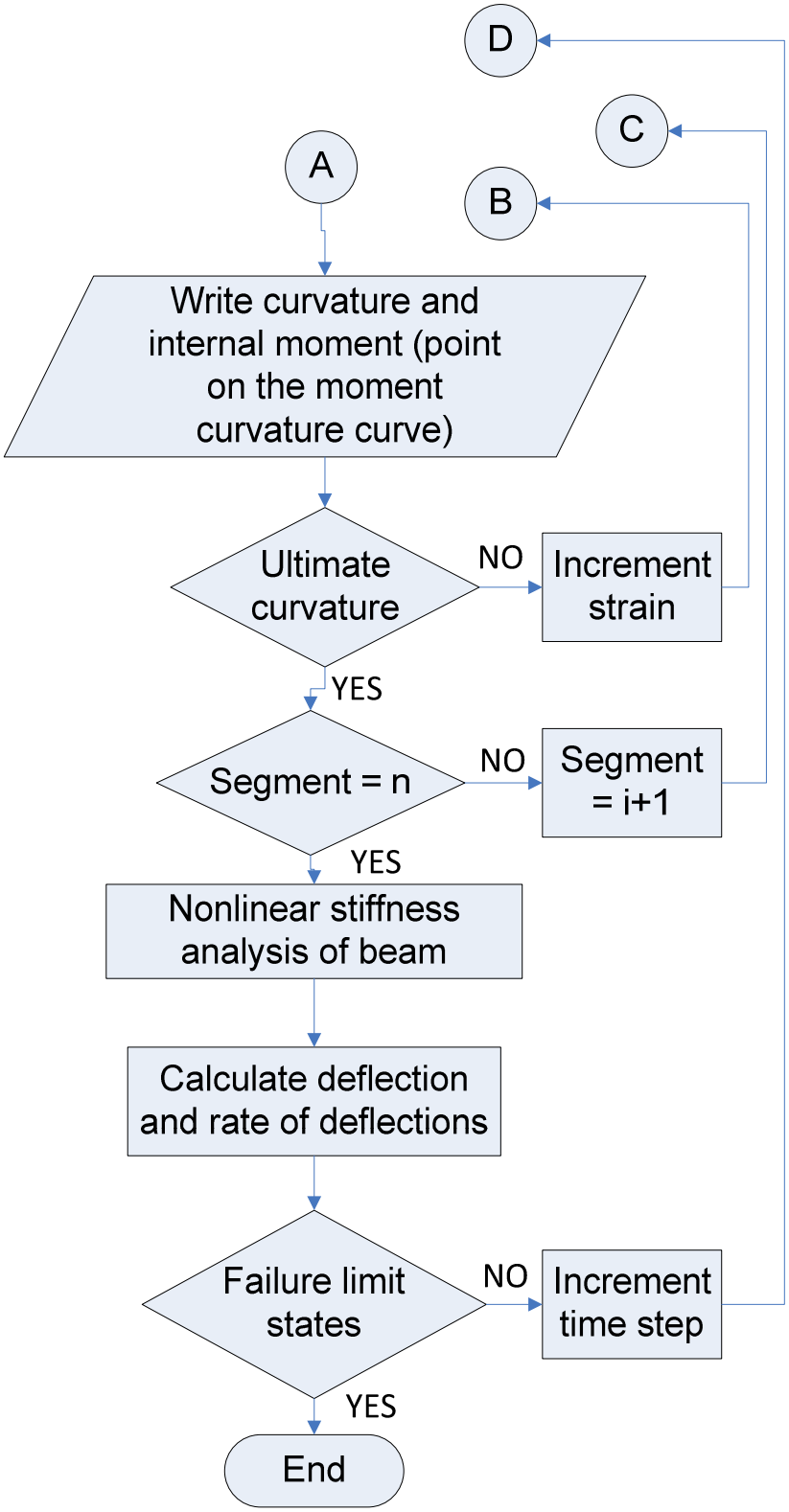

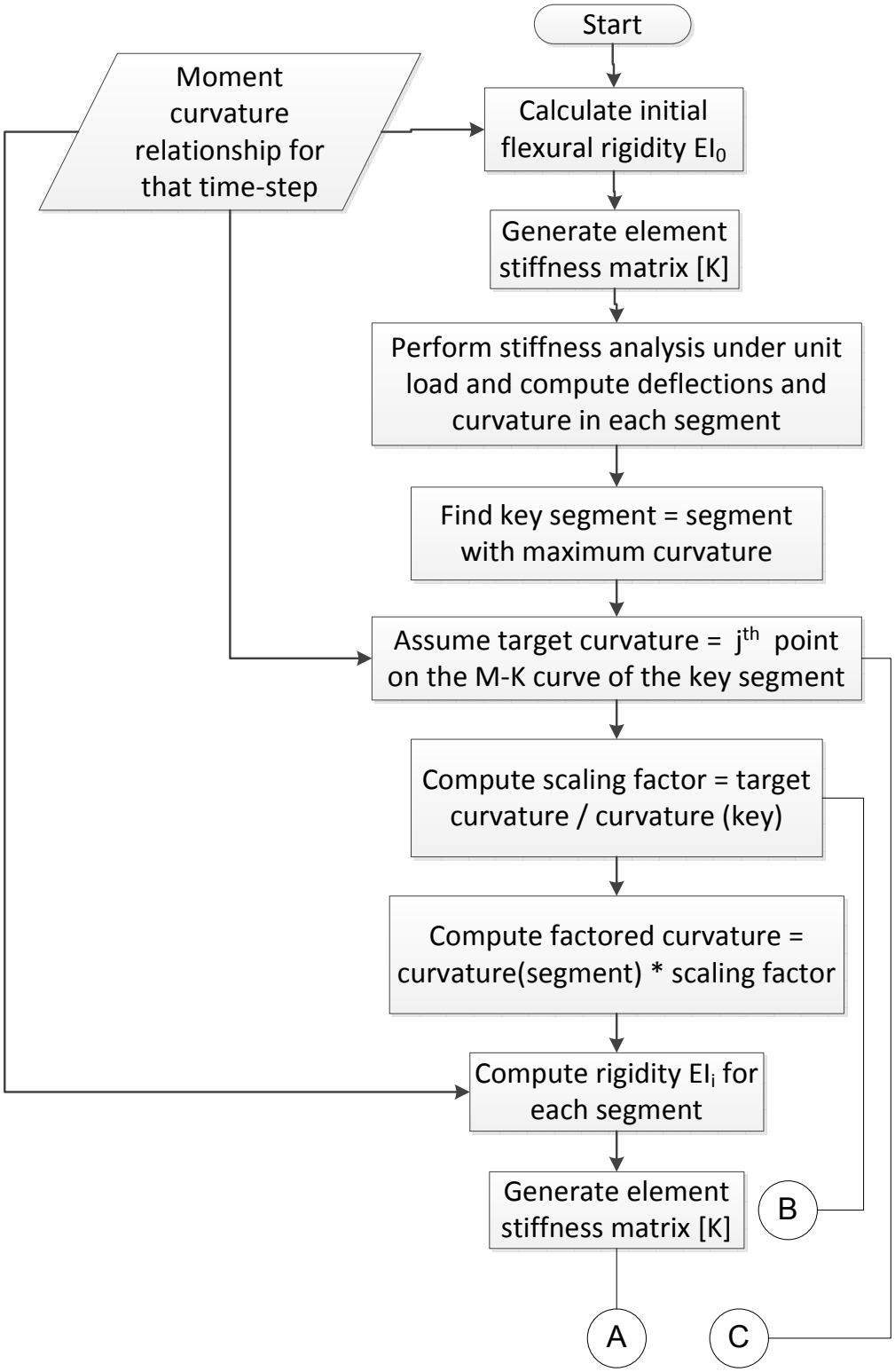

Fig. 4.2 (b) - Flowchart showing the steps associated with the stiffness analysis subroutine

Fig. 4.2 (b) Contd. - Flowchart showing the steps associated with the stiffness analysis subroutine

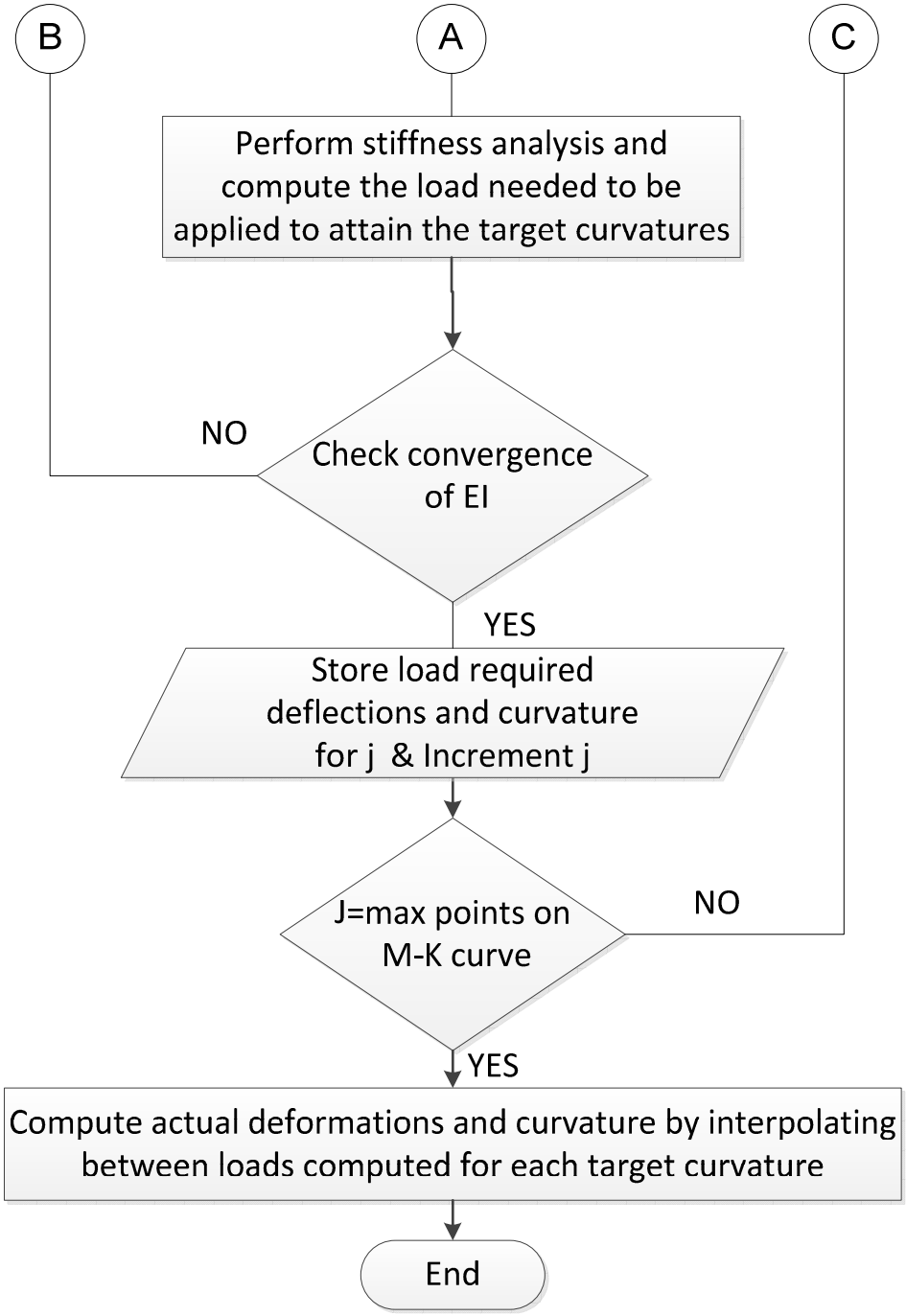

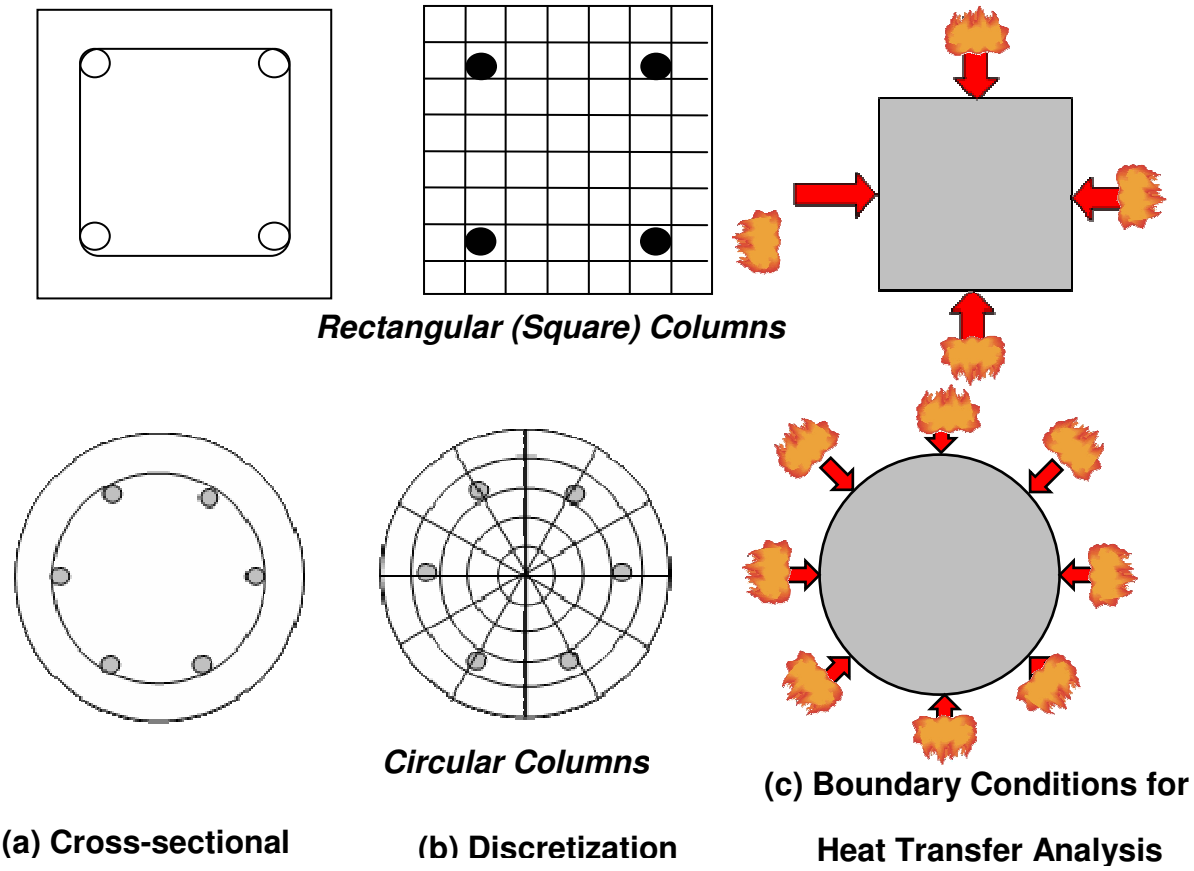

Fig. 4.3 - Cross-section of an RC column and its Discretization for Fire Resistance Analysis

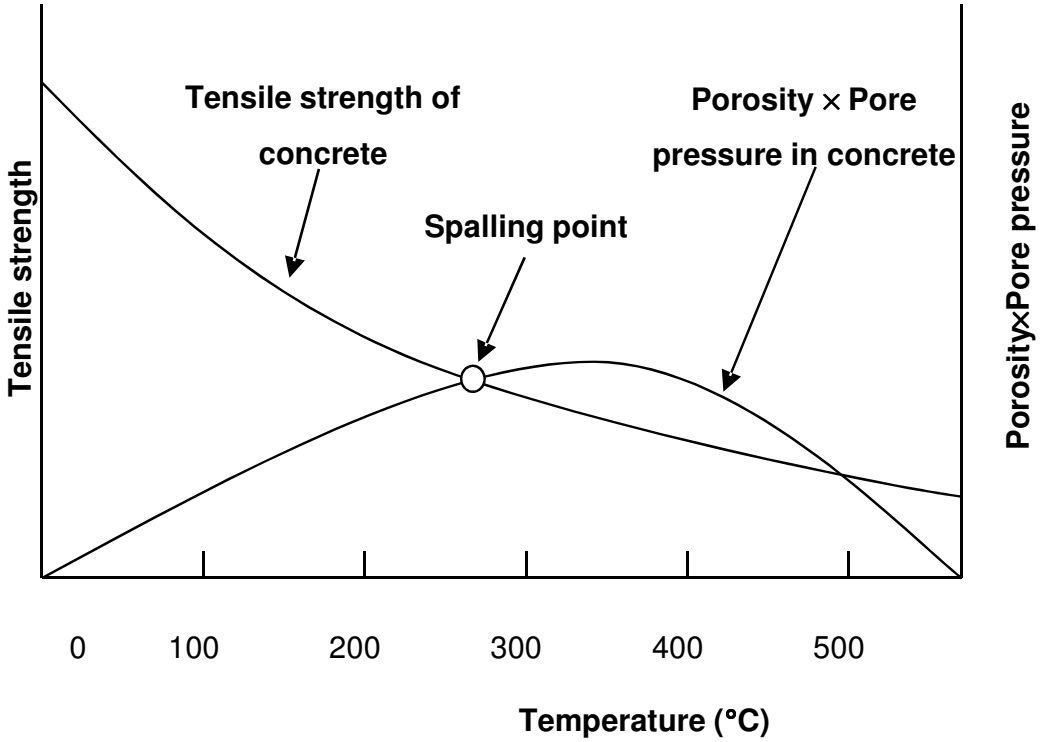

(a) Change in pore pressure and tensile strength of concrete with temperature

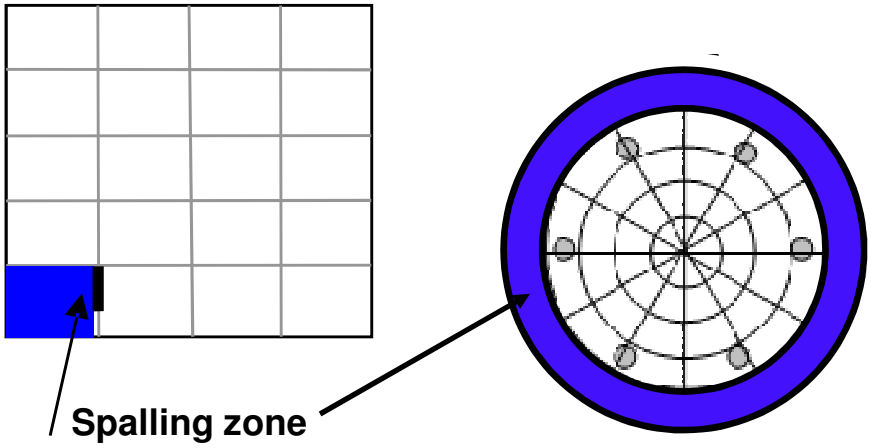

(b) Illustration of spalled area for rectangular and circular RC columns

Fig. 4.4 - Illustration of Spalling Prediction in a Concrete Segment

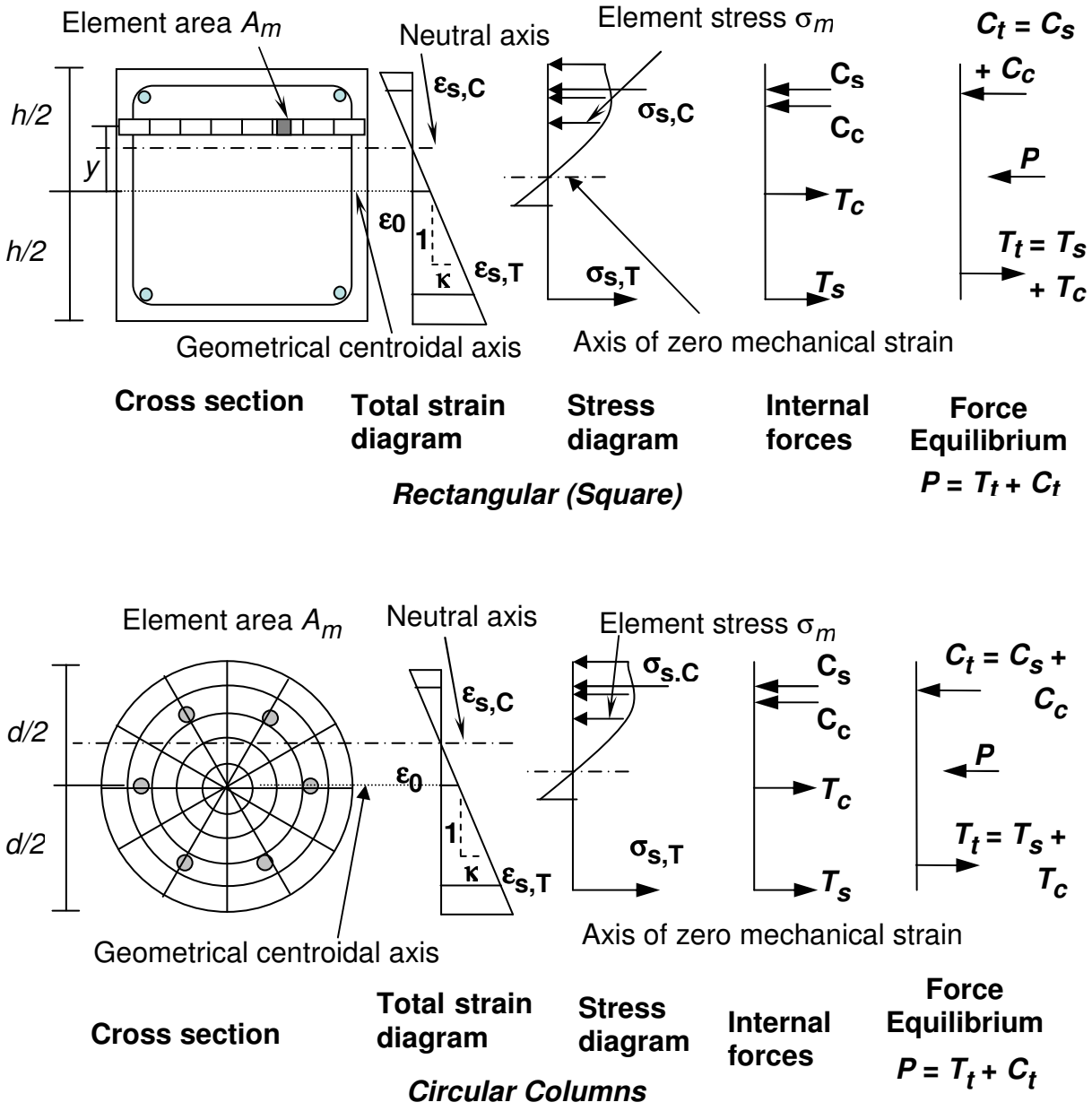

Fig. 4.5 - Variation of Strain, Stress and Internal Forces in a Typical RC Column Cross-section Exposed to Fire

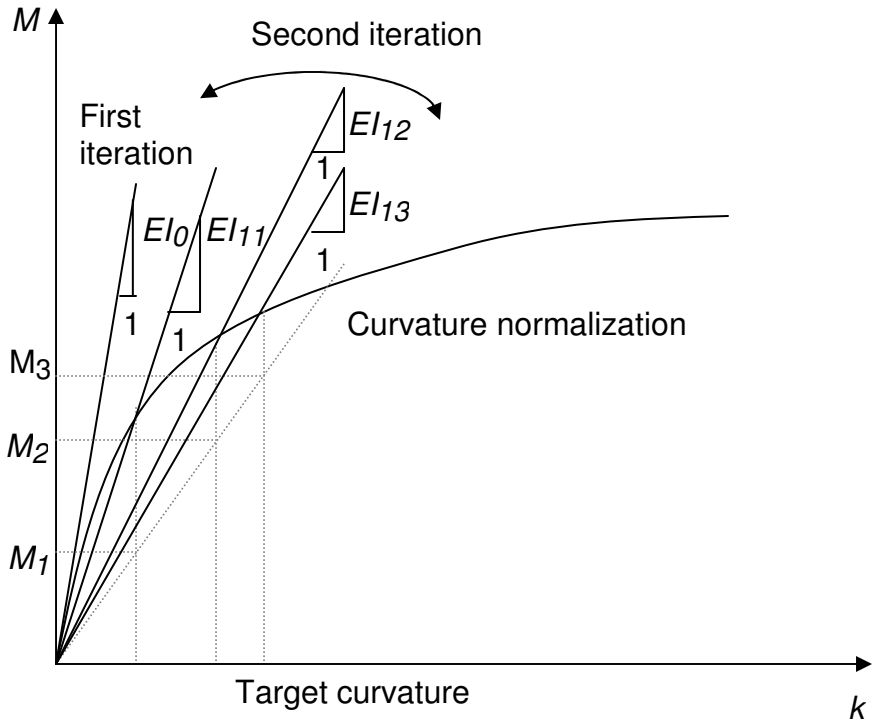

(a) Moment curvature curve for a column segment

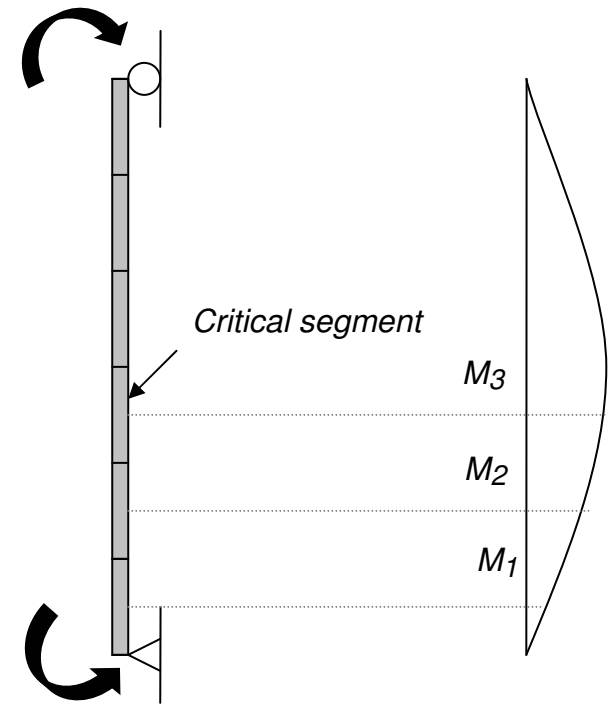

(b) Column (c) Bending moment diagram

Fig. 4.6 - Illustration of Curvature Controlled Iterative Procedure used for Structural Analysis

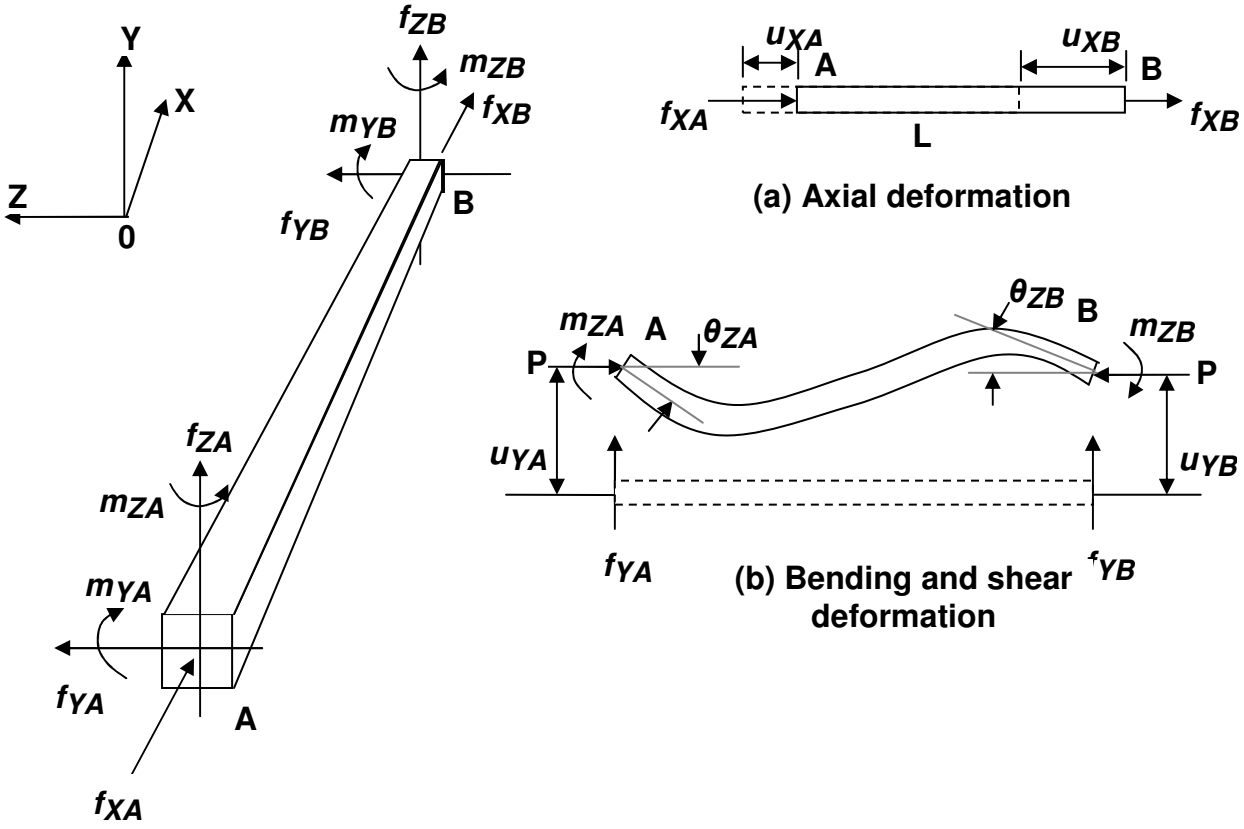

Fig. 4.7– Independent deformation of a column segment

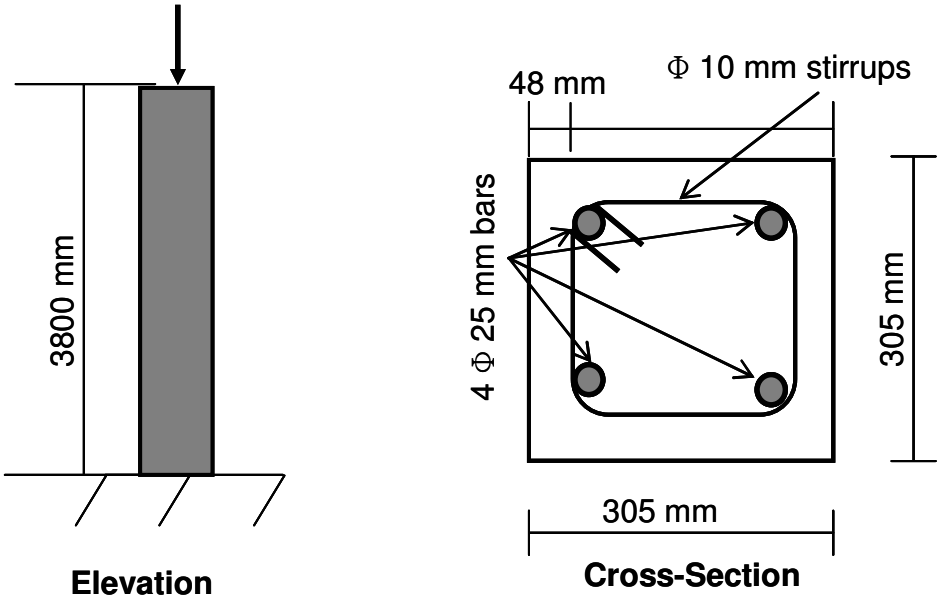

Fig. 4.8–Elevation and cross-section of the RC column used for discretization effect case study

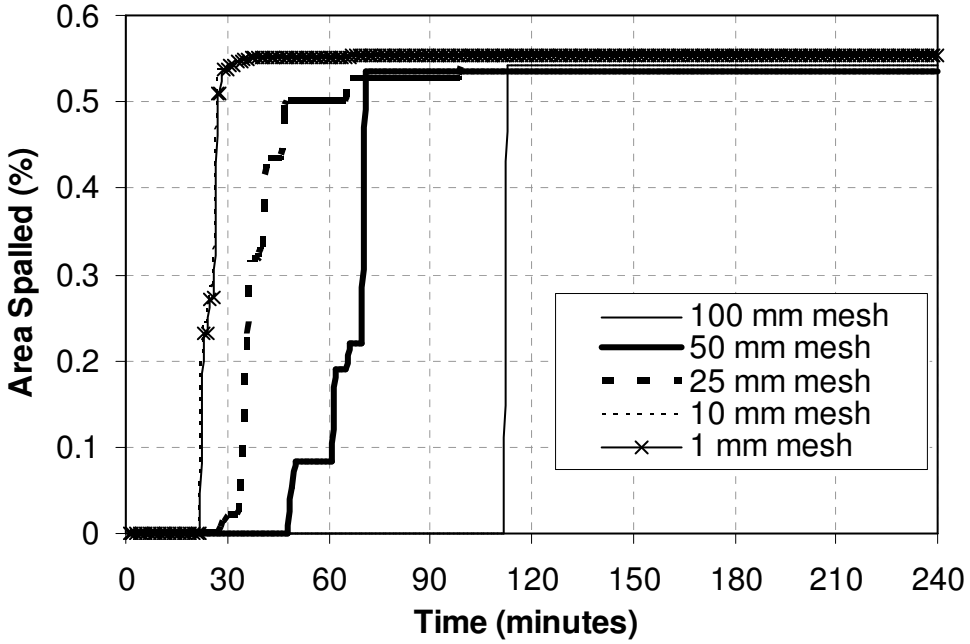

(a) Prediction of spalled area

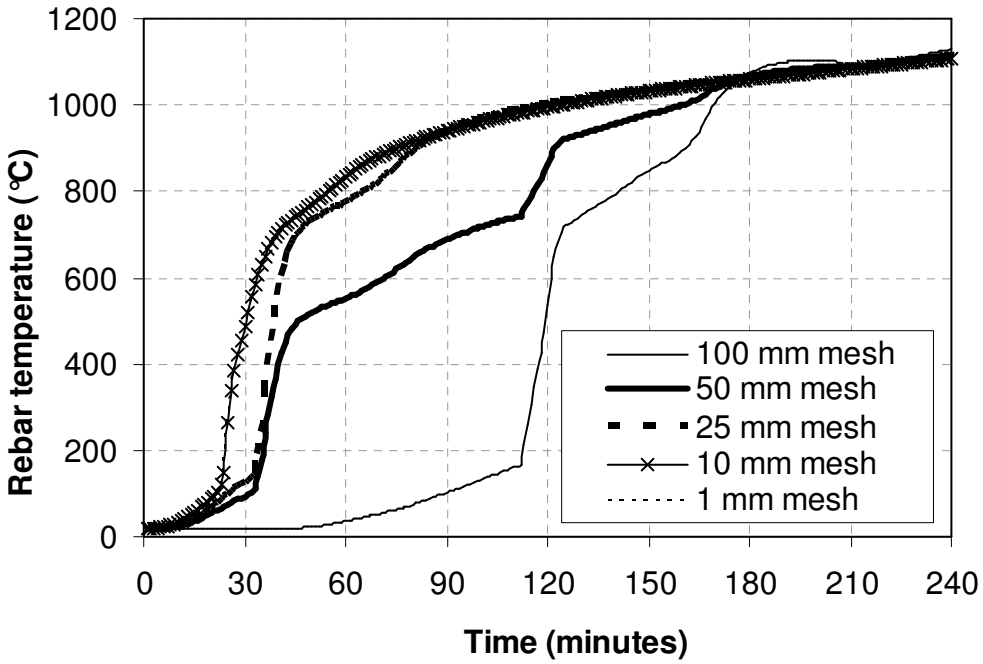

(b) Rebar temperature

Fig. 4.9– Effect of mesh size on fire-induced spalling and thermal response predictions

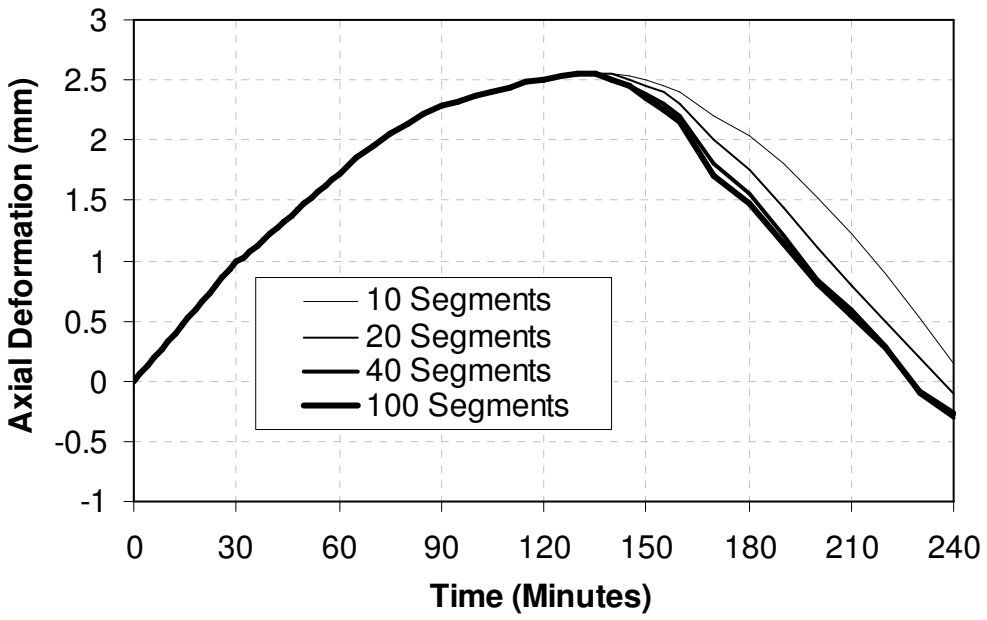

Fig. 4.10–Effect of segment discritization on axial deformation prediction in an RC column

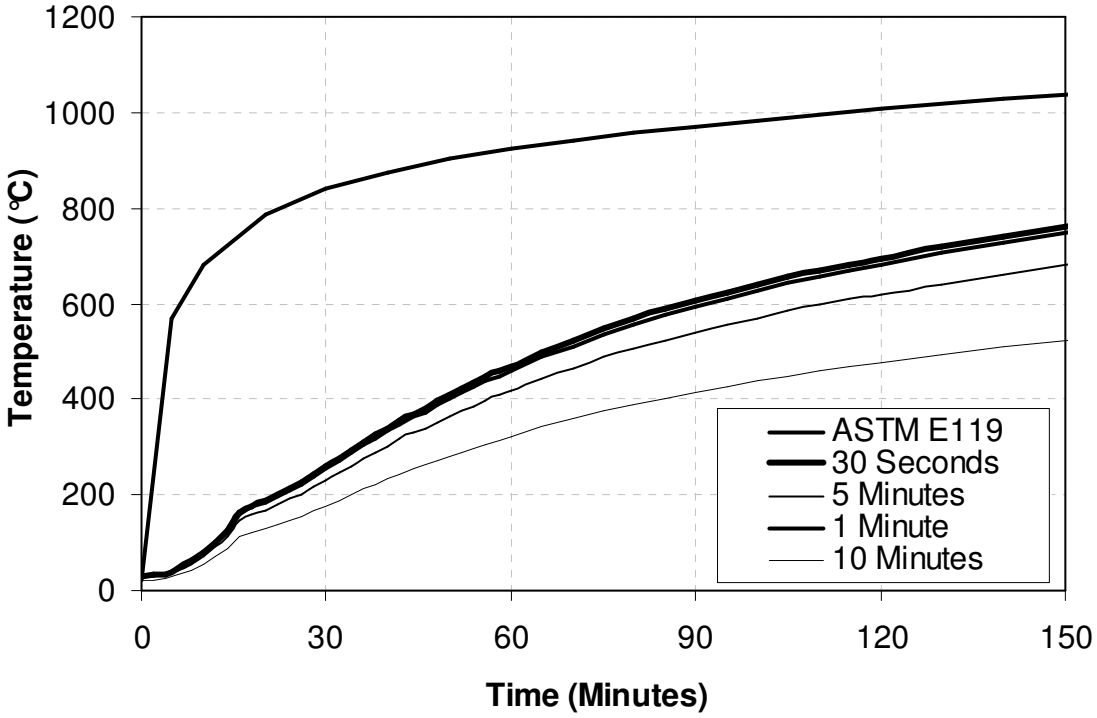

(a) Sensitivity of thermal analysis

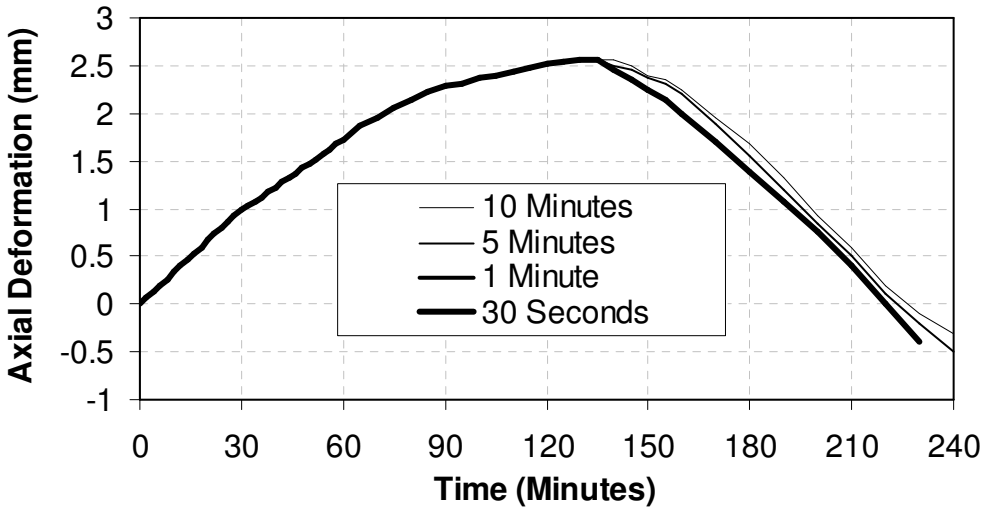

(b) Sensitivity of structural analysis

Fig. 4.11–Effect of time step on fire response prediction in RC columns

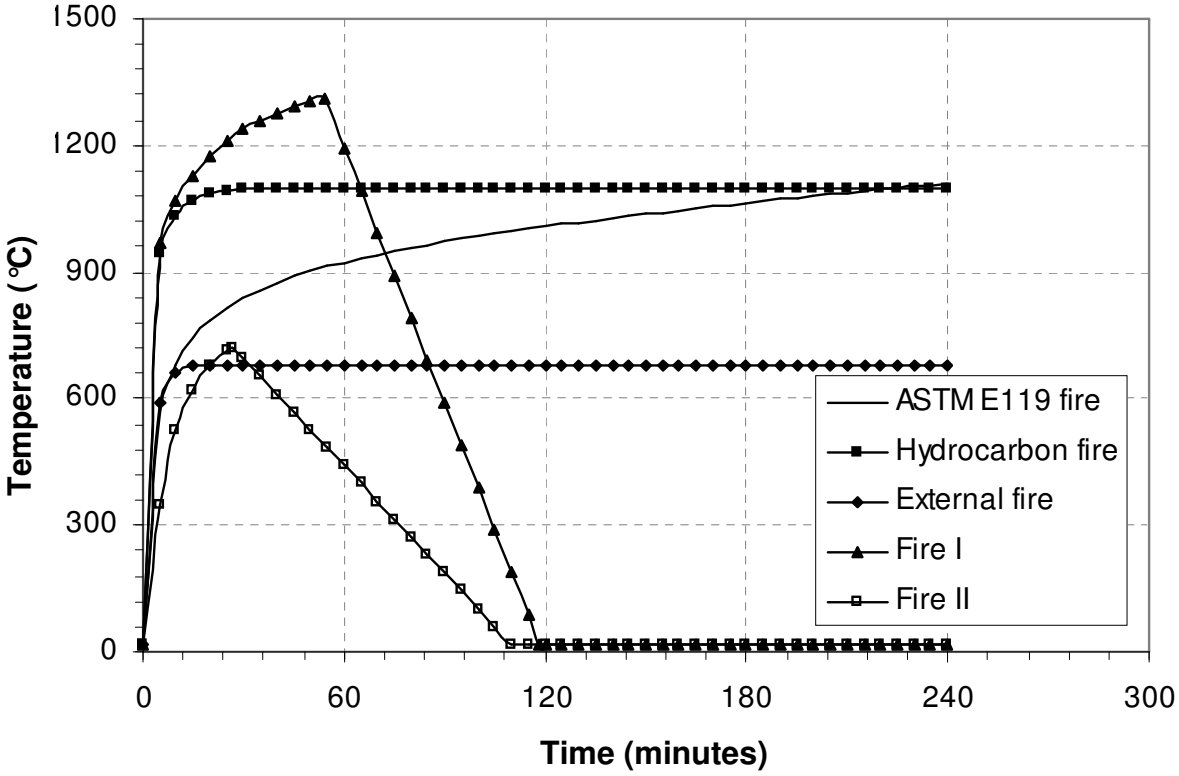

Fig. 4.12– Different fire scenarios incorporated in the model

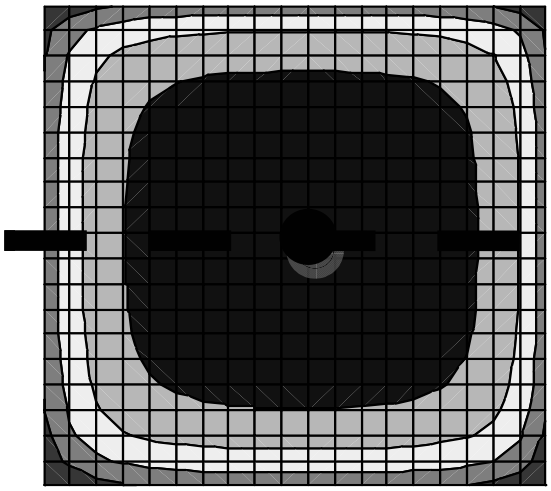

(a) Thermal gradients after 60 minutes in a RC column

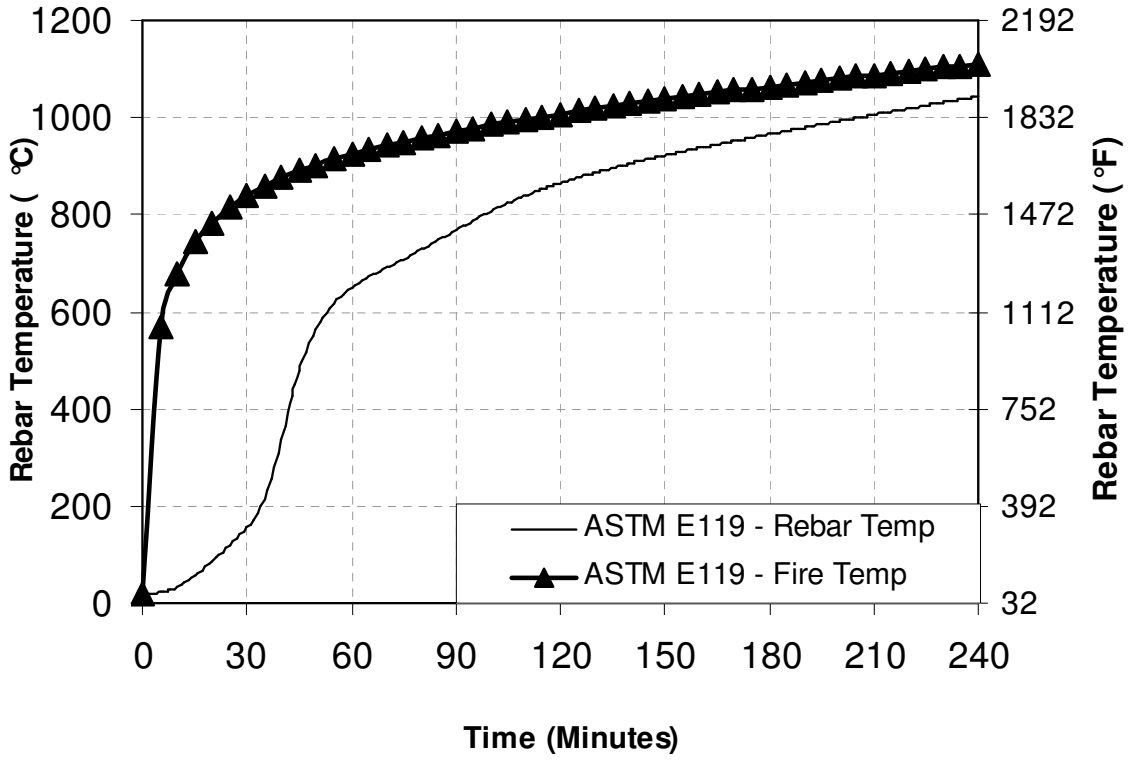

(c) Rebar temperature in RC column

Fig. 4.13– Typical response parameters generated in the fire resistance analysis

Fig. 4.13 Contd. – Typical response parameters generated in the fire resistance analysis

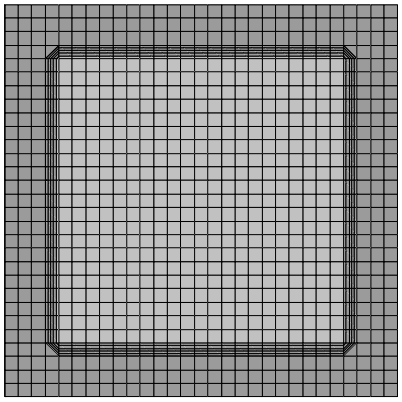

(c) Spalled are after 60 minutes in RC columns

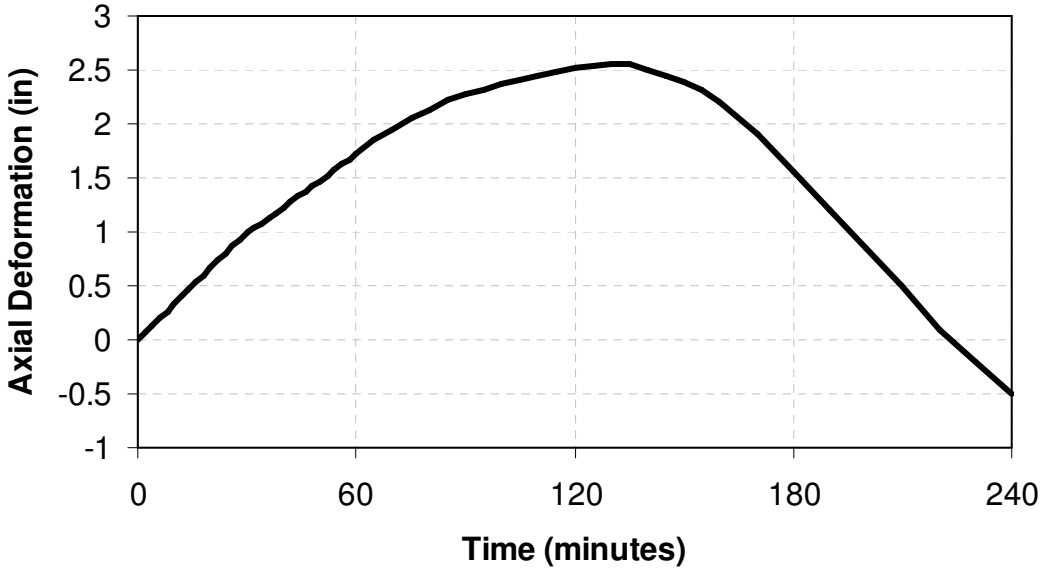

(d) Axial deformation in RC columns

Fig. 4.13 Contd. – Typical response parameters generated in the fire resistance analysis

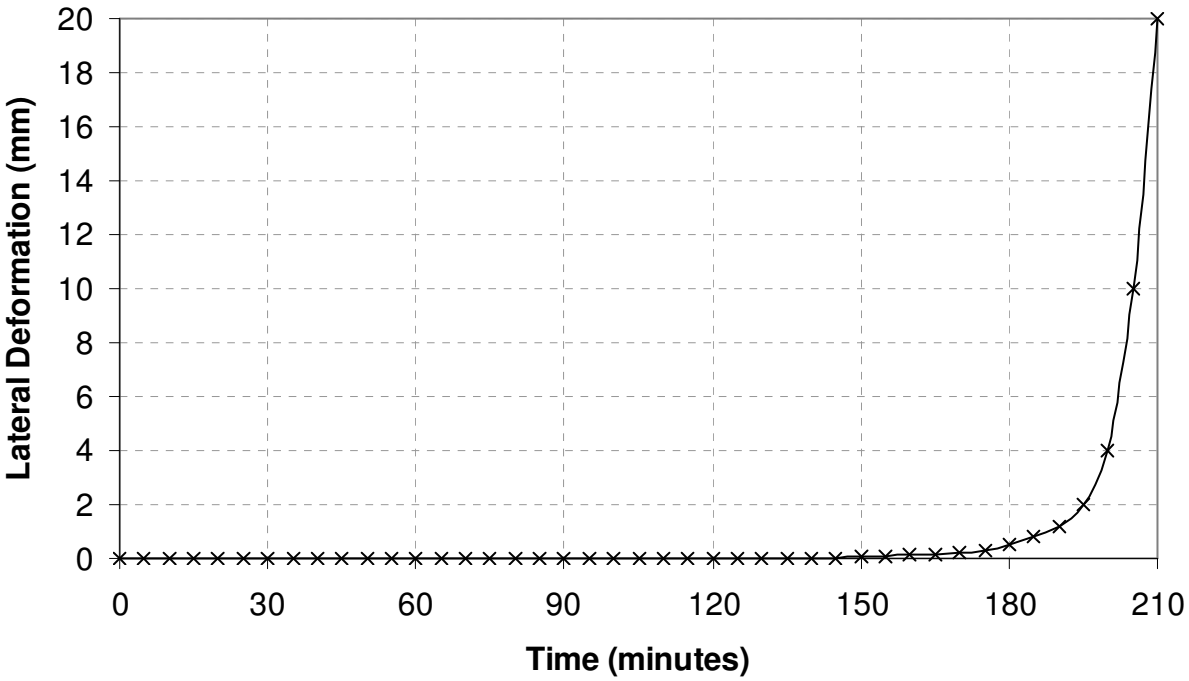

(e) Lateral deformation in RC column

CHAPTER 5

5 VALIDATION STUDIES

This chapter is mainly based on the following journal papers:

- Kodur, V., Dwaikat M. and Raut N., (2007) "Macroscopic Finite Element Models for Tracing the Response of Concrete Structures Under Fire Conditions", Proceedings: Fire Design of Concrete Structures from Materials Modeling to Structural Performance, FIB Workshop, University of Coimbra, Portugal, pp 327-341.
- Kodur V., Dwaikat M. and Raut N., (2009) "Macroscopic FE Models for Tracing the Fire Response of Reinforced Concrete Members", Engineering Structures Journal, V. 31 No. 10, pp. 2368-2379.
- Raut N. and Kodur V., (2009) "Behavior of High Strength Concrete Columns under Design Fire Scenarios", Proceedings: ASCE Structures Congress, Austin, TX.
- Raut N., Kodur V., and Szoke S (2010) "A Macroscopic Finite Element Computer Model for Tracing Fire Response of Reinforced Concrete Columns", Proceedings: ACI Spring Convention, Chicago, IL.
- Raut N. and Kodur V., (2010) "Modeling the Fire Response of Reinforced Concrete Columns under Biaxial Bending", 6th International Conference on Structures in Fire, East Lansing, USA.
- Raut N. and Kodur V., (2010) "Modeling the Fire Response of Reinforced Concrete Columns Under Biaxial Bending", Accepted, ACI Structural Journal.
- Raut N. and Kodur V., (2010) "Behavior of Circular Reinforced Concrete Columns Under Fire Conditions", Communicated, Journal of Structural Fire Engineering.

- Raut N. and Kodur V., (2010) "Computer Model for Predicting the Fire Response of Reinforced Concrete Columns ", Accepted, ACI Special Publication.

5.1 General

The validity of the macroscopic finite element model, presented in Chapter 4, is established in this chapter by comparing predictions from the model with data from fire resistance tests on RC columns. For the validation two sets of data were selected, fire tests reported in literature and secondly the fire resistance experiments carried out as a part of the current study (Chapter 3). Critical response parameters, such as cross-sectional temperatures, axial deformation, extent of fire-induced spalling, failure time, and failure modes were compared for validating the model.

It should be noted that high temperature material properties, structural parameters (boundary conditions and geometry), and the discretization (idealization of member and time steps) used in the analysis has influence on the results from finite element analysis. The optimum mesh size and time steps developed through sensitivity study, presented in Chapter 4, was used for discretization of the columns. High temperature material properties vary within their domain as discussed in Chapter 2. It is not possible to get exact high temperature properties of concrete and reinforcing steel due to complexity and effort involved in the process. Hence high temperature property relations specified in codes and standards were used. Details of the material properties, discretization parameters and boundary conditions used in the validation studies is presented in the following section.

5.2 Validation of Numerical Model

To establish the validity of the fire resistance model, 12 RC columns that were tested in different research programs were selected for the analysis. The first six columns are the ones that were tested in the literature to generate data to study the effect of parameters such as different concrete strengths, cross-sectional shapes and bending (eccentric loading). It should be noted that, there is no test data on RC columns under uni/biaxial bending arising from 1-, 2-, 3-side fire exposure. However, limited fire test data are available for RC columns under uniaxial eccentric loading and two representative columns (one NSC and one HSC) were chosen amongst the columns used for validation studies.

The remaining six columns selected for validation were the columns tested at MSU whose results are presented in Chapter 3. Details of the geometric and material properties and load level for the columns are given in Table 5.1 and 5.2.

5.2.1 Column Discretization and Material Models

Since all the tests validated below were carried out in North America, high temperature material properties (thermal properties and constitutive relationships), used in the analyses, were as per ASCE [1999] provisions for normal strength concrete and reinforcement steel while property relations as per Kodur et al. [2004] were used for high strength concrete. These material property relations are discussed in Chapter 2 and presented in Appendix A. The column (length) was divided into 40 segments of equal length and the mid-plane of each segment was assumed to represent the segmental behavior. The cross-section of each segment was divided with a mesh of elemental size of 10 mm. For circular columns, the cross-section of each segment was represented as single line using axisymmetry (see Chapter 4) and was divided with an elemental size of 10 mm. The details of the column discretization are shown in Figure 4.3. The time domain was divided into increments of one minute and the transient analysis was carried out at

each time step. The fire resistance was computed based on strength failure criterion (either by crushing of concrete, or buckling of the column) as described in Chapter 4.

5.2.2 Columns Tested in Literature

To establish the validity of the model under wide range of scenarios, comprehensive analysis was carried out on tested columns with different characteristics.

5.2.2.1 Axially Loaded Rectangular Columns

The first two columns selected for validation study were taken from fire tests reported by Lie and Woolerton [1988] and Kodur et al. [2003] and are designated as Columns I3 and HSC2-1. These columns were axially loaded and represent typical NSC and HSC columns. The geometric and material properties of the tested columns are taken from the literature and are summarized in Table 5.1. These columns were analyzed by applying the computer model presented in Chapter 4 and the temperatures, deformations, and failure times from the analysis were compared with the measured values from the fire test in Figures 5.1 and 5.2, and Table 5.1.

Figure 5.1 (a) shows the cross-sectional dimensions and thermocouple layout for column I3. The predicted temperatures at three different cross-sectional locations, for column I3, are compared with the measured values, in Figure 5.1(b). It can be seen that the predicted temperatures are generally in good agreement with the measured values. The temperatures follow expected trend with higher values close to the fire exposed surface. The temperatures in rebar (thermocouple TC9) are higher than the concrete temperatures (located at quarter-depth (TC29) and mid-depth (TC31)) as it is closest to the column surface.

Figure 5.1(c) shows axial deformation as a function of fire exposure time for NSC column I3. It can be seen that model predictions are in close agreement with the measured axial deformations throughout the fire exposure time. The axial deformations increase initially and this is primarily

due to expansion resulting from high thermal strain (thermal expansion) in concrete and rebars which occurs due to the rise in cross-sectional temperature. After steel yield concrete starts to take over load. This leads to a decrease in the axial deformations (contraction) as a result of loss of strength and stiffness in the column. The faster rate of increase in deformation prior to failure of the column is mainly due to the significant high temperature creep deformations resulting from very low stiffness of the column, as well as very high temperatures in concrete and rebars.

Figure 5.2(a) shows the cross-sectional dimensions and thermocouple layout for column HSC2-1 while, Figure 5.2 (b) shows the temperature comparisons for that column. The predictions from the model are in good agreement with the measured temperature throughout the temperature range. Spalling was observed in this column and the time at which it began was reported in the literature. The model predictions indicate that fire induced spalling starts at about 13 minutes, which is close to the observed time (10 minutes) recorded in test. Measured test temperatures at thermocouple located at the centre of the column (mid-depth (TC5)), shows that there is a sudden rise in temperature after 180 minutes as seen in Figure 5.2(b). This can be attributed to possible damage to the thermocouple due to occurrence of large cracks in concrete resulting from reduced strength/stiffness, thus exposing the thermocouple to higher temperatures. This is not captured in the model as the model cannot account for the occurrence of load induced cracks or their propagation. The effect of this variation in the temperature is reflected partially in the higher fire resistance time predicted by the model.

Figure 5.2(c) shows the axial deformation comparisons for HSC column HS2-1. The prediction from the model is generally in good agreement with the measured axial deformation. The column shows similar trend to that of NSC column with expansion in the early stages followed by contraction of the column. There is lesser expansion in the HSC columns due to faster

degradation of strength with rise in temperature thus leading to high axial compression. Also the applied load ratio is higher for the HSC column causing higher compressive stresses in the column.

The fire resistance values from the tests and the numerical model are compared and are tabulated in Table 5.1. The predicted fire resistance for NSC column I3 obtained from macroscopic FEM based on strength failure criteria was 205 minutes, which is close to the measured fire resistance in the test (218 minutes). The failure of this column was predicted to be due to crushing of concrete as observed in the tests. Similarly for column HS2-1 the predicted fire resistance is 310 minutes (crushing failure) based on strength criteria as compared to the measured fire resistance were 299 minutes (crushing failure) for column HS2-1

5.2.2.2 Eccentrically Loaded Rectangular Columns

Two eccentrically loaded columns, III3 and HSC2-9, (one NSC and one HSC) reported by Lie and Woolerton [1988] and Kodur et al. [2003] respectively were used for further validating the numerical model under eccentric loading. The geometric and material properties of the tested columns are taken from the reported studies and are summarized in Table 5.1. Both columns had load applied eccentrically along one axis. The response of the columns was evaluated using the above described model and fire resistance was evaluated based on strength failure criterion. Predicted results from the analysis are compared to the measured values from the fire test in Figures 5.3 and 5.4, and Table 5.1.

Figure 5.3(a) shows the layout, cross-sectional dimensions and thermocouple locations for column III3. The predicted temperatures at three different cross-sectional locations (mid-depth (TC31), quarter-depth (TC29) and rebar (TC9)), for column III3, are compared with the measured values, in Figure 5.3(b). It can be seen that the measured temperature at mid-depth of

concrete is lower than that at the rebars and this is due to the lower thermal conductivity and higher thermal capacity of concrete which slows down heat penetration to the inner layers of concrete. It can be seen that the predicted temperatures are generally in good agreement with the measured values. The temperatures follow expected trend with higher values close to the exposed surface. The rebar temperature is higher than that at concrete quarter-depth and mid-depth, as it is closest to the column surface.

Figure 5.3(c) shows axial deformations as a function of fire exposure time for NSC column III3. It can be seen that model predictions are in close agreement with the measured axial deformations throughout the fire exposure time. Similar to column I3 the axial deformation increases initially and is then followed by a decrease in the axial deformation. Also, due to the eccentricity of the applied load, the increased P-δ effect resulting from bending of the column, contributes to faster increase in deformations prior to failure of the column.

Predictions from fire resistance analysis of HSC column HSC2-9 is compared with test data in Figure 5.4. Figure 5.4(a) shows the cross-sectional dimensions and thermocouple layout for column HSC2-9. Figure 5.4(b) shows that the predicted temperatures from the model are in good agreement with the measured temperature. Similar to columns HSC2-1, this column was made of high strength concrete and hence it experienced spalling. The model predictions indicate occurrence of fire induced spalling at about 13 minutes, which is close to the time (15 minutes) observed in test. This occurrence of spalling causes sudden rise in temperatures (measured and predicted) between 15 – 25 minutes.

Figure 5.4(c) shows the axial deformation comparisons for HSC column HS2-8. The deformation trend is similar to the columns discussed above with expansion in the early stages followed by contraction of the column. Similar to column HSC2-1, there is lesser expansion in column

HSC2-9 due to faster degradation of strength thus leading to high axial compression. Also the applied load ratio is higher for the HSC column causing higher compression in the column. The prediction from the model is in good agreement with the measured axial deformation.

These fire resistance from the analysis and tests are tabulated in Table 5.1. The fire resistance of column III3 obtained from macroscopic FEM was 195 minutes which is close to the measured fire resistance in the test (181 minutes). The predicted failure was through buckling and this is in agreement with the observed failure pattern. Similarly for column HS2-9 the predicted and measured fire resistance is 123 and 117 minutes respectively based on the strength criteria. The model predicted column HSC2-9 to fail through crushing which is similar to that reported in the test.

5.2.2.3 Axially Loaded Circular Columns

The validity of the macroscopic finite element model for circular RC columns is established by comparing the predictions from the analysis with the fire test data reported by Lie and Woolerton [1988]. The geometric and material properties of the tested columns III11 and III12 are taken from the literature and are summarized in Table 5.1. Predicted results from the analysis are compared to the measured values from the fire test in Figures 5.5 and 5.6, and Table 5.1.

Figures 5.5(a) and 5.6(a) show the cross-sectional dimensions and thermocouple layout for columns III11 and III12 respectively. The predicted temperatures in concrete at mid-depth, quarter-depth and rebar in column III 11 and 12 are compared with the measured values in test, in Figures 5.5(b) and 5.6(b) respectively. The temperatures follow expected trend with higher values close to the exposed surface. As discussed before, the measured temperature at mid-depth (TC17) and quarter depth (TC16) of concrete are lower than that at the rebars (TC4). It can also be seen that the model can predict the cross-sectional temperatures with good accuracy.

Figures 5.5(c) and 5.6(c) show axial deformations as a function of fire exposure time for column III 11 and 12. It can be seen that model predictions are in close agreement with the measured axial deformations throughout the fire exposure time. The axial deformations increase initially followed by a decrease in the axial deformations, similar to the other columns presented above.

The fire resistance of column III 11 obtained from macroscopic FEM based on strength failure criteria was 255 minutes which is close to the measured fire resistance in the test (245 minutes). The predicted failure was through crushing and this is in agreement with the observed failure pattern. Similarly for column III 12 the predicted and measured fire resistance is 232 and 220 minutes respectively based on the strength criteria. The model predicted column III 12 to fail through crushing similar to what was observed in the test. This validation illustrates that the macroscopic finite element model is capable of predicting fire response of circular RC columns.

5.2.3 Columns Tested at MSU

The six tested RC columns, whose results are discussed in Chapter 3, were analyzed using the macroscopic finite element model presented in Chapter 4. Each column is analyzed under the fire scenarios they were exposed to in tests and is given in Table 5.2. Failure time is recorded when the column is no longer capable of supporting the applied load. The predicted spalling and fire resistance values obtained from the analyses are summarized in Table 5.3.

For concrete and reinforcement, high temperature material properties/relationships specified in the ASCE Manual [1992] are used in the analysis. The thermal properties of concrete and steel are assumed to be the same for both heating and cooling phase. For mechanical properties, linear interpolation between high temperature strength and residual strength is used to estimate the strength of both concrete and reinforcing steel in the cooling phase. The residual strengths for any concrete element or steel rebar are determined based on the maximum temperature attained

in that element (or rebar). For mechanical properties, linear interpolation between high temperature strength and residual strength obtained from Kumar [2003] is used to estimate the strength of both concrete and reinforcing steel in the cooling phase. However, the residual strength of reinforcing steel is assumed based on the residual strength tests conducted by Neves et al. [1996] on reinforcing steel. Up to 500°C, residual strength of reinforcing steel is assumed to be similar to room temperature strength. However, the residual strength is assumed to decrease linearly with temperature till it reaches 0.7 of the of the room temperature strength at 800°C.

The validity of the model is established by comparing predictions from the model with measured temperatures, deflections and fire resistance in Figure 5.4 and Table 5.2. While fire resistance times from all six columns are presented in Tbale 5.2, temperature and axial deformation trends are presented only for three columns NSC1, HSC1 and HSCP1. The NSC and HSC columns were assumed to have a permeability of the order 10^{-17} and 10^{-19} respectively. Usually HSC has lower permeability ranging in the order of 10^{-18} or lower and the susceptibility to fire induced spalling increases with decrease in permeability [Kodur and Dwaikat 2009]. Columns HSCP1 and HSCP2, made from HSC with polypropylene fibers were assumed to have permeability of the order 10^{-19} same as that of HSC. But once the concrete in these columns attain 160°C the permeability was reset to 10^{-18} to account for the increase in permeability resulting from melting of polypropylene fibers [Khalifa et al., 2001].

Figure 5.7(a) shows the cross-sectional dimensions and thermocouple layout for all the columns. Figures 5.7(b), (c) and (d) show the predicted and measured rebar temperature as a function of fire exposure time for columns NSC1, HSC1 and HSCP1. It can be seen that there is good agreement between the measured and the predicted rebar temperatures throughout the fire

exposure time for the two columns. However, for column HSC1, the model predicts slightly higher temperatures than the measured ones. This can be attributed to the severe spalling observed in column HSC1. The model accounts for spalling but under idealistic conditions and assumed uniform permeability of 10^{-19} which may not be the case since permeability might vary across the cross section as discussed below.

The non-uniformity of spalling of the column in the fire tests can be attributed to the cracking in the tension zone of the column (when buckling) due to applied loading. Cracking facilitates the escape of steam and thus reduces the build-up of pore pressure under fire conditions [Dwaikat and Kodur 2009]. In addition to cracking, curing conditions also influence the permeability of concrete. The top surface of the columns was covered with burlap that was soaked with water (common practice for curing RC members). This results in better curing conditions for the top part of the column which enhances hydration of concrete leading to reduced porosity (permeability) in the top part of the column. This can lead to slight variations in temperature predictions. Predicting slightly higher temperature generally leads to conservative fire resistance of the RC column. Similarly a slight difference was observed in the predicted rebars temperature for column HSCP1 (see Figure 5.7 (d)). This can be attributed to the fact that the permeability may vary from that assumed as the actual permeability is not known after the fibers have melted. Also thermal properties of the concrete (thermal conductivity, specific heat etc.) used in the analysis (taken from ASCE manual) might be slightly different from that of the concrete used in the tested columns. It was not possible to measure the actual high temperature thermal properties since it involves significant effort and time.

The predicted and measured axial deformations are compared in Figure 5.7(e) for the same three columns (NSC1, HSC1 and HSCP1). The figure shows that there is a good agreement between

the measured and the predicted axial deformations for all three columns. However, for column HSC1, the model predicted higher axial deformation than the measured values. This can be mainly attributed to the discrepancy between predicted and measured rebar temperatures as shown in Figure 5.4(c). Similar observation can be made for column HSCP1.

The comparison of the measured and predicted spalling in column HSC1 is shown in Figure 5.7(f) as a function of fire exposure time. The extent of spalling in the tested column was measured after the column was removed from the furnace. Observations were made during the test in order to record the time when spalling started and stopped. Volumetric measurements were made on the post fire test columns in order to calculate the quantity of concrete lost due to spalling. For column HSC1, the model predicts spalling to start at about 10 minutes and stop at about 29 minutes after fire exposure. The visual observations recorded in the test indicated that spalling started and stopped at about 15 and 33 minutes after fire exposure, respectively. Figure 5.7(f) shows that the model can predict spalling progression with a reasonable level of accuracy. The measured and predicted start and end times of spalling and the extent of spalling at the end of fire tests are presented in Table 5.3. It should be noted that spalling is dependent on a number of variables and accurate test data on these variables is hard to measure. Nevertheless, reasonable spalling predictions were obtained and thus, for qualitative assessment, the proposed spalling sub-model is deemed to be sufficient. The properties provided by the ASCE manual [1992], which were used in the thermal calculation in the model are more towards the upper limit (worst case scenario) of the thermal properties [Kodur et al. 2008]. Thus the rise in temperature in concrete is faster leading to earlier inset of spalling. But overall, the measured volume of spalling at the end of the test is higher than that predicted by the model. This is because when the column fails more concrete is lost due to the crushing of concrete. This cannot be separated from the

concrete spalled due to fire as the measurements were done after the column had failed. This results in the higher temperature prediction by the model as stated in the prior sections.

The predicted fire resistance is compared to the measured fire resistance values in Table 5.2. For the columns NSC1 and HSC1, which were subjected to ASTM E119 standard fire, the model predicts fire resistance of 176 minutes (crushing failure) and 57 minutes (buckling failure) respectively as compared to 183 minutes (crushing failure) and 61 minutes (buckling failure) observed in the test. While for columns HSC3 and HSCP2, which were subjected to design fires with a cooling phase, the model predicts fire resistance of 63 minutes (buckling failure) and 213 minutes (crushing failure) respectively as compared to 75 minutes (buckling failure) and 221 minutes (crushing failure) measured in the test. The model predicts no failure in columns HSC2 and HSCP2 (burnt-out conditions) due to recovery of strength resulting from cooling phase of fire. For these two columns no failure occurred in fire tests. The model predictions are in good agreement with measured fire resistance values for the six tested RC columns. It can be seen that the model predicts lesser fire resistance for the columns. This can be attributed to the fact that ASCE material properties (which are more towards upper limit of the range of values available in the literature) were used in the model (see Appendix A). These comparisons illustrate that the numerical model can reasonably predict the behavior of different types of concrete columns (NSC, HSC, HSCP). The predictions can further be improved by using the actual variation of permeability, and thermal properties for specific concrete strength (types), data of which is not easy to generate for specific columns.

Though detailed comparisons are presented only for three columns, the predicted temperatures, deformations, spalling, and fire resistance also compared well with test data for the other three columns tested at MSU.

5.3 Summary

The validity of the computer model developed as part of the current study is established by comparing perditions from the model with test data. Six columns from the literature along with the six columns tested as a part of this study (see Chapter 3) were used for the validation study. For all the columns, the model predictions match well with the measured test parameters. In the validation, predicted spalling, temperatures, axial deformations, and fire resistance were compared with measured values in fire resistance tests. Based on these comparative studies, it is concluded that the microscopic finite element model is capable of predicting the fire response of RC columns under realistic fire, loading and eccentricity scenarios. However, additional tests on parameters such as biaxial bending of RC columns due to 1-, 2-, or 3-side exposure, or due to bi-eccentric loading, are necessary for further validation of the numerical model presented in Chapter 4. In the following chapter, the validated model will be applied to conduct parametric studies to investigate the influence of various parameters on the fire resistance of RC columns.

Table 5.1– Properties and results for RC columns used in the validation study

Property	**Column I3**	**Column HS2-1**	**Column III3**	**Column HS2-9**	**Column III11**	**Column III12**
Cross section (mm)	305 × 305	406 × 406	305 × 305	406 × 406	355 Φ	355 Φ
Length (m)	3.8	3.8	3.8	3.8	3.8	3.8
Support conditions	Fixed-Fixed	Fixed-Fixed	Fixed-Fixed	Pinned-Pinned	Fixed-Fixed	Fixed-Fixed
Reinforcement	4 ϕ 25 mm bars	8ϕ 25m bars	4 ϕ 25 mm bars	8ϕ 25mm bars	4 ϕ 25 mm bars	4 ϕ 25 mm bars
Concrete cover to centre of rebars (mm)	48	48	48	48	48	48
f'_c (MPa)	34.8	75	35.7	127	39.7	39.7
f_y (MPa)	444	400	444	400	444	444
Applied axial load (kN) (P)	800	3895	1000	4981	993	993
Load Eccentricity (mm)	0	0	24	25	44	44
Load ratio	0.70	0.76	0.875	0.97	0.87	0.87
Aggregate type	Siliceous	Carbonate	Siliceous	Carbonate	Siliceous	Siliceous
Measured fire resistance in tests (minutes)	218	299	181	118	245	220
Predicted fire resistance using model (minutes)	205	310	195	123	255	232

Table 5.2 Summary of test parameters and comparison with fire resistance tests at MSU

Column designation	Test #	Fire exposure	Concrete type	Concrete Strength (Mpa)		Test day concrete strength (MPa)	Load ratio (%)	Relative humidity (%)	Fire resistance (minutes)		Extent of spalling measured
				28 Day	Test Day				Measured	Predicted	
NSC1	I	ASTM E119	NSC	39	51	51	0.4	81.5	183	176	Minor
HSC1	I	ASTM E119	HSC	91	106	106	0.4	81.1	61	57	Medium-Severe
HSC2	II	SF	HSC	91	107	107	0.4	87.5	NF	NF	Severe
HSC3	II	SF	HSC	91	107	107	0.6	86.6	75	63	Severe
HSCP1	III	LF	HSCP	85	93	93	0.4	91.8	NF	NF	Nil
HSCP2	III	LF	HSCP	85	93	93	0.6	92.5	221	213	Nil

NF - No Failure

Table 5.3 Summary of spalling predictions and measurements

Column designation	Spalling Duration Measured (mins in the fire test)		Extent of spalling (%)	
	Start	End	Measured	Predicted
NSC1	-	-	15	0
HSC1	15	33	40	35
HSC2	15	35	43	35
HSC3	15	27	40	39
HSCP1	-	-	0	0
HSCP2	-	-	0	0

- No spalling recorded

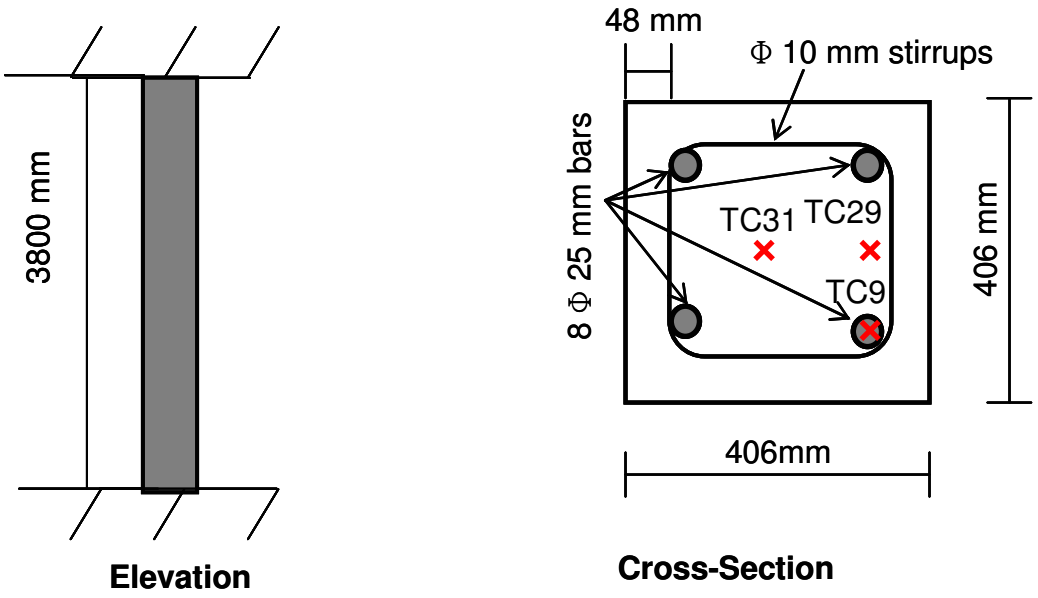

(a) Column details and thermocouple locations

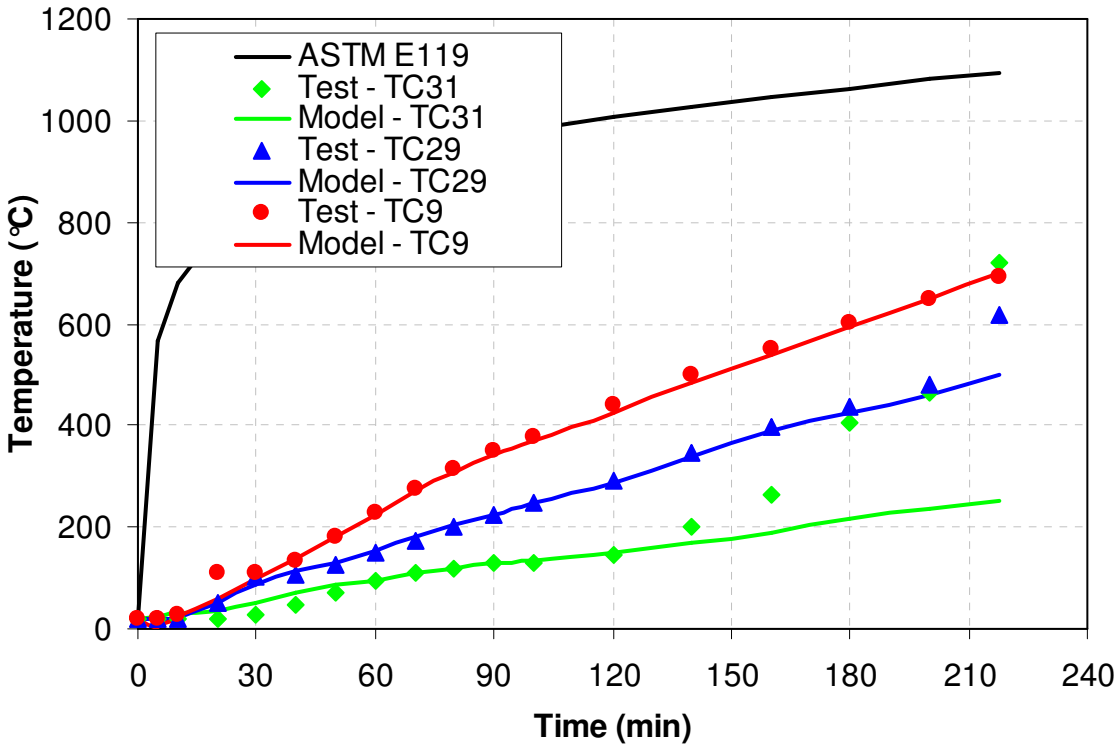

(b) Comparison of predicted and measured temperatures

Fig. 5.1. Cross-sectional dimensions and comparison of predicted and measured temperatures and deformations for concentrically loaded NSC column I3.

Fig. 5.1. Contd. Cross-sectional dimensions and comparison of predicted and measured temperatures and deformations for concentrically loaded NSC column I3.

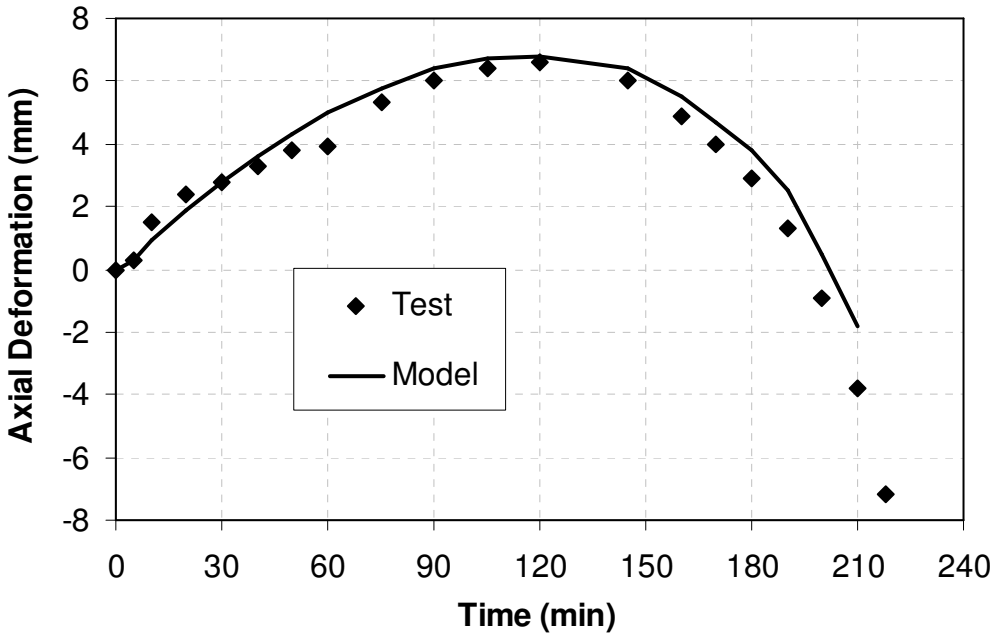

(c) Comparison of predicted and measured axial deformations

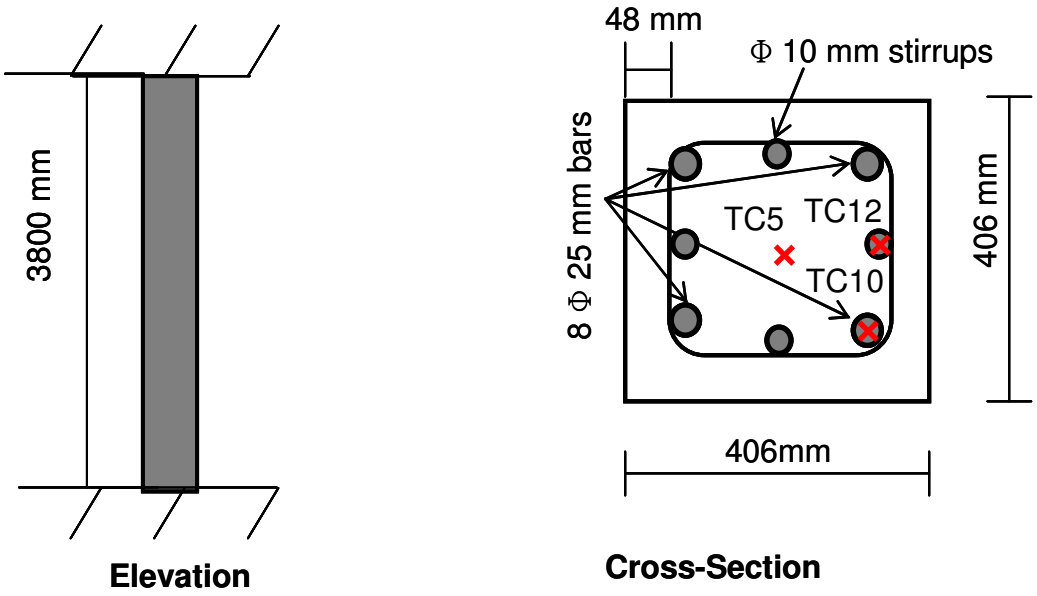

(a) Column details and thermocouple locations

Fig. 5.2. Cross-sectional dimensions and comparison of predicted and measured temperatures and deformations for concentrically loaded HSC column HSC2-1.

Fig. 5.2. Contd. Cross-sectional dimensions and comparison of predicted and measured temperatures and deformations for concentrically loaded HSC column HSC2-1.

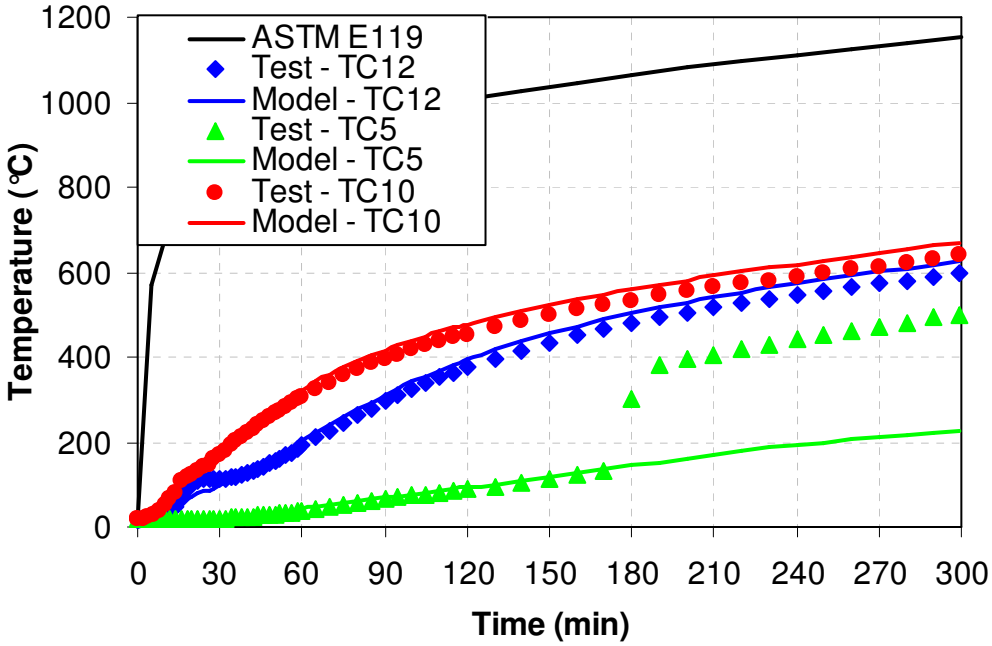

(b) Comparison of predicted and measured temperatures

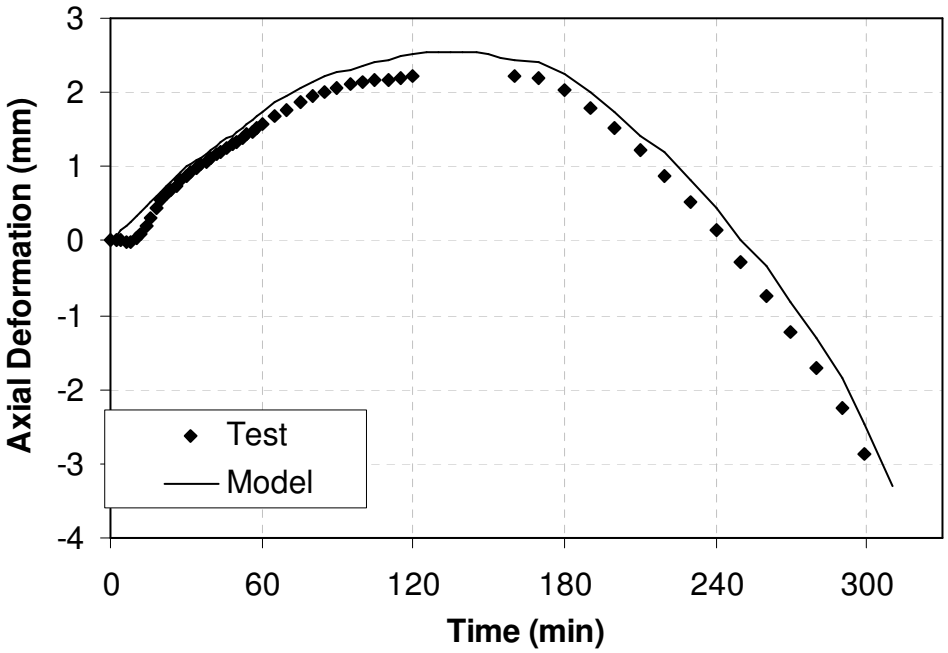

(c) Comparison of predicted and measured axial deformations

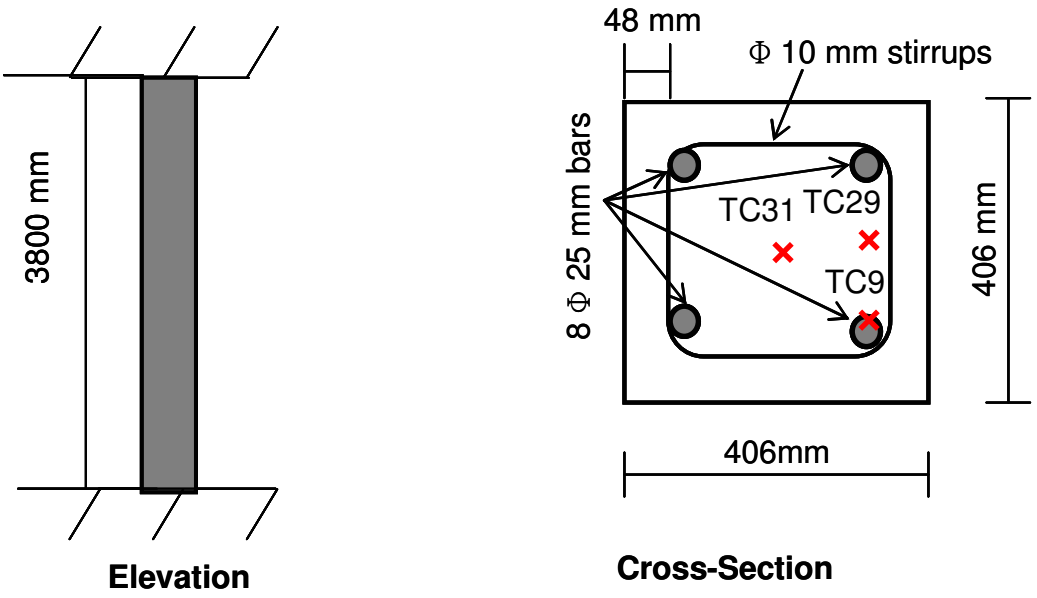

(a) Column details and thermocouple locations

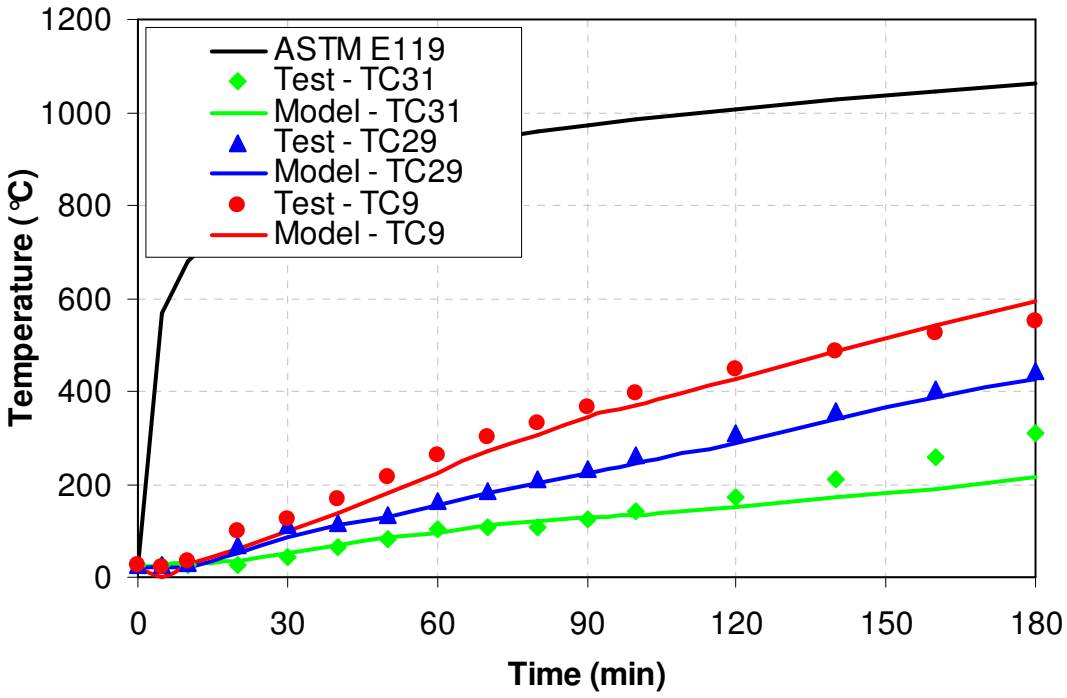

(c) Comparison of predicted and measured temperatures

Fig. 5.3. Cross-sectional dimensions and comparison of predicted and measured temperatures and deformations for eccentrically loaded NSC column III3.

Fig. 5.3. Contd. Cross-sectional dimensions and comparison of predicted and measured temperatures and deformations for eccentrically loaded NSC column III3.

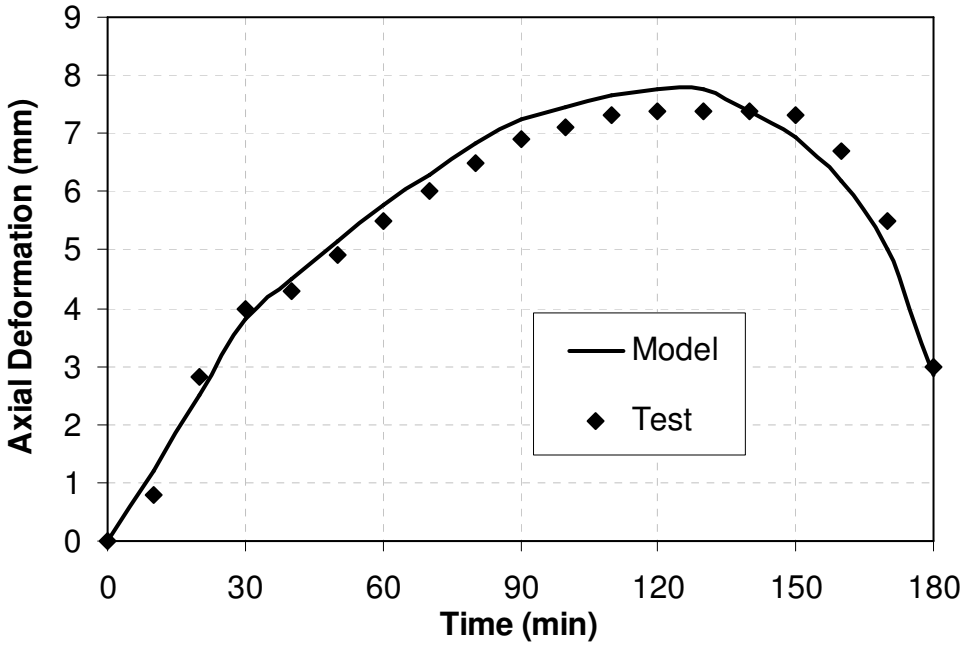

(c) Comparison of predicted and measured axial deformations

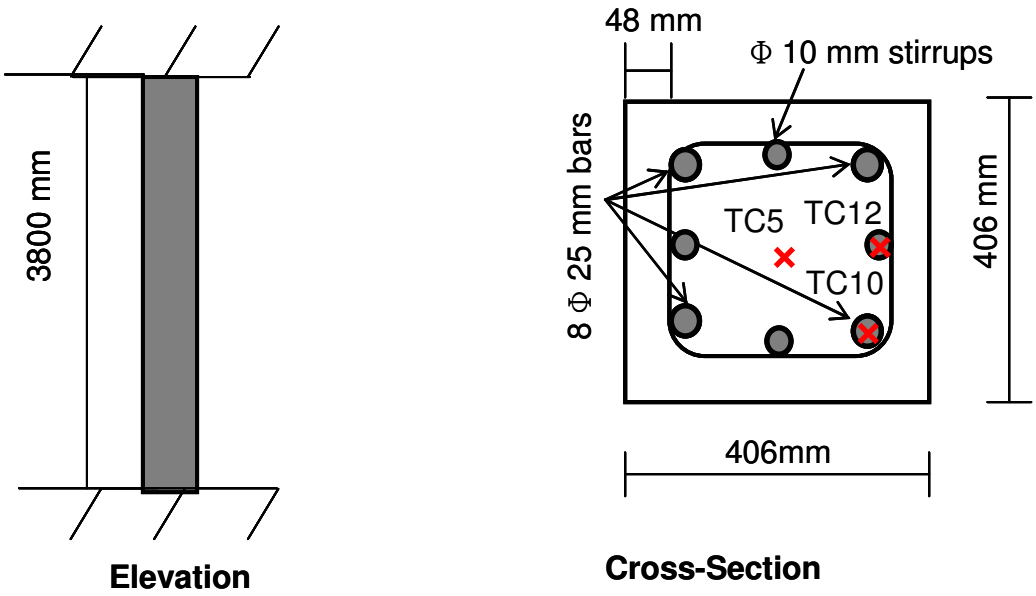

(a) Column details and thermocouple locations

Fig. 5.4. Cross-sectional dimensions and comparison of predicted and measured temperatures and deformations for eccentrically loaded HSC column HSC2-9.

Fig. 5.4. Contd. Cross-sectional dimensions and comparison of predicted and measured temperatures and deformations for eccentrically loaded HSC column HSC2-9.

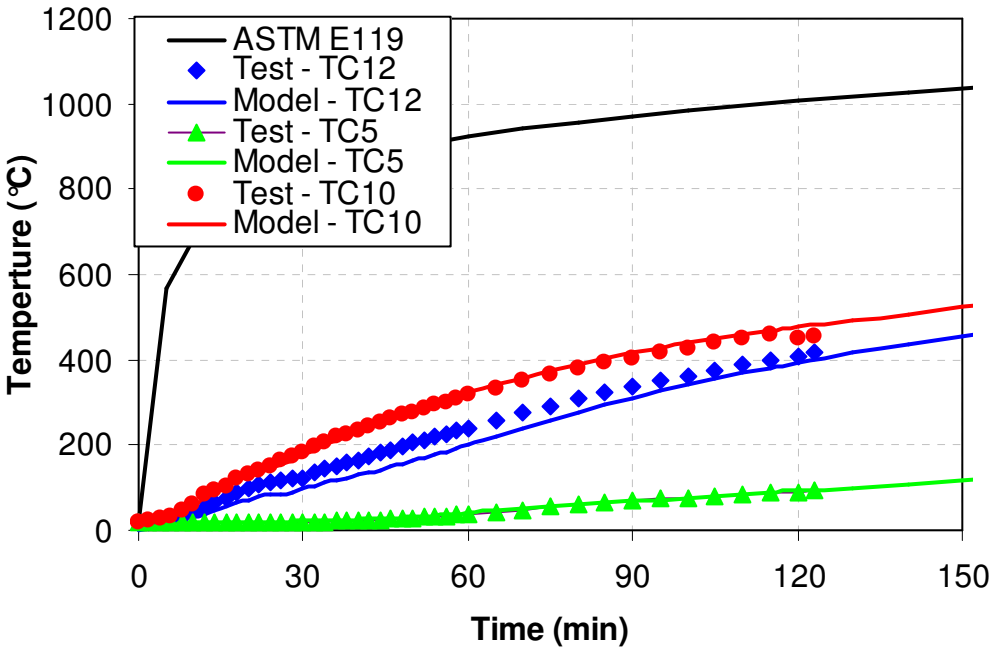

(b) Comparison of predicted and measured temperatures

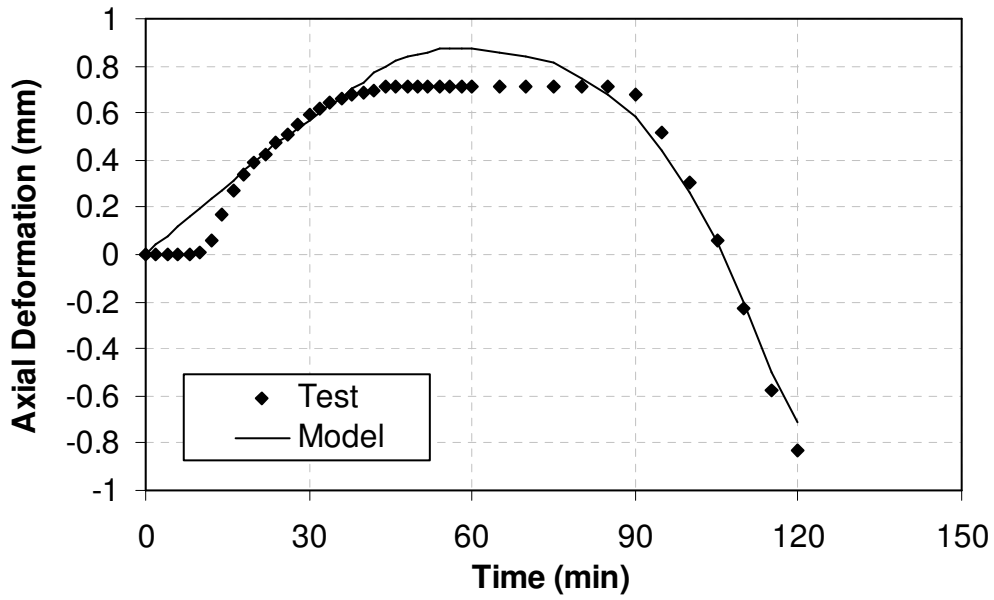

(c) Comparison of predicted and measured axial deformations

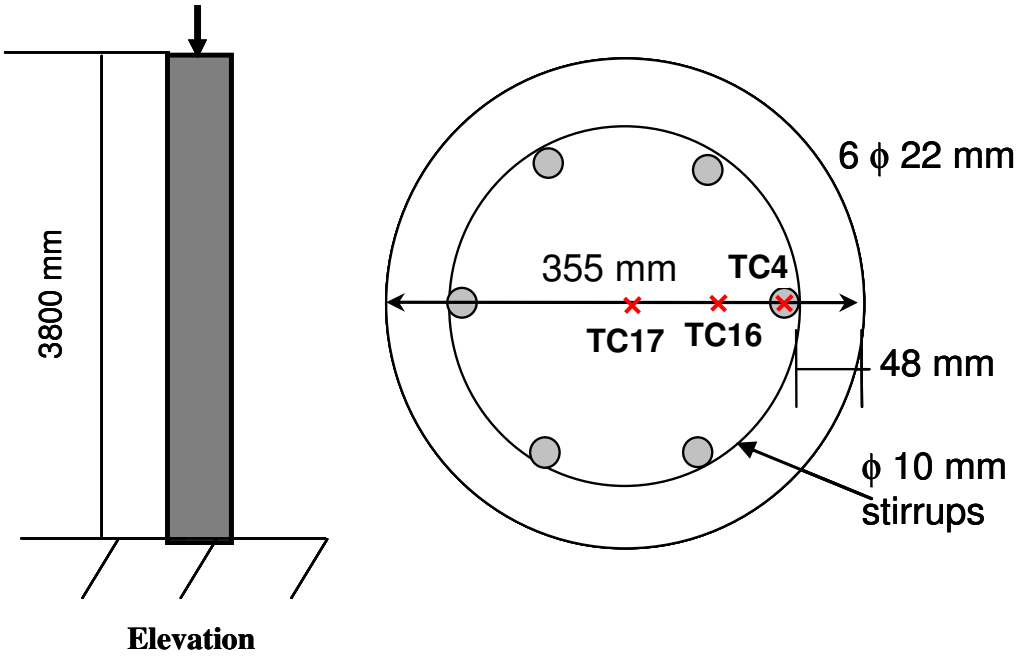

(a) Column details and thermocouple locations

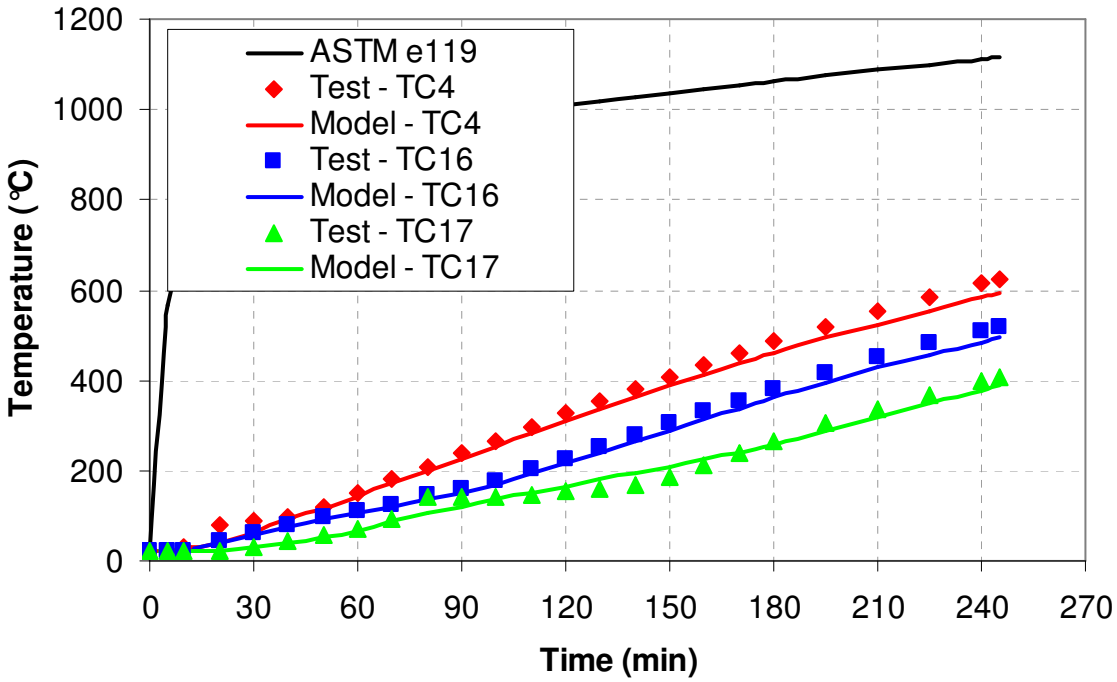

(b) Comparison of predicted and measured temperatures

Fig. 5.5. Cross-sectional dimensions and comparison of predicted and measured temperatures and deformations for concentrically loaded circular NSC column III11.

Fig. 5.5. Contd. Cross-sectional dimensions and comparison of predicted and measured temperatures and deformations for concentrically loaded circular NSC column III11.

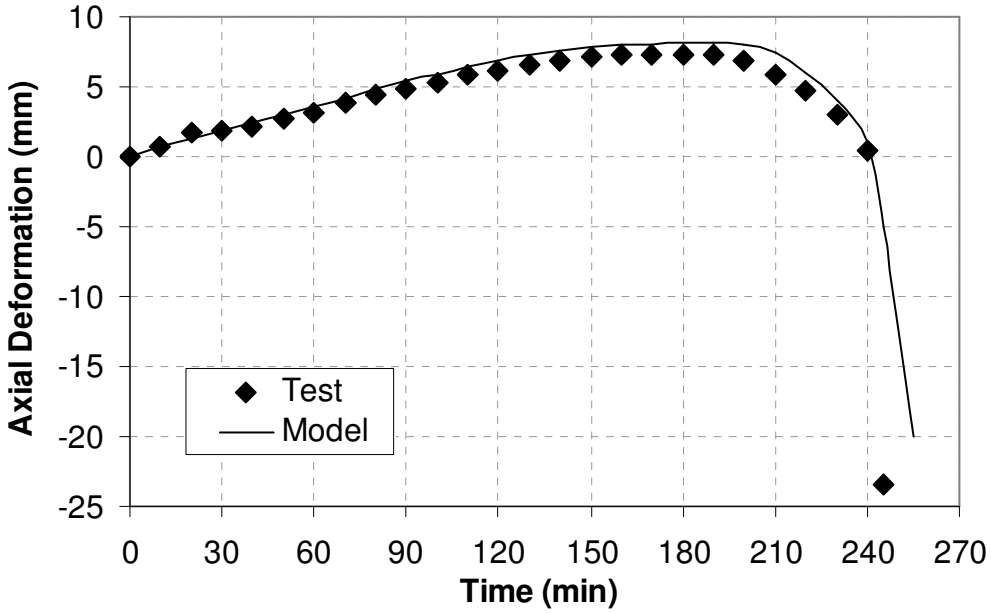

(c) Comparison of predicted and measured axial deformations

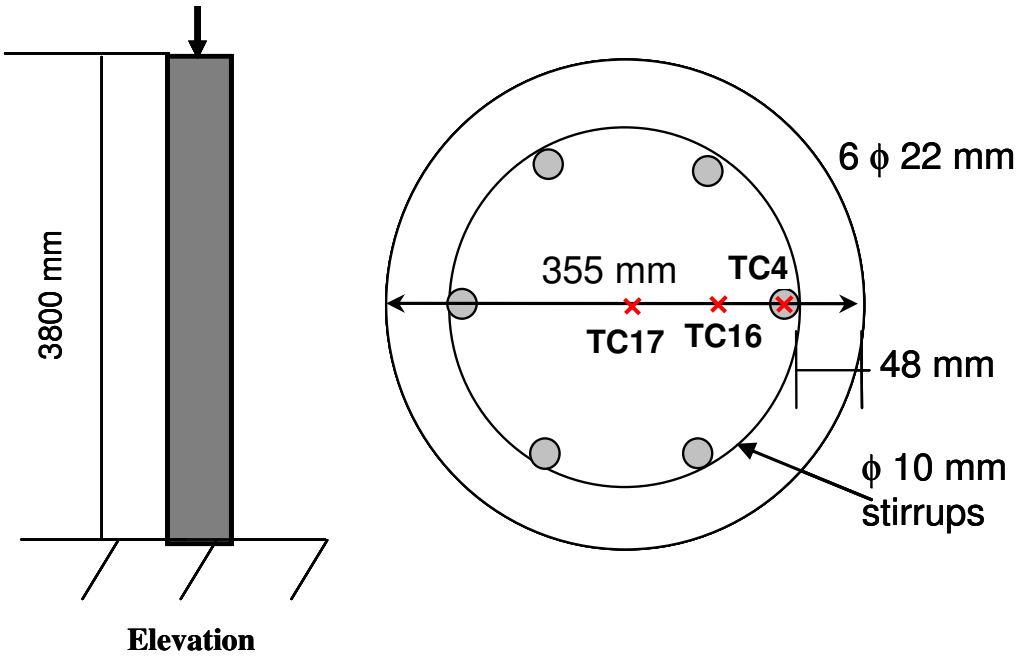

(a) Column details and thermocouple locations

Fig. 5.6. Cross-sectional dimensions and comparison of predicted and measured temperatures and deformations for concentrically loaded circular NSC column III12.

Fig. 5.6. Contd. Cross-sectional dimensions and comparison of predicted and measured temperatures and deformations for concentrically loaded circular NSC column III12.

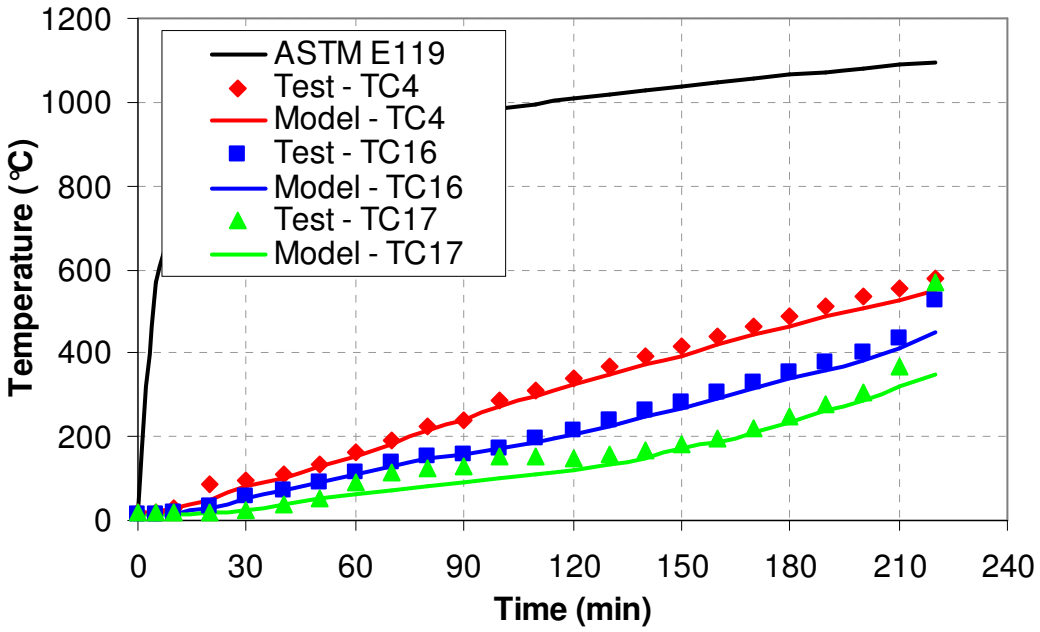

(b) Comparison of predicted and measured temperatures

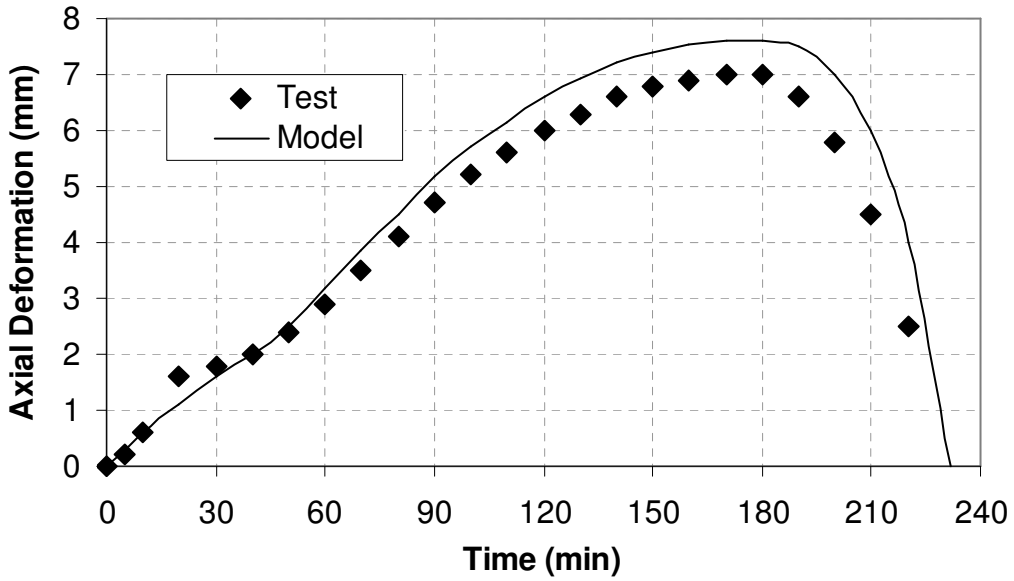

(c) Comparison of predicted and measured axial deformations

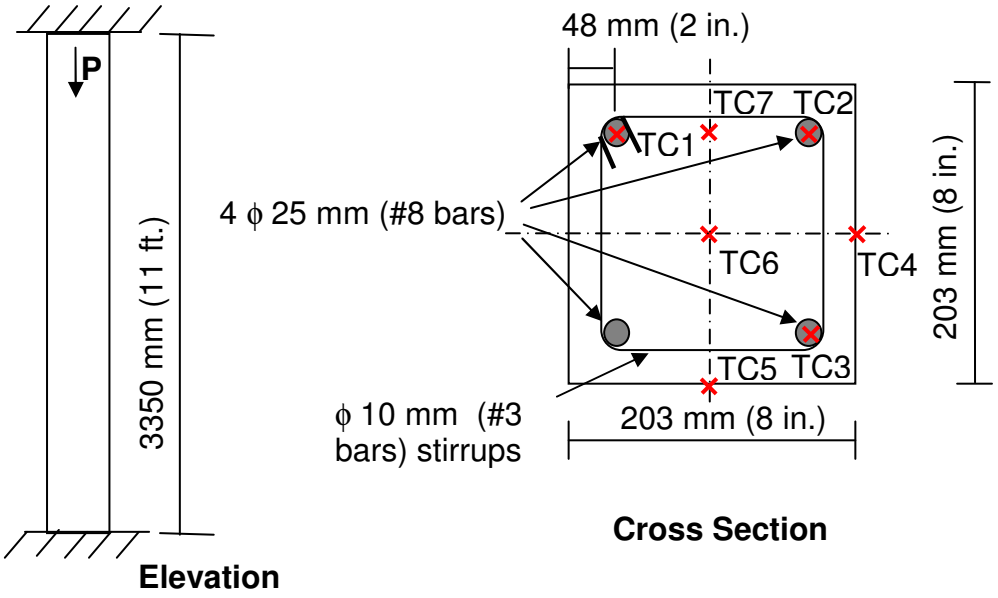

(a) Cross-sectional details and thermocouple locations

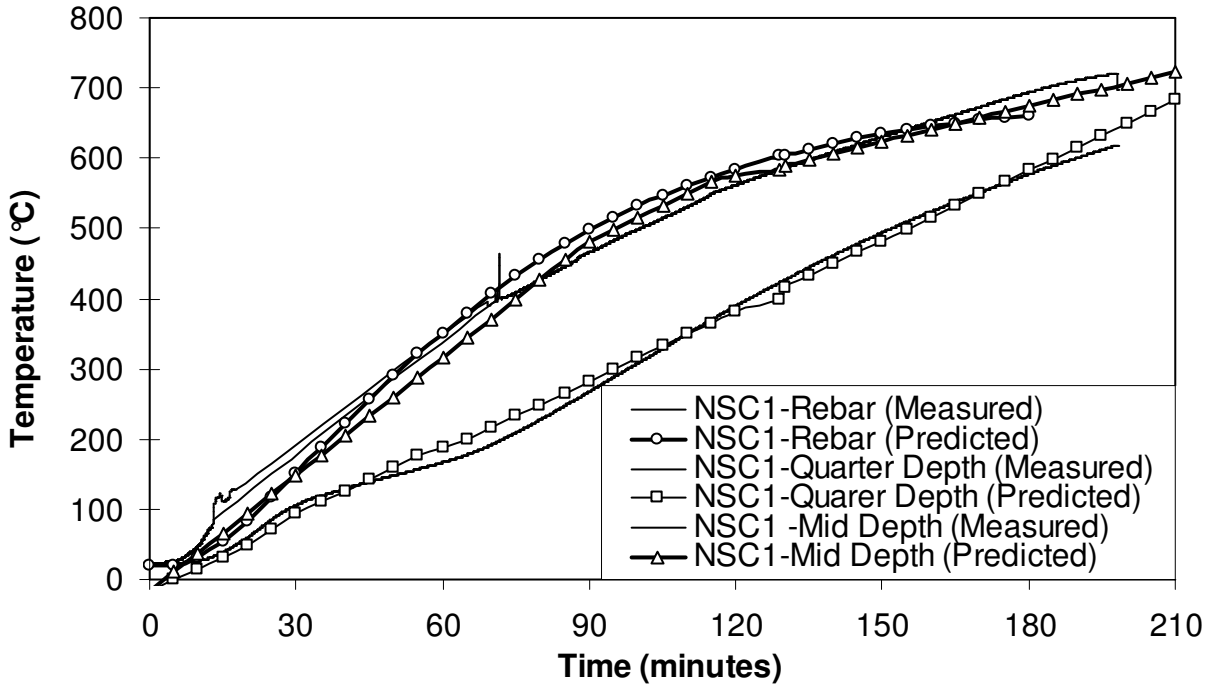

(b) Comparison of predicted and measured temperatures – NSC1

Fig. 5.7. Cross-sectional dimensions and comparison of predicted and measured temperatures, deformations and spalled area for concentrically loaded RC columns tested at MSU.

Fig. 5.7. Contd. Cross-sectional dimensions and comparison of predicted and measured temperatures, deformations and spalled area for concentrically loaded RC columns tested at MSU.

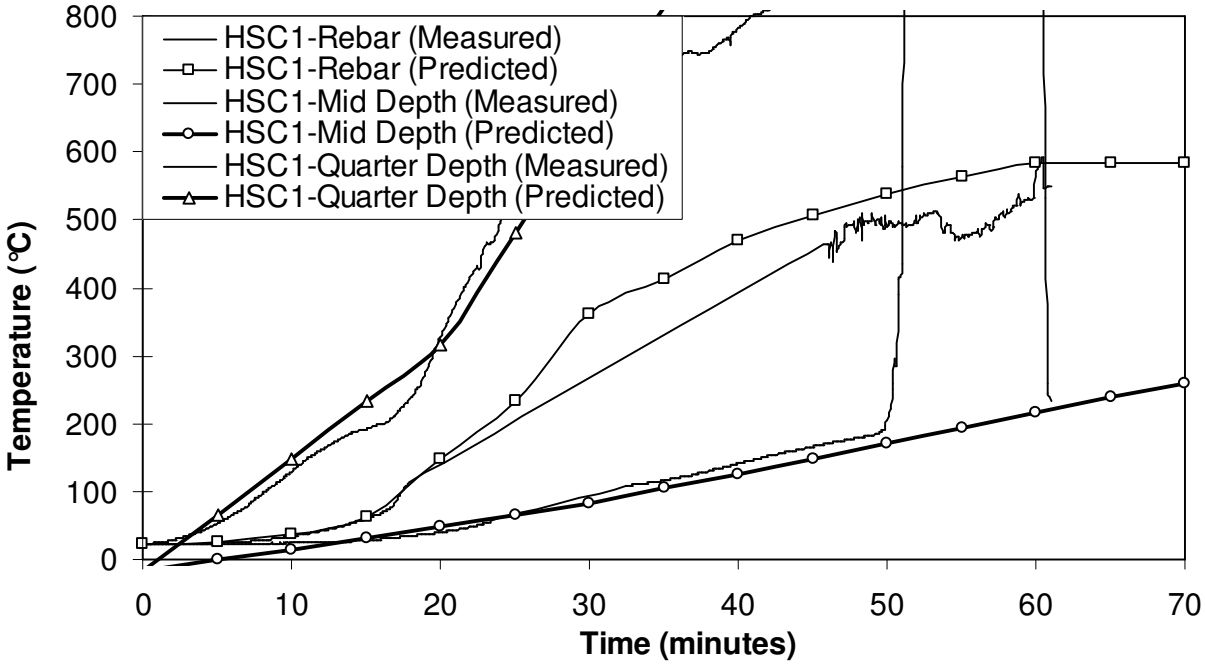

(c) Comparison of predicted and measured temperatures – HSC1

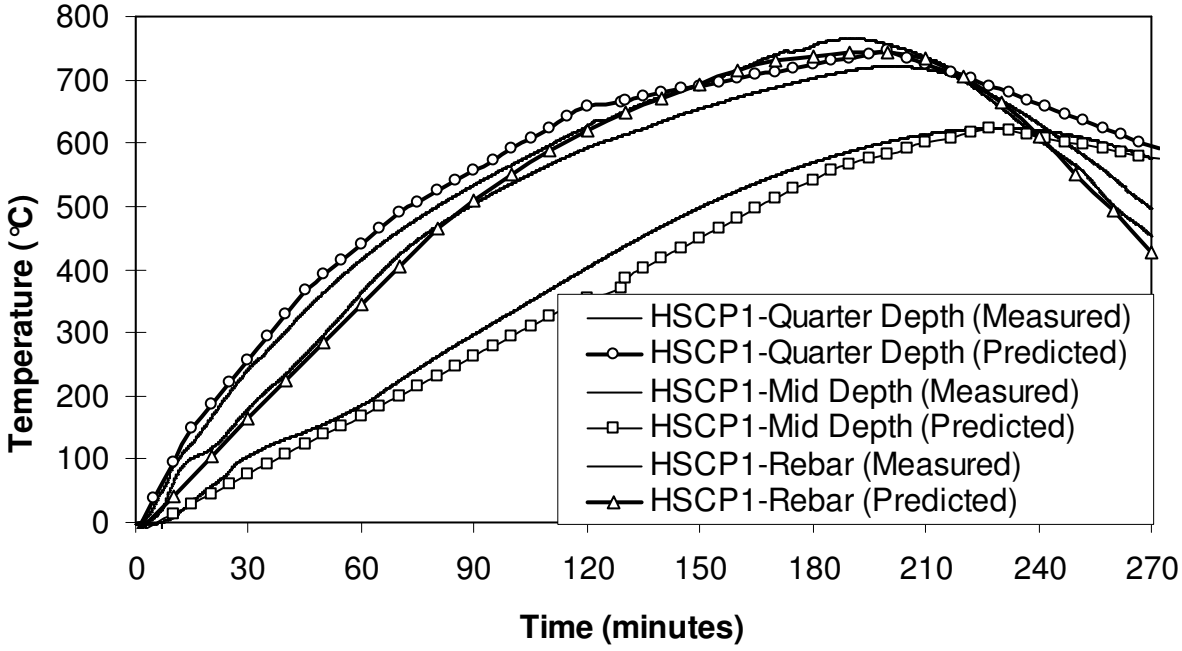

(d) Comparison of predicted and measured temperatures – HSCP1

Fig. 5.7. Contd. Cross-sectional dimensions and comparison of predicted and measured temperatures, deformations and spalled area for concentrically loaded RC columns tested at MSU.

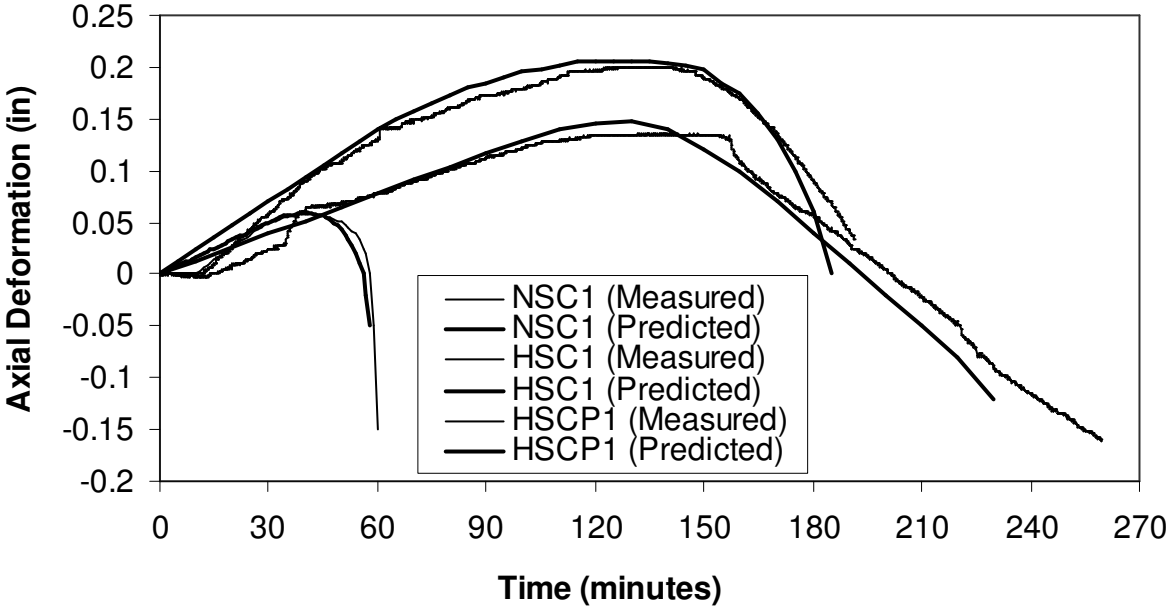

(e) Comparison of predicted and measured axial deformations

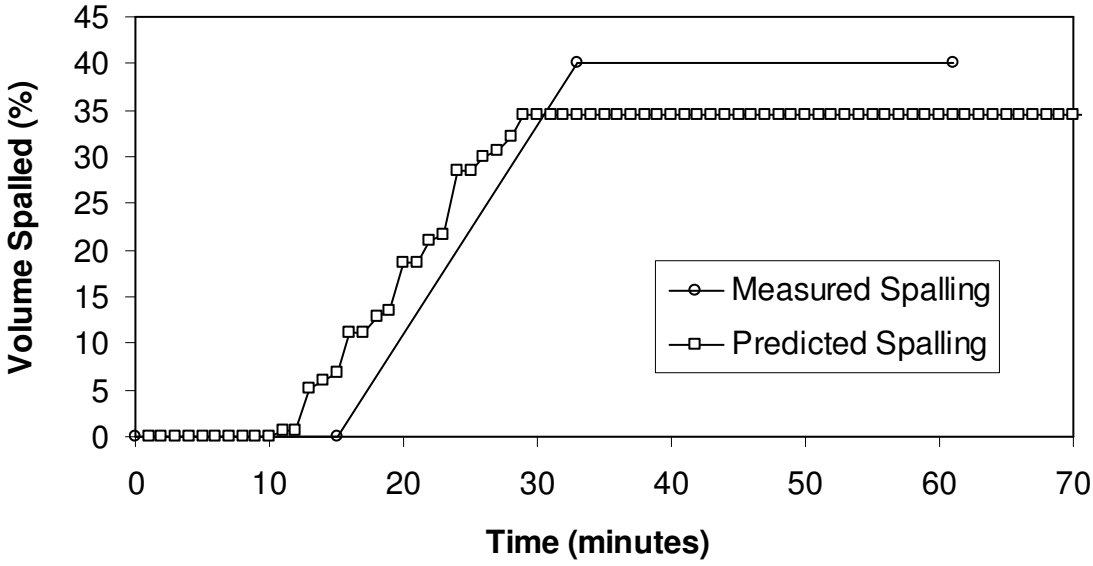

(f) Comparison of predicted and measured spalled area – HSC1

CHAPTER 6

6 PARAMETRIC STUDIES

This chapter is mainly based on the following journal papers:

- Kodur V., Dwaikat M. and Raut N., (2009) “Macroscopic FE Models for Tracing the Fire Response of Reinforced Concrete Members“, Engineering Structures Journal, V. 31 No. 10, pp. 2368-2379.
- Raut N. and Kodur V., (2009) “Behavior of High Strength Concrete Columns under Design Fire Scenarios”, Proceedings: ASCE Structures Congress, Austin, TX.
- Kodur V. and Raut N., (2009) "Design Equation for Predicting Fire Resistance of Reinforced Concrete Columns", Structural Concrete, V. 10, No. 2, pp. 73-86.
- Raut N., Kodur V., and Szoke S (2010) “A Macroscopic Finite Element Computer Model for Tracing Fire Response of Reinforced Concrete Columns”, Proceedings: ACI Spring Convention, Chicago, IL.
- Raut N. and Kodur V., (2010) “Modeling the Fire Response of Reinforced Concrete Columns under Biaxial Bending”, 6th International Conference on Structures in Fire, East Lansing, USA.
- Raut N. and Kodur V., (2010) "Modeling the Fire Response of Reinforced Concrete Columns Under Biaxial Bending", Accepted, ACI Structural Journal.
- Raut N. and Kodur V., (2010) "Behavior of Circular Reinforced Concrete Columns Under Fire Conditions", Communicated, Journal of Structural Fire Engineering.
- Raut N. and Kodur V., (2010) "Computer Model for Predicting the Fire Response of Reinforced Concrete Columns ", Accepted, ACI Special Publication.

6.1 General

Fire performance of reinforced concrete columns is influenced by a large number of factors. Parametric studies can generate data to quantify the influence of various factors on fire resistance and also identify the critical parameters. The ideal method is to undertake a number of runs using the numerical model developed in Chapter 4. Results from such parametric studies are influenced by the accuracy of the high temperature property relations for concrete and reinforcing steel. As seen in Chapter 2, there is large variation in reported high temperature properties of concrete and moderate variation in properties of reinforcing steel. Thus, the parametric studies are conducted using the average material properties (obtained by averaging the worst and best case scenarios of material properties) [Dwaikat 2009]. The reason for using the average material properties is the fact that fire is a rare event, and therefore fire design is generally performed using the most likely expected (average) material properties [Buchanan 2002, Dwaikat 2009]. Thus, it is reasonable to use the average high temperature properties to carry out the parametric studies. It should be noted that the effect of the studied parameters on the fire resistance of RC columns is not significantly influenced by variation in the high temperature property relations.

6.2 Factors Influencing Fire Resistance

A state-of-the-art review presented in Chapter 2 clearly indicated that several factors influence the fire response of RC columns. Some of these factors have been studied before and their effect is quantified in the previous studies reported in the literature [Lie and Woolerton, 1988, Ali et al., 2001, Kodur, 2003]. The main factors influencing the fire response of RC columns established from literature are:

- Column cross-sectional size,
- Concrete cover thickness,
- Aggregate type,
- Load ratio, and
- Reinforcement ratio.

However some of the critical factors influencing the fire response of RC columns are not yet studied. These are:

- Eccentricity of load (uniaxial and biaxial),
- Fire scenario,
- Face exposure (1-, 2-, 3-, or 4- side), and
- Concrete strength (permeability)

The above factors were not studied in literature due to lack of models that account for biaxial bending. Further some of these critical factors have greater influence in case of columns made of new types of concrete (HSC) due to the possible occurrence of fire induced spalling. Many of the above factors generate either uniaxial or biaxial bending during exposure to fire. Hence a detailed parametric study was undertaken, using the numerical model, to quantify the influence of different exposure conditions, fire scenarios, bi-eccentric loading, and effect of concrete type (permeability) on the fire resistance of RC columns and the results are presented in Section 6.4.

6.3 Numerical Studies

A numerical study was undertaken to quantify the effect of critical factors that were not previously studied. The effect of other parameters, that are already existing in literature is discussed in Chapter 7.

6.3.1 Column Characteristics

For the parametric studies, 68 RC columns, as listed in Table 6.1, were selected with varying parameters. The columns were assumed to be fixed at both ends. The fire scenarios and geometric properties of RC columns used in the analysis are shown in Table 6.1 and Figure 6.1. The variables included the permeability (strength) of concrete, number of sides exposed to fire, load eccentricity, column size, load ratio, and fire scenario. Thirty eight columns were assumed to be made of NSC with a compressive strength of 30 MPa, while remaining 30 columns were made of HSC with compressive strength of 100 MPa. The permeability of NSC was assumed to be in the order of 10^{-17}, while the permeability of 15 HSC columns was taken to be 10^{-18} and the remaining 15 HSC columns to be 10^{-19}. The columns were reinforced with steel rebars having yield strength of 400 MPa. The reinforcement ratio was maintained at 2% for all the columns which lies within the minimum and maximum limits specified in ACI 318 [2008].

6.3.2 Analysis Details

The parameters varied in the analysis include three different concrete cross-sections, five load ratios (30%, 40%, 50%, 60% and 70%), two concrete types (NSC and HSC), five exposure conditions (1-side, 2-adjacent sides, 2-opposite sides, 3-sides, and 4-sides), three uniaxial eccentricities (25mm, 50mm, and 75mm along X-axis), and six biaxial eccentricities (25mm, 50mm, and 75 mm along X and Y-axes). In addition, to investigate the effect of fire scenario, some of the columns were analyzed under three standard fire exposures (ASTM E119 [2008] standard fire, ASTM E1529 [1993] hydrocarbon fire and External fire [Buchanan, 2002]) and two design fire exposures (Fire I, and Fire II). The time temperature curves for the five fire scenarios are given in Figure 6.2.

The fire resistance analyses of RC columns were carried out by incrementing time at one minute intervals. The column along its length was divided into 40 equal segments. Each segment was then discretized into quadrilateral elements of 10 mm size for the analysis. The discretization and analysis procedure is similar to that adopted in validation of the model, which is presented in detail in Chapter 5. High temperature material properties for concrete and steel were used as per the ASCE manual [ASCE, 2007]. The ties were assumed to be bent at 135° and thus spalling was assumed to occur in the concrete outside the ties and none inside the tie core [Kodur et al, 2004]. The pore pressure, cross-sectional temperature, axial deformation and lateral deformation were computed at every time step and the results were used to evaluate failure. Strength limit state was applied to determine failure, time at which column can no longer carry the applied load.

6.4 Results of Parametric Studies

Results from the parametric studies are presented in Table 6.1 and Figures 6.3 to 6.19. Table 6.1 gives the details of the columns and the predicted fire resistances while the figure present the time-axial deformation and time-lateral deformation curves for the analyzed columns. The effect of the studied parameters on the thermal response of the column (rebar and concrete temperatures) is not presented here because many of these parameters such as load ratio, and load eccentricity do not influence the temperature rise of the columns. The effect of each of the parameters on the fire response is discussed below.

6.4.1 Effect of Fire Exposure Conditions

RC columns in buildings can be subjected to fire scenarios from 1-, 2-, 3-, or 4-sides. In order to quantify the effect of various exposure types (1-, 2-, 3- side), 30 columns were analyzed. Three column sizes (203 mm, 406 mm and 610 mm) were considered in the analysis by exposing them to ASTM E119 standard fire from all four sides. These three column sizes (203 mm, 406 mm

and 610 mm) were also analyzed with concentrically applied load but with 1-side, 2- opposite sides, 2- adjacent sides and 3- sides exposed to fire. The properties of these columns are tabulated in Table 6.1.

Figures 6.3-6.5 show the response of RC columns exposed to fire with different exposure conditions. The temperature and deformation progression in columns CE0, CE1, CE3 & CE4 (see Table 6.1 for parameters varied) are plotted in Figure 6.3-6.5. Since these four columns have different number of faces exposed to fire, thermal gradients develop differently in these columns. It can be seen from Figure 6.3 that the thermal gradients in column CE0 (exposed on 4 sides) at 45 minutes into fire exposure are symmetric about both the axes, while the thermal gradients for column CE1 and CE4 (exposed on 3-sides and 1-side respectively) are symmetric about one axis. These gradients (in columns CE1 and CE4) cause the column to bend along the axis of eccentricity (uniaxial bending). The thermal gradients for column CE3 (exposed on 2 adjacent sides) are not symmetric about any axes along the member orientation. The axis of symmetry is oriented at an angle to the member axes and thus this causes the column to experience biaxial bending.

Figure 6.4 shows the variation of the axial deformation of these four columns as a function of fire exposure time for different fire exposure conditions. It can be seen that the columns undergoing bending (CE1, CE3, and CE4) have shorter expansion zone since the eccentricity causes bending and thus the total downward deformation (contraction) of the column is higher (see Figure 6.4). Column CE3 undergoes biaxial bending and thus has significantly less area of concrete resisting bending. Therefore this column suffers higher compressive axial deformation as compared to columns CE1 and CE4 (uniaxial bending) and thus demonstrates lesser fire resistance.

Figure 6.5 shows progression of lateral deformation in all four columns as a function of time. It can be seen that the lateral deformations of all the columns are zero till the columns are in expansion phase. This is as expected as an expanding column cannot deform laterally. The lateral deformations occur after the column begins to contract. These lateral deformations are very small for most of the fire duration until just prior to failure, where the high temperature creep strains play a significant role and concrete has lost significant stiffness. Also, the moments acting on the column get magnified with time due to P-δ effect and thus the lateral deformations increase exponentially. It should be noted that, even though the thermal gradients in column CE0 are symmetric, it undergoes lateral deformation as all the columns were analyzed with the applied load subjected to some minimum eccentricity (2% of column width) in order to account for geometric nonlinearity and represent the realistic conditions.

It can be seen from Table 6.1 that fire exposure conditions (1-, 2-, 3-, or 4-side exposure) has significant influence on the fire resistance (failure time) of RC columns. The fire resistance reduces from 253 minutes, under four side exposure, to 226, 177 and 240 minutes when subjected to 3-, 2-, 1-side fire exposure respectively. As discussed above, this reduction can be attributed to the development of thermal gradients and associated bending (uniaxial or biaxial) effects.

6.4.2 Effect of Load Eccentricity

RC columns can also be subjected to eccentric loading, due to eccentric connection of adjoining beams and also due to the resisting moments from these beams. The effect of eccentricity on fire resistance was studied by analyzing 15 RC columns under ASTM E119 standard fire exposure. The columns were loaded to 50% of their ultimate load capacity (calculated as per ACI 318) applied at eccentricities of 0 mm, 25 mm, 50 mm and 75 mm. The axial load on the column was

assumed to act at an eccentricity (X axis in some cases and both X and Y axes in the rest) as given in Table 6.1. When the load is eccentric there is additional moment acting on the column along with the axial force. The fire resistance of an RC column decreases with increased eccentricity. This can be attributed to the fact that, as the eccentricity increases the moment due to applied loading also increases, thus subjecting the column to higher bending. This leads to faster degradation of column strength and stiffness due to increased P-δ effect. For comparison, the predictions for five columns (CE0, CE5, CE6, CE54, and CE58) are presented in detail in Table 6.1. As an example fire resistance of uniaxially eccentrically loaded columns CE5 (e = 25mm) and CE6 (50 mm) is 221 minutes and 198 minutes respectively, which is lower than that of axially loaded column (CE0) of 253 minutes.

When the load is applied eccentric to both axes, a column will be subjected to additional moments in both the axes. Also, since the neutral axis not only shifts but also rotates due to biaxial bending, the sectional area available farther away from the neutral axis (necessary for higher moment capacity) is much lesser. This further reduces the fire resistance of the RC column. It can be seen that the fire resistance of bi-eccentrically loaded column CE54 (208 minutes) is lower than that of eccentrically (uniaxial) loaded column CE5 (221 minutes) as CE54 has moments acting along both axes. Similar to uniaxially eccentric loading case, fire resistance decreases with increased biaxial eccentricity (fire resistance of CE58 = 148 minutes) as the moments acting on the column increase.

Figure 6.6 shows the variation of the axial deformation of these five columns as a function of fire exposure time for different loading cases. It can be seen that the columns with increased eccentricity have shorter expansion zone since the eccentricity causes bending of the column and the total expansion of the column is lower as can be seen in Figure 6.6. Figure 6.7 shows the

progression of lateral deformation at mid-height with time for the five columns. Similar to previous columns the lateral deformations of all columns are zero till the columns are in expansion zone.

6.4.3 Effect of Column Size

Three RC columns (203mm, 406mm, and 610mm), per scenario (different exposure, load eccentricity, and concrete strength), were analyzed to study the effect of cross-sectional size on fire performance. All columns were analyzed under ASTM E119 standard fire. All columns were assumed to carry an axial load equal to 50% of their design capacity applied. In order to compare the behavior of columns with different sizes three columns namely, CE0, CE8, and CE16, are compared as they are exposed on all four sides to fire and are subjected to concentric loading. No spalling was predicted in these three columns as they were made of NSC. As seen in Table 6.1, column CE0 (of 406 mm) has a higher fire resistance of 253 minutes as compared to column CE8 (of 203 mm) which has a fire resistance of 155 minutes. This is as expected as there is larger mass of concrete available to act as a heat sink in column CE0 and thus the overall temperature rise within the column is lower than that of column CE8. This results in slower strength loss in concrete and steel rebars and thus has higher load carrying capacity. Similarly column CE16 (of 610mm) has the highest fire resistance (297 minutes) amongst the three sizes. Thus it is seen that the fire resistance increases with the increase in cross-section size.

It should be noted that the thermal expansion increases with column size (see Figure 6.8) due to larger mass of concrete being heated up before the column starts losing significant amount of strength and contracting. Figure 6.8 shows the axial deformation for the three columns while Figure 6.9 shows the lateral deformations for these columns.

It should be noted that under biaxial bending the increase in fire resistance with column size may not be the same. Hence, the behavior of three other columns namely, CE3, CE11, and CE19, is also compared. All these three columns have a concentrically applied load, but are exposed to fire on two adjacent sides. The axial and deformations of these three columns are shown in Figure 6.10 and Figure 6.11 respectively. These figures show similar trends for columns CE0, CE8, and CE16, with larger columns undergoing more expansion and demonstrating higher fire resistance time. But, it can be seen from Table 6.1 that the increase in fire resistance with column size is lower than the condition when all four sides are exposed to fire. The fire resistance of columns CE3, CE11, and CE19 is 177, 136, and 220 minutes respectively. Since under biaxial bending the neutral axis rotates and thus the area available farther away from the neutral axis (which is most effective in providing flexural strength) is less than under axially loaded columns. Thus the increase in the column dimensions does not significantly increase the flexural strength of the column under biaxial bending.

6.4.4 Effect of Fire Severity

To illustrate the effect of fire scenario combined with biaxial bending effects, four RC columns CE60, CE61, CE62, and CE63 were analyzed under standard and design fire scenarios. The columns were analyzed under three standard and two design fire exposures (see Figure 6.2) by subjecting them to bi-eccentric load (50 mm). The three standard fire scenarios are ASTM E119 standard fire [2008], hydrocarbon standard fire [1993], and external fire as per Eurocode [Buchanan, 2002]. There is no decay phase in the standard fire curves but in realistic fires, there always exists a decay phase, since the fuel or ventilation runs out leading to compartment burnout. Thus, the remaining two fire scenarios are used to represent more realistic (design) fire exposure.

Figures 6.12 and 6.13 show the axial and lateral deformations for these columns. It can be seen, from Table 6.1 and Figure 6.12 that the lowest fire resistance of 98 minutes is obtained for the column CE60 exposed to the hydrocarbon fire as compared to 148 minutes for column CE58 under the ASTM E119 standard fire exposure. This is due to the steep increase in temperature for the hydrocarbon fire as shown in Figure 6.2. The axial deformation of CD60 is also lower than that of CE58 in the expansion phase due to higher loss in strength and stiffness in the column. Also, the fire resistance for the column exposed to the external fire (CE61) is higher than that for the column under ASTM E119 standard fire. This is on expected line, and is due to the fact that the maximum fire temperature attained for external fire exposure is low when compared to that of ASTM E119 standard fire. The columns exposed to design fire scenarios (CE62 and CE63) do not attain failure. Thus the columns survive complete burn-out under design fire exposure.

Comparing fire response of columns CE60 to CE63 it can be seen that the reduction or increase in fire resistance of a column due to change in the fire scenario is very prominent. For example the fire resistance of the column CE58 reduced by 31% when fire scenario changed from ASTM E119 to hydrocarbon fire (column CE60). This can be attributed to the fact that the change in the fire time-temperature profiles affects the temperature in the outer layer of concrete. This in turn reduced the strength and stiffness of the concrete which contributes more towards flexural strength of the column.

6.4.5 Effect of Load Level

Four RC columns, namely; CE64, CE65, CE66, and CE67 were analyzed to study the effect of load level on fire resistance under 30%, 40% 60% and 70% load ratio, applied at an eccentricity of 50 mm along both axis. All columns were analyzed under ASTM E119 standard fire and results are presented in Table 6.1. Figures 6.14 and 6.15 show the axial and lateral deformations

for these columns as compared to column CE58 which is loaded to 50% of its capacity. As seen in Table 6.1, fire resistance decreases with increase in the load level. The drop in the fire resistance with increased load level is higher than that observed from literature [Lie and Woolerton, 1988] (where in a drop of approximately 10% in fire resistance per 25 mm of load eccentricity was recorded) under axial loading case only. This can be attributed to increase in moments acting due to the eccentricity which further increase with load level resulting is early failure of the column. Also the rate of deformation increases significantly in the later stages of fire exposure for highly loaded columns and this is mainly resulting from higher creep strains and P-δ effect in these columns (see Figure 6.14).

6.4.6 Effect of Concrete Strength (Permeability)

The effect of concrete strength for the three column sizes (203 mm, 406 mm and 610 mm) was quantified by analyzing columns under 1-, 2-opposite, 2-adjacent, 3- and 4- side exposure. The columns studied were assumed to be made of HSC. These columns were analyzed assuming a permeability of the order 10^{-18} and 10^{-19}. Thus 30 different scenarios were analyzed and the details are provided in Table 6.1.

Figure 6.16 shows the spalled area for columns CE24 and CE39. Both columns were exposed to ASTM E119 standard fire on all four sides. Column CE24 has a permeability of 10^{-18} while column CE39 has permeability of 10^{-19}. The progression of spalling with time as predicted by the numerical model is presented in Figure 6.17. It can be seen that spalling starts at 12 minutes for column CE39 since the permeability of this column is lower compared to CE24 where spalling starts after 28 minutes of dire exposure. The amount of concrete spalled after 30 minutes of fire exposure is 10% and 46% for columns CE24 and CE39 respectively.

In order to compare the behavior of RC columns of varying strengths, columns, CE0, CE24, and CE39 were compared. Figures 6.18 and 6.19 show the axial and lateral deformation plots for these three columns. It can be seen that as the permeability of concrete decreases, more spalling occurs in the column cross-section, thus increasing the slenderness of the column, which in turn leads to buckling and failure of the column. This is seen in the lesser expansion of the HSC columns (CE24 and CE39) as compared to NSC column CE0. It can be seen from Table 6.1 that fire resistance drops to 231 minutes from 253 minutes with reduction in permeability from the order of 10^{-17} (CE0) to 10^{-18} (CE24). The fire resistance further drops to 202 minutes when the permeability further decreases to the order of 10^{-19} (CE39). This can be attributed to fire-induced spalling occurring in the HSC columns. This not only reduces the cross-section of the column, but also considerably reduces the second moment of inertia about the neutral axis (due to loss of mass farther away from the axis) and thus leads to early failure of the column. Similarly reduction in fire resistance is observed for concentrically loaded, but exposed to fire on two adjacent faces, columns CE3, CE27, and CE42. This is due to the fact that the concentrically applied load does not remain concentric due to occurrence of uneven spalling. Since two adjacent sides of the columns are exposed to fire, thermal gradients develop which lead to spalling of concrete from the two exposed faces. It should be noted that, even though the column is subjected to biaxial bending, the loss of strength and stiffness in the column section is smaller due to slower rise in temperature as compared to 4-sides exposed to fire. Also the amount of spalling and thus the amount of concrete area lost is lesser as compared to 4-sides exposed to fire.

6.5 Summary

This chapter presents results of parametric studies to illustrate the influence of critical factors, specially related to biaxial bending effect and HSC, on the fire response of RC columns. The effect of load ratio, load eccentricity (uniaxial and biaxial), column size, different faces exposed to fire (1-, 2-, 3-, 4-side), fire scenario, and concrete strength (permeability) on fire response of concrete columns is quantified. Time-axial deformation and time-lateral deformation curves are presented for the analyzed columns along with the predicted fire resistance times. Resulkts indicate that these factors have significant influence on fire behavior of RC columns since they induce biaxial bending effects on the column under later stages of fire exposure. Load eccentricity has a significant influence of fire response of RC columns and the fire resistance reduces due to P-δ effects. Different exposure conditions affect fire resistance of RC columns with 2 adjacent sides of fire exposure being the worst case (least fire resistance) and 2 opposite sides exposure being the best case (highest fire resistance) scenario. The reduction in fire resistance due to increased load level is higher for columns subjected to biaxial bending than axially loaded columns. Increased column size leads to higher fire resistance. This increase is smaller when columns are subjected to biaxial bending. Fire resistance of HSC columns are highly affected by biaxial bending due to the occurrence of spalling. Thus these parameters must be duly accounted for in fire resistance design of RC columns. Results from these parametric studies are utilized in Chapter 7 to develop rational design approach for evaluating fire resistance of RC columns.

Table 6.1 Properties and results for RC columns used in the numerical study

Concrete	Column	Size (mm)	Fire Scenario‡	Fire Exposure	Applied Load (kN)	Eccentricity (mm)		Permeability	Fire resistance (mins)
						X	Y		
NSC	CE0	406	F1	4	1410	0	0	-17	253
	CE1	406	F1	3	1410	0	0	-17	226
	CE2	406	F1	2O†	1410	0	0	-17	281
	CE3	406	F1	2A†	1410	0	0	-17	177
	CE4	406	F1	1	1410	0	0	-17	240
	CE5	406	F1	4	1410	25	0	-17	221
	CE6	406	F1	4	1410	50	0	-17	198
	CE7	406	F1	4	1410	75	0	-17	165
	CE8	203	F1	4	400	0	0	-17	155
	CE9	203	F1	3	400	0	0	-17	145
	CE10	203	F1	2O†	400	0	0	-17	170
	CE11	203	F1	2A†	400	0	0	-17	136
	CE12	203	F1	1	400	0	0	-17	149
	CE13	203	F1	4	400	25	0	-17	138
	CE14	203	F1	4	400	50	0	-17	111
	CE15	203	F1	4	400	75	0	-17	85
	CE16	610	F1	4	3190	0	0	-17	297
	CE17	610	F1	3	3190	0	0	-17	216
	CE18	610	F1	2O†	3190	0	0	-17	329
	CE19	610	F1	2A†	3190	0	0	-17	220
	CE20	610	F1	1	3190	0	0	-17	259
	CE21	610	F1	4	3190	25	0	-17	260
	CE22	610	F1	4	3190	50	0	-17	224
	CE23	610	F1	4	3190	75	0	-17	188

Table 6.1 Contd. Properties and results for RC columns used in the numerical study

HSC	CE24	406	F1	4	1410	0	0	-18	231
	CE25	406	F1	3	1410	0	0	-18	188
	CE26	406	F1	2O†	1410	0	0	-18	250
	CE27	406	F1	2A†	1410	0	0	-18	164
	CE28	406	F1	1	1410	0	0	-18	203
	CE29	203	F1	4	400	0	0	-18	127
	CE30	203	F1	3	400	0	0	-18	121
	CE31	203	F1	2O†	400	0	0	-18	155
	CE32	203	F1	2A†	400	0	0	-18	107
	CE33	203	F1	1	400	0	0	-18	127
	CE34	610	F1	4	3190	0	0	-18	280
	CE35	610	F1	3	3190	0	0	-18	229
	CE36	610	F1	2O†	3190	0	0	-18	303
	CE37	610	F1	2A†	3190	0	0	-18	198
	CE38	610	F1	1	3190	0	0	-18	230
	CE39	406	F1	4	1410	0	0	-19	202
	CE40	406	F1	3	1410	0	0	-19	164
	CE41	406	F1	2O†	1410	0	0	-19	221
	CE42	406	F1	2A†	1410	0	0	-19	129
	CE43	406	F1	1	1410	0	0	-19	179
	CE44	203	F1	4	400	0	0	-19	89
	CE45	203	F1	3	400	0	0	-19	99
	CE46	203	F1	2O†	400	0	0	-19	130
	CE47	203	F1	2A†	400	0	0	-19	89
	CE48	203	F1	1	400	0	0	-19	101
	CE49	610	F1	4	3190	0	0	-19	261
	CE50	610	F1	3	3190	0	0	-19	195
	CE51	610	F1	2O†	3190	0	0	-19	271
	CE52	610	F1	2A†	3190	0	0	-19	163
	CE53	610	F1	1	3190	0	0	-19	205

Table 6.1 Contd. Properties and results for RC columns used in the numerical study

NSC	CE54	406	F1	4	1410	25	25	-17	208
	CE55	406	F1	4	1410	25	50	-17	183
	CE56	406	F1	4	1410	25	75	-17	141
	CE57	406	F1	4	1410	50	25	-17	180
	CE58	406	F1	4	1410	50	50	-17	148
	CE59	406	F1	4	1410	50	75	-17	104
	CE60	406	F2	4	1410	50	50	-17	98
	CE61	406	F3	4	1410	50	50	-17	155
	CE62	406	F4	4	1410	50	50	-17	NF*
	CE63	406	F5	4	1410	50	50	-17	NF*
	CE64	406	F1	4	940	50	50	-17	211
	CE65	406	F1	4	1175	50	50	-17	177
	CE66	406	F1	4	1645	50	50	-17	102
	CE67	406	F1	4	1880	50	50	-17	71

* NF – No Failure

† O – Opposite sides exposed to fire; A – Adjacent sides exposed to fire

‡ Refer to Figure 6.2 for explanation of fire scenarios

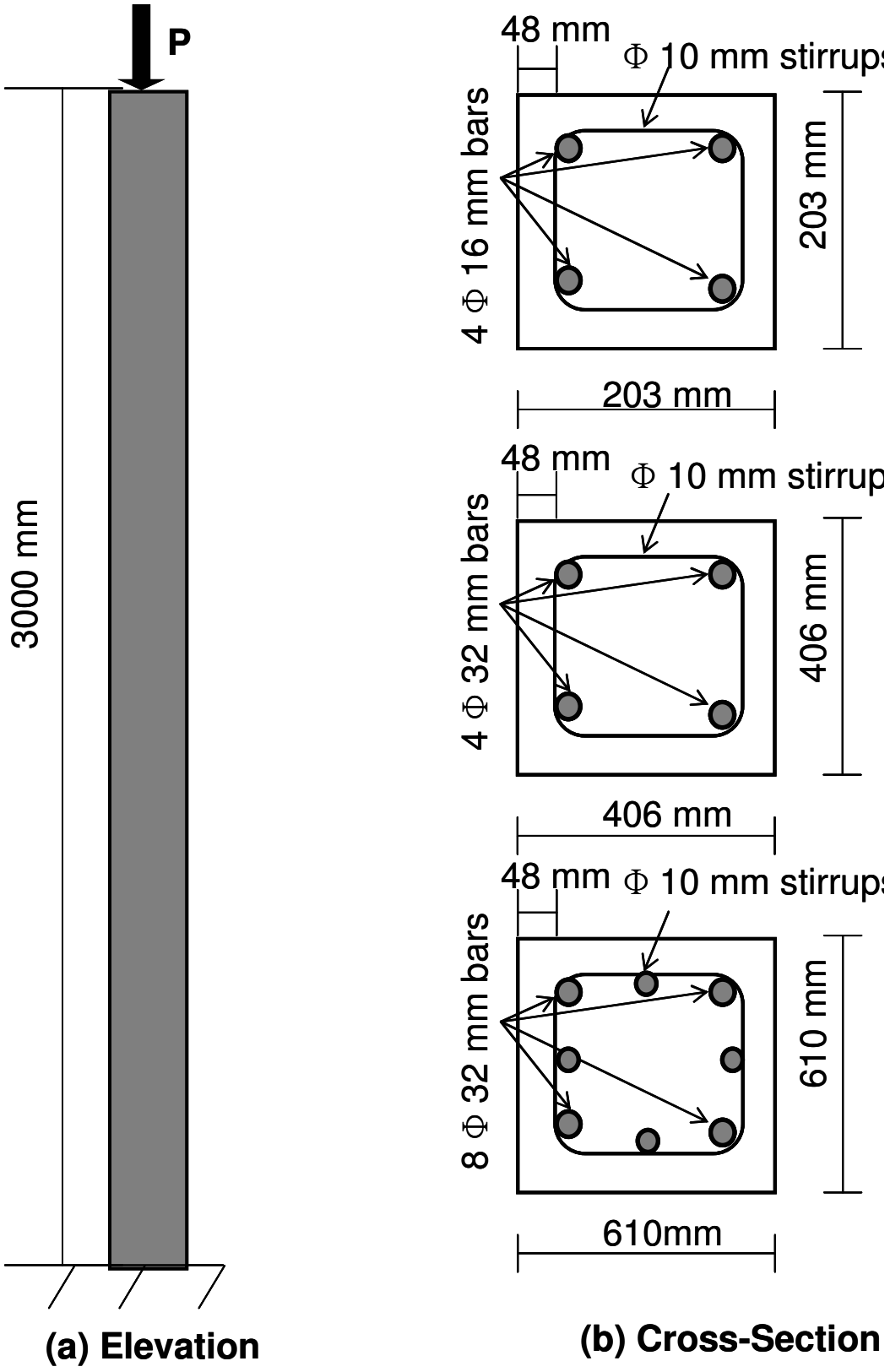

Fig. 6.1. Details of column analyzed in numerical studies.

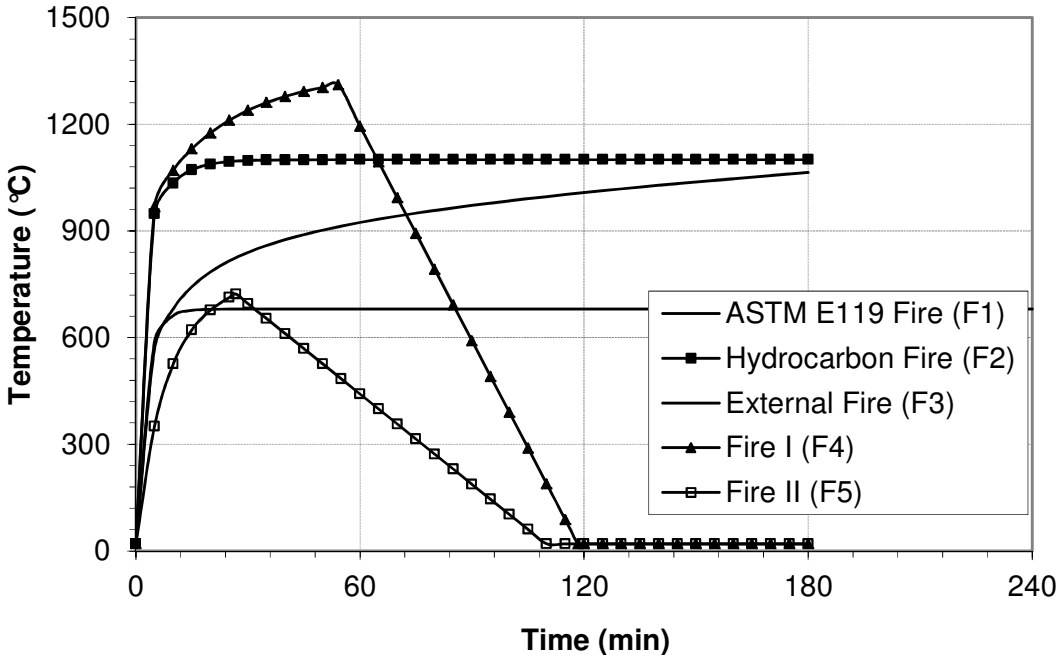

Fig. 6.2. Various Fire Scenarios used in the Analysis.

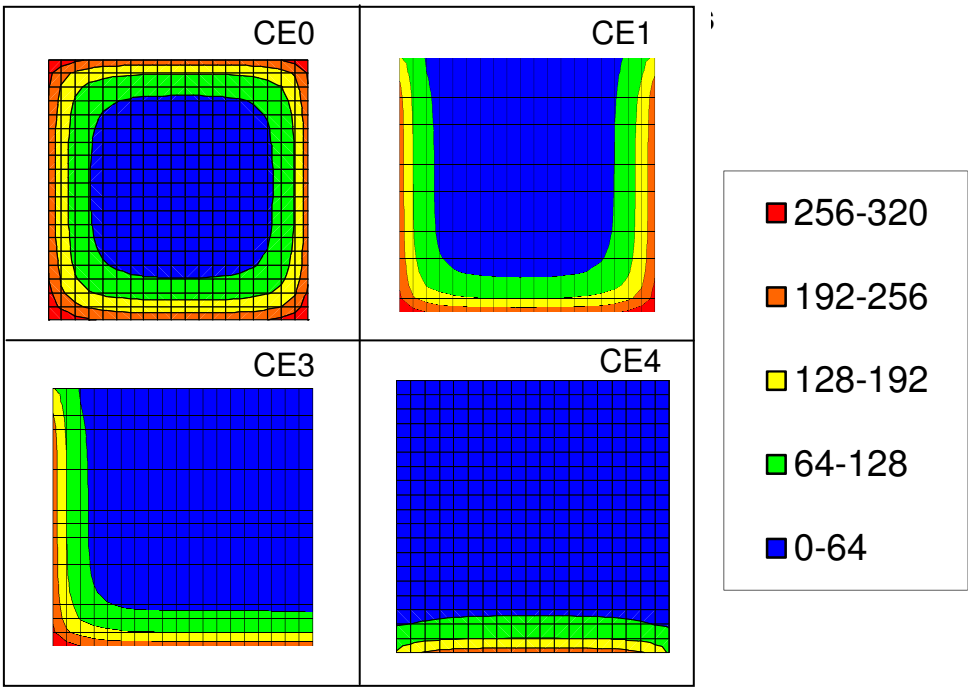

Fig. 6.3. Thermal gradients after 45 minutes in RC columns CE0, CE1, CE3 and CE4

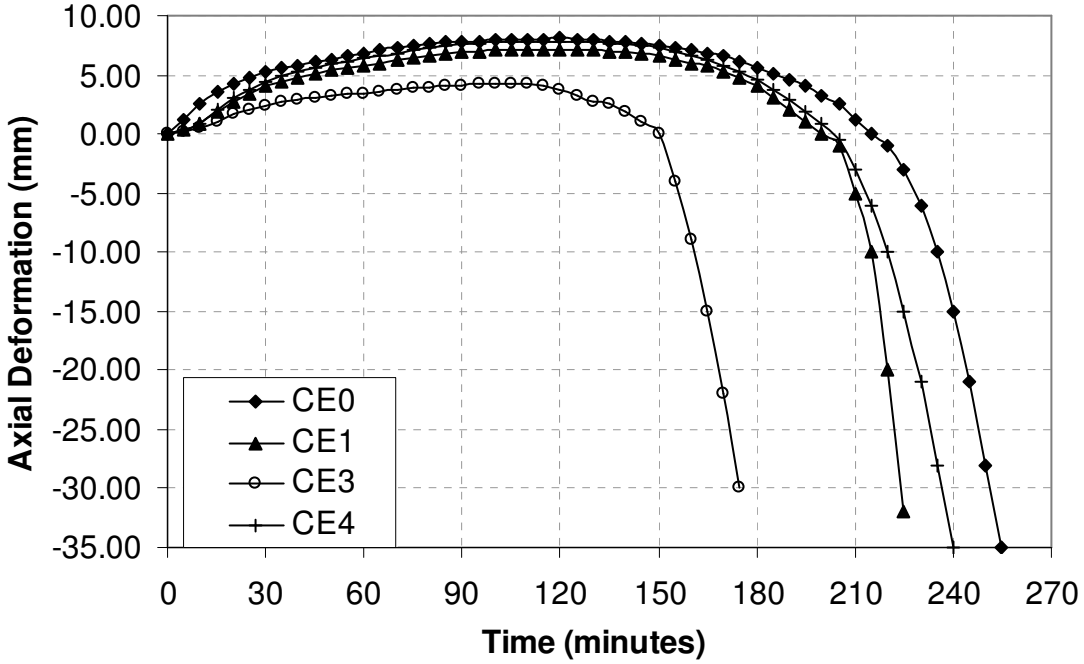

Fig. 6.4. Axial deformation of RC columns (CE0, CE1, CE3, & CE4) exposed to different face exposure

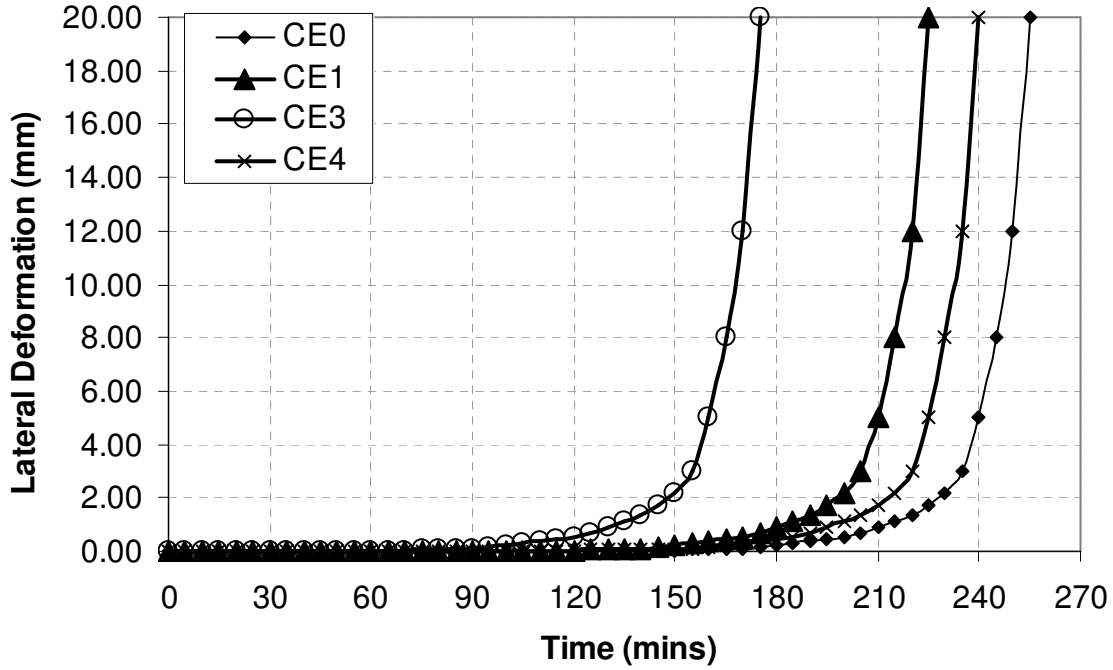

Fig. 6.5. Lateral deformation of RC columns (CE0, CE1, CE3, & CE4) exposed to different face exposure

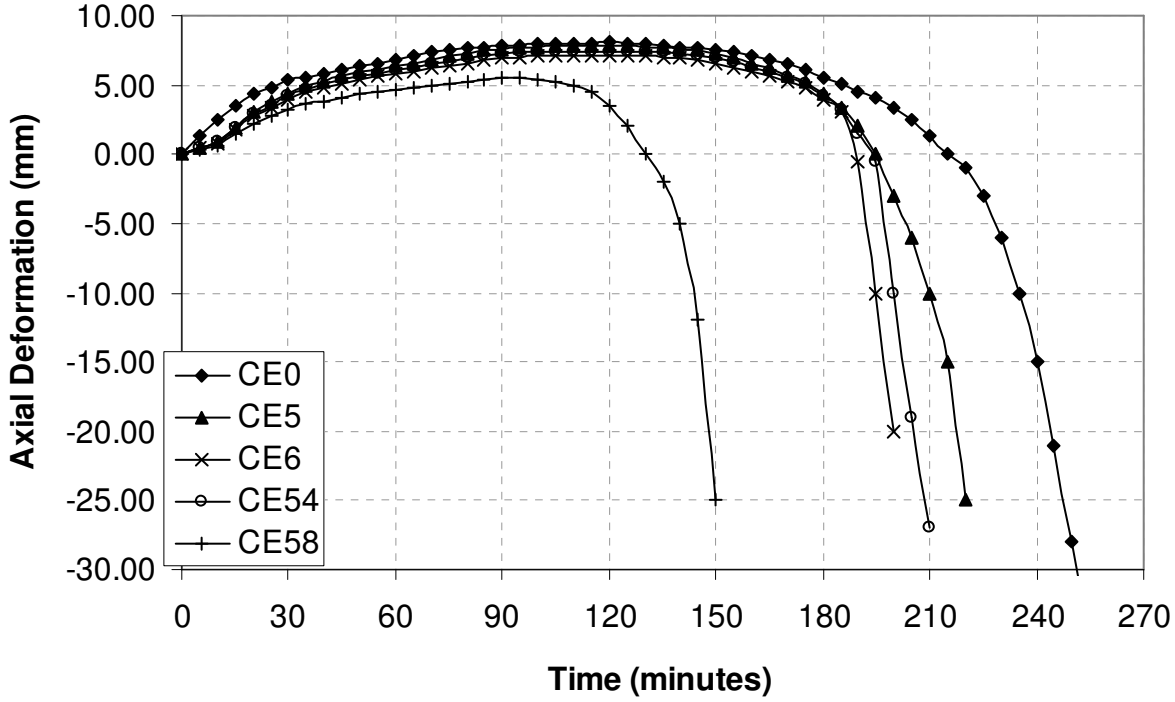

Fig. 6.6. Axial deformation of RC columns (CE0, CE5, CE6, CE54 & CE58) under different eccentric loadings

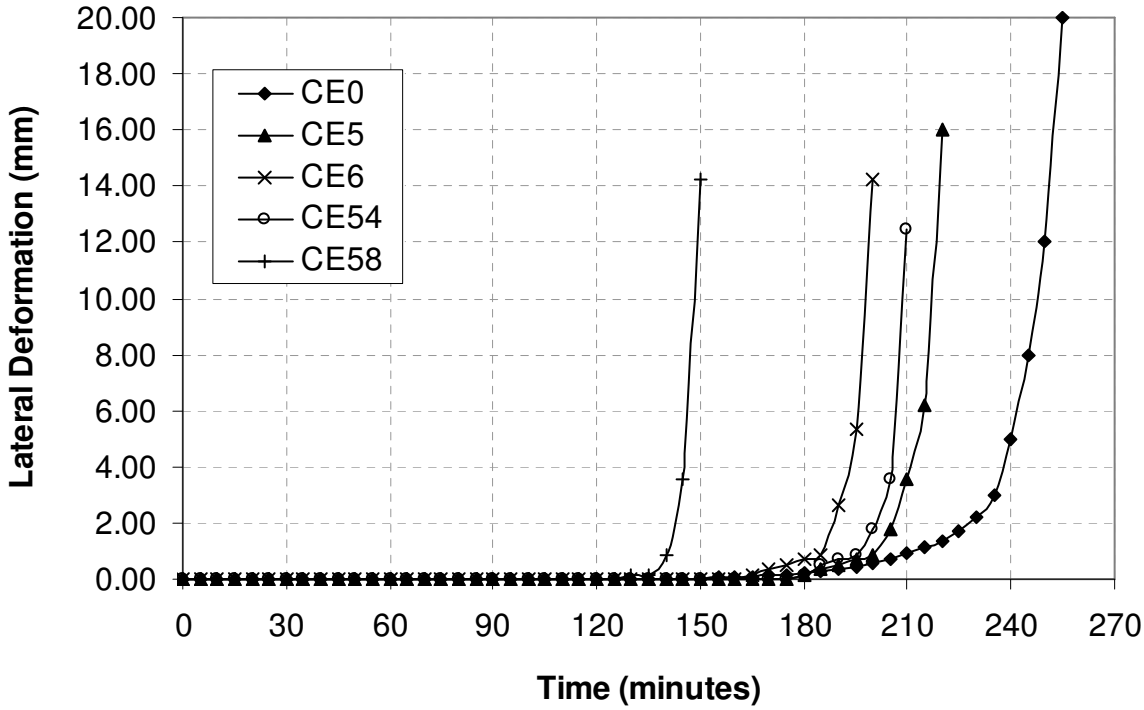

Fig. 6.7. Lateral deformation of RC columns (CE0, CE5, CE6, CE54 & CE58) under different eccentric loadings

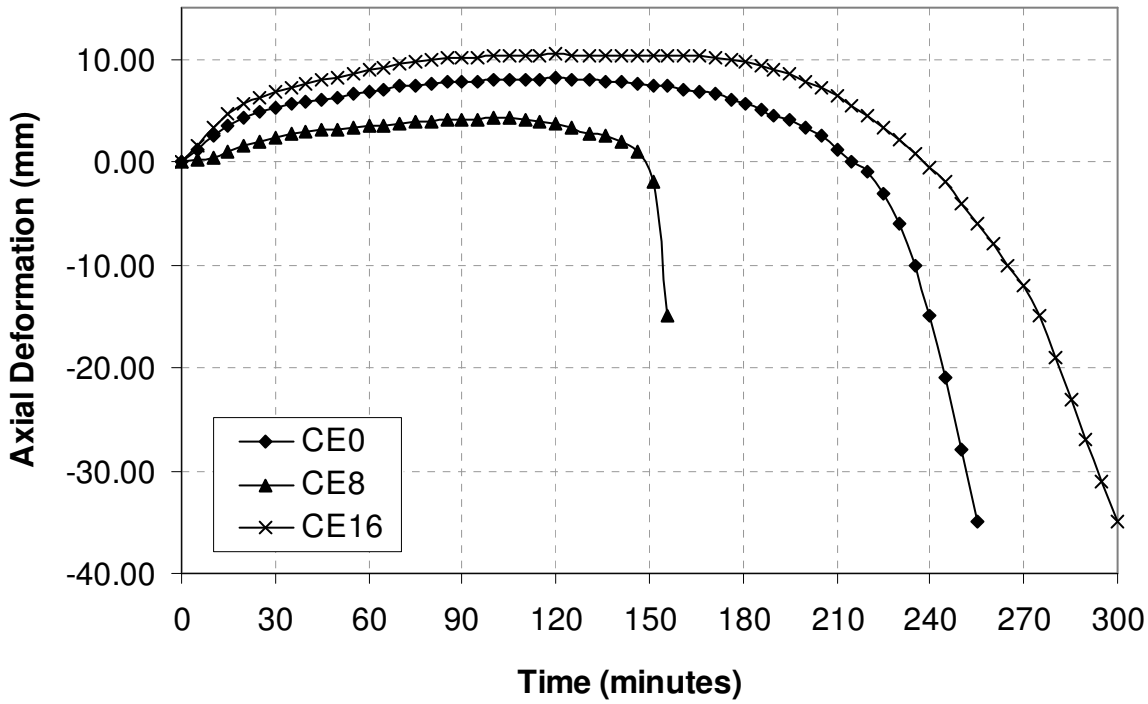

Fig. 6.8. Axial deformation of RC columns (CE0, CE8, and CE16) under different sizes

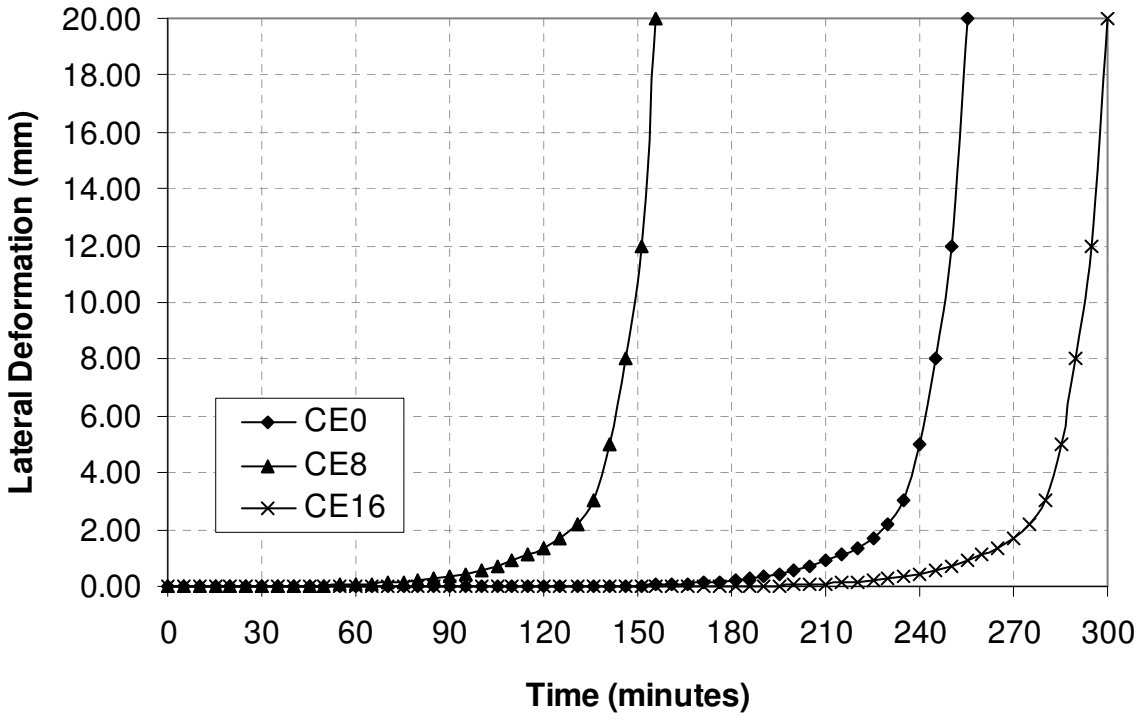

Fig. 6.9. Lateral deformation of RC columns (CE0, CE8, and CE16) under different sizes

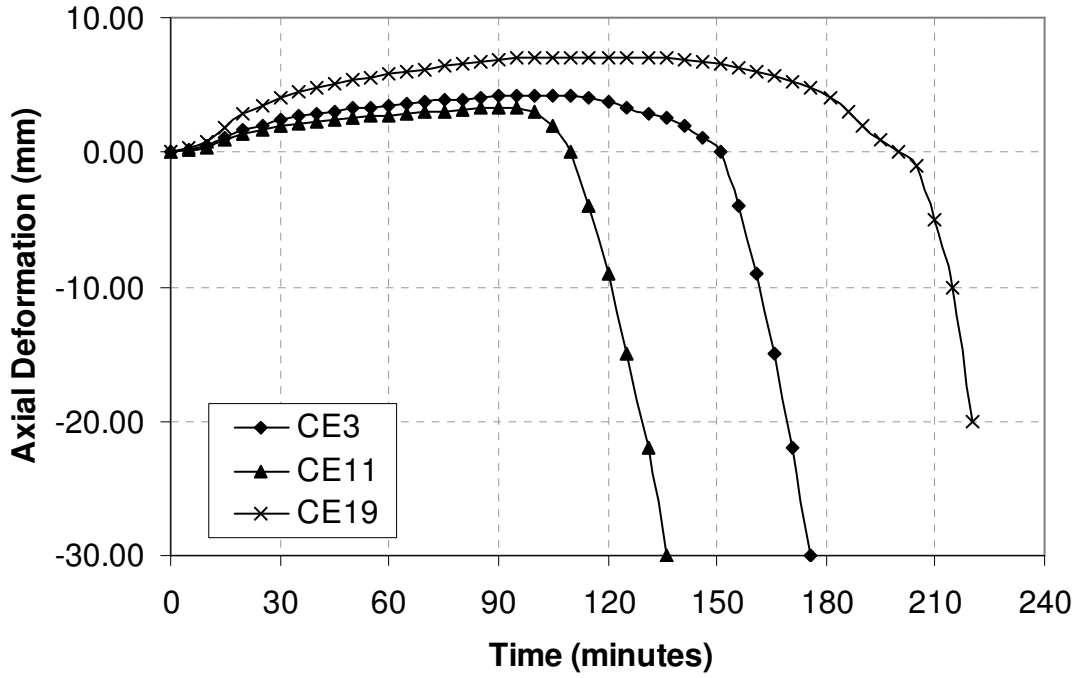

Fig. 6.10. Axial deformation of RC columns (CE3, CE11, and CE19) under different sizes

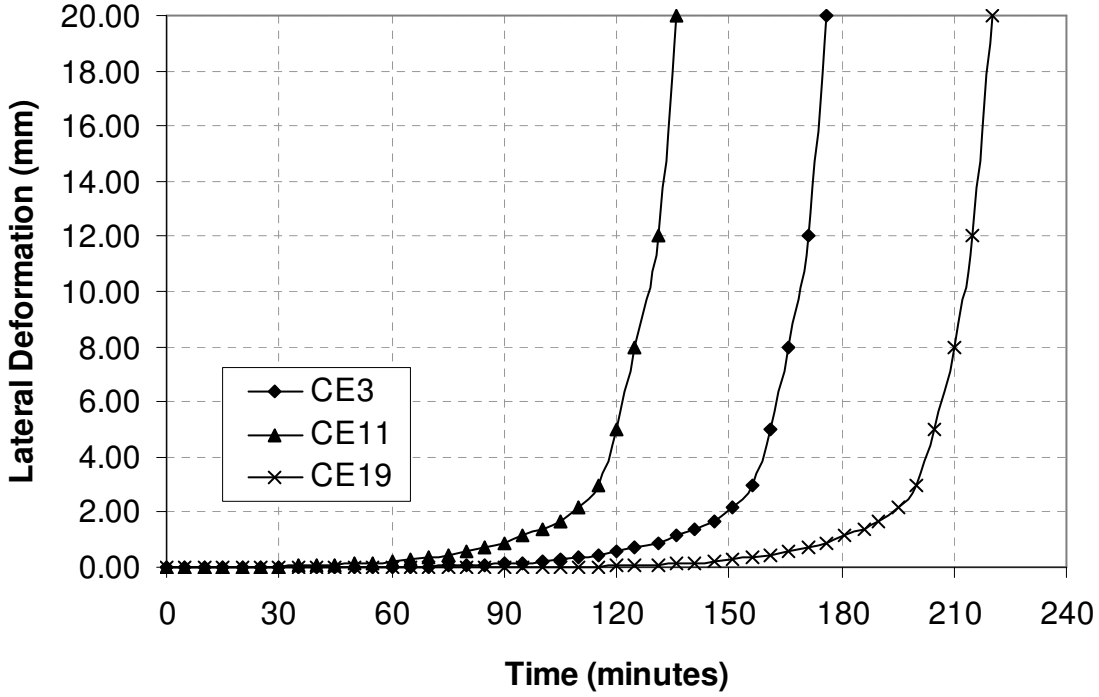

Fig. 6.11. Lateral deformation of RC columns (CE3, CE11, and CE19) under different sizes

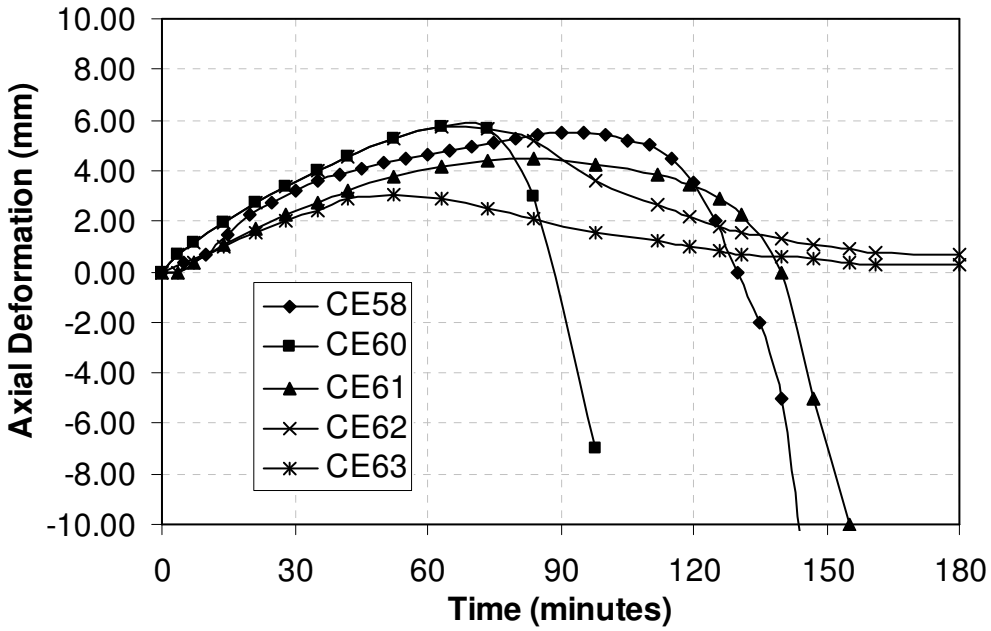

Fig. 6.12. Axial deformation of RC columns (CE58, CE60, CE61, CE63, and CE63) under different fire scenarios

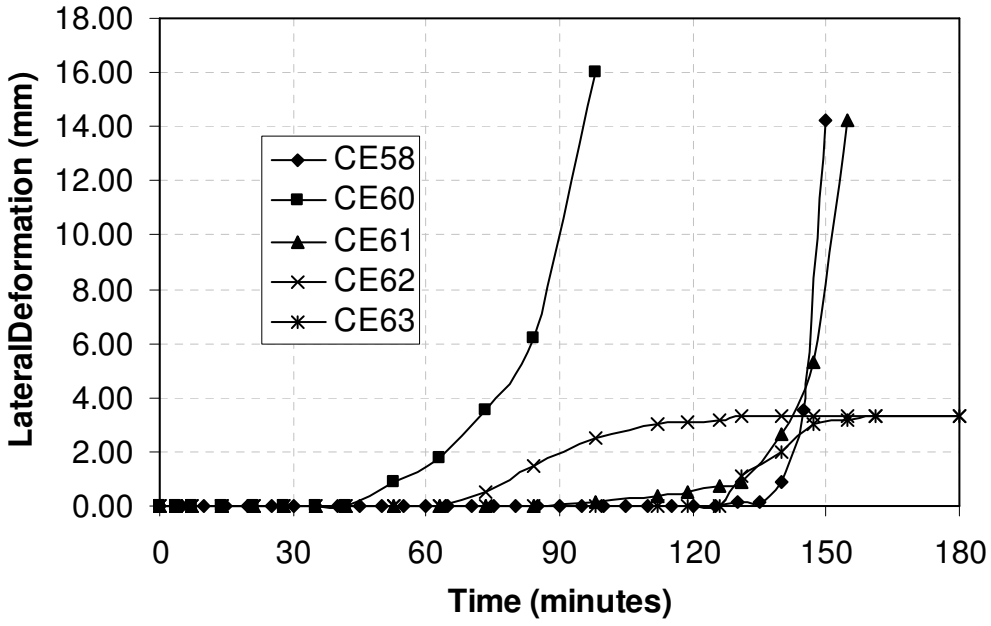

Fig. 6.13. Lateral deformation of RC columns (CE58, CE60, CE61, CE63, and CE63) under different fire scenarios

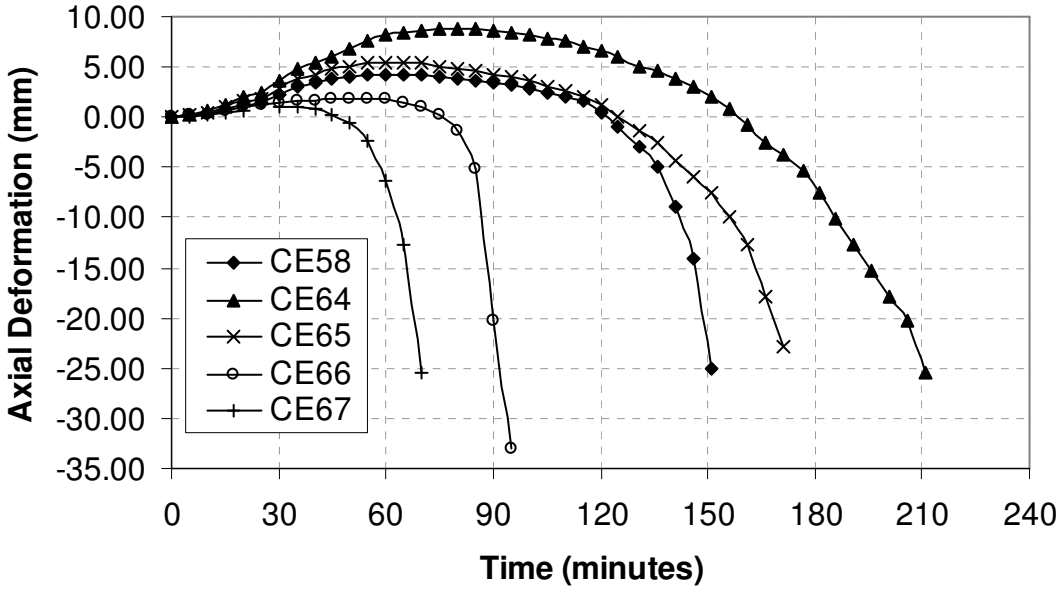

Fig. 6.14. Axial deformation of RC columns (CE58, CE64, CE65, CE66, and CE67) under different load levels

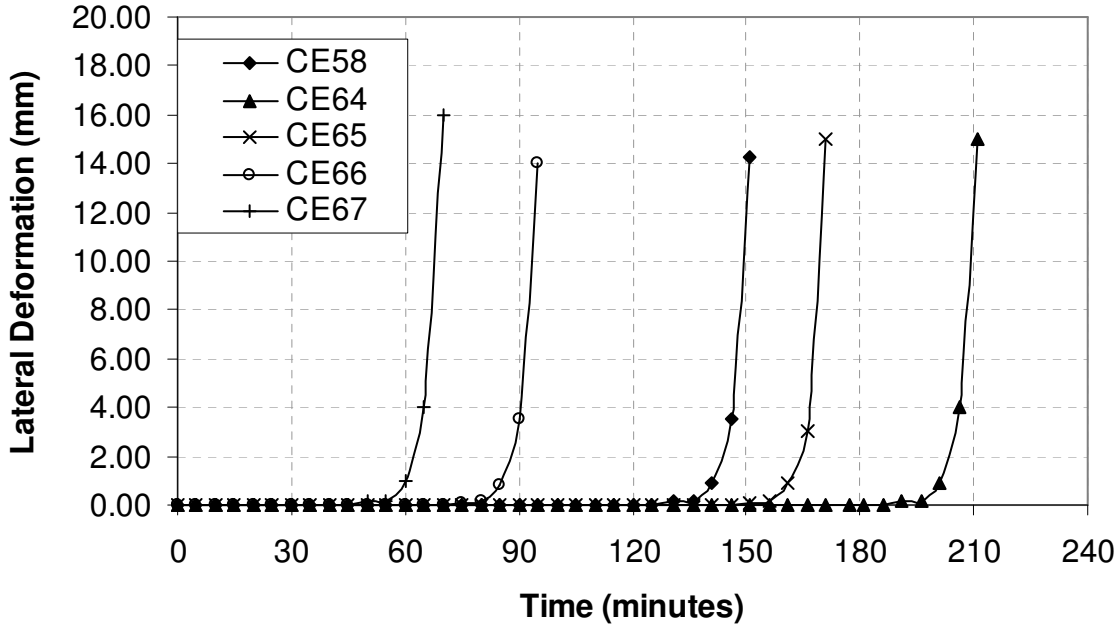

Fig. 6.15. Lateral deformation of RC columns (CE58, CE64, CE65, CE66, and CE67) under different load levels.

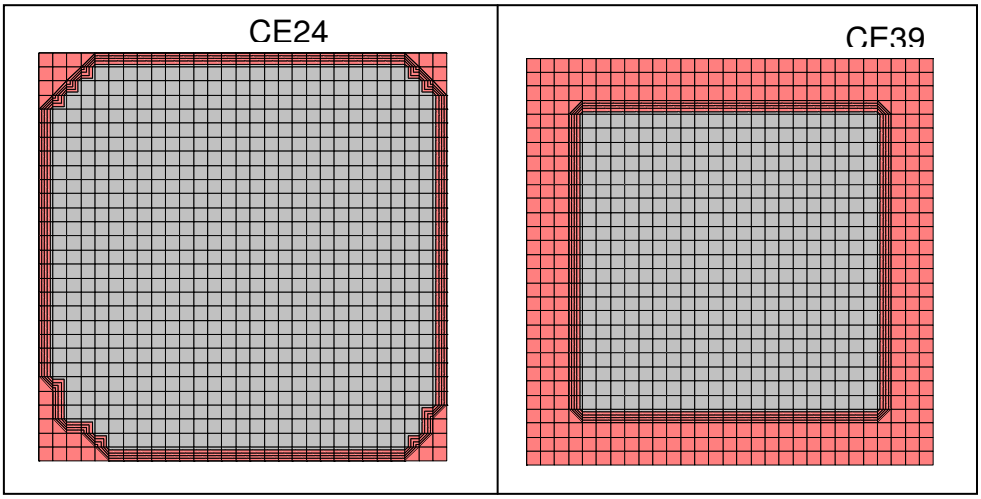

Fig. 6.16. Spalled area after 30 minutes for columns CE24 and CE39

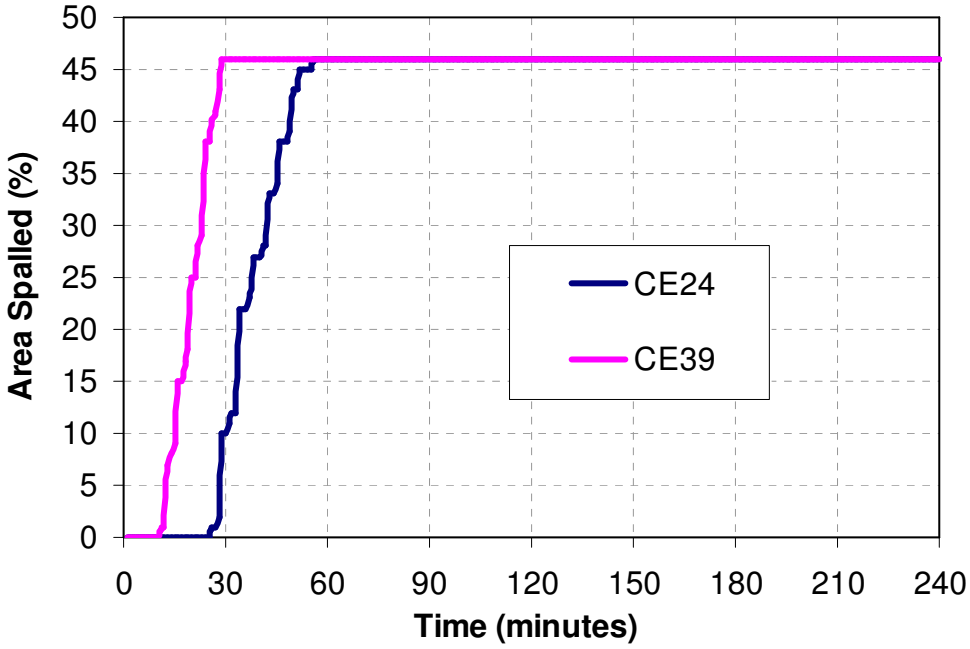

Fig. 6.17. Progression of spalling with time for columns CE24 and CE39

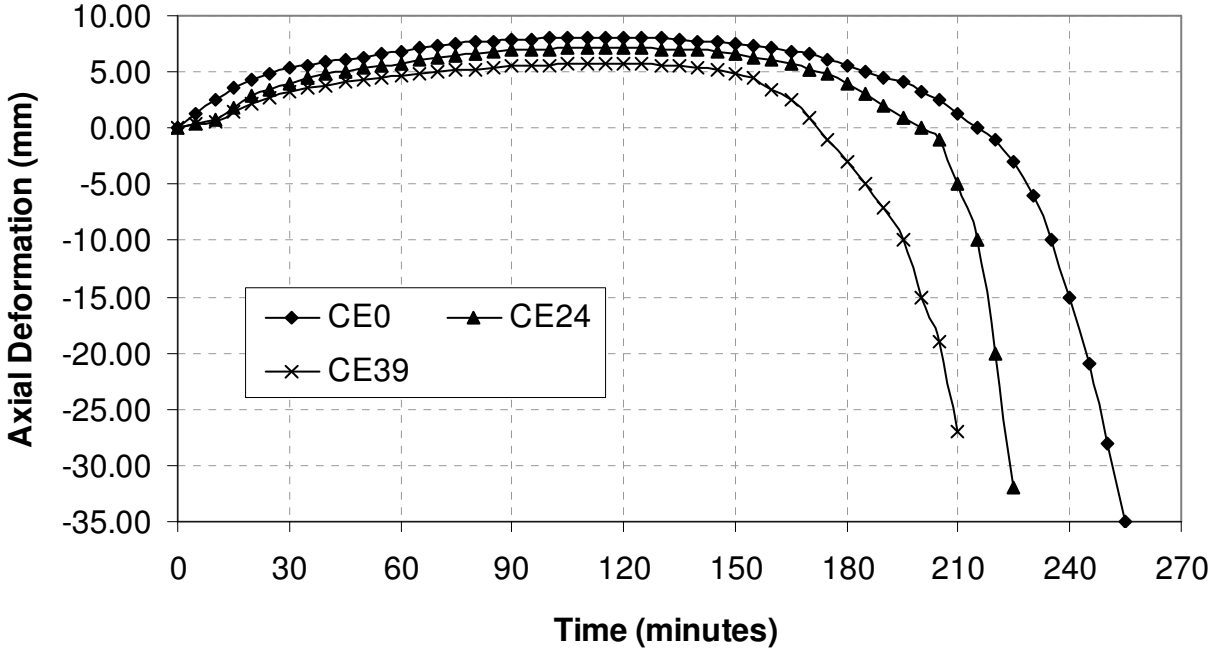

Fig. 6.18. Axial deformation of RC columns (CE0, CE24, and CE39) under different concrete types.

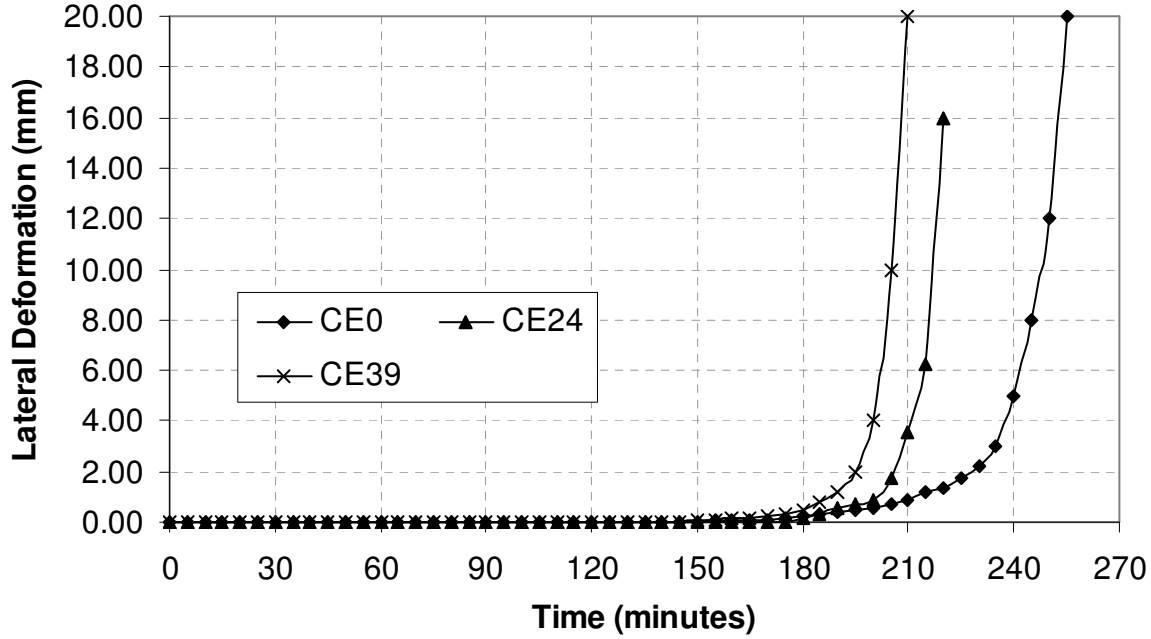

Fig. 6.19. Lateral deformation of RC columns (CE0, CE24, and CE39) under different concrete types.

CHAPTER 7

7 DESIGN GUIDELINES

This chapter is mainly based on the following journal papers:

- Kodur V. and Raut N., (2009) "Design Equation for Predicting Fire Resistance of Reinforced Concrete Columns", Structural Concrete, V. 10, No. 2, pp. 73-86.

7.1 General

There are major drawbacks in the current fire resistance provisions since critical factors such as load level, eccentricity (uniaxial and biaxial) of loading, spalling, 1-, 2-, 3- sided exposure, and realistic fire scenario are not taken into consideration in evaluating fire resistance of RC columns. To overcome these drawbacks, a rational approach for predicting the fire resistance of RC columns is developed in this chapter. The proposed approach comprises of two steps, namely; an empirical equation for evaluating fire resistance of an RC column under a standard fire exposure and then establishing time equivalency between standard and design fire exposure. Data generated from parametric studies and fire resistance experiments, as well as those reported in literature, is utilized to develop this rational design methodology for evaluating fire resistance of RC columns. The validity of the proposed approach is established by comparing the fire resistance predictions with those obtained from detailed numerical studies and fire resistance tests.

7.2 Critical Factors Influencing Fire Resistance

There have been numerous fire tests and few numerical studies for evaluating fire resistance of reinforced concrete columns exposed to "standard fire" as discussed in Chapter 2. Data from published tests and numerical studies was utilized to quantify the effect of parameters such as cross sectional size, cover thickness, reinforcement ratio, aggregate type, load, and load eccentricity on fire resistance and is presented in Table 7.1. The parametric studies, presented in Chapter 6 and Table 6.1, quantified the effect of parameters such as concrete strength, different face exposure, and eccentric loading which were not studied in the experimental studies presented in Table 7.1.

All these parameters are not independent and thus their influence is interrelated. Hence, statistical software was used to obtain the variation of fire resistance with respect to these parameters. A multivariate regression analysis was carried out to establish the best fit of the multi-dimensional surface with respect to the data and the significant parameters. The influence of different factors on fire resistance is discussed below. Figures 7.1 to 7.12 present this fitted curve for different parameters under consideration.

7.2.1 Effect of Load Ratio

It is well established that increased load on a column leads to lesser fire resistance. Figure 7.1 shows the reduction in fire resistance as a function of load ratio (defined as the ratio of axial load acting on the column to the load-carrying capacity of the column at room temperature). Load ratio is a better measure for evaluating fire resistance than the applied load acting on the column, as the load ratio represents the extent to which the column is stressed. The capacity of an RC column can be calculated as per ACI 318 specifications and assuming that the column is not slender. The column is assumed to be non-slender for calculation purposes, in order to facilitate better comparison of the actually applied load. Thus, load ratio can be determined as:

$$L_R = \frac{P}{P_{cap}} \quad [7.1]$$

In which:

L_R = load ratio, P = axial load acting on the column, and P_{cap} = axial load carrying capacity of the column computed as per ACI provisions and is given by:

$$P_{cap} = 0.8\left(0.85 A_c \cdot f_c' + A_s \cdot f_y\right) \quad [7.2]$$

where:

A_c = area of concrete, f'_c = characteristic strength of concrete, A_s = area of steel, and f_y = yield strength of steel.

In Figure 7.1, the fire resistance of an RC column is shown as a function of load ratio for three selected slenderness ratios. It can be seen that the load ratio has a significant influence on the fire resistance of the column. Also, the rate of decrease in fire resistance is predominant for increased slenderness ratio of the column. This trend indicates that load ratio and slenderness ratio are interrelated and have significant influence on fire resistance of RC columns.

7.2.2 Effect of Slenderness Ratio

It can be seen from the data in Tables 7.1 and 6.1, that the geometric properties, mainly cross sectional dimensions, length, and support conditions, play a significant role in determining the fire resistance of RC columns. This could be attributed to the fact that buckling becomes a prominent factor with deteriorating stiffness that results with increased fire duration. These factors can be expressed in terms of slenderness ratio (SR) which can be defined as:

$$S_R = \frac{L_e}{r} \quad [7.3]$$

where:

L_e = effective length of the column (depends on support conditions) and r = radius of gyration of the column

The influence of slenderness ratio on the fire resistance of RC columns is shown in Figure 7.2 for three different load ratios. As slenderness increases, the fire resistance of the column decreases due to decreased resistance to buckling. The decreased resistance to buckling can be attributed to the fact that higher slenderness is an indicative of lower flexural stiffness $\left(\frac{EI}{L}\right)$. Thus slenderness ratio has significant influence on fire resistance of RC columns.

7.2.3 Effect of Cover Thickness

The effect of concrete cover on fire resistance of RC members is well established and has been recognized in most codes and standards. This is attributed to the fact that, concrete cover has direct influence on the temperature rise in rebar which in turn dictates the load carrying capacity of the column. Generally, reinforcing steel loses nearly 50% of its strength at about 550°C. Thus, fire resistance increases with cover thickness since increased cover thickness delays the temperature rise in the reinforcing steel, which in turn slows the loss load carrying capacity of the RC column. The influence of cover thickness on fire resistance of RC columns for different load ratios is shown in Figure 7.3. It can be seen that the fire resistance increases linearly with cover thickness for different load ratios. The effect is slightly more significant for lower load ratios. Overall cover thickness has moderate influence on fire resistance of RC columns.

7.2.4 Effect of Reinforcement Ratio

The effect of reinforcement ratio on fire resistance is illustrated in Figure 7.4 where the fire resistance of RC columns is plotted as a function of reinforcement ratio for different load ratios.

It can be seen that an increase in reinforcement ratio leads to lower fire resistance in RC columns. This can be attributed to the fact that for the same cross sectional area of column there is more steel present whose properties deteriorate fast with temperature. Steel loses its strength with the rise in its temperature at a faster rate than concrete. This leads to reduction in fire resistance of the RC columns. Overall, the reinforcement ratio has a moderate influence on fire resistance of RC columns.

7.2.5 Effect of Aggregate Type

A review of fire test data indicates that the aggregate type has moderate influence on fire resistance of RC columns. Of the two commonly used aggregates, carbonate aggregate (predominantly consisting of limestone) provides higher fire resistance than the siliceous aggregate (predominantly consisting of quartz) [Kodur, 2003]. This is mainly due to enhanced heat capacity of carbonate aggregate concrete in the 600-800°C temperature range as a result of an endothermic reaction which occurs due to dissociation of dolomite in carbonate aggregate. The heat capacity of carbonate aggregate concrete in this temperature range is 10 times higher than that of siliceous aggregate concrete, as seen in Figure 2.3 [Kodur, 2003]. The thermal conductivity of carbonate aggregate also partially contributes in enhanced fire resistance. Thus, carbonate aggregate concrete columns provides about 10% higher fire resistance than columns made with siliceous aggregate concrete.

7.2.6 Effect of Load Eccentricity

Data from limited fire tests and parametric studies indicate that eccentric loads can have significant influence on fire resistance of RC columns. The effect of load eccentricity on fire resistance is illustrated in Figure 7.5 where the fire resistance of RC columns is plotted as a function of load eccentricity ratio (defined as ratio of load eccentricity to column width) for

different load ratios. The fire resistance decreases with increased load eccentricity. This is mainly due to the fact that an eccentric load introduces an additional moment on the column. This leads to buckling of the column which produces significant lateral deflections. The effect of eccentricity can be significant under fire conditions due to reduced stiffness of the column. With the reduction in column strength the lateral deflection increases subjecting the column to additional moments due to p-δ effects, which in turn produces more deflections. Overall, buckling induces additional stresses in the column and results into earlier failure. Also it can be seen that the rate of decrease in fire resistance is more prominent for higher slenderness ratio.

This reduction in fire resistance is amplified even more when the load is eccentric about both the axes. Figure 7.6 shows the plot for reduction in fire resistance due to increase in load eccentricity in second axis with a constant eccentricity along first axis. It can be seen that the fire resistance decreases quadratically with increase in the eccentricity along the second axes. Thus it can be said that biaxial eccentricity has high influence on fire resistance of RC columns.

7.2.7 Effect of Number of Sides of Fire Exposure

The fire resistance of the different sized (203, 406, and 610mm) columns under 1-, 2-, or 3- side exposure is also shown in Figure 7.7. As discussed above the fire resistance of RC columns reduces when exposed to 1- or 3- side exposure due to the development of thermal gradients along one axis and reduces even further when exposed to fire on 2-adjacent sides due to the development asymmetric thermal gradients along both axes. However the fire resistance increases when the column is exposed to fire on 2- opposite sides, since in this case the thermal gradients remain symmetric along both axes but the rise in temperature across the cross-section is slower due to only 2 faces being exposed. Figure 7.7 also shows the variation of fire resistance of the three sizes of columns (203, 406, and 610mm) under increasing eccentricity of load. This

is helpful in comparing the effects of various exposure conditions. For example, in case of a column of size 406 mm i-side or 3-side exposure will create conditions equivalent to a column exposed to fire on 4-sides but with a load eccentricity of 25 mm. While, a 2-adjacent side exposed column would has fire resistance equivalent to an eccentricity of 50mm.

7.2.8 Effect of Concrete Strength

Results from fire tests indicate that concrete strength (within the range of normal strength concrete) has moderate influence on the fire resistance of RC columns. However, for higher strengths of concrete (greater than 70 MPA), the influence of concrete strength on fire resistance can be significant due to the occurrence of spalling, and faster degradation of strength with temperature. Recorded observations from various fire test programs have indicated that spalling is not a major concern in normal strength concrete (NSC) columns, and so the effect of spalling is not generally taken into account. The effect of concrete strength on fire resistance can be reflected through the use of load ratio as the actual load carrying capacity of the column depends on concrete strength.

The concrete strength can be related to the permeability of concrete, with higher strength corresponding to lower permeability. The variation of fire resistance with permeability for the three different column sizes, when all four sides are exposed to fire is plotted in Figure 7.8. It can be seen that the fire resistance decreases with the decrease in permeability. This is as expected since the reduction of permeability leads to higher spalling and thus lower load carrying capacity. Figures 7.9-7.12 show similar plots for 1-, 2 adjacent, 2 opposite, and 3- side exposure conditions. The decrease in fire resistance with the decrease in permeability follows a trend, similar to 4- side exposure, for the other fire exposures.

7.2.9 Summary

The above discussion clearly shows that load ratio, slenderness ratio, face exposure, concrete strength (permeability) and load eccentricity have a significant influence on fire resistance of RC columns. Factors such as concrete cover, percentage of reinforcing steel, and aggregate type have moderate influence on the fire resistance of RC columns. Results from the parametric studies are utilized in the following section to develop an approach for evaluating fire resistance of RC columns.

7.3 Methodology for Evaluating Fire Resistance

An empirical equation, which accounts for the above discussed significant parameters, is developed for predicting the fire resistance of RC columns. For developing such an equation, results of experimental studies taken from literature (Table 7.1) and parametric studies presented in Chapter 6 (Table 6.1) are utilized. Details on the development of the empirical equation are presented in the following sections. The approach is developed in two steps; first evaluating the fire resistance of RC columns exposed to standard fire scenario, and then accounting for design fire scenarios.

Contrary to the current prescriptive approaches, the goal of the proposed method is not to determine the fire resistance of an RC column under design fire exposure, but to determine if an RC column can survive in a design fire scenario [Dwaikat, 2009; Fike, 2010]. In general, the design approach involves two steps, namely:

- Evaluating the fire resistance of the RC column (R) under standard fire exposures, using a simplified equation,

- Determining the area under the design fire and standard fire time-temperature curves up to failure in standard fire (i.e. R min), and then checking failure of the columns (under a design fire exposure) which is said to occur when:

$$A_D > A_S \quad \Rightarrow \quad \text{Failure} \qquad [7.4]$$

where:

A_S = Area under standard fire time-temperature curve up to failure (i.e. R min)

A_D = Area under design fire time-temperature curve up to failure (i.e. R min)

The proposed approach is developed by giving full consideration to critical parameters, (key parameters for performance-based fire safety design as discussed in Chapter 2), that influence the fire resistance of RC columns. In the second step fire scenario is accounted for in evaluating the time equivalent.

7.4 Fire Resistance Equation for Standard Fire Conditions

7.4.1 General

In the proposed approach, the first step is to evaluate the fire resistance of an RC column under standard fire exposure. Based on the relationship between the fire resistance and the parameters discussed in Section 7.2, an equation was developed such that its predictions had minimal variation from the measured test values [Kodur and Raut, 2009]. The expression was developed through curve fitting technique by fitting a polynomial curve to data which incorporates all the significant parameters. Statistical software was used to find a polynomial that accurately fit the data. For better prediction of fire resistance the proposed equation has to account for critical parameters. This is achieved by giving due consideration to these critical parameters through coefficients. These coefficients are arrived at as explained in following sections.

7.4.2 Accounting for Different Face Exposures

In order to account for different face exposures, in rectangular columns, the change of fire resistance due to different exposure conditions can be expressed in terms of a fictitious eccentricity referred to as equivalent eccentricity (see Figure 7.7). Thus the reduction in fire resistance (for 1- 2-adjacent and 3- side exposure) can be considered to be resulting from an eccentrically applied load. The reduction in fire resistance with the increase in load eccentricity, for different column sizes under 4-side exposure is shown in Figure 7.7. The fire resistance obtained for these column sizes under axial load and 1-, 2-, 3- side exposure is superposed on the above plots in Figure 7.7. Thus, the equivalent eccentricity for a particular case (e.g. 1- side exposure) for the each of the column sizes can be calculated. An equation can be fit using regression analysis in order to predict their trend. It should be noted that since the exposure condition of 2-opposite faces exposed increases the fire resistance. The equivalent eccentricity for this case was calculated by extrapolating on the negative side and calculating a fictitious negative equivalent eccentricity (see Figure 7.7).

Figure 7.13 shows the variation of equivalent eccentricities with increase in column size. Four different plots are shown for 1-, 2 opposite- 2 adjacent- and 3- side exposure. Trend lines are fitted in order to predict the equivalent eccentricity for a particular size of the column under different exposure conditions. In order to incorporate the effect of different side exposure, Eq (2) can be modified by changing the parameter E_c to be the sum of the applied load eccentricity E_{ap} and the equivalent eccentricity E_{eq} arising from 1-, 2-, 3-side fire exposure or spalling.

7.4.3 Accounting for Concrete Strength (Permeability)

As seen from the Figures 7.8-7.12 it can be assumed that the fire resistance decreases linearly with decrease in the order of permeability. That means fire resistance reduces exponentially with the reduction in permeability. Thus an exponential function has been arrived at for computing the spalling factor for the simplified equation. Since the rate of decrease is pretty similar for all the exposure conditions, only the amplitude of the exponential equation was modified to incorporate the effect of different exposure conditions. And this is merged with the coefficient which accounts for different face exposure in the equivalent eccentricity calculations. The details of the equation are provided later in this section.

7.4.4 Accounting for Eccentric Loading

Figure 7.6 shows that the fire resistance decreases quadratically with increase in the eccentricity along the second axes. In order to account for this the calculation of the coefficient kec in Eq. 2 is modified to account for eccentricity (Ed2) induced due to fire induced biaxial bending. This way the effect of biaxial bending can be accounted in the simplified equation.

7.4.5 Proposed Fire Resistance Equation

Based on the results generated from parametric studies presented and statistically fitted curves, the following equation was develop for evaluating fire resistance of RC columns:

$$R = C_t \left[8 \times k_{sh} \times k_{cp} \times \left(30 - \left(S_R + 5\right) \times \left(L_R - 0.2\right)\right)\right]^{0.94} \qquad [7.5]$$

where:

R = fire resistance in minutes, S_R = slenderness ratio of the column, L_R = load ratio of the column

C_t = a constant based on aggregate type used in concrete

C_t = 1.0 for siliceous aggregate concrete

C_t = 1.1 for carbonate aggregate concrete

k_{cp} = a constant based on the cover thickness and the percentage steel and is given by:

$$k_{cp} = \frac{[(C_e - 82) \times (S_P + 10.5) + 870]}{390} \quad [7.6]$$

where:

C_e = effective concrete cover thickness (mm), S_p = percentage of steel in column,

k_{sh} = a constant based on the shape of the column

$$k_{sh} = k_{ec} \times k_{sp} \quad [7.7]$$

k_{ec} = a constant based on the load eccentricity, load ratio and slenderness ratio

k_{sp} = a constant to account for spalling

These are given by:

$k_{ec} = 1$, when Ec = 0 (concentric loads),

Else,

$$k_{ec} = \frac{[(S_R - 243) \times (Ec - 768) - 83250]}{99880} \times k_{e2} \quad [7.8]$$

where:

$k_{e2} = 1$, when E_{c2} = 0 (no eccentricity along Y axis) or when circular column,

$$k_{e2} = \left[\frac{[(7600 + E_{d2}) \times (Ec + 550) + 870]}{3600000}\right]^{-1}$$, otherwise [7.9]

Ec = Total eccentricity and is given by:

$$Ec = E_{ap} + E_{eq}$$ [7.10]

where: E_{ap} = applied eccentricity along X axis

E_{eq} = Equivalent eccentricity arising from 1-, 2-, 3-side exposure

$E_{eq} = 0$, for circular cross section

$$E_{eq} = -\frac{d^2 + 930d - 73000}{3000}$$, when 2-adjacent sides exposed

$$E_{eq} = -\frac{d^2 + 1000d - 115000}{5000}$$, when 3- sides exposed

$$E_{eq} = -\frac{d^2 + 900d - 120000}{5000}$$, when 1- side exposed

$E_{eq} = -17$, when 2-opposite sides exposed

where: *d* is the size of the column in mm

And:

$k_{sp} =$ 1, when perm ≥ 10^{-17} m^2

$k_{sp} =$ 1, when perm < 10^{-17} m^2, but polypropylene fibers (1%-2% by volume) present in concrete mix.

$$k_{sp} = \frac{[log(perm) + 20]}{2.75}$$; for rectangular columns when perm < 10^{-17} m^2

$$k_{sp} = \frac{[log(perm) + 25]}{2.5}$$; for circular columns when perm < 10^{-17} m^2

where: perm = intrinsic permeability of concrete (m^2),

The equation was developed using the test and numerical data on columns subjected to ISO 834 or ASTM E119 fire exposure. Since the time temperature profile of both these standard fires is similar the equation can be used for either of the two fire exposures.

7.5 Fire Resistance under Design Fire Exposure

The expression presented above is valid for standard fire exposure only. However in reality, the columns will be exposed to fire scenarios with a cooling phase which can have significant influence on fire performance. To account for this the proposed methodology is extended to cover design fire scenarios by establishing time equivalency between standard and design fire scenarios and is based on equivalent area under the fire curve (time-temperature curve) concept. The equal are concept describes two fires to have the same fire severity if the area under the time-temperature curve is the same for both fires. Since RC column will either fail in less time in a design fire than in standard fire, or will survive complete compartment burnout, only the severity of the fire up to the time of column failure under standard fire exposure needs to be compared. It should however be pointed out that determining the time of failure for the column in a design fire is not the objective, it is rather to determine if the column will fail in the design fire or withstand complete compartment burnout.

The proposed approach can be applied to establish equivalency (survival of a column) between a standard and design fire. As a first step, the fire resistance of the RC column under standard fire

is evaluated using Eq. 7.2. To determine if the column will fail in a design fire, the area under both the standard and the design fire time temperature curves is determined at the time the column fails in the standard fire. If the area under the standard fire curve is greater than the area under the design fire curve, the column will not fail in the design fire, that is to say the column will survive complete compartment burnout. If however, the area under the standard fire curve is less than that under the design fire curve, the column will fail in the design fire. Most notably, in the latter case, the column will fail in less time in the design fire than in the standard fire.

The application of this approach is illustrated in Fig. 7.14 which shows the time temperature curves corresponding to the standard (ASTM E-119) and a design fire exposure. Knowing the basic details of the column, the fire resistance of the column under standard fire exposure can be estimated by applying Eq. 2. Once both the design fire and the failure time of the column under standard fire exposure are known, the area under the standard fire time temperature curve (Area A in Fig. 7.14) and the area under the design fire time temperature curve (Area B in Fig. 7.14) can be determined at the time of column failure under standard fire exposure. If the area under the standard fire curve (Area A) is less than the area under the design fire curve (Area B) the column is said to have failed in the design fire, and most notably in less time than in the standard fire. If however, the area under the standard fire curve (Area A) is greater than that under the design fire curve (Area B) the column is said to not have failed in the design fire, that is to say the column will survive complete compartment burnout [Fike 2010].

The approach proposed here is predicated on the concept that design fires have a similar initial rate of temperature increase, and most design fires achieve higher initial temperatures than the standard fire exposure. It should be noted that the proposed method is not applicable for design

fires that do not have a similar initial temperature rise as that of the ASTM E-119 fire exposure (up to ten minutes of fire exposure).

7.6 Validation of Proposed Approach

The validity of the proposed approach in evaluating fire resistance of RC columns is established by comparing the predictions from the proposed simplified equation with results from numerical studies (using the computer model developed in Chapter 4) and from fire resistance tests for both standard and design fire scenarios. The validation for column exposed to standard fire scenario and columns exposed to design fire scenarios is presented in two separate sections.

7.6.1 RC Columns Exposed to Standard Fire Scenario

Twenty two tested RC columns, form literature, were selected for this validation. Further, a separate set of 40 columns were analyzed using the computer model, presented in Chapter 4, under standard fire exposure. Two cross-sectional sizes of 305 mm and 508 mm were used in this study. Both circular as well as rectangular columns are validated. All columns, analyzed using the numerical model, were designed as per ACI 318 specifications. The properties of the RC columns selected for this validation, together with predicted values of fire resistance, is provided in Table 7.2.

Figures 7.15 and 7.16 show the comparison of the predicted (using proposed expression) fire resistance to the measured fire resistance values during tests. Figure 7.15 shows the comparison of predicted and measured fire resistance for RC columns with concentric loads while Figure 7.16 illustrates the comparison of predicted and measured fire resistance for RC columns with eccentric loads The 'safety limit' line in these figures represents the boundary where the predictions from proposed equation exactly coincide with the test measurements. Any prediction

above the ‘safety limit’ line indicates that the proposed expression overestimates the fire resistance and hence is unconservative.

The comparison of the predictions from the proposed model with the measured test data for columns with eccentricity is shown in Figure 7.16. It can be seen that the predictions from the proposed equation compare well with the test results, and are conservative for most of the columns. Further over conservatism can be seen in columns with a comparatively lower slenderness ratio (lesser than 4000mm).

Similarly Figure 7.17 shows the comparison of the predicted (using developed expression) fire resistance to the predicted (using numerical model) fire resistance values. While Figure 7.18 shows the prediction of the equation as compared to test and numerical model values for circular columns

It can be seen in Figures 7.15-7.18 that the predictions from the proposed equation compare well with the test results, and are conservative for most of the columns. There are minor variations in the predictions from the model and this can be attributed to the fact that the behavior of the column under fire is quite complex and would require a complex equation for its representation. But in order to achieve easy applicability, a simplified equation is developed such that it is sufficient for practical purposes. The predicted fire resistance values are unconservative for three columns which have a fire resistance less than 60 minutes. Also, the predictions from the equation are highly conservative for fire resistance beyond 4 hours. This may not be a major drawback since in most practical applications fire resistance ratings of 1 to 4 hours is required for RC columns. Also, the equation overestimates the fire resistance for column I6 which has a fire resistance of 3 hours.

7.6.2 RC Columns Exposed to Design Fire Scenarios

The proposed approach was also applied to the 60 different scenarios to determine if the columns fail or survive complete compartment burnout. The columns were analyzed using the numerical model and the proposed approach. Table 7.3 presents the data on the various scenarios considered and the failure time as determined by the numerical model and whether or not the column is determined to fail using the proposed method. The column designations are the same as provided in Table 6.1. In 20 out of the 60 column-fire combinations analyzed, both the numerical model and proposed approach indicated that no failure occurs in the column. This high percentage of survivability can be attributed to the fact that the decay phase of the fire allows the column to regain part of its strength and stiffness, resulting in a fire exposure that is less severe than the "standard" fire exposure. Thus it can be said that the proposed approach is capable of predicting the survivability of the RC columns with good accuracy.

Of the 40 remaining scenarios, both the numerical model and proposed approach predicted failure in 37 of them. The failure of RC column can be attributed to the high severity of fires encountered in these cases. Again, the agreement between the actual (numerical model) failure and that predicted by the proposed approach indicates the validity of the proposed approach. Further, for another 3 scenarios, while failure was not observed in the numerical model, the proposed approach predicted failure. This can be attributed to fires that are similar to ASTM E-119 for the considered time period, entering the decay phase possibly only minutes before the column failed under ASTM E-119 fire exposure. This can however be taken as conservative for design purposes.

It should be noted that this method predicts whether or not an RC column will survive the design fire exposure. As such, there is a built in factor of safety in that all columns designed according

to this method will have sufficient fire resistance to withstand complete burnout of the probabilistic fires to which the column would be exposed, rather than satisfying specific fire resistance requirements. It might be possible to achieve more deterministic results using more sophisticated methods, but that would increase the complexity of the calculations and make the approach less practical for use in design.

7.6.3 Comparison with Codes and Standards

To further validate the proposed equation, fire resistance predictions from the equation are compared to those obtained from the current codes of practice (see Table 7.4). this is undertaken for loaded columns exposed to standard fire exposure. Figure 7.19 shows the comparison of fire resistance as obtained from current provisions in ACI code, with those predicted by the proposed equation. Details of columns characteristics can be found in Table 7.1. It can be seen that ACI code underestimates the fire resistance (significantly) for most of the RC columns. This is mainly due to the fact that ACI provisions give only fire resistance ratings (to the nearest hour or 90 minutes). These ratings are mostly based on concrete cover thickness requirements and minimum section dimensions but do not account for significant factors such as load ratio, slenderness, etc. The proposed equation gives better predictions of fire resistance than the ACI code estimates and is closer to the safety line.

Figure 7.20 shows the comparison of fire resistance values from the proposed equation with those obtained from Eurocode provisions. It can be seen that the Eurocode predictions are comparable to those of the proposed equation for most of the columns. However, the Eurocode equation does account for minimum eccentricity but does not account for eccentricity explicitly thus rendering it unconservative in such cases.

Similarly, Figure 7.21 compares the fire resistance predictions from the proposed equation with those obtained based on Australian code provisions. It can be seen that the predictions from the Australian code have significant variability and are often unconservative throughout the range of the data. However, predictions from the proposed equation are closer to safety line and provide better estimate of fire resistance.

7.7 Design Applicability

7.7.1 General

Newer types of concrete such as HSC possess improved strength and durability properties as compared to conventional concrete; however they are susceptible to spalling and faster degradation of strength and spalling under certain fire conditions. In practical situations columns are often subjected to biaxial bending due to eccentricity of load or different exposure conditions. For evaluating realistic fire resistance of RC columns, the effect of biaxial bending occurring form load eccentricity, 1-, 2-, 3-, side exposure and fire induced spalling are to be considered. The proposed expression provides a convenient way of obtaining fire resistance of RC columns subjected to spalling, and thus can be used for estimating fire resistance in lieu of full-scale standard fire resistance tests or detailed numerical analysis. It incorporates significant parameters that influence the fire resistance of RC column. Also, the equation uses parameters such as slenderness ratio, percentage of steel, eccentricity etc. which are used to calculate the load carrying capacity of RC columns at ambient temperature. Thus, the proposed equation provides a simple but rational approach for computing the fire resistance of an RC column exposed to a fire. The proposed equation provides better estimate of fire resistance than those predicted by current codes of practice. Therefore, this equation can be considered for incorporation in codes and standards.

7.7.2 Design Example

To illustrate the applicability of the proposed approach in a design situation, the procedure is applied to evaluate the fire resistance of RC column III14 [Lie and Woolerton, 1988]. Details on the properties of the column are presented in Table 7.1(a) and Figure C.1. The fire resistance calculations from the proposed equation are carried out under fixed-fixed support condition. The results from the proposed equation are compared with fire resistance values from current codes and standards. The column is also checked (using the proposed method) for sustaining failure under design fire, Fire I, shown in Figure 6.2 Details of the calculations are given in Appendix C. The fire resistace of this columns under standard fire exposure was evaluated based on the proposed equation. Based on the concrete cover thickness and column cross-sectional size, load ratio, and eccentricity the standard fire resistance (R) was found from Eqn [7.5] to be 162 minutes.

The fire resistance is also evaluated based three widely used codes of practice, namely; ACI 216.1, Eurocode 2 and Australian code [AS 3600]. Detailed calculations of fire resistance are given in Appendix C and summary of results are given in Table C.1. It can be seen from the table that there is large variation in the fire resistance computed as per current code provisions. It can also be seen that the proposed equation predicts conservative fire resistance for simply supported beam compared to the three codes of practice. This reveals that current codes may not be fully conservative under some scenarios.

However, under design fire exposure (Fire I in Figure 6.2) the area under the design fire time-temperature curve (A_D) is higher than the area under standard fire time-temperature curve (A_S). Thus failure will occur in that column under the given design fire scenario. Detailed calculations of time equivalent are given in Appendix C.

7.7.3 Limitations

The proposed method offers a practical approach for evaluating the fire resistance of RC columns exposed to fire. However, the applicability of this method is limited to the range of parameters that were considered in the numerical study which formed the basis for developing this approach. The explicit limitations for the proposed methods are as follows:

- Fire resistance (R) duration: 1 – 4 hours.
- Type of fire exposure: ASTM E119 standard fire, equivalent standard fire scenarios such as ISO 834 standard fire, or any design fire whose initial temperature rise is similar to standard fire and has a decay phase.
- Specified 28 day compressive strength (f'_c): 25 – 100 MPa
- Size of column (rectangular or circular): 200 – 600 mm
- Percentage of longitudinal steel: 1 – 4 %
- Effective length of column: 2000 – 4500 mm
- Load Eccentricity: 0 – $0.75 \times b$ where b is the cross sectional dimension of the column in the direction of eccentricity.
- Modified tie configuration (135° bent) i.e. no spalling within the core of concrete.

Aggregate type: Siliceous and carbonate aggregate.

7.8 Summary

The development of a simplified approach for evaluating the fire resistance of RC columns is presented in this chapter. The equation developed based on data from parametric studies and tests from literature comprises of two main steps: evaluating the fire resistance under standard

fire exposure and establishing time equivalency between standard and design fire scenarios. The approach accounts for various parameters that have significant influence on the fire resistance of RC columns such as fire scenario, load ratio, load eccentricity (uniaxial and biaxial), different face exposure (1-, 2-, 3-, or 4-side), concrete strength, and slenderness ratios. The validity of the proposed approach is established by comparing perditions with results from detailed finite element analysis and fire tests. The proposed method provides a simple but rational approach for computing the fire resistance of an RC column exposed to standard or design fire scenarios. The approach facilitates a rational methodology for achieving desired fire resistance by varying parameters such as column dimensions, length and load. The proposed equation provides a better estimate of fire resistance than those predicted by current codes of practice.

Table 7.1(a). Fire resistance of RC columns with concentric loads obtained in standard fire tests

Column	End Conditions	Size (mm)	A_s/A_C %	Agg. type †	Slenderness ratio	Load ratio	Fire resistance (mins)
I1	FF	305	2.19	S	22	0.00	240
I2	FF	305	2.19	S	22	0.50	170
I3	FF	305	2.19	S	22	0.28	218
I4	FF	305	2.19	S	22	0.26	220
I7	FF	305	2.19	S	22	0.37	208
I8	FF	305	2.19	S	22	0.64	146
I9	FF	305	2.19	S	22	0.44	187
II2	FF	305	2.19	S	22	0.31	201
II3	FF	305	2.19	S	22	0.30	210
II4	FF	305	2.19	S	22	0.29	227
II5	FF	305	2.19	S	22	0.27	234
III14	FF	305	2.19	S	22	0.37	183
II1	FP	305	2.19	S	31	0.11	340
III1	FP	305	2.19	S	31	0.28	242
III2	FP	305	2.19	S	31	0.34	220
T3	PP	305	2.19	S	43	0.34	221
III11*	FF	356	2.34	S	21	0.42	245
III12*	FF	356	2.34	S	21	0.44	220
I5	FF	407	2.47	S	16	0.00	300
II10	FF	407	2.47	S	16	0.43	262
I6	FF	203	2.75	S	33	0.13	180
II11	FF	407	3.97	S	16	0.45	285
II8	FF	305	4.38	S	22	0.25	252
II9	FF	305	4.38	S	22	0.36	225
II12‡	FF	407	3.97	S	16	0.44	213

Table 7.1(a). Contd. Fire resistance of RC columns with concentric loads obtained in standard fire tests

I10	FF	305	2.19	C	22	0.29	510
I11	FF	305	2.19	C	22	0.38	366
I12	FF	305	2.19	C	22	0.63	216
III4	/FF	305	2.19	C	22	0.35	328

* indicates circular columns

** Columns analyzed using SAFIR

† S – Siliceous Aggregate; C – Carbonate Aggregate

‡ All columns except Column II12 had 48 mm cover to main reinforcement. Column II12 had 64 mm cover.

Table 7.1(b). Fire resistance of RC columns with eccentric load as obtained in standard fire tests

Column	End Conditions	Size (mm)	A_S/A_C %	Aggregate type †	Slenderness ratio	Load Ecc	Load ratio	Fire resistance (mins)
CS27	PP	300	2.09	S	55	5	0.37	48
CS28	PP	300	2.09	S	43	5	0.46	57
CS29	PP	300	2.09	S	54	5	0.48	38
CS14	PP	200	4.71	S	82	10	0.17	49
CS22	PP	200	4.71	S	100	10	0.12	40
CS30	PP	300	2.09	S	54	10	0.32	55
CS31	PP	300	2.09	S	54	10	0.43	57
CS35	PP	200	2.31	S	99	10	0.15	40
CS37	PP	200	2.31	S	99	10	0.11	49
CS39	PP	200	2.31	S	99	10	0.08	72
CS13	PP	300	2.09	S	55	15	0.26	85
CS23	PF	300	2.09	S	39	15	0.26	160
CS15	PP	200	4.71	S	82	20	0.14	36
CS1	PP	300	2.09	S	43	30	0.29	86
CS4	PP	300	2.09	S	55	30	0.26	63

Table 7.1(b). Contd. Fire resistance of RC columns with eccentric load as obtained in standard fire tests

CS6	PP	300	2.09	S	67	30	0.24	61
CS11	PP	300	2.09	S	55	30	0.23	80
CS12	PP	300	2.09	S	55	30	0.23	69
CS20	PF	300	2.09	S	31	30	0.28	111
CS25	PP	300	2.09	S	55	30	0.25	93
NRC	FF	305	2.19	S	22	44	0.27	167
CS21	PF	300	2.09	S	31	50	0.26	125
CS36	PP	200	2.31	S	99	50	0.10	35
CS38	PP	200	2.31	S	99	50	0.07	52
NRC	FF	305	2.19	S	22	58	0.27	225
CS18	PP	200	4.71	S	82	60	0.10	49
CS26	PP	300	2.09	S	55	60	0.19	135
NRC	FF	305	2.19	S	22	61	0.25	210
NRC	FF	305	2.19	S	22	81	0.28	170
CS16	PP	300	2.09	S	55	90	0.16	75
CS19	PP	200	4.71	S	82	100	0.08	53
CS34	PP	200	2.31	S	99	100	0.08	31
CS17	PP	300	2.09	S	55	150	0.13	65
CS24	PF	300	2.09	S	39	150	0.09	89
CS32	PP	300	2.09	S	54	150	0.09	49
CS33	PP	300	2.09	S	54	150	0.15	50

† S – Siliceous Aggregate; C – Carbonate Aggregate

Table 7.2 (a). Fire resistance data of rectangular RC columns used for validating proposed equation

Concrete	Column	Size (mm)	Fire Exposure	Applied Load (kN)	Eccentricity (mm)		Permeability	Fire resistance from Numerical study (mins)	Fire resistance from equation (mins)
					X	Y			
NSC	CE60	305	4	800	0	0	-17	202	172
	CE61	305	3	800	0	0	-17	181	155
	CE62	305	2O	800	0	0	-17	225	191
	CE63	305	2A	800	0	0	-17	142	122
	CE64	305	1	800	0	0	-17	192	164
	CE65	305	4	800	25	0	-17	177	152
	CE66	305	4	800	50	0	-17	158	136
	CE67	305	4	800	75	0	-17	132	114
	CE68	508	4	2210	0	0	-17	238	202
	CE69	508	3	2210	0	0	-17	173	148
	CE70	508	2O	2210	0	0	-17	263	223
	CE71	508	2A	2210	0	0	-17	176	151
	CE72	508	1	2210	0	0	-17	207	176
	CE73	508	4	2210	25	0	-17	208	177
	CE74	508	4	2210	50	0	-17	179	153
	CE75	508	4	2210	75	0	-17	150	129
HSC	CE76	305	4	800	0	0	-18	185	158
	CE77	305	3	800	0	0	-18	150	129
	CE78	305	2O	800	0	0	-18	200	171
	CE79	305	2A	800	0	0	-18	131	113
	CE80	305	1	800	0	0	-18	162	139
	CE81	508	4	2210	0	0	-18	224	190
	CE82	508	3	2210	0	0	-18	183	157
	CE83	508	2O	2210	0	0	-18	242	205
	CE84	508	2A	2210	0	0	-18	158	136
	CE85	508	1	2210	0	0	-18	184	157

Table 7.2 (a). Contd. Fire resistance data of rectangular RC columns used for validating proposed equation

NSC	CE86	305	4	800	25	25	-17	166	142
	CE87	305	4	800	25	50	-17	146	126
	CE88	305	4	800	25	75	-17	113	98
	CE89	305	4	800	50	25	-17	144	124
	CE90	305	4	800	50	50	-17	118	102
	CE91	305	4	800	50	75	-17	83	73
TEST	HSC1	406	4	6436	0	0	-19	239	203
	HSC2	406	4	5900	0	0	-19	224	190
	HSC3	406	4	7400	0	0	-19	104	90
	HSC4	305	4	3145	0	0	-19	266	225
	HSC5	305	4	3145	0	0	-19	290	245
	HSC6	305	4	3145	0	0	-19	266	225
	21BC	200	4	344	0	0	-17	107	71
	31BC	300	4	944	0	0	-17	63	63
	31CC	300	4	608	0	0	-17	123	82
	33AC	300	4	560	0	0	-17	69	57
	22BC	200	4	384	0	0	-17	97	94
	III3	305	4	544	0	0	-17	181	183
	CS27	300	4	592	5	0	-17	48	42
	CS13	300	4	416	15	0	-17	85	58
	CS4	300	4	416	30	0	-17	63	55
	CS36	200	4	80	50	0	-17	35	26
	CS19	200	4	64	100	0	-17	53	26
	CS33	300	4	240	150	0	-17	50	41

Table 7.2 (b). Fire resistance data of circular RC columns used for validating proposed equation

Column type	Concrete	Column	Size (mm)	Applied load (kN)	Load level (%)	Eccentricity (mm)	Permeability	Fire resistance from Numerical study (mins)	Fire resistance from equation (mins)
						X			
Analyzed columns	NSC	CV1	305	640	40	25	-17	219	186
		CV2	305	640	40	50	-17	180	154
		CV3	305	960	60	25	-17	183	157
		CV4	305	960	60	50	-17	151	130
	HSC	CV5	305	1270	40	25	-19	113	98
		CV6	305	1270	40	50	-19	93	81
		CV7	305	1900	60	25	-19	95	83
		CV8	305	1900	60	50	-19	78	68
Tested columns	NSC	C1	305	1260	59	0	-18	156	134
		C2	305	1770	83	0	-18	131	113
		C3	508	1450	57	0	-18	187	160
		C4	508	1900	75	0	-18	163	140

Table 7.3: Fire resistance equivalency as predicted by macroscopic finite element model (MFEM) (Chapter 4) and the proposed approach

Column →	CE0		CE1		CE3		CE4		CE58		CE27	
Type of Fire Exposure ↓	MFEM Failure (min)	Predicted Failure	MFEM Failure (min)	Predicted Failure	MFEM Failure (min)	Predicted Failure	MFEM Failure (min)	Predicted Failure	MFEM Failure (min)	Predicted Failure	MFEM Failure (min)	Predicted Failure
ASTM	253	NA	226	NA	177	NA	240	NA	148	NA	160	NA
FIRE 1	73	Y	65	Y	53	Y	71	Y	44	Y	51	Y
FIRE 2	95	Y	81	Y	77	Y	90	Y	56	Y	69	Y
FIRE 3	NF	N	NF	N	183	N	NF	N	167	N	165	N
FIRE 4	NF	N	NF	N	NF	N	NF	N	174	N	NF	N
FIRE 5	NF	N	NF	N	NF	N	NF	N	NF	N	NF	N
FIRE 6	73	Y	65	Y	53	Y	71	Y	44	Y	51	Y
FIRE 7	103	Y	81	Y	77	Y	90	Y	56	Y	69	Y
FIRE 8	NF	N	NF	N	NF	N	NF	Y	NF	N	NF	Y
FIRE 9	NF	N	NF	N	NF	N	NF	N	NF	Y	NF	N
FIRE 10	NF	N	NF	N	NF	N	NF	N	NF	N	NF	N

NA – Not Applicable

NF – No Failure

Table 7.4. Fire resistance comparison from proposed equation with code provisions

Column	Fire resistance (mins)				
	Test	Proposed Eqn.	ACI	Eurocode	Australian Code
21BC	107	71	30	70	98
31BC	63	63	60	59	118
31CC	123	82	60	84	227
33AC	69	57	60	87	177
22BC	97	94	30	87	83
III3	181	183	180	230	258
CS27	48	42	90	78	84
CS13	85	58	90	92	135
CS4	63	55	90	91	119
CS36	35	26	30	72	445
CS19	53	26	30	102	262
CS33	50	41	60	102	283

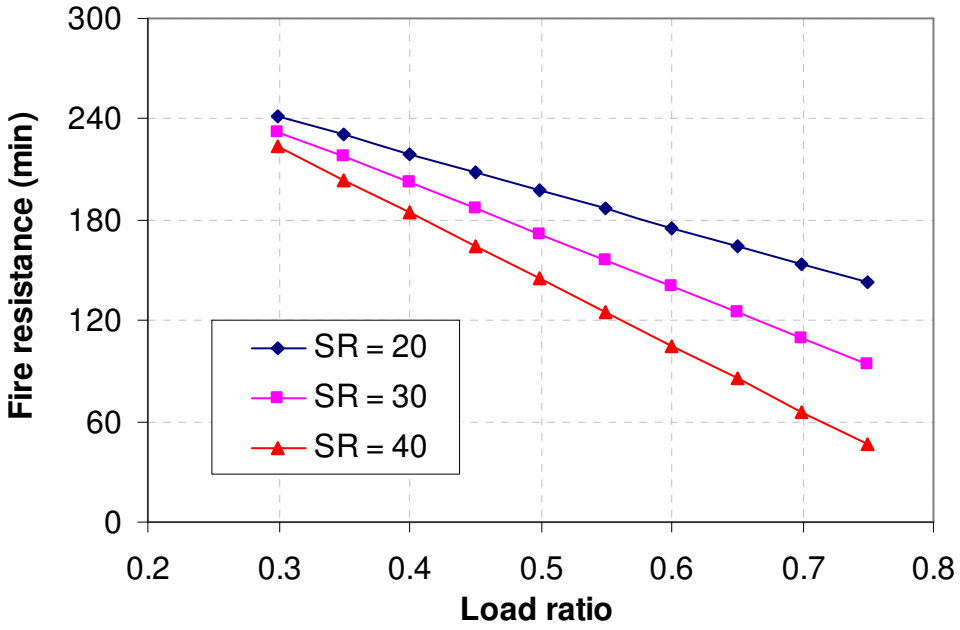

Fig. 7.1- Fire resistance as a function of load-ratio for RC columns

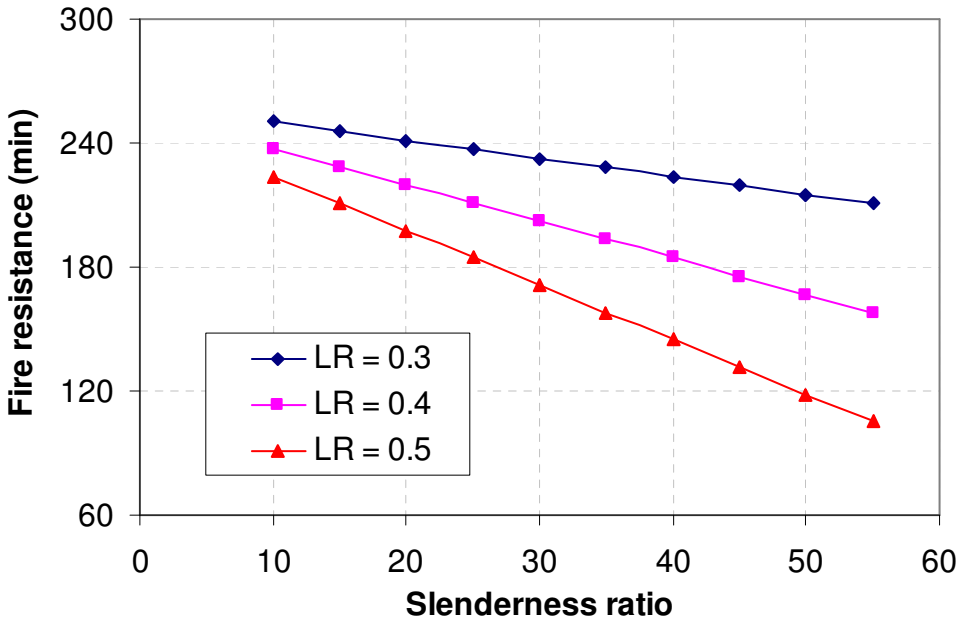

Fig. 7.2- Fire resistance as a function of slenderness-ratio for RC columns

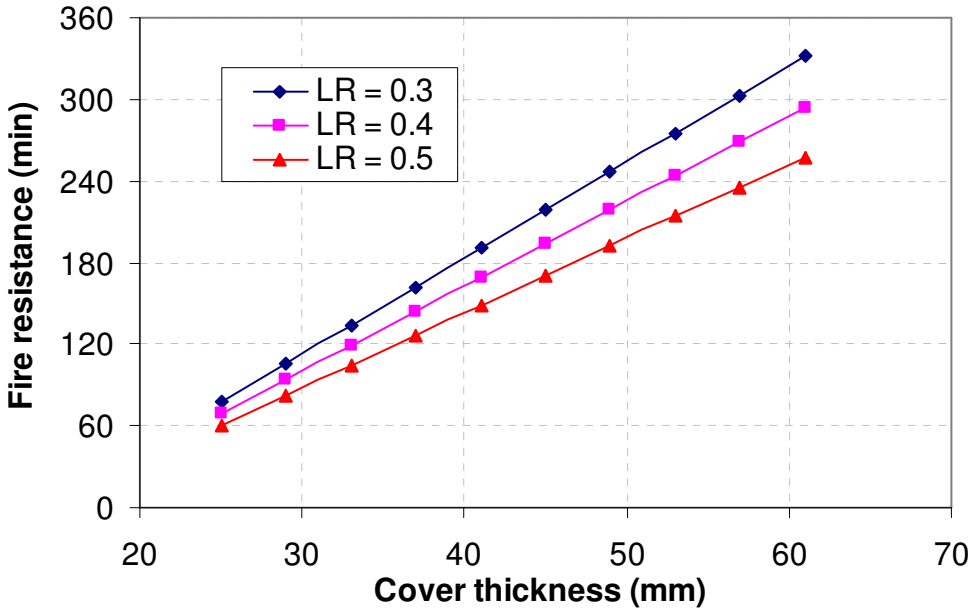

Fig. 7.3- Fire resistance as a function of cover thickness for RC columns

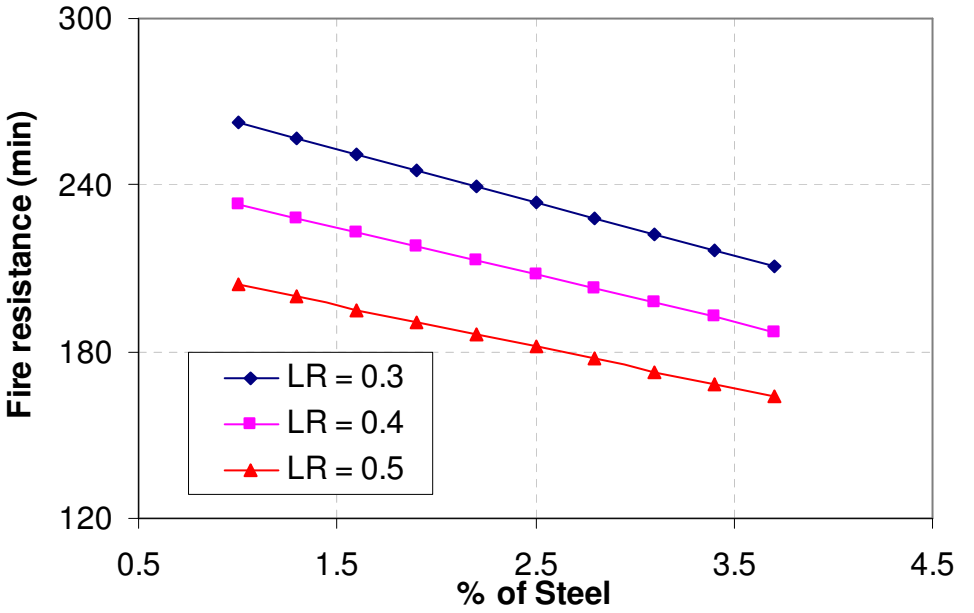

Fig. 7.4- Fire resistance as a function of percentage of steel for RC columns

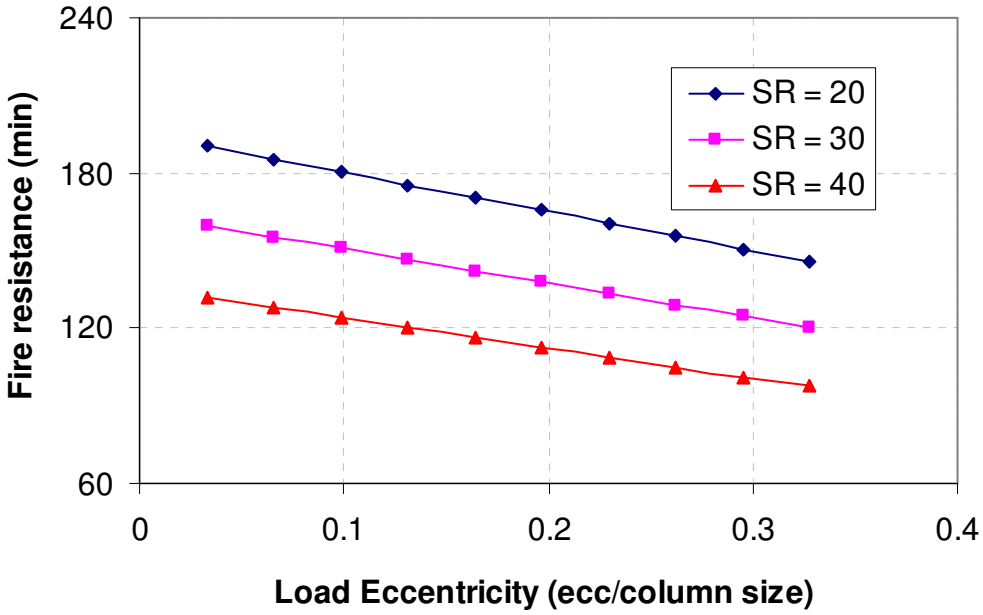

Fig. 7.5- Fire resistance as a function of load eccentricity for RC columns

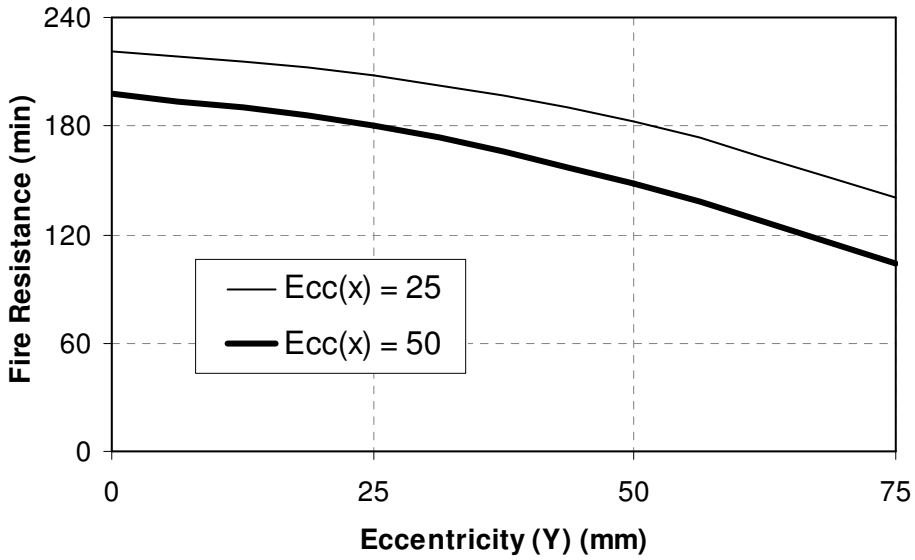

Fig. 7.6- Variation of fire resistance with eccentricity along Y axis for different eccentricities along X axis

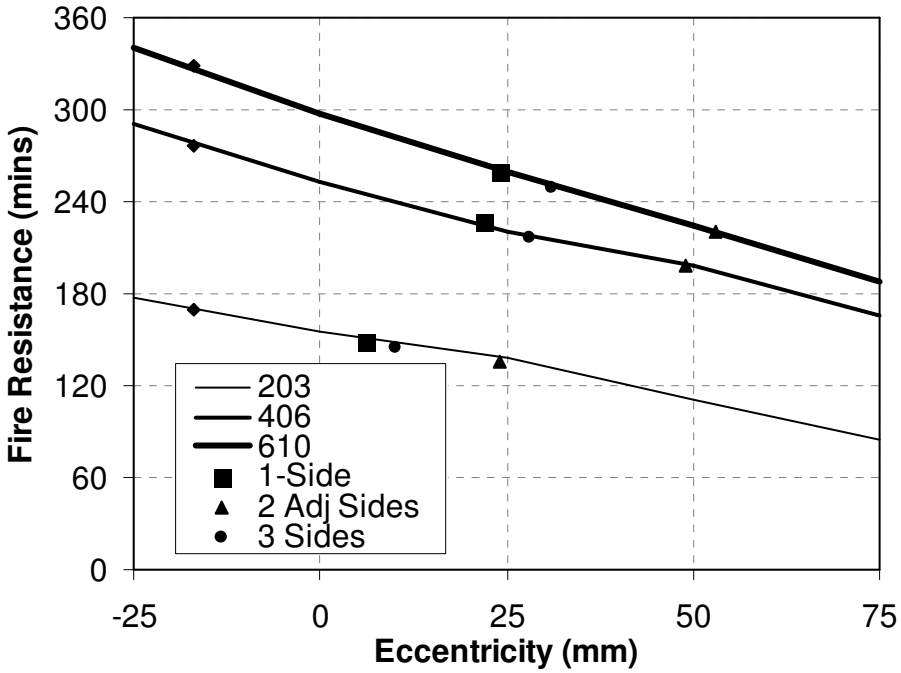

Fig. 7.7- Variation of fire resistance with eccentricity and exposure condition

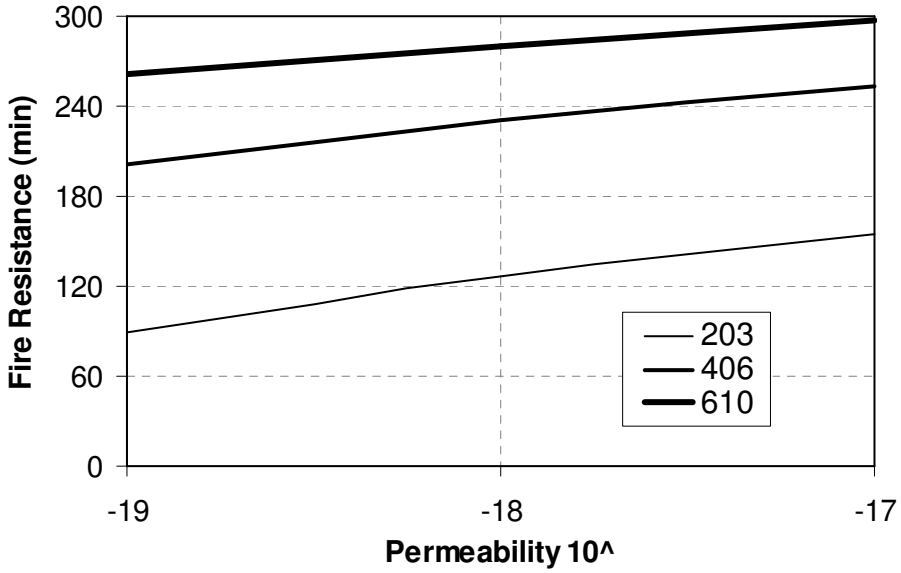

Fig. 7.8- Variation of fire resistance with permeability under 4-side exposure for different column sizes conditions

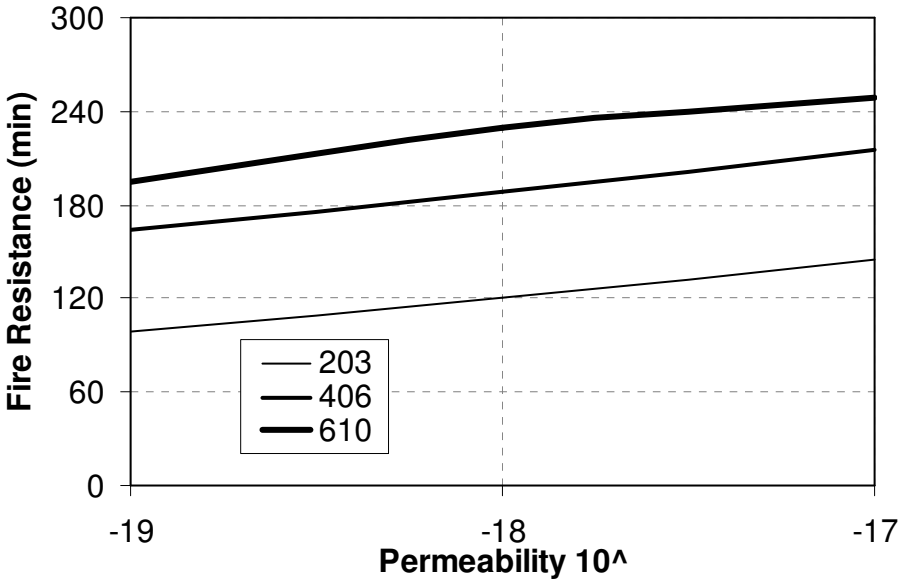

Fig. 7.9- Variation of fire resistance with permeability under 3-side exposure for different column sizes conditions

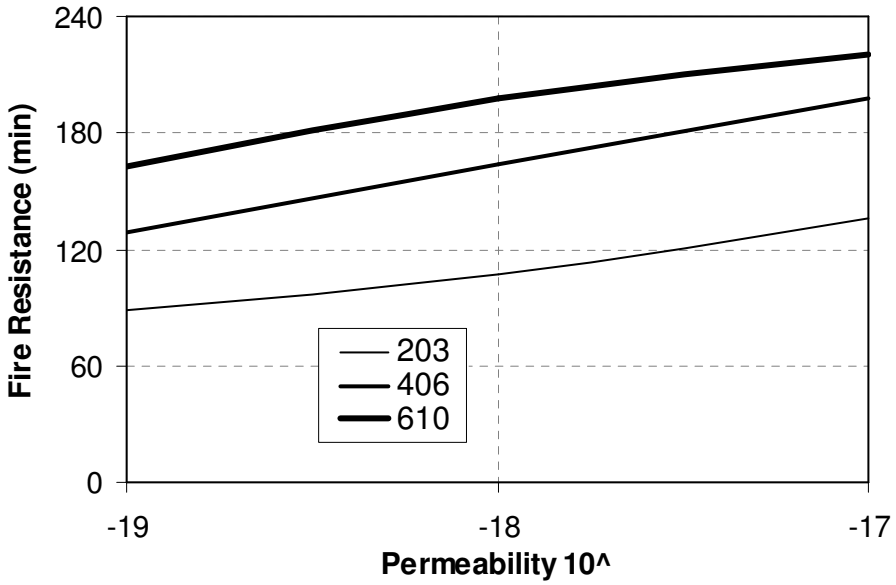

Fig. 7.10- Variation of fire resistance with permeability under 2-adjacent side exposure for different column sizes conditions

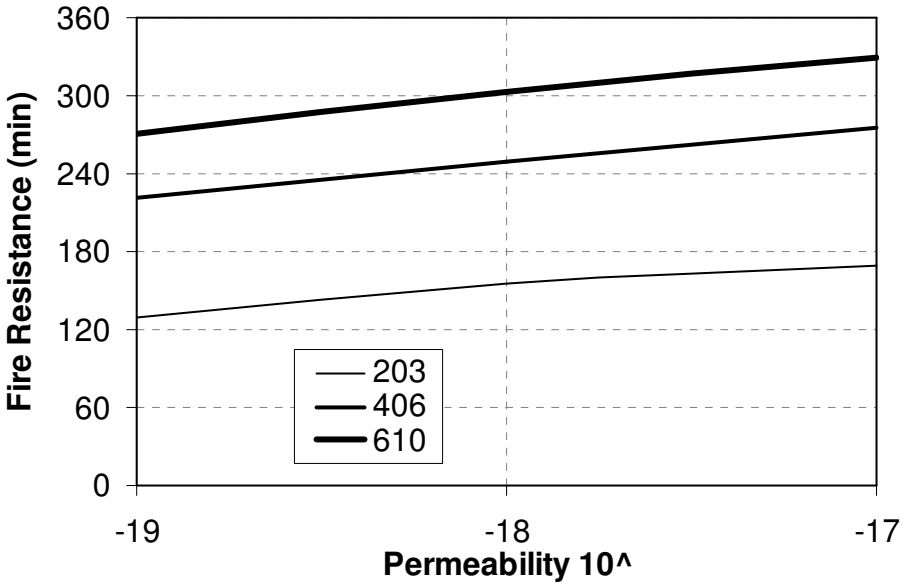

Fig. 7.11- Variation of fire resistance with permeability under 2-opposite side exposure for different column sizes conditions

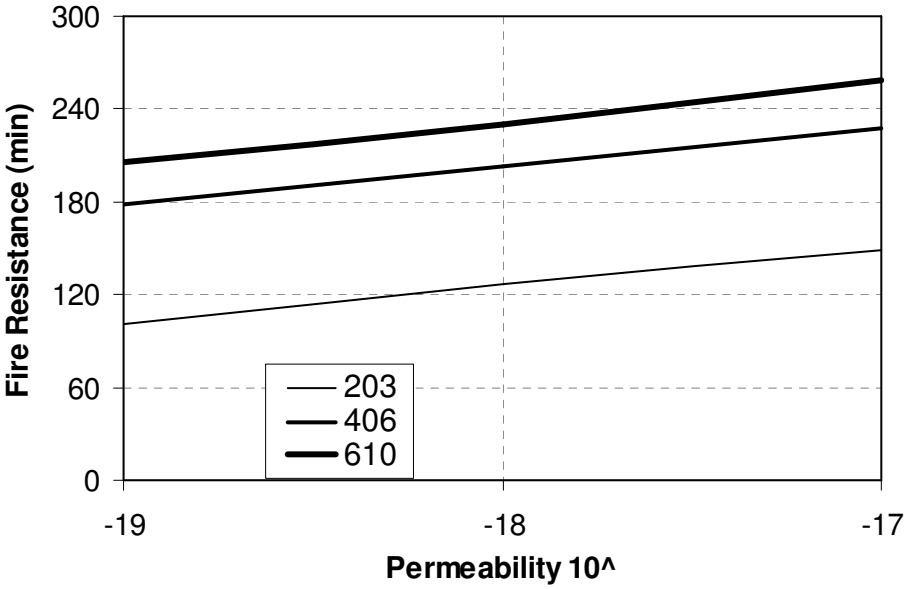

Fig. 7.12- Variation of fire resistance with permeability under 1-side exposure for different column sizes conditions

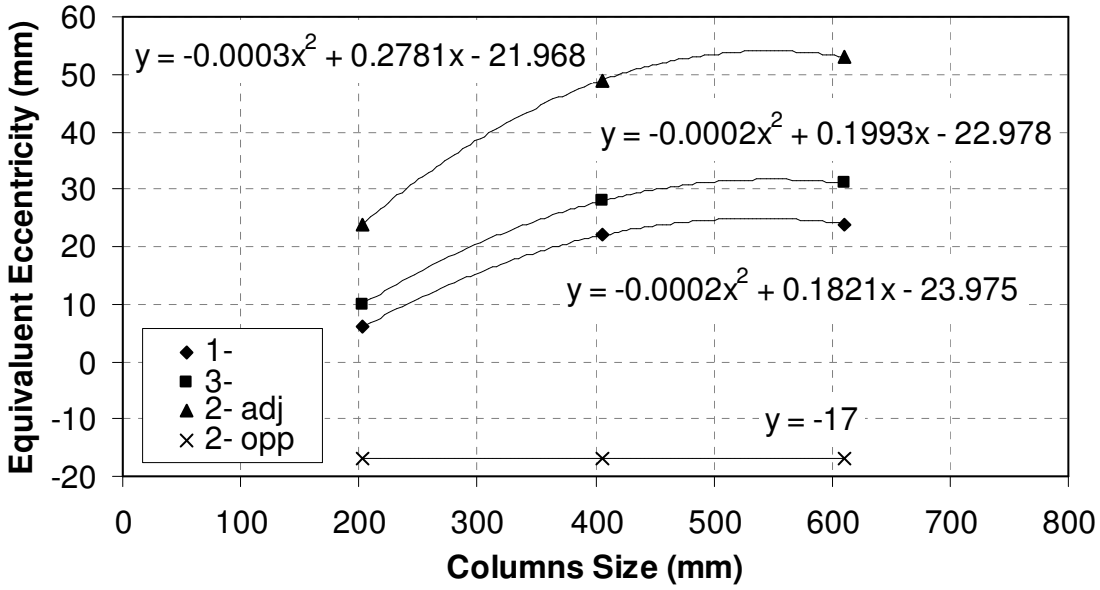

Fig. 7.13- Variation of equivalent eccentricity for different exposure conditions

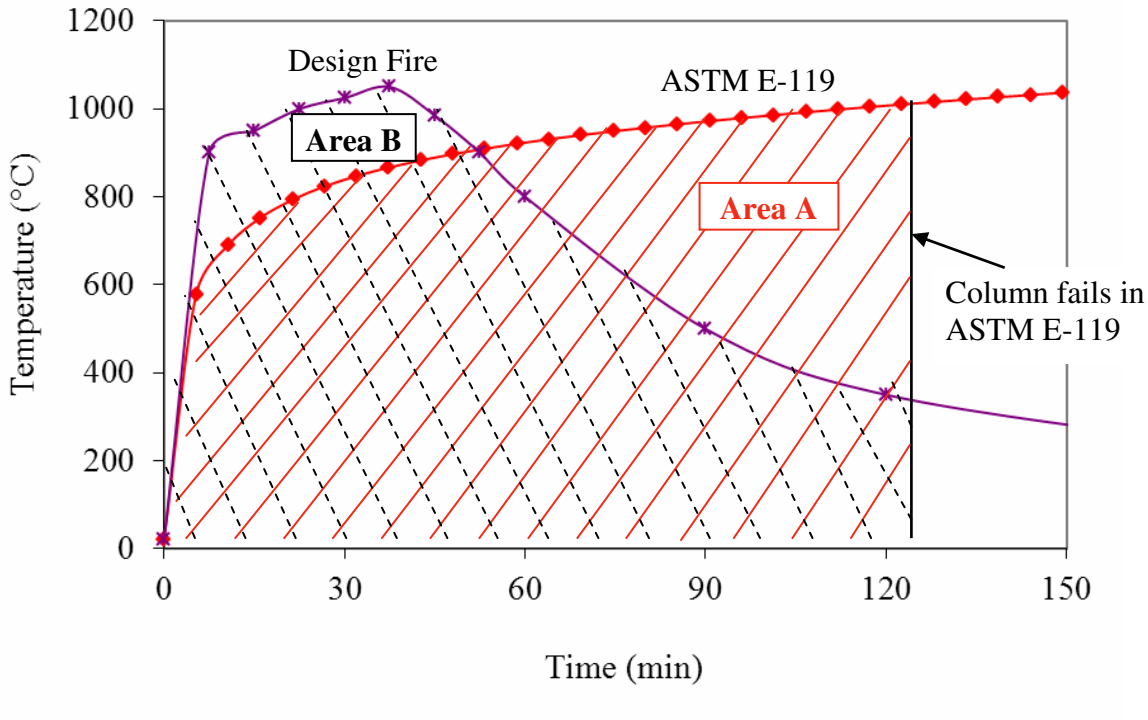

Fig. 7.14- Calculation of time equivalency between design fire and standard fire

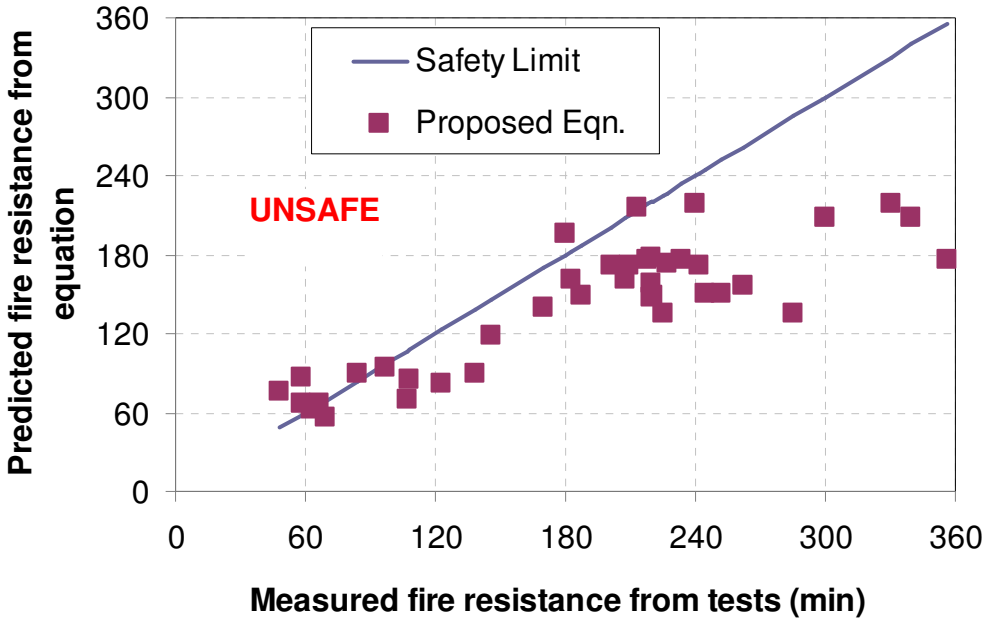

Fig. 7.15- Comparison of predicted and measured fire resistance for NSC columns with concentric load under standard fire

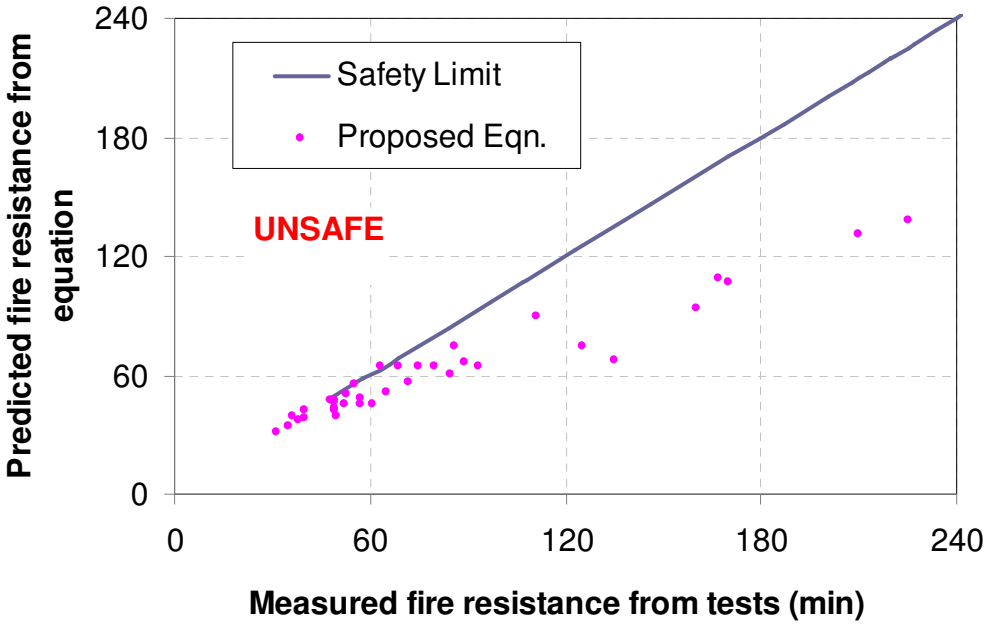

Fig. 7.16- Comparison of predicted and measured fire resistance for NSC columns with eccentric load under standard fire

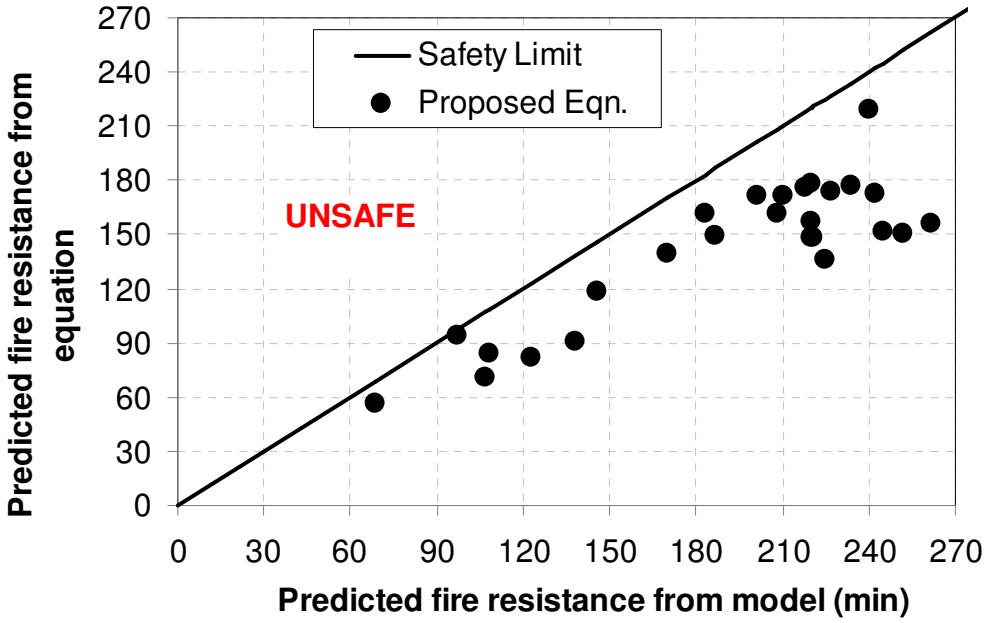

Fig. 7.17- Comparison of predicted fire resistance form the proposed equation with the predicted fire resistance from numerical model

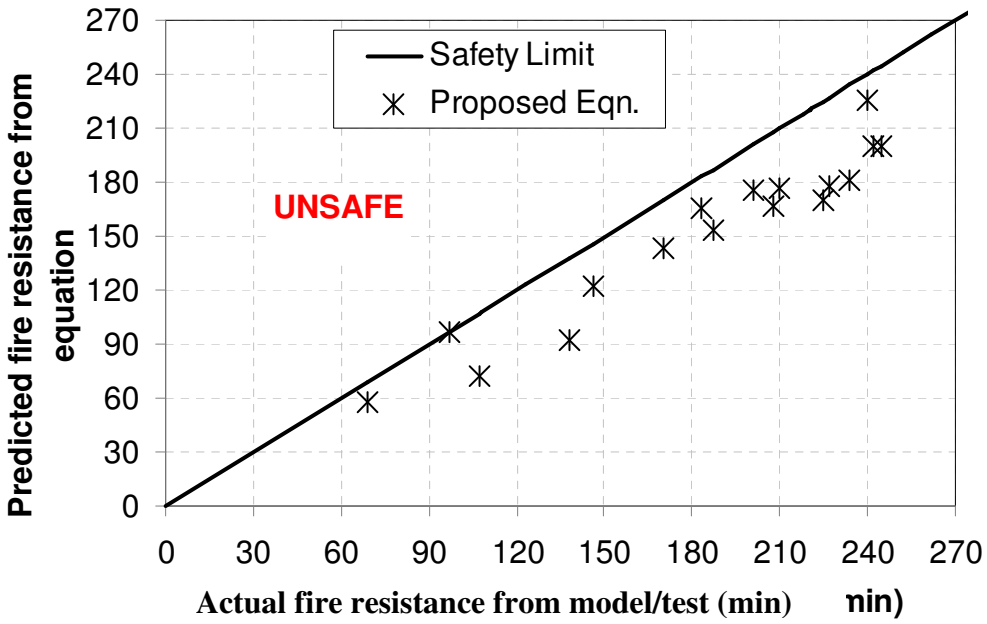

Fig. 7.18- Comparison of predicted fire resistance from the proposed equation with actual fire resistance values (tests) and values from model for circular columns

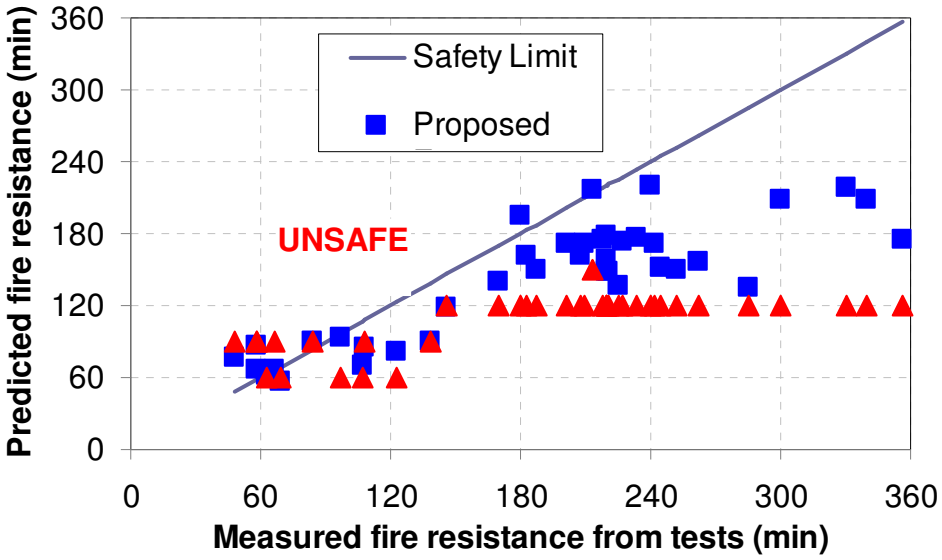

Fig. 7.19- Comparison of fire resistance predicted from the proposed equation with ACI provisions

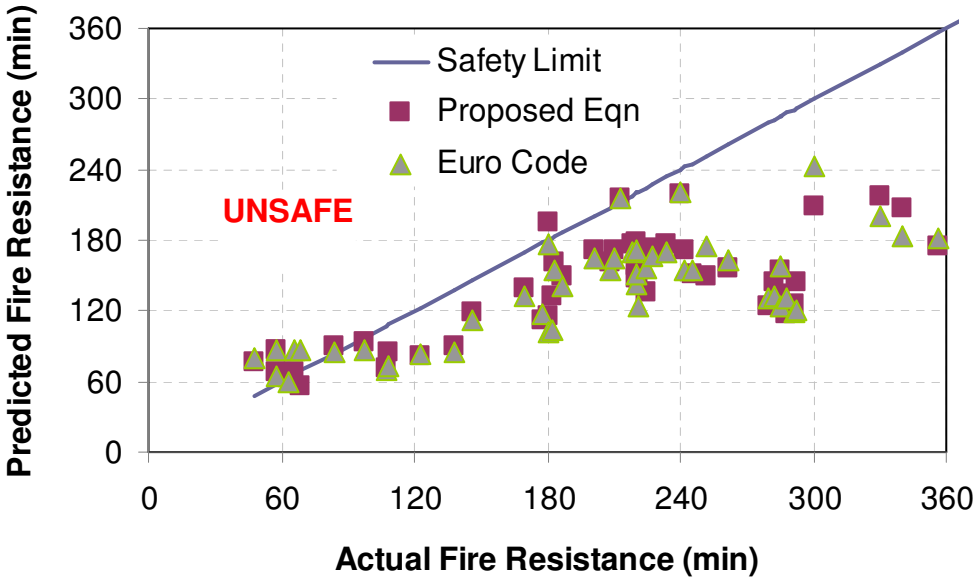

Fig. 7.20- Comparison of fire resistance predicted from the proposed equation with Eurocode equation

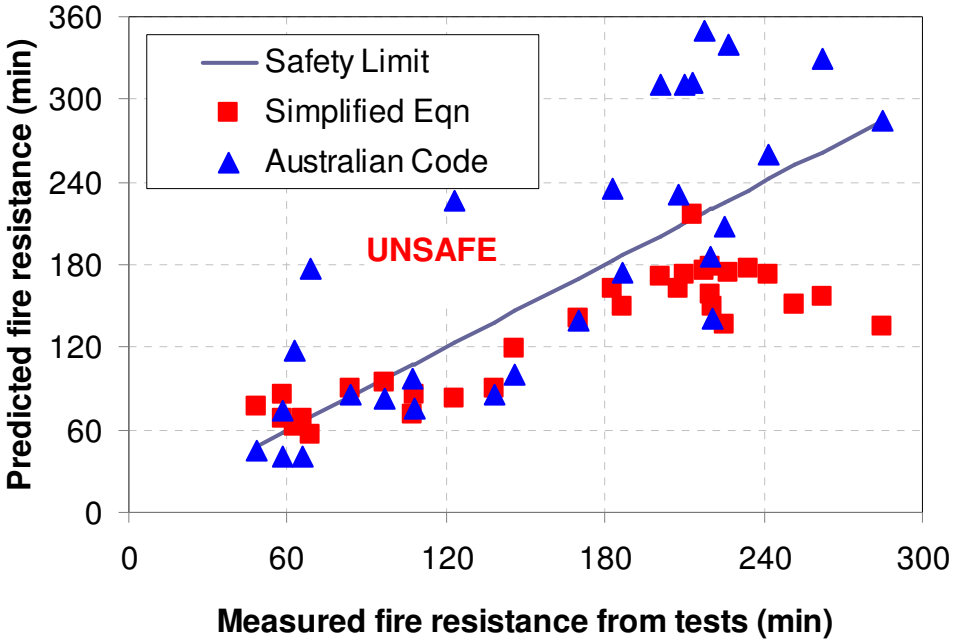

Fig. 7.21- Comparison of fire resistance predicted from the proposed equation with Australian code provisions

CHAPTER 8

8 CONCLUSIONS AND RECOMMENDATIONS

8.1 General

Fire resistance of RC columns is currently evaluated based on standard fire conditions and no consideration is given to a number of realistic conditions, including biaxial bending effects that arise under realistic fire conditions. This is mainly due to lack of understanding on the response of RC columns under realistic fire, loading, and restraint scenarios. To study the response of RC columns realistic under fire conditions a numerical model was developed for tracing the response of RC columns under realistic fire, loading and exposure conditions. The model is based on macroscopic finite element approach and uses time-dependent moment-curvature relationships to trace the response of the columns from pre-fire stage to failure under fire conditions. All of the critical factors, namely; high temperature material properties, fire induced spalling, different strain components, different exposure (1-, 2-, 3-, or 4-side) conditions and bi-eccentric loading, that have significant influence on fire response of RC columns, are accounted for in the analysis.

For validating the numerical model, fire tests on six RC columns were conducted under varying fire, concrete strength, presence of fiber, and load level conditions. The columns comprised of one NSC, three HSC and two HSC columns with polypropylene fibers, and they were tested under one standard and two design fires. Data from fire tests was utilized to validate the numerical model for various response parameters such as temperatures, deformations, spalling, and fire resistance. The validated numerical model was applied to conduct parametric studies to quantify the influence of various factors on the fire response of RC columns. Finally, data from parametric studies was utilized to develop a rational design approach for evaluating the fire resistance of RC columns. The proposed design approach accounts for significant parameters

that govern the fire response of RC column, and thus provide better fire resistance estimates as compared to current code provisions.

8.2 Key Findings

Based on the information presented in this study, the following key conclusions are drawn:

- There is very limited information on the fire performance of RC columns, especially under design fires scenarios, fire-induced spalling and fire-induced biaxial bending (due to bi-eccentric loading, uneven spalling, or different face exposures). Also, to date, there is no rational approach for evaluating fire resistance of RC columns under biaxial bending effects.
- Data from fire resistance tests on six RC columns indicate that:
    - HSC columns have lower fire resistance as compared to NSC columns, mainly due to occurrence of spalling and faster reduction strength and stiffness at elevated temperatures.
    - HSC columns can survive burnout conditions (no failure) under typical design fire scenarios due to regaining part of concrete strength and stiffness upon cooling.
    - Addition of polypropylene fibers helps mitigating spalling, by providing channels for moisture to escape and thus enhancing fire resistance of HSC columns.
- The proposed macroscopic finite element model is capable of predicting the fire response of RC columns, in the entire range: from pre-fire stage to collapse stage, with a good amount of accuracy. This model accounts for critical parameters such as different fire scenarios, high temperature material properties, various strain components, fire induced spalling, restraint effects and biaxial bending in RC columns arising form 1-, 2-, 3-side exposure, uneven spalling or eccentric loading.

- Data from parametric and experimental studies indicate that the main factors that significantly influence fire resistance of RC columns are load ratio, slenderness ratio, concrete strength (permeability), and biaxial bending arising from face exposure (1-, 2-, or 3-side), load eccentricity, and uneven spalling. Specifically:
    - Load eccentricity has a significant influence of fire response of RC columns and the fire resistance reduces by about 20% for every 25 mm increase in load eccentricity arising due to uniaxial bending or P-δ effects. The fire resistance can reduce by about 30% in biaxial bending situations.
    - Different exposure conditions affect fire resistance of RC columns with 2 adjacent sides of fire exposure being the worst case (least fire resistance) and 2 opposite sides exposure being the best case (highest fire resistance) scenario.
    - For a typical RC column, the fire resistance can decrease by about 15%, 40%, and 10% when the fire exposure changes from 4-sided to 3-, 2-, or 1-sided exposure respectively. This change in exposure conditions lead to thermal gradients that translate to eccentricity of load.
    - The reduction in fire resistance due to increased load level is higher for columns subjected to biaxial bending than axially loaded columns. The fire resistance drops by about 30 minutes for each 10% increase in the load ratio when column undergoes biaxial bending as compared to about 15 minutes drop under axial loading.
    - Increased column size leads to higher fire resistance (40% for every 100mm increase in size). The increase is smaller (about 25% for every 100mm increase in size) when columns are subjected to biaxial bending. The fire resistance increases

quadratically with increase in column size since the area farthest away from the central core is more efficient in resisting bending.

- Fire resistance of HSC columns are highly affected by biaxial bending due to the occurrence of spalling. The fire resistance in HSC column can drop by about 50% due to loss of cross-section and thus the flexural rigidity.

- A simplified expression is proposed for evaluating fire resistance of RC columns. The proposed equation can evaluate the fire resistance of RC column subject to spalling, 1-, 2-, 3-, of 4-side fire exposure and bi-eccentric loading with accuracy sufficient for practical applications. The approach also provides a method for predicting the survivability of RC columns under design fire scenarios. The proposed approach provides better fire resistance predictions than those obtained from current code provisions.

8.3 Recommendations for Future Research

While this study has advanced the state-of-the-art with respect to fire response of RC columns, further research is required to fully characterize the complex behavior of concrete columns especially under biaxial bending effects. The following are some of the key recommendations for further research in this area:

- Currently there is a lack of test data on fire behavior of RC columns under biaxial bending, either arising from bi-eccentric loading or from different face exposures. Future research can be directed towards generating such test data which is very valuable for validating the numerical models.
- The macroscopic finite element model can be further advanced by incorporating coupling between hydro-thermal and structural models. Such advancement enables the model to

consider the influence of mechanical response (such as stresses, and cracking) on the hydro-thermal analysis and spalling predictions in concrete.

- The effect of tie configuration in mitigating spalling is well established through experimental studies. This effect can be incorporated in the finite element numerical model presented here by accounting for the hoop pressure due to pore-pressure, poisons effect, and due to the buckling effect of unconfined rebars. This will facilitate prediction of local failure of RC columns.
- The moment-curvature based microscopic finite element numerical model, presented here, can be extended to RC columns with FRP-strengthening. This can be achieved by extending thermal and structural sub-models to account for high temperature properties of FRP and insulation material. The numerical procedures should be enhanced to account for shear and bond effects, since these factors may be critical FRP-strengthened RC columns.
- The current constitutive models for high temperature material properties of concrete and steel (including high temperature creep strain in concrete and reinforcing steel, and also transient strain in concrete), particularly in the cooling phase, are not sufficiently accurate. Improvements in such constitutive models will help to enhance the accuracy of the model predictions under design fire scenarios. Also, similar models for newer types of concrete (fly ash concrete, self-consolidating concrete, high strength concrete with polypropylene or steel fibers) need to be developed.
- Strain gage measurements would have been a useful source of data to fully validate the model under combined effects of applied load and fire, and to quantify the different strain components under fire exposure. The high temperature strain gages currently available in

the market do not provide reliable measurements under fire exposure, and thus there is a need for developing reliable high temperature strain gages. Similarly, measurement of lateral deformations can also provide additional validation points for numerical models and thus there is a need for designing an accurate lateral deformation technique for RC columns tested under fire.

8.4 Research Impact

Uniaxial and biaxial bending can arise in RC columns under fire situations due to 1-, 2-, 3-side fire exposure, uneven spalling, or bi-eccentric loading. The research undertaken as part of this study develops fundamental understanding on the response of RC columns under fire induced biaxial bending. The current approach of evaluating fire resistance through standard fire tests on full-scale RC columns does not consider these effects and thus has a number of drawbacks. An alternative is to use numerical models for predicting fire resistance. However, the current calculation methods do not account for important factors such biaxial bending (arising from 1-, 2-, 3-side exposure, uneven spalling, or bi-eccentric loading), design fire scenarios, and restraint effect. The proposed numerical model and design approach provide a convenient way of obtaining fire resistance of RC columns, and thus can be used for estimating fire resistance in lieu of full-scale standard fire resistance tests and can be utilized for studying detailed fire response of RC columns under fire conditions.

Further, the current fire resistance provisions in codes and standards [ACI 216.1 2007, Eurocode 2 2004, AS3600] are prescriptive and do not account for realistic conditions such as loading, fire, face exposure, and spalling effects. Thus, the current design approaches are not applicable for undertaking rational and cost-effective fire safety solutions. The design approach proposed from this study can be applied to evaluate fire resistance under realistic fire, loading and face exposure

scenarios. The proposed equation expresses fire resistance in terms of structural parameters, and thus the approach is attractive for incorporation in codes and standards. Such rational design approach will contribute to reduced loss of life and property damage in fire incidents.

APPENDICES

APPENDIX A

High Temperature Material Relationships

Table A.1 – Constitutive Relationships for High Temperature Properties of Concrete

	Normal strength concrete – [ASCE Manual 1992]
Stress-strain relationships	$$\sigma_c = \begin{cases} f'_{c,T}\left[1-\left(\dfrac{\varepsilon-\varepsilon_{max,T}}{\varepsilon_{max,T}}\right)^2\right], & \varepsilon \le \varepsilon_{max,T} \\ f'_{c,T}\left[1-\left(\dfrac{\varepsilon_{max,T}-\varepsilon}{3\varepsilon_{max,T}}\right)^2\right], & \varepsilon > \varepsilon_{max,T} \end{cases}$$ $$f'_{c,T} = \begin{cases} f'_c & ,20\,°C \le T \le 450\,°C \\ f'_c\left[2.011-2.353\left(\dfrac{T-20}{1000}\right)\right] & ,450\,°C < T \le 874\,°C \\ 0 & ,874\,°C < T \end{cases}$$ $$\varepsilon_{max,T} = 0.0025 + \left(6.0T + 0.04T^2\right)\times 10^{-6}$$

Table A.1 (Continued) – Constitutive Relationships for High Temperature Properties of Concrete

Thermal Capacity	Siliceous Aggregate Concrete: $$\rho c = \begin{cases} 0.005T + 1.7 & 20\,°C \le T \le 200\,°C \\ 2.7 & 200\,°C < T \le 400\,°C \\ 0.013T - 2.5 & 400\,°C < T \le 500\,°C \\ 10.5 - 0.013T & 500\,°C < T \le 600\,°C \\ 2.7 & 600\,°C < T \end{cases}$$ Carbonate Aggregate Concrete: $$\rho c = \begin{cases} 2.566 & 20\,°C \le T \le 400\,°C \\ 0.1765\,T - 68.034 & 400\,°C < T \le 410\,°C \\ 25.00671 - 0.05043\,T & 410\,°C < T \le 445\,°C \\ 2.566 & 445\,°C < T \le 500\,°C \\ 0.01603\,T - 5.44881 & 500\,°C < T \le 635\,°C \\ 0.16635\,T - 100.90225 & 635\,°C < T \le 715\,°C \\ 176.07343 - 0.22103\,T & 715\,°C < T \le 785\,°C \\ 2.566 & 785\,°C < T \end{cases}$$

Table A.1 (Continued) – Constitutive Relationships for High Temperature Properties of Concrete

	Normal strength concrete – [ASCE Manual 1992]
Thermal Conductivity	Siliceous Aggregate Concrete: $k_c = \begin{cases} -0.000625T + 1.5 & 20\,°C \le T \le 800\,°C \\ 1.0 & 800°C < T \end{cases}$ Carbonate Aggregate Concrete: $k_c = \begin{cases} 1.355 & 20\,°C \le T \le 293\,°C \\ -0.00124IT + 1.7162 & 293\,°C < T \end{cases}$
Thermal Strain	All types: $\varepsilon_{th} = \left[0.004\left(T^2 - 400\right) + 6\left(T - 20\right)\right] \times 10^{-6}$

Table A.1 (Continued) – Constitutive Relationships for High Temperature Properties of Concrete

	High strength concrete – [Kodur et al. 2004]
Stress-strain relationships	$$\sigma_c = \begin{Bmatrix} f'_{c,T}\left[1-\left(\dfrac{\varepsilon_{max,T}-\varepsilon}{\varepsilon_{max,T}}\right)^{H}\right] & \varepsilon \le \varepsilon_{max,T} \\ f'_{c,T}\left[1-\left(\dfrac{30(\varepsilon-\varepsilon_{max,T})}{(130-f'_c)\varepsilon_{max,T}}\right)^{2}\right] & \varepsilon > \varepsilon_{max,T} \end{Bmatrix}$$ $$f'_{c,T} = \begin{Bmatrix} f'_c[1.0-0.003125(T-20)] & T < 100°C \\ 0.75 f'_c & 100°C \le T \le 400°C \\ f'_c[1.33-0.00145T] & 400°C < T \end{Bmatrix}$$ $$\varepsilon_{max,T} = 0.0018 + \left(6.7 f'_c + 6.0T + 0.03T^2\right)\times 10^{-6}$$ $$H = 2.28 - 0.012 f'_c$$

Table A.1 (Continued) – Constitutive Relationships for High Temperature Properties of Concrete

Thermal Capacity	Siliceous Aggregate Concrete: $$\rho c = \begin{cases} 0.005T + 1.7 & 20\,°C \le T \le 200\,°C \\ 2.7 & 200\,°C < T \le 400\,°C \\ 0.013T - 2.5 & 400\,°C < T \le 500\,°C \\ -0.013T + 10.5 & 500\,°C < T \le 600\,°C \\ 2.7 & 600\,°C < T \le 635\,°C \end{cases}$$ Carbonate Aggregate Concrete: $$\rho c = \begin{cases} 2.45 & 20\,°C \le T \le 400\,°C \\ 0.026T - 12.85 & 400\,°C < T \le 475\,°C \\ 0.0143T - 6.295 & 475\,°C < T \le 650\,°C \\ 0.1894T - 120.11 & 650\,°C < T \le 735\,°C \\ -0.263T + 212.4 & 735\,°C < T \le 800\,°C \\ 2 & 800\,°C < T \le 1000\,°C \end{cases}$$

Table A.1 (Continued) – Constitutive Relationships for High Temperature Properties of Concrete

	High strength concrete – [Kodur et al. 2004]
Thermal Conductivity	Siliceous Aggregate Concrete: $k_c = 0.85(2 - 0.0011T) \qquad 20°C < T \leq 1000°C$ Carbonate Aggregate Concrete: $k_c = \begin{cases} 0.85(2 - 0.0013T) & 20°C \leq T \leq 300°C \\ 0.85(2.21 - 0.002T) & 300°C < T \end{cases}$
Thermal Strain	All types: $\varepsilon_{th} = \left[0.004\left(T^2 - 400\right) + 6(T - 20)\right] \times 10^{-6}$

Table A.1 (Continued) – Constitutive Relationships for High Temperature Properties of Concrete

	Normal strength and high strength concrete – [Eurocode 2 2004]
Stress-strain relationships	$$\sigma_c = \frac{3\varepsilon f'_{c,T}}{\varepsilon_{c1,T}\left(2 + \left(\frac{\varepsilon}{\varepsilon_{c1,T}}\right)^3\right)} \quad , \varepsilon \leq \varepsilon_{cu1,T}$$ For $\varepsilon_{c1(T)} < \varepsilon \leq \varepsilon_{cu1(T)}$, the Eurocode permits the use of linear as well as nonlinear descending branch in the numerical analysis. For the parameters in this equation refer to Table A2
Thermal Capacity	Specific heat (J/kg°C) $c = 900$, for $20°C \leq T \leq 100°C$ $c = 900 + (T - 100)$, for $100°C < T \leq 200°C$ $c = 1000 + (T - 200)/2$, for $200°C < T \leq 400°C$ $c = 1100$, for $400°C < T \leq 1200°C$ Density change (kg/m^3) $\tilde{n} = \tilde{n}(20°C)$ = Reference density for $20°C \leq T \leq 115°C$ $\tilde{n} = \tilde{n}(20°C)\ (1 - 0.02(T - 115)/85)$ for $115°C < T \leq 200°C$ $\tilde{n} = \tilde{n}(20°C)\ (0.98 - 0.03(T - 200)/200)$ for $200°C < T \leq 400°C$ $\tilde{n} = \tilde{n}(20°C)\ (0.95 - 0.07(T - 400)/800)$ for $400°C < T \leq 1200°C$ Thermal Capacity = $\tilde{n} \times c$

Table A.1 (Continued) – Constitutive Relationships for High Temperature Properties of Concrete

		Normal strength and high strength concrete – [Eurocode 2 2004]
Thermal Conductivity	***All types***	Upper limit: $k_c = 2 - 0.2451\,(T/100) + 0.0107\,(T/100)2$ $for\ 20°C \le T \le 1200°C$ Lower limit: $k_c = 1.36 - 0.136\,(T/100) + 0.0057\,(T/100)2$ $for\ 20°C \le T \le 1200°C$
Thermal Strain	***Siliceous aggregate***	$\mathring{a}_{th} = -1.8\times10^{-4} + 9\times10^{-6}T + 2.3\times10^{-11}T^3$ $for\ 20°C \le T \le 700°C$ $\mathring{a}_{th} = 14\times10^{-3}$ $for\ 700°C < T \le 1200°C$
	Carbonate aggregate	$\mathring{a}_{th} = -1.2\times10^{-4} + 6\times10^{-6}T + 1.4\times10^{-11}T^3$ $for\ 20°C \le T \le 805°C$ $\mathring{a}_{th} = 12\times10^{-3}$ $for\ 805°C < T \le 1200°C$

Table A.2. Values for the Main Parameters of the Stress-strain Relationships of NSC and HSC at Elevated Temperatures (Eurocode 2)

Temp. °F	Temp. °C	NSC						HSC		
		Siliceous Agg.			Calcareous Agg.			$f'_{c,T} / f'_c(20^\circ C)$		
		$\frac{f'_{c,T}}{f'_c(20^\circ C)}$	$\varepsilon_{c1,T}$	$\varepsilon_{cu1,T}$	$\frac{f'_{c,T}}{f'_c(20^\circ C)}$	$\varepsilon_{c1,T}$	$\varepsilon_{cu1,T}$	Class1	Class2	Class3
68	20	1	0.0025	0.02	1	0.0025	0.02	1	1	1
212	100	1	0.004	0.0225	1	0.004	0.023	0.9	0.75	0.75
392	200	0.95	0.0055	0.025	0.97	0.0055	0.025	0.9	0.75	0.70
572	300	0.85	0.007	0.0275	0.91	0.007	0.028	0.85	0.75	0.65
752	400	0.75	0.01	0.03	0.85	0.01	0.03	0.75	0.75	0.45
932	500	0.6	0.015	0.0325	0.74	0.015	0.033	0.60	0.60	0.30
1112	600	0.45	0.025	0.035	0.6	0.025	0.035	0.45	0.45	0.25
1292	700	0.3	0.025	0.0375	0.43	0.025	0.038	0.30	0.30	0.20
1472	800	0.15	0.025	0.04	0.27	0.025	0.04	0.15	0.15	0.15
1652	900	0.08	0.025	0.0425	0.15	0.025	0.043	0.08	0.113	0.08
1832	1000	0.04	0.025	0.045	0.06	0.025	0.045	0.04	0.075	0.04
2012	1100	0.01	0.025	0.0475	0.02	0.025	0.048	0.01	0.038	0.01
2192	1200	0	-	-	0	-	-	0	0	0

Table A.3 – Constitutive Relationships for High Temperature Properties of Reinforcing Steel

	ASCE Manual [1992]
Stress-strain relationships	$$\sigma_s = \begin{cases} \dfrac{f(T,0.001)}{0.001}\varepsilon_s & \varepsilon_s \le \varepsilon_p \\ \dfrac{f(T,0.001)}{0.001}\varepsilon_p + f(T,\varepsilon_s - \varepsilon_p + 0.001) - f(T,0.001) & \varepsilon_s > \varepsilon_p \end{cases}$$ $$f(T,x) = 6.9(50 - 0.04T)\left[1 - exp\left((-30 + 0.03T)\sqrt{x}\right)\right]$$ $$\varepsilon_p = 4 \times 10^{-6} f_{y,20}$$ where: σ_s and ε_s = stress (MPa) and strain in steel reinforcement, respectively, and $f_{y,20}$ is the yield strength of reinforcing steel (MPa) at room temperature.
Thermal Strain	$$\varepsilon_{ths} = \left[0.004\left(T^2 - 400\right) + 6(T - 20)\right] \times 10^{-6} \qquad T < 1000°C$$

Table A.3 (Continued) – Constitutive Relationships for High Temperature Properties of Reinforcing Steel

	Eurocode 2 [2004]
Stress-strain relationships	$$\sigma_s = \begin{cases} \varepsilon_s E_{s,T} & \varepsilon_s \le \varepsilon_{sp,T} \\ f_{sp,T} - c + (b/a)\left(a^2 - \left(\varepsilon_{sy,T} - \varepsilon_s\right)^2\right)^{0.5} & \varepsilon_{sp,T} < \varepsilon_s \le \varepsilon_{sy,T} \\ f_{sy,T} & \varepsilon_{sy,T} < \varepsilon_s \le \varepsilon_{st,T} \\ f_{sy,T}\left(1 - \dfrac{\varepsilon_s - \varepsilon_{st,T}}{\varepsilon_{su,T} - \varepsilon_{st,T}}\right) & \varepsilon_{st,T} < \varepsilon_s \le \varepsilon_{su,T} \\ 0.0 & \varepsilon_s > \varepsilon_{su,T} \end{cases}$$ Parameters $$\varepsilon_{sp,T} = \frac{f_{sp,T}}{E_{s,T}} \quad \varepsilon_{sy,T} = 0.02 \quad \varepsilon_{st,T} = 0.15 \quad \varepsilon_{su,T} = 0.2$$ Functions $$a^2 = \left(\varepsilon_{sy,T} - \varepsilon_{sp,T}\right)\left(\varepsilon_{sy,T} - \varepsilon_{sp,T} + \frac{c}{E_{s,T}}\right)$$ $$b^2 = c\left(\varepsilon_{sy,T} - \varepsilon_{sp,T}\right)E_{s,T} + c^2$$ $$c = \frac{\left(f_{sy,T} - f_{sp,T}\right)^2}{\left(\varepsilon_{sy,T} - \varepsilon_{sp,T}\right)E_{s,T} - \left(f_{sy,T} - f_{sp,T}\right)}$$ Values of $f_{sp,T}$, $f_{sy,T}$ and $E_{s,T}$ can be obtained from Table A.4

Table A.3 (Continued) – Constitutive Relationships for High Temperature Properties of Reinforcing Steel

Thermal Strain	$\varepsilon_{ths} = \begin{Bmatrix} 1.2\times10^{-5}T + 0.4\times10^{-8}T^2 - 2.416\times10^{-4} & 20°C \le T < 750°C \\ 1.1\times10^{-2} & 750°C \le T < 860°C \\ 2\times10^{-5}T - 6.2\times10^{-3} & 20°C \le T < 750°C \end{Bmatrix}$

Table A.4. Values for the Main Parameters of the Stress-strain Relationships of Reinforcing Steel at Elevated Temperatures (Eurocode 2)

Steel Temperature T (^{o}C)	f_{yT} / f_y	f_{sp} / f_y *	E_{sT} / E_s *
20	1	1	1
100	1	1	1
200	1	0.807	0.9
300	1	0.613	0.8
400	1	0.42	0.7
500	0.78	0.36	0.6
600	0.47	0.18	0.31
700	0.23	0.075	0.13
800	0.11	0.05	0.09
900	0.06	0.0375	0.0675
1000	0.04	0.025	0.045
1100	0.02	0.0125	0.0225
1200	0	0	0

* f_y and E_s are yield strength and modulus of elasticity at room temperature

APPENDIX B

Calculation Load Carrying Capacity of the Testes Columns

Table B.1 –Parameters Assumed for 8 X 8 inch Columns

Parameter	**Value**
Section dimensions	8” x 8”
Steel reinforcement	4#6
Yield strength of steel	60 ksi
Span length	11’
Clear concrete cover	1.5”

Table B.2 – Summary Table

Beam	**Parameter**	**Value**
Column 1	Concrete strength	6 ksi
	Moment Capacity	30 k.ft
	Axial load	157 k
Column 2	Concrete strength	18 ksi
	Moment Capacity	66 k.ft
	Axial load	285 k

LOAD CALCULATIONS

NSC Column

Length of column = 11 ft.

Pin ended

Radius of gyration $r = 0.3 \times h$

Where h = dimension of column in the direction of eccentricity

$\therefore h = 8$

$$\therefore r = 0.3 \times 8 = 2.4in$$

$$kl_u = 1 \times 11 = 11ft$$

slenderness ratio $= \dfrac{kl_u}{r} = \dfrac{11 \times 12}{2.4} = 55$

$$22 < \frac{kl_u}{r} < 100 \text{ from 10.12.2}$$

Hence the column is slender and moment magnification method should be used.

Load carrying capacity of eccentrically loaded column assuming it to be non-slender

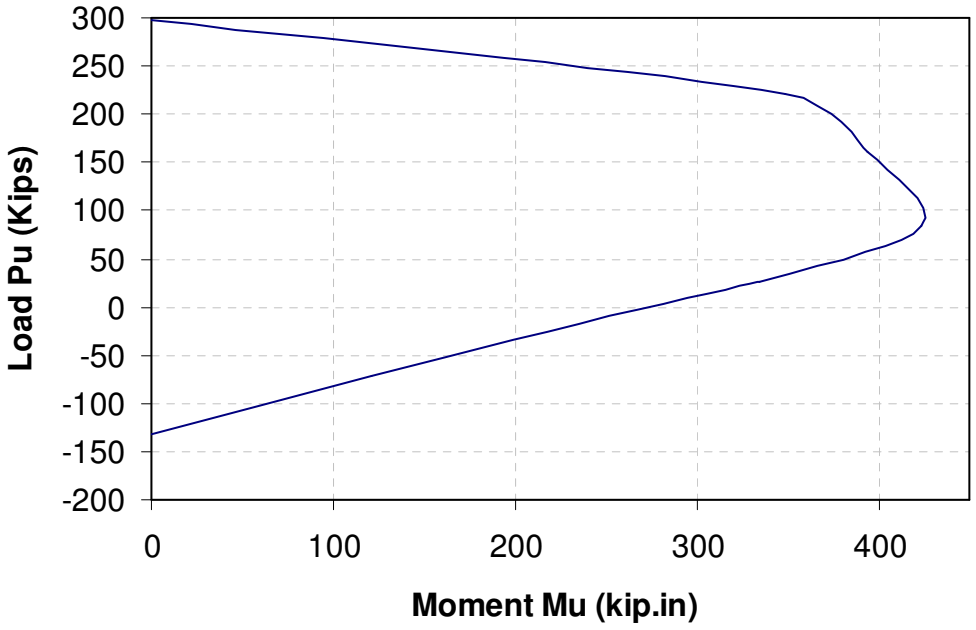

Fig. B.1. P-M Diagram for NSC column

Modulus of Elasticity of concrete

$$E_c = 33 \cdot w^{1.5} \cdot \sqrt{f_c'} = 33 \times 150^{1.5} \times \sqrt{6000} = 4.7 \times 10^6 \ psi$$

Moment of inertia of gross section $I_g = \dfrac{b \times h^3}{12} = \dfrac{8 \times 8^3}{12} = 341.33in^4$

Assume $\beta_d = 0.5$

Flexural rigidity

$$EI = \frac{E_c \times I_g / 2.5}{1 + \beta_d} = \frac{4.7 \times 10^6 \times 341.33 / 2.5}{1 + 0.0} = 0.64 \times 10^9 \, lbs \cdot in^2$$

Euler buckling load $P_c = \frac{\pi^2 EI}{(kL_u)^2} = \frac{\pi^2 \, 0.64 \times 10^9}{17424} = 400000 lbs$

Moment magnification factor $\delta_{ns} = \frac{C_m}{1 - (P_u / \phi \cdot P_c)} = \frac{1}{1 - (P_u / 0.65 \times 400)}$

Actual moment carrying capacity $Mn = \delta_{ns} \cdot P_u \cdot e_{min}$

$e_{min} = 0.6 + 0.03 \times h = 0.6 + 0.03 \times 8 = 0.84 in$

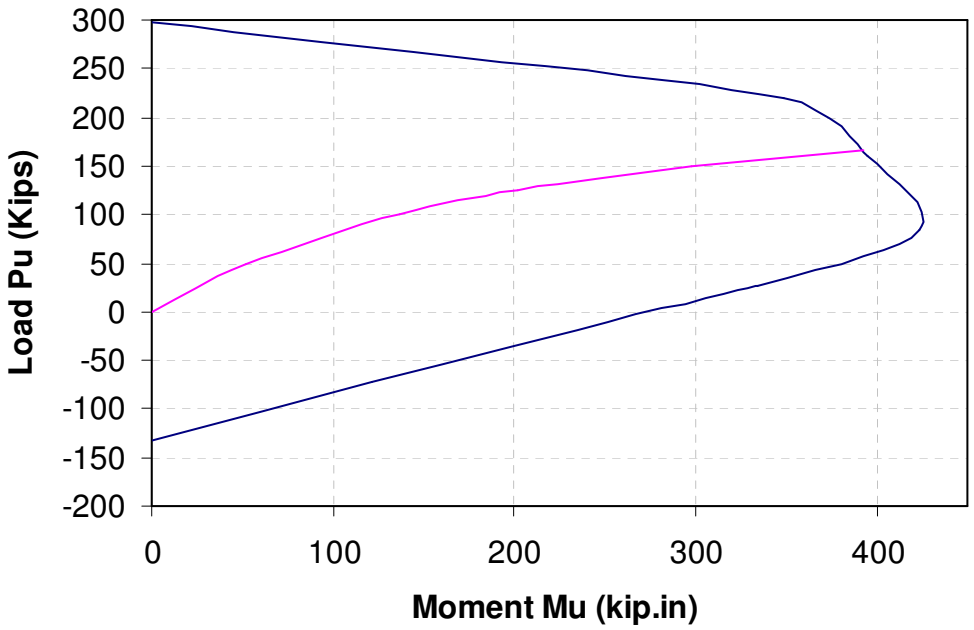

Fig. B.2. Load Carrying Capacity of NSC column

$P_u = 157kip$

$M_u = 30kip \cdot ft$

$e = 0.84in$

HSC Column

Length of column = 11 ft.

Pin ended

Radius of gyration $r = 0.3 \times h$

Where h = dimension of column in the direction of eccentricity

$$\therefore h = 8$$

$$\therefore r = 0.3 \times 8 = 2.4in$$

$$kl_u = 1 \times 11 = 11ft$$

slenderness ratio $= \frac{kl_u}{r} = \frac{11 \times 12}{2.4} = 55$

$$22 < \frac{kl_u}{r} < 100$$ from 10.12.2

Hence the column is slender and moment magnification method should be used.

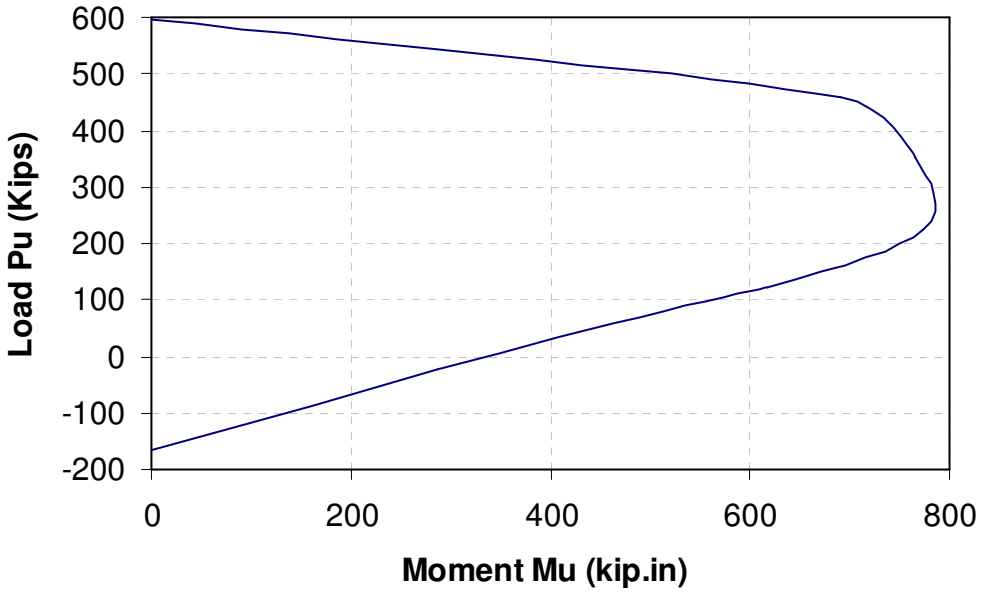

Fig. B.3. P-M Diagram for HSC column

Modulus of Elasticity of concrete $E_c = 33 \cdot w^{1.5} \cdot \sqrt{f'_c} = 33 \times 150^{1.5} \times \sqrt{18000}$

$E_c = 8.13 \times 10^6 \ psi$

Moment of inertia of gross section $I_g = \frac{b \times h^3}{12} = \frac{8 \times 8^3}{12} = 341.33 in^4$

Assume $\beta_d = 0.5$

Flexural rigidity

$$EI = \frac{E_c \times I_g / 2.5}{1 + \beta_d} = \frac{8.13 \times 10^6 \times 341.33 / 2.5}{1 + 0.0} = 1.11 \times 10^9 \, lbs \cdot in^2$$

Euler buckling load $P_c = \frac{\pi^2 EI}{(kL_u)^2} = \frac{\pi^2 \cdot 1.11 \times 10^9}{(17424)} = 630000 lbs$

Moment magnification factor $\delta_{ns} = \frac{C_m}{1 - (P_u / \phi \cdot P_c)} = \frac{1}{1 - (P_u / 0.75 \times 630)}$

Actual moment carrying capacity $Mn = \delta_{ns} \cdot P_u \cdot e_{min}$

$e_{min} = 0.6 + 0.03 \times h = 0.6 + 0.03 \times 8 = 0.84in$

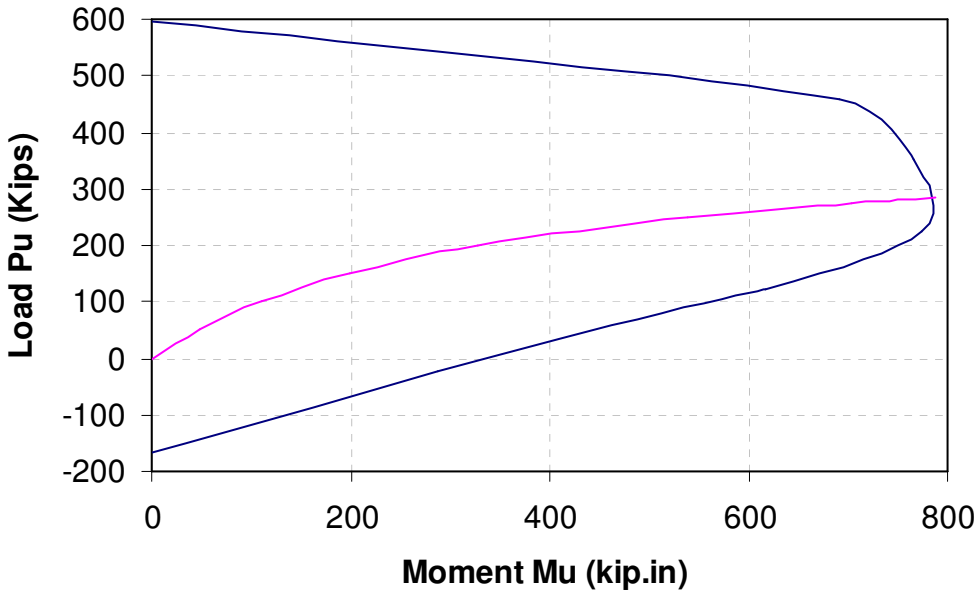

Fig. B.4. Load carrying capacity of HSC Column

$P_u = 285kip$

$M_u = 66kip \cdot ft$

$e = 0.84in$

APPENDIX C

Worked Example using Proposed Simplified Approach

To illustrate the applicability of the proposed equation in design practice, the fire resistance of a RC column is evaluated. Figure C.1 shows the elevation and cross sectional details of an RC column, tested by Lie and Woolerton [1988], considered for analysis. The column, fabricated with siliceous aggregate concrete, had an applied load of 1178 KN. The measured fire resistance of the column, in the test is 183 minutes. The fire resistance calculations from the proposed equation, and also using the provisions of different codes of practice, is presented below. The column is also checked for survivability under a design fire (Fire I) exposure shown in Figure 6.2.

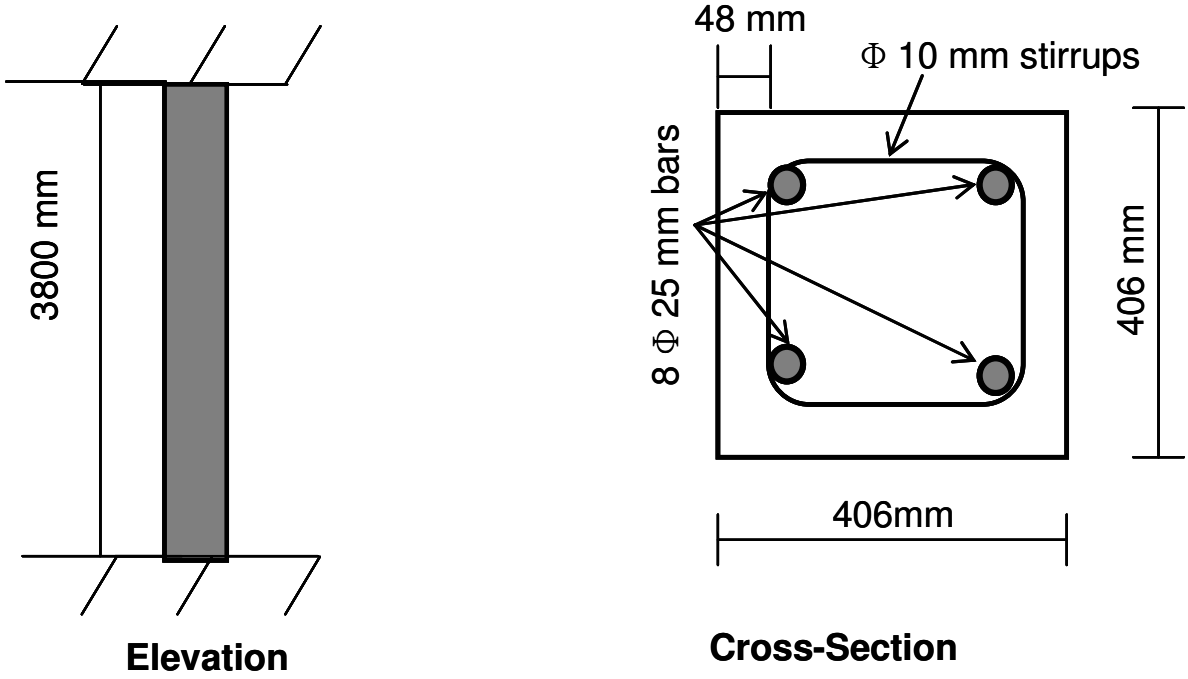

Fig. C.1- Elevation and cross-sectional details of Columns III14 [Lie and Woolerton, 1988]

Proposed Equation

$$R = C_t\left[8 \times k \times \left((S_R + 5) \times (0.2 - L_R) + 30\right)\right]^{0.94}$$

$$S_p = \frac{A_s}{A} \times 100 = \frac{\left(4 \times \frac{\pi \times 1^2}{4}\right)}{12 \times 12} \times 100 = 2.18$$

$C_e = 48$ mm

$$k = \frac{\left[(C_e - 82) \times (S_P + 10.5) + 870\right]}{390} = \frac{\left[(48 - 82) \times (2.18 + 10.5) + 870\right]}{390} = 1.11$$

Radius of gyration = $r = \sqrt{\frac{b^2}{12}} = \sqrt{\frac{305^2}{12}} = 88.05$ mm

$$S_R = \frac{l_e}{r} = \frac{0.5 \times 3810}{88.05} = 21.64$$

Load carrying capacity = $P_{Cr} = 0.8\left(0.85 \times A_c \times f_c' + A_s \times f_y\right)$

$$P_{Cr} = 0.8\left(0.85 \times \left((305 \times 305) - 1963\right) \times 31 + 1963 \times 444\right) = 3198kN$$

Load Ratio = $L_R = \frac{P}{P_{Cr}} = \frac{1178}{3198} = 0.37$

Here $C_t = 1.0$ as siliceous aggregate is used

$$R = C_t\left[8 \times k \times \left((S_R + 5) \times (0.2 - L_R) + 30\right)\right]^{0.94}$$

$$R = 1.0\left[8 \times 1.11 \times \left((43.27 + 5) \times (0.2 - 0.37) + 30\right)\right]^{0.94} = 162\,min$$

Eurocode Method

The empirical expression for fire resistance calculation is given by

$$R = 120\left(\frac{R_{\eta fi} + R_a + R_l + R_b + R_n}{120}\right)^{1.8}$$

$$\omega = \frac{A_s \times f_y}{A_c \times f_c'} = \frac{1964 \times 444}{((305 \times 305) - 1964) \times \left(\frac{31}{0.85 \times 1.5}\right)} = 0.39$$

$$b' = 305 \text{ mm}$$

$$l_{o,fi} = 3.81 \text{ m}$$

$$a = 48 \text{ mm}$$

$$\mu_{fi} = 0.32$$

$$R_{nfi} = 83\left[1.00 - \mu_{fi}\frac{(1+\omega)}{(0.85/\alpha_{cc}) + \omega}\right] = 83\left[1.00 - 0.32\frac{(1+0.39)}{(0.85/1) + 0.39}\right] = 56.15$$

$$R_a = 1.60(a - 30) = 1.60(48 - 30) = 28.2$$

$$R_l = 9.60(5 - l_{o,fi}) = 9.60(5 - 0.5 \times 3.81) = 29.7$$

$$R_b = 0.09b' = 0.09 \times 305 = 27.45$$

$$R_n = 0$$

$$R = 120\left(\frac{R_{\eta fi} + R_a + R_l + R_b + R_n}{120}\right)^{1.8}$$

$$R = 120\left(\frac{56.15 + 28.2 + 29.7 + 27.45 + 0}{120}\right)^{1.8} = 161 min$$

Australian Code Method

The fire resistance of an RC column is given by

$$FRP = \frac{\left(k \cdot f_c'^{1.3} \cdot D_c^{3.3} \cdot D_g^{1.8}\right)}{\left(10^5 \cdot N^{*1.5} \cdot L_e^{0.9}\right)}$$

$$\frac{A_s}{A_g} = \frac{3.14}{305 \times 305} = 3.37 \times 10^{-5}$$

$$\therefore k = 1.5$$

$$D_c = 305 \text{ mm}$$

$$D_g = 305 \text{ mm}$$

$$N^* = 1178 \text{ KN}$$

$$L_e = 3810 \text{ mm}$$

$$FRP = \frac{\left(k \cdot f_c'^{1.3} \cdot D_c^{3.3} \cdot D_g^{1.8}\right)}{\left(10^5 \cdot N^{*1.5} \cdot L_e^{0.9}\right)} = \frac{\left(1.5 \times 31^{1.3} \times 305^{3.3} \times 305^{1.8}\right)}{\left(10^5 \times 1178^{1.5} \times 3810^{0.9}\right)} = 234 \, min$$

ACI method

The fire resistance of the column using the ACI provisions presented in Table 1 for a 305 mm column made of siliceous aggregate concrete is 3 hours i.e. 180 min. Using the provisions based on concrete cover to the main reinforcement, the fire resistance for a 48mm cover is found to be 180min.

Summary

Based on the above calculation the fire resistance calculated from various codes and the proposed equation is shown in table A1 below.

Table C.1. Prediction of fire resistance values for column III 14 using different codes.

Fire Resistance (min)	Measured (test)	Proposed Equation	ACI	Eurocode	Australian Code
Column III14	183	162	180	161	234

Survivability under Design Fire Exposure

A_S = Area under standard fire time-temperature curve =

A_D= Area under standard fire time-temperature curve =

$\because A_D > A_S$

The columns will fail under design fire (Fire I) exposure.

REFERENCES

REFERENCES

1. ACI-216.1 (2007). Code requirements for determining fire resistance of concrete and masonry construction assemblies. Farmington Hills, MI, American Concrete Institute.

2. ACI-318 (2008). Building Code Requirements for Reinforced Concrete and Commentary. Farmington Hills, MI, American Concrete Institute.

3. Aldea, C. M., J. M. Franssen, et al. (1977). Fire test on normal and high strength reinforced concrete columns. Gaithersburg, Maryland, USA, National Institute of Science and Technology.

4. Ali, F. A., D. O'Connor, et al. (2001). "Explosive spalling of high strength concrete columns in fire." Magazine of Concrete Research 53(3): 197-204.

5. Ali, F. A., N. Ali, et al. (2004). "Outcomes of a major research on fire resistance of concrete columns." Fire Safety Journal 39: 433-445.

6. Anderberg Y., and Thelandersson S. (1976), "Stress and Deformation Characteristics of Concrete at High Temperatures, 2. Experimental Investigation and Material Behaviour Model", Lund Institute of Technology, Sweden.

7. Anderberg, Y. (1997), "Spalling Phenomenon of HPC and OC", International Workshop on Fire Performance of High Strength Concrete, NIST SP 919, Gaithersburg, MD, pp. 69-75.

8. Anderberg, Y. and S. Thelandersson (1976). Stress and deformation characteristics of concrete at high temperatures, 2-Experimental investigation and material behaviour model. Lund, Sweden Bulletin 54, Lund Institute of Technology.

9. AS-3600 (2001). Concrete Structures. Australia, Committee BD-002.

10. ASTM Test Method E1529 (1993), "Standard Test Methods for Determining Effects of Large Hydrocarbon Pool Fires on Structural Members and Assemblies", American Society for Testing and Materials, West Conshohocken, PA.

11. ASTM-E119 (2007). Standard test methods for fire tests of building construction and materials. West Conshohocken, PA, American Society for Testing and Materials.

12. Balendran, R. V., N. Abid, et al. (2003). "Flexural and Split Cylinder Strengths of HSC at Elevated Temperatures." Fire Technology 39(47-61).

13. Bazant Z.P. (1997), “Analysis of Pore Pressure, Thermal Stress and Fracture in Rapidly Heated Concrete”, International Workshop on Fire Performance of High Strength Concrete, NIST SP 919, Gaithersburg, MD, pp. 155-164.

14. Bazant Z.P., and Kaplan M.F. (1996), Concrete at High Temperature, Longman.

15. Bazant Z.P., and Thonguthai W. (1978), "Pore pressure and Drying of Concrete at High Temperature", Journal of the Engineering Mechanics Division, ASCE, 104(EM5), pp. 1059-1079.

16. Benmarce, A. and M. Guenfoud (2005). "Experimental behavior of high strength concrete columns in fire." Magazine of Concrete Research 57(5): 283-287.

17. Bilodeau, A., V. M. Malhotra, et al. (1998). Hydrocarbon Fire Resistance of High Strength Normal Weight and Light Weight Concrete Incorporating Polypropylene Fibres. International Symposium on High Performance and Reactive Powder Concrete. Sherbrooke, QC: 271-296.

18. Bratina, S., B. Cas, et al. (2005). "Numerical modeling of behavior of reinforced concrete columns in fire and comparison with Eurocode 2." International Journal of Solids and Structures 42(21-22): 5715-5733.

19. Buchanan, A. (2002). Structural Design for Fire Safety. Chichester, Wiley.

20. Campbell T.I., and Kodur V.R. (1990), "Deformation Controlled Nonlinear Analysis of Prestressed Concrete Continuous Beams", PCI Journal, PCI, pp. 42-55.

21. CAN/ULC-S101 (2004). Code for the design of concrete structures for buildings. Rexdale, ON, Canada, Canadian Standards Association (CSA).

22. Castillo, C. and A. J. Durrani (1990). "Effect of Transient High Temperature on High-Strength Concrete." ACI Materials Journal 87(1): 47-53.

23. Chan, S. Y. N., G. F. Peng, et al. (1999). "Fire Behavior of High-Performance Concrete Made with Silica Fume at Various Moisture Contents." ACI Materials Journal 96(3): 405-409.

24. Chang, Y. F., Y. H. Chen, et al. (2006). "Residual stress–strain relationship for concrete after exposure to high temperatures." Cement and Concrete Research 36: 1999-2005.

25. Cheng, F. P., V. R. Kodur, et al. (2005). "Stress-Strain Curves for High Strength Concrete at Elevated Temperatures." Journal of Materials in Civil Engineering 16(1): 84-94.

26. Danielsen, U. (1997). Marine Concrete Structures Exposed to Hydrocarbon Fires, SINTEF – The Norwegian Fire Research Institute: 56-76.

27. Diederichs, U., U. M. Jumppanen, et al. (1988). Material properties of high strength concrete at elevated temperature. IABSE 13th Congress, Helsinki.

28. Diederichs, U., U. M. Jumppanen, et al. (1995). High Temperature Properties and Spalling Behavior of High Strength Concrete. Fourth Weimar Workshop on High Performance Concrete, HAB Weimar, Germany.

29. Dwaikat, M. B. (2009). Flexural response of reinforced concrete beams exposed to fire. East Lansing, Michigan, USA, Doctoral Thesis, Michigan State University. Doctoral: 117-163.

30. Dwaikat, M.B. and Kodur, V.K., (2009) "Hydrothermal Model for Predicting Fire Induced Spalling in Concrete Structural Systems", Fire Safety Journal, 44(3), pp. 425-434.

31. EC2-1-2 (2004). Design of concrete structures – Part 1-2, General rules – Structural Fire design, CEN.

32. Eurocode 1 (2002), "EN 1991-1-2: Actions on Structures. Part 1-2: General Actions - Actions on Structures Exposed to Fire", European Committee for Standardization, Brussels, Belgium.

33. Feasey, R., and Buchanan, A.H. (2002), "Post Flash-over Fires for Structural Design", Fire Safety Journal, 37(1), pp. 83-105.

34. Felicetti, R., P. G. Gambarova, et al. (1996). Residual mechanical properties of high-strength concretes subjected to high-temperature cycles. 4th International Symposium on Utilization of High-Strength/High-Performance Concrete, Paris, France.

35. Flynn, D. R. (1999). Response of High Performance Concrete to Fire Conditions: Review of Thermal Property Data and Measurement Techniques, MetSys Corportation, US.

36. Franssen, J. M. and J. C. Dotreppe (2003). "Fire tests and calculation methods for circular concrete columns." Fire Technology 39: 80-97.

37. Franssen, J. M., V. K. Kodur, et al. (2004). User Manual for SAFIR, University of Liege, Belgium.

38. Fu, Y. F., Y. L. Wong, et al. (2005). "Stress–Strain Behaviour of High–Strength Concrete at Elevated Temperatures." Magazine of Concrete Research 57(9): 535-544.

39. Furumura, T., T. Abe, et al. (1995). Mechanical Properties of High Strength Concrete at High Temperatures. 4th Weimar Workshop on High Performance Concrete: Material Properties and Design, Hochschule für Architektur und Bauwesen (HAB), Weimar, Germany.

40. Gawin D., Majorana C.E., and Schrefler B.A. (1999), "Numerical Analysis of Hygro-thermic Behaviour and Damage of Concrete at High Temperature", Magazine of Cohesive Frictional Material, 4, pp. 37-74.

41. Hammer, T. A. (1995). High strength concrete phase 3, spalling reduction through material design. SP6 Fire Resistance. S. S. a. Concrete.

42. Harada, T., J. Takeda, et al. (1972). Strength, Elasticity and Thermal Properties of Concrete Subjected to Elevated Temperatures. International Seminar on Concrete for Nuclear Reactor. A. S. P. SP34-21. Detroit, MI, USA. 34: 377-406.

43. Harmathy T.Z. (1967), "A comprehensive Creep Model", Journal of Basic Engineering, 89(2), pp. 496-502.

44. Harmathy T.Z. (1969), "Simultaneous Moisture and Heat Transfer in Porous Systems with Particular Reference to Drying". I & E C Fundamentals, 8(1).

45. Harmathy T.Z. (1971), "Moisture and Heat Transport with Particular Reference to Concrete", National Council of Canada, NRCC 12143.

46. Harmathy, T. Z. (1970). "Thermal properties of concrete at elevated temperatures." ASTM Journal of Materials 5(1): 47-74.

47. Harmathy, T. Z. (1993). Fire safety design and concrete. New York, NY, John Wiley & Sons, Inc.

48. Harmathy, T. Z. and L. W. Allen (1973). "Thermal Properties of Selected Masonry Unit Concretes." Journal of American Concrete Institute 70: 132-142.

49. Hertz, K. (1991). Danish investigations on silica fume concretes at elevated temperatures. ACI 1991 Spring Convention, Boston, MA.

50. Hertz, K. (2003). "Limits of Spalling of Fire-Exposed Concrete." Fire Safety Journal 38(2): 103-116.

51. Huang C.L. (1979), "Multi-Phase Moisture Transfer in Porous Media Subject to Temperature Gradient", International Journal of Heat and Mass Transfer, 22, pp. 1295-1307.

52. Kalifa P., Chene G., and Galle C. (2001), “High-Temperature Behavior of HPC with Polypropylene Fibers: From Spalling to Microstructure”, Cement and Concrete Research, 31, pp. 1487-1499.

53. Kanema M., Noumowe A., Gallias J., and Cabrillac R. (2007), "Pearmeability and Mechanical Properties of Concrete at High Temperatures", Concrete Under Sever Concditions: Environment & Loading, CONSEC’07 Tours, France.

54. Khoury G.A. (2009), “Concrete spalling assessment methodologies and polypropylene fibre toxicity analysis in tunnel fires”, Structural Concrete, 9(1), pp. 11-18.

55. Khoury G.A., Grainger B.N., and Sullivan P.J.E. (1985), “Strain of Concrete during Fire Heating to 600 °C”, Magazine of Concrete Research, 37, pp. 195-215.

56. Khoury, G. A. (1996). Performance of Heated Concrete-Mechanical Properties. London, U.K., Nuclear Installations Inspectorate, Imperial College.

57. Khoury, G. A. (2006). "Strain of heated concrete during two thermal cycles. Part 1: Strain over two cycles, during first heating and at subsequent constant temperature." Magazine of Concrete Research 58(6): 367-385.

58. Khoury, G. A. (2006). "Strain of heated concrete during two thermal cycles. Part 2: Strain during first heating and at subsequent thermal cycle." Magazine of Concrete Research 58(6): 387-400.

59. Khoury, G. A. (2006). "Strain of heated concrete during two thermal cycles. Part 3: Isolation of strain components and stain model development." Magazine of Concrete Research 58(7): 421-435.

60. Kodur, V. K. (1999). "Performance based fire resistance design of concrete-filled steel columns." Journal of Constructional Steel Research 51(1): 21-36.

61. Kodur, V. K. and R. McGrath (2006). "Effect of silica fume and confinement on fire performance of high strength concrete columns." Canadian Journal of Civil Engineering 33: 93-102.

62. Kodur, V. R. (2000). Spalling in High Strength Concrete Exposed to Fire - Concerns, Causes, Critical parameters and Cures. ASCE Structures Congress, Philadelphia, U.S.A.

63. Kodur, V. R. (2003). Fire resistance design guidelines for high strength concrete columns, National Research Council, Canada: 1-11.

64. Kodur, V. R. and L. Phan (2007). "Critical Factors Governing the Fire Performance of High Strength Concrete Systems." Fire Safety Journal 42: 482-488.

65. Kodur, V. R. and M. A. Sultan (2003). "Effect of Temperature on Thermal Properties of High-Strength Concrete." Journal of Materials in Civil Engineering 15(2): 101-107.

66. Kodur, V. R. and R. McGrath (2003). "Fire endurance of high strength concrete columns." Fire Technology-Special Issue 39(1): 73-87.

67. Kodur, V. R., F. P. Cheng, et al. (2003). "Effect of Strength and Fiber Reinforcement on the Fire Resistance of High Strength Concrete Columns." ASCE Journal of Structural Engineering 129(2): 253-259.

68. Kodur, V. R., M. M. S. Dwaikat, et al. (2008). "High Temperature Properties of Concrete for Fire Resistance Modeling of Structures." ACI Material Journal 105(5): 517-527.

69. Kodur, V. R., T. C. Wang, et al. (2004). "Predicting the fire resistance behavior of high strength concrete columns." Cement and Concrete Composites 26(2): 141-153.

70. Kumar A. (2003), "Behaviour of RCC Beams after Exposure to Elevated Temperatures", Journal of the Institution of Engineers (India): Civil Engineering Division, 84(3), pp. 165-170.

71. Lau, A. and M. Anson (2006). "Effect of High Temperatures on High Performance Steel Fibre Reinforced Concrete." Cement and Concrete Research 36: 1698-1707.

72. Lawson, J. R., L. T. Phan, et al. (2000). Mechanical Properties of High Performance Concrete After Exposure to Elevated Temperatures. US.

73. Li, M., C. X. Qian, et al. (2004). "Mechanical properties of high-strength concrete after fire." Cement and Concrete Research 34(6): 1001-1005.

74. Lie, T. T. (1992). Structural fire protection. New York,NY, ASCE Committee on Fire Protection, Structural Division, American Society of Civil Engineers: 225-229.

75. Lie, T. T. and B. Celikkol (1991). "Method to calculate the fire resistance of circular reinforced concrete columns." ACI Materials Journal 88(1): 84-91.

76. Lie, T. T. and J. L. Woolerton (1988). Fire Resistance of Reinforced Concrete Columns – Test Results, National Research Council Canada.

77. Lie, T. T. and R. J. Irwin (1993). "Method to calculate the fire resistance of reinforced concrete columns with rectangular cross section." ACI Structural Journal 90(1): 52-60.

78. Lie, T. T. and V. R. Kodur (1995). Mechanical Properties of Fibre-Reinforced Concrete at Elevated Temperatures, IRC-NRC.

79. Lie, T. T. and V. R. Kodur (1995). Thermal Properties of Fibre-Reinforced Concrete at Elevated Temperatures, IRC-NRC.

80. Lie, T. T. and V. R. Kodur (1996). "Thermal and Mechanical Properties of Steel-Fibre-Reinforced Concrete at Elevated Temperatures." Canadian Journal of Civil Engineering 23: 511-517.

81. Mindess S., Young J. F., and Darwin D. (2003), Concrete, 2nd Edt., Prentice Hall, Pearson Education Inc., Upper Saddle River, NJ 07458.

82. Nassif, A. (2006). "Postfire full stress–strain response of fire-damaged concrete." Fire and Materials 30: 323-332.

83. Naus D.J. (2006), "The Effect of Elevated Temperatures on Concrete Materials and Structures – A Literature Review", U.S. Nuclear Regulatory Commission, Office of Nuclear Regulatory Research, Washington, DC 20555-0001.

84. Neves I. C., Rodrigues J. C., and Loureiro A. P. (1996), "Mechanical Properties of Reinforcing and Prestressing Steels after Heating," Journal of Materials in Civil Engineering, 8(4), 1996, pp. 189-194.

85. Phan, L. T. (1996). Fire performance of high-strength concrete: A report of the state-of-the-art. Gaithersburg, MD, National Institute of Standard and Technology.

86. Phan, L. T. and N. J. Carino (2003). "Code Provisions for High Strength Concrete Strength - Temperature Relationship at Elevated Temperatures." Materials and Structures 36(256): 91-98.

87. Phan, L. T., J. R. Lawson, et al. (2000). Heating, spalling characteristics and residual properties of high performance concrete. Fifteenth Meeting of the UJNR Panel on Fire Research and Safety. USA, NIST. 2.

88. Phan, L. T., J. R. Lawson, et al. (2001). "Effects of elevated temperature exposure on heating characteristics, spalling, and residual properties of high performance concrete." Materials and Structures 34(2): 83-91.

89. Purkiss, J.A. (2007), "Fire Safety Engineering : Design of Structures", 2nd edition, Butterworth-Heinemann, UK.

90. Saad, M., S. A. Abo-El-Enein, et al. (1996). "Effect of temperature on physical and mechanical properties of concrete containing silica fume." Cement & Concrete Composites 26: 669-675.

91. Sahota M.S., and Pagni P.G. (1979), "Heat and Mass Transfer in Porous Media Subjecte to Fire". International Journal of Heat and Mass Transfer, 22, pp. 1069-1081.

92. Savva, A., P. Manita, et al. (2005). "Influence of elevated temperatures on the mechanical properties of blended cement concretes prepared with limestone and siliceous aggregates." Cement & Concrete Composites 27(2): 239-248.

93. Scheider U. (1988), "Concrete at High Temperatures – A General Review", Fire Safety Journal, 13, pp. 55-68.

94. Schneider U., and Herbst H.J. (1989), "Permeabiliteat und Prositaet von Beton bei hohen Temperaturen", Deutscher Ausschuss fuer Stahlbeton, 403, pp. 23-52.

95. SFPE (2008), "SFPE Handbook of Fire Protection Engineering, 4th edition, Editor: DiNenno P.J., National Fire Protection Association, Quincy, MA.

96. Shin, K. Y., S. B. Kim, et al. (2002). "Thermo-Physical Properties and Transient Heat Transfer of Concrete at Elevated Temperatures." Nuclear Engineering and Design 212(1-3): 233-241.

97. Sullivan, P. J. E. (2004). "A Probabilistic Method of Testing for the Assessment of Deterioration and Explosive Spalling of High Strength Concrete Beams in Flexure at High Temperature." Cement & Concrete Composites 26(2): 155-162.

98. Tan, K. H. and Y. Yao (2003). "Fire resistance of four-face heated reinforced concrete columns." Journal of Structural Engineering 129(9): 1220-1229.

99. Tan, K. H. and Y. Yao (2004). "Fire resistance of reinforced concrete columns subjected to 1-, 2-, and 3-face heating" Journal of Structural Engineering 130(11): 1820-1828.

100. Van-Geem, M. G., J. Gajda, et al. (1996). Thermal Properties of Commercially Available High Strength Concretes. Skokie, IL, US, Portland Cement Association.

101. Van-Geem, M. G., J. Gajda, et al. (1997). "Thermal Properties of Commercially Available High Strength Concretes." Cement, Concrete, & Aggregates 19: 38-53.

102. Wang, Y. C., P. M. H. Wong, et al. (2003). Mechanical properties of fibre reinforced polymer reinforcing bars at elevated temperatures, IRC – NRCC.

103. Williams B.K. (2004), “Fire Performace of FRP-Strengthened Reinforced Concrete Flexural Memebers”, PhD Thesis, Queen’s University, Kongston, Ontario, Canada.

104. Xiao, J., M. Xie, et al. (2006). "Residual Compressive Behaviour of Pre-heated High-performance Concrete with Blast–furnace–slag." Fire Safety Journal 41: 91-98.